Table of Contents

List of Figures

List of Tables

Nomenclature

C	Compressive strength (MPa)
d	Diameter (m)
D	Density (kg/m^3)
F_{max}	Maximum applied load (N)
h	Plank constant (6.62×10^{-34} Js)
I	Current (amp)
k	Absorption coefficient
L_c	Crystalline length of coke or anode (Å)
M	Mass (kg)
R	Absolute reflectance
s	Scattering coefficient
t	Time (s)
v	Voltage drop (mV)
V	Volume (m^3)
W	Total load on the sample at failure (N)
W_a	Work of adhesion (N/m)

Greek Symbols

Y_{SV}	Interfacial tension between solid and vapor (Nm^{-1})
Y_{SL}	Interfacial tension between solid and liquid (Nm^{-1})
Y_{LV}	Interfacial tension between liquid and vapor (Nm^{-1})
ε	Frequency of the x-ray radiation (Hz)
θ	Contact angle of coal tar pitch on coke bed (°)
λ	Wavelength (nm)
ρ	Density of pitch (kg/m^3)
σ_{max}	Bending stress (N/m^2)

Abbreviations

ANN	Artificial neural network
ANOVA	Analysis of variance
BAD	Baked anode density (kg/m^3)
BMP	Ball mill product
DAD	Dry aggregate density (kg/m^3)
DBT	Dibenzothiophene
df	Deegree of freedom
DR	Dusting rate for air/CO_2 reactivity ($mg/cm^2.h$)
ER	Electrical resistivity of anode (μΩm)
FD	Filter dust
FT-IR	Fourier transform infrared spectroscopy
GAD	Green anode density (kg/m^3)

LMV	Linear multivariable analysis
NMR	Nuclear magnetic resonance spectroscopy
OPM	Optical microscopy
QI	Quinoline insoluble
SCC	Standard calcined coke
SE	Sum of errors
SEM	Scanning electron microscopy
SER	Specific electrical resistivity of coke (μΩm)
SS	Sum of squares
TBD	Tapped bulk density (kg/m^3)
TCD	Thermal conductivity detector
TGA	Thermogravimetric analysis
TI	Toluene insoluble
TR	Total air/CO_2 reactivity rate ($mg/cm^2.h$)
TR_i	Initial air/CO_2 reactivity rate ($mg/cm^2.h$)
TR_f	Final air/CO_2 reactivity rate ($mg/cm^2.h$)
UCC	Under-calcined coke
VBD	Vibrated bulk density (kg/m^3)
XPS	X-ray photoelectron spectroscopy
XRD	X-ray diffraction

CHAPTER 1

INTRODUCTION

1.1 Background

1.1.1 Production of aluminum

The use of aluminum is experiencing sustained growth throughout the world. Over the last few decades, the growth rate is annually 2-3% because of the exceptional properties of aluminum. Its flexibility, corrosion resistance, light weight, and infinite capacity to be recycled makes it a highly useful material in many areas of daily life and a viable solution in helping to protect the environment. In 2006, aluminum's main applications were focused in the fields of transport (27%), building and construction (20%), packaging (16%), electrical supplies (10%), machinery and equipment (8%), and sustainable consumer products (7%). Aluminum is one of the major industries in Québec and Canada. North America produces 7% of worldwide demand. The favourable socio-economic conditions led Canada to take the third place among all the aluminum producing countries in the world [1-3] (Figure 1.1). In 2014, China produced 43% of the global aluminum production [3]. Canada produced 60% of the tonnage of primary aluminum in North America in 2013 [4]. Over 90% of this production comes from Québec. In 2011, aluminum industries ranked third among the major export industries of Québec, with 11% of total exports [2].

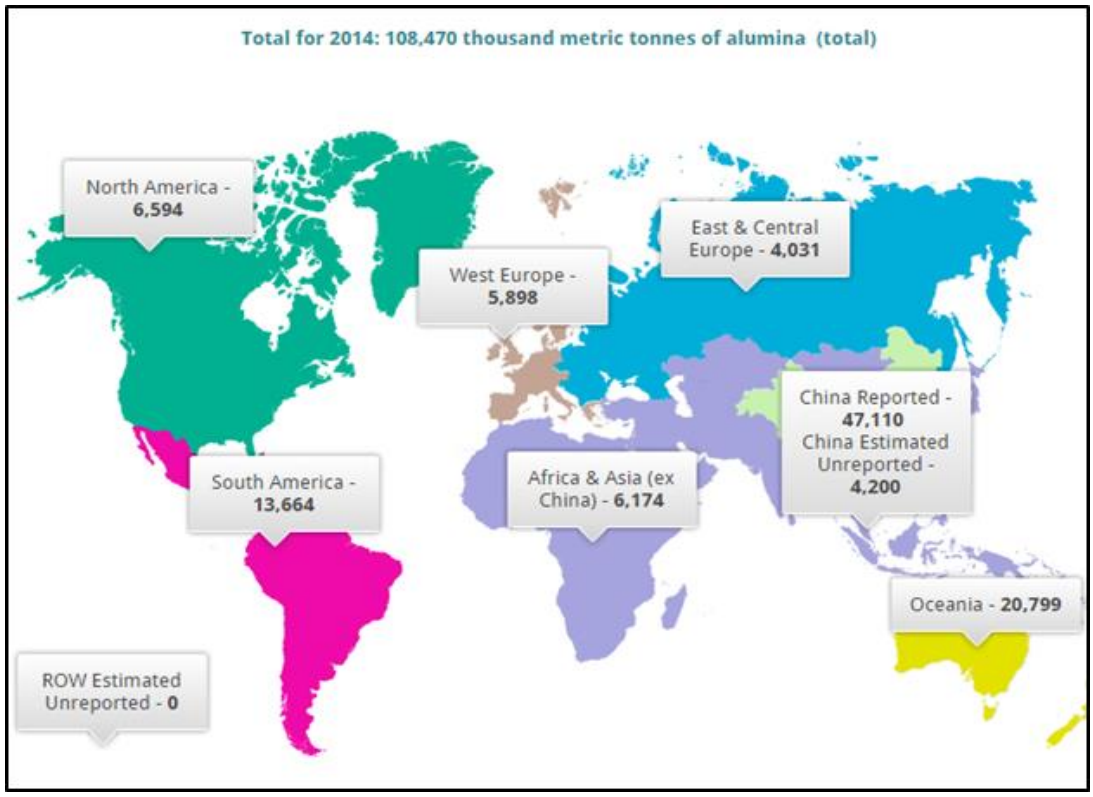

Figure 1.1 Worldwide primary aluminum production in 2014 [3]

The primary aluminum production is carried out using the Hall –Heroult process which is an electrolytic process that separates metal aluminum from aluminum oxide and produces carbon dioxide as the by-product. The whole process takes place in an electrolytic cell known as 'pot' where alumina is dissolved in a bath of sodium aluminum fluoride called cryolite (Na_3AlF_6) at approximately 960°C. High-amperage direct electrical current at low voltage is applied through the carbon anode which is immersed in molten electrolyte. The aluminum metal collects on the top of the cathode, and it is syphoned out at regular intervals for further processing [5]. The following equation represents the reaction in the cell:

$$2Al_2O_3(l) + 3C(s) \rightarrow 4Al(l) + 3CO_2(g) \quad \textbf{(1.1)}$$

(1.890 kg) (0.334 kg) (1 kg) (1.224 kg)

Several ferrous and non-ferrous metals are produced via electrochemical processes where carbon is used as electrodes at industrial-scale production of these metals [6]. Theoretical requirement for aluminum production is 334 kg carbon per tonne of aluminum metal. However, more than 400 kg of carbon is used to produce one tonne of aluminum. This carbon used in the form of carbon anodes represents about 15% of the production cost [7]. The carbon anodes are consumed during the electrolysis process and have to be replaced every 2-4 weeks depending on the size, density and reactivity (air and CO_2) of the anode and the operating conditions of the electrolytic cell. Electricity consumption during electrolysis has a significant effect on the total production cost, and a small increase in anode resistance considerably decreases the efficiency and economy of the process [5].

1.1.2 Production of carbon anodes

Green petroleum coke is calcined in a calciner. Calcined petroleum coke and recycled butts and anodes (called ‘dry agrregate’) are separated to different fractions required for a predetermined recipe by crushing and screening. The dry aggregate is preheated to around 150-180°C to ensure that, during mixing, pitch wets and penetrates into the particles. Coal tar pitch is utilized as a binder which binds the dry aggregate together to produce anodes. Liquid pitch is heated to about 200°C and added to the mixer or the kneader. Mixing time should be optimum to attain homogenous paste. Thereafter, anode paste is compacted in a vibrocompactor or in a hydraulic press. After compaction, anode is cooled using water or

air as the cooling medium. Then, green anodes are baked in a baking furnace at around 1000-1300°C; and after rodding, baked anodes are used in electrolysis to produce primary aluminum.

Thus, carbon anodes are made by baking a compacted mixture of calcined coke, recycled anode butts, recycled green and baked anodes, and coal tar pitch. Good interaction between coke and pitch is essential for the generation of a satisfactory bond between these two components. Efficient wetting of the coke particles by the binder is required so that the binder could penetrate through coke pores and fill the voids between the coke particles. This keeps the structure together and reduces electrical resistivity [7]. Wettability of coke by pitch determines the quality of bonding between these two components and thereby greatly affects the final anode properties. Good bonding generates high density, good mechanical properties, and structurally-sound anode material. The interaction between dry aggregate and binder depends on the binder characteristics, i.e., softening point, chemical composition, surface tension, viscosity, and the characteristics of the filler such as particle size, texture, chemical functional groups on the surface, and porosity [8]. Details of anode production steps are explained in the Figure 1.2.

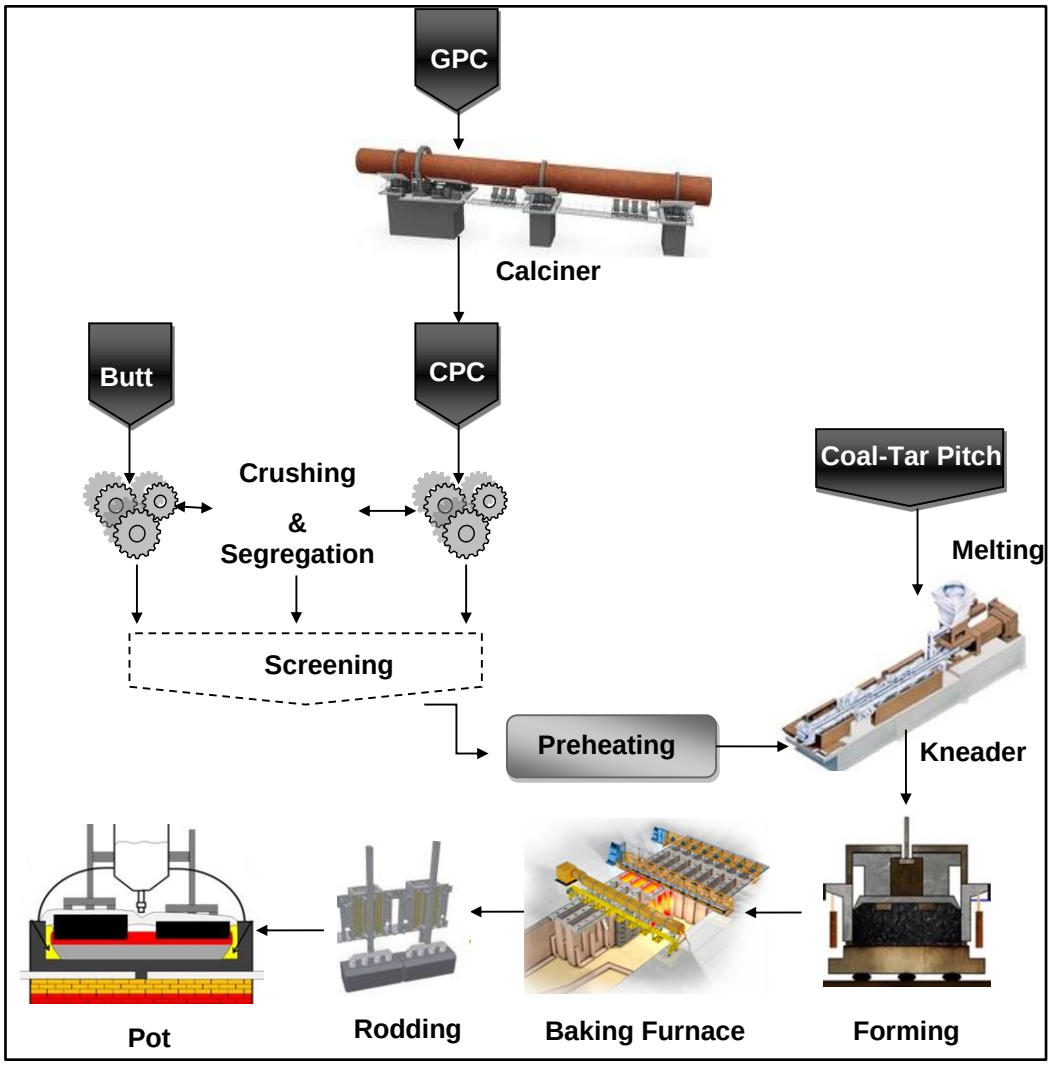

Figure 1.2 Carbon anode fabrication steps for primary aluminum production

Prebaked anodes consist of about 65-68% petroleum coke, 20-30% anode butts and, 13-15% coal tar pitch. Different chemical and physical properties of the petroleum coke i.e. porosity, grain stability, impurities, bulk density, reactivity, mechanical structure, surface characteristics, etc. significantly affect the properties, behavior, and the performance of anodes during the electrolysis [1].

In the last few years, the available anode-quality petroleum coke has been deteriorating throughout the world. Therefore the anode recipe should be optimized according to the availability of raw materials so that the anode quality could be improved or kept constant. The anode production plant uses three different granulometry ranges in order to obtain best particle packing to achieve higher density. In the plant, each granulometry range is blended in such a way that the strong aspects of individual coke fractions can be used to maximize the anode performance as each fraction has its specific impact on anode properties. Blending strategy plays an important role in determining anode properties as each individual fraction has its own importance. Increasing the fine content in formulation will certainly increase the density of the anodes by filling the coke pores and the inter-particle voids. Nevertheless, higher quantity of fines has undesirable effects on mechanical properties of anode and also increases the binder demand. However, larger fractions of coke and anode butt provide mechanical strength to the anodes; but simultaneously, the impurity content (especially sodium) of anode butt increases the anode reactivity [5].

Calcination of green petroleum coke increases its grain stability, and this improves the mechanical strength of the anode. Calcination minimizes the particle shrinkage which then minimizes the cracking of the anode during baking. It also ensures that the pore structure is accessible to pitch which increases the density and reduces the electrical resistivity of the anode. Calcination of coke reduces the coke reactivity by decreasing the number of highly reactive carbon atoms on the edge with respect to the carbon atoms in the crystal basal plane. Calcination of coke significantly reduces the volatile release from the coke during anode baking [5]. However, it is reported in the literature that using under-calcined coke in

anode production might reduce total anode consumption and dusting in electrolysis cell. In general, standard calcined coke is less reactive than pitch. Pitch reacts more than coke causing disintegration of the anode structure. Using under-calcined coke leads to similar reactivities for coke and pitch after baking; thereby, this makes the anode consumption more homogeneous. Nevertheless, the effect of using under-calcined coke on the anode reactivity is dependent on the baking temperature of the anode. At high baking temperatures, the reactivity of the anodes made from under-calcined coke and standard calcined coke is similar [9-11].

1.2 Statement of the problem

For efficient aluminum production, anodes should have certain properties such as high density, low electrical resistivity, high mechanical strength, high thermal shock resistance, and low air/CO_2 reactivity. In the aluminum reduction cell, carbon anode is part of the electrical circuit. Due to high carbon consumption during electrolysis, it is required to change the anode every 14-28 days depending on the anode size and current density. In this process, the high electrical resistance of anode is one of the main contributors to the energy consumption and cost during electrolysis. High density anodes have lower electrical resistivity. Therefore, a small improvement in density as well as electrical conductivity will improve the efficiency and economy of the operation.

It is important to reduce the carbon consumption during electrolysis from both economical and environmental aspects. Various reactions which consume additional carbon take place in the cell. The three main consumption reactions other than electrolytic

consumption are air burn, formation of CO, and selective oxidation which also causes dusting. Air burn takes place near the top of the anode and produces CO_2 (air reactivity). Due to reactivity imbalance between coke and pitch, selective oxidation takes place which could lead to dustingl. In addition, CO_2 produced during electrolysis at the anode/electrolyte interface can react with anode carbon resulting in CO formation (CO_2 reactivity). If the anode is dense and less porous, the reaction takes place only on the surface of the anode. If an anode is porous, CO_2 gas can penetrate through the pores of the anode resulting in further reaction inside as well.

In order to produce high quality carbon anodes, it is required to investigate the various aspects of anode manufacturing process (kneader performance, temperature distribution in baking furnace, vibro compactors and compaction times), to improve the dry aggregate recipe, and to develop a method (ANN model) that helps to determine possible recipes for better quality anodes.

1.3 Objectives

The general objective of this project is to study the effects of coke type and coke properties (particle size distribution, porosity, bulk density, crystalline structure, chemical composition, particle shape) on anode properties (density, specific electrical resistance, CO_2/air reactivity, and mechanical properties). In addition, this study also aims to develop a recipe for the production of high density, low electrical resistivity as well as low air/CO_2 reactivity anodes.

The specific objectives are:

1. To carry out a detailed literature review.

2. To study the effect of coke properties such as crystalline length, coke granulometry (size and shape), bulk density on anode properties, especially density, specific electrical resistivity, air/CO_2 reactivity, and mechanical properties.

a) The effect of coke granulometry on anode properties: The aim of this part is to comprehend the effect of medium and fine particles as well as recycled butt materials on the green anode density as well as baked anode density, specific electrical resistivity, air/CO_2 reactivity, and mechanical properties.

b) To study the effect of under-calcined coke on anode air/CO_2 reactivity and dusting. Also, to study the combined effect of crystalline length, baking temperature, and sulfur content of the coke on air/CO_2 reactivity and dusting of anode.

3. To study the wetting of different types of coke (cokes with different crystallinity, cokes from different suppliers, cokes with different S content, shot coke, etc.) with different pitches at different temperatures. This identifies the coke and pitch pairs suitable for anode production. The measurement of the wettability of a coke by a pitch gives also a good idea of optimum mixing conditions.

4. To characterize industrial anodes and compare their properties with those produced at UQAC so that the recipe developed at UQAC could be transferred to the industry:

a) To develop a reliable optical method to quantify pitch and pores in green and baked anodes.

b) To investigate the effect of different production parameters on the distribution of pitch in green and baked anodes.

c) To develop an ANN (Artificial Neural Network) model in order to understand the influence of process parameters and anode properties on anode CO_2 reactivity.

5. To develop a method to extract pitch from a paste to evaluate the performance of an industrial kneader. This practice will help detect the changes in coke granulometry during kneading.

1.4 Scope

In this project, a holistic study of the type and characteristics of coke and its impact on anode properties has been undertaken. The project consists of studies at both microscopic and macroscopic levels to find the relation between coke characteristics and anode properties.

This thesis consists of seven chapters. Following the introduction given in Chapter 1, detailed literature review is discussed in Chapter 2, where a brief background is given on coke and carbon anodes. The methodology used in this project is given in Chapter 3. In Chapter 4, detailed studies on the wetting characteristic of a variety of cokes and pitches are presented. This chapter consists of four major subdivisions. In the first subdivision, the results on the wettability of petroleum cokes from different suppliers by coal tar pitch are given. In the following two subdivisions, the influence of coke crystallinity on wetting is

explained based on the experimental results and the wetting behaviour of recycled butts is compared to that of calcined coke. In the last subsection, two different statistical methods are used to identify the effect of impurities and surface compositions of raw materials on wettability, and the results are presented. It is important to identify the best coke/pitch pairs as well as to have an idea on the optimal mixing conditions to be used during anode preparation. Anode properties are closely related to coke properties, and factors affecting coke properties also affect anode properties. It is essential to identify the chemical functionality of the petroleum coke as it can interact with pitch chemically leading to better bonding. It is also important to identify the type of interaction (physical or chemical) taking place between coke and pitch, which helps identify the suitable coke/pitch combinations during anode production. A large number of analysis methods to study coke-pitch interactions including wetting were used. Each method gives complementary information. The effect of coke crystallinity on wetting is the subject of the subsequent subdivision.

The characterization of laboratory made anodes produced with different recipes using cokes with different crystallinity is the subject of Chapter 5. This chapter is also divided in two subsections, starting with the development of new anode recipes and the characterization of anodes produced from different recipes along with the development of an ANN model for predicting the densities of green anodes made of different recipes. In order to develop a recipe for high quality carbon anodes (high density, low electrical resistivity, low reactivity), the effect of coke granulometry and particle shape during the anode manufacturing process needs to be investigated. Coke granulometry is directly related to the mechanical and physical properties of anodes. In addition, an ANN model,

which can predict green density of anodes based on their dry aggregate density, was developed. Also, this macroscopic-level investigation is linked intimately with the above microscopic-level study on coke-pitch interaction. This chapter ends with the presentation of the results of the study on air and CO_2 reactivity of anodes produced from coke with different crystalline lengths and sulfur contents, and baked at two different temperatures. Use of under-calcined coke is getting a lot of interest according to research results recently published on aluminum production as it seems to reduce the overall reactivity of anode in the electrolytic cell and thus total anode consumption. This is a relatively new topic and some publications on this topic are contradictory. The effect of the under-calcination of coke is also dependent on the baking conditions used in the plants. This study was aimed at understanding fundamentally the effect of the degree of coke calcination combined with sulfur content and baking temperatures on anode properties. Under-calcined coke can be substituted partially or fully to produce anodes with lower reactivity. This will reduce the CO_2 emissions as well. Hence, a comprehensive study was undertaken to determine the impact of the under-calcination of coke, baking temperature, and sulfur content on anode performance.

Chapter 6 is mostly focuses on the characterization of industrial anodes and the influence of process parameters and raw materials on anode properties. In the first part of this chapter, the results of pitch distributions in green and baked anodes, which were measured using an image analysis technique developed during the study by the UQAC/AAI Chaire, are presented. A statistical study was conducted for a better understanding of the influence of process parameters, equipment, and raw materials used. In the following

subsection in this chapter, an ANN model, which was developed to understand the influence of anode properties and process parameters on anode CO_2 reactivity, is explained and results are presented. Industrial kneader performance is the subject of the last part of Chapter 6 where a rapid, inexpensive, and environmentally viable pitch extraction method was introduced which can be used to monitor the distribution of size fractions in green anodes. This part of study would help understand the problems regarding the production of anodes at industrial scale. Finally, in the last chapter, the conclusions and recommendations are given.

This thesis gives an overview of the project and the methodology used and summarizes the available literature related to the above studies in order to demonstrate that this work is a step forward in the process of carbon anode manufacturing.

1.5 Originality

The originality of this project is , in general, its comprehensiveness in using a systematic approach starting with a study of coke-pitch interactions at the microscopic level, then investigating anode fabrication under different conditions for different types of cokes of interest, and finally correlating anode properties with all important coke characteristics and properties as well as with anode fabrication conditions. This will allow the production of high quality anodes with desired properties.

A new anode recipe, which resulted in improved anode properties, was proposed based on the predictions of the developed ANN model. The recipe was tested and validated in the

laboratory. This recipe has a good potential for application in the plant. The approach used which involves the utilization of an ANN model is highly original.

A detailed wettability study with a number of cokes and pitches was carried out under the same conditions. The effect of particle shape and the presence of butts on the wettability of coke by pitch were studied. In the literature, there are different studies carried out under different conditions which make their comparison difficult. The current study covers many aspects including the structure of cokes and chemistry of pitch and coke surfaces which explain the wetting behavior observed. This is also an original scientific contribution.

In the literature, there are studies on the effect of Lc, baking temperature, and the coke sulfur content on anode properties. However, no study was found on the investigation of the effect of these three parameters together under the same conditions as it is done during this study.

Another originality of this study is the investigation of pitch redistribution during the cooling of green anodes. To our knowledge, there is no similar study.

During mixing, the coarse particles may break, which changes the anode recipe and, consequently, the anode properties. The available method for testing the particle size distribution in paste is expensive and long and uses toxic solvents. An inexpensive, quick, and environmentally-friendly method was developed during this study, which is also original.

Usually, CO_2 reactivity and dusting is measured using the ASTM standard, which is a seven-hour test. It is difficult to understand what happens in the plant with such a short test. During this study, 21-hour CO_2 and dusting tests were carried out to gain better

understanding of the CO_2 reactivity, especially, the dusting phenomenon during electrolysis and the influence of different operational parameters affecting them. This has not been done before.

CHAPTER 2

LITERATURE REVIEW

This section summarizes the information available based on the published literature on the different properties of calcined petroleum coke, the effect of different coke properties on carbon anode properties, the influence of different raw material properties on wetting phenomena, and the effect of anode production parameters on pitch and pore distribution in carbon anodes.

2.1 Raw materials and their impact on anode quality

Raw materials (calcined petroleum coke, coal tar pitch, recycled anode butts, scrapped green and baked anodes) have a great influence on anode quality. The effect of raw materials and formulation has been considered as an essential factor for anode production [5]. Some of the raw material properties to be considered are:

1. Purity, structure, and porosity of coke [12]

2. Binder demand, wetting capability, mixing conditions (especially temperature and time)

3. Recycled material properties.

In anode manufacturing, raw materials are required in large quantity and acquired from different sources which might have different properties. This may cause homogeneity problem. Also the impurity level of petroleum coke has been increasing which directly affects the mechanical and physical properties of anodes. In addition, it has been observed that there is a change in QI (quinoline insolubles) content and softening point of the pitches

[5]. The publications available in the literature on this specific topic of interest of the current project are summarized below.

2.1.1 Petroleum coke

Coke quality is dependent on the coke production technology. The chemical and structural properties of the green coke are influenced by coking conditions. Physical and mechanical properties of green cokes are controlled by coke microstructure and volatile matter. Coke calcination removes the moisture content and volatile combustible matter and modifies the coke structure [13].

Green petroleum coke is produced as a by-product of petroleum refining. It is produced by delayed coking or by fluid coking. Petroleum coke has a weak amorphous structure. In green coke, the pores of the matrix are filled with a hardened residuum remaining from the coker feed [5, 14, 15]. Cokes obtained from high asphaltenes feedstock contain higher concentrations of sulfur and metals than cokes produced from feedstock which have high aromatic content [16, 17]. Most of the sulfur in coke exists as organic sulfur bound to the carbon matrix [14]. Other forms of sulfur found in coke include sulphates and pyritic sulfur, but these rarely make up more than 0.02% of the total sulfur in coke [14]. Metals, mainly vanadium and nickel, come from the asphaltenes fraction, and calcium and sodium from desalting process. Some metals are present in coke; but, they are not chemically bonded thus become part of the ash and particulates [5]. Volatile matter content, trace elements, density, and granulometry are the major parameters which characterize green cokes [18]. Calcination of coke is a heat treatment process for green coke up to a

temperature of approximately 1150-1250°C. Before using it as anode raw material, green coke is calcined for numerous reasons such as increasing C/H ratio, grain strength, thermal conductivity, and purity, and reducing electrical resistivity, air reactivity, and shrinkage during the baking of anode [19]. Calcination of coke removes the moisture and the volatile matter (hydrogen, methane, tar) to avoid cracking due to grain shrinkage during the baking of the carbon anode and also to ensure the access of binder pitch to its pores during mixing [5]. Cokes from different sources have different volatile content, microstructure, and impurity level; and it is necessary to calcine each coke differently to get the optimum quality for anode-grade coke [12, 18]. Identical green cokes can be calcined under identical conditions, and their various blends can also be calcined under similar conditions [18]. Rotary kiln and rotary hearth are the types of calciner used frequently for green coke calcination process. Processing techniques have a great influence on the mechanical and structural (L_c) properties of the calcined coke [20-22].

Structurally, sponge coke is preferred for anode production because it has a combination of low impurity levels, low air and CO_2 reactivity, a moderate coefficient of thermal expansion (CTE), good density and enough open porosity to allow good interlocking and bonding with a binder pitch. The sponge coke structure is intermediate between the extremes of needle coke and highly isotropic coke. Shot coke is the most isotropic form of coke. Cokes and their micrographs showing their typical structures are given in Figure 2.1. If used in large percentages in the aggregate, shot coke can also cause mechanical strength problems due to the lack of open macro-porosity and inability of pitch to penetrate the fine porosity to create coke-pitch bridges [23, 24].

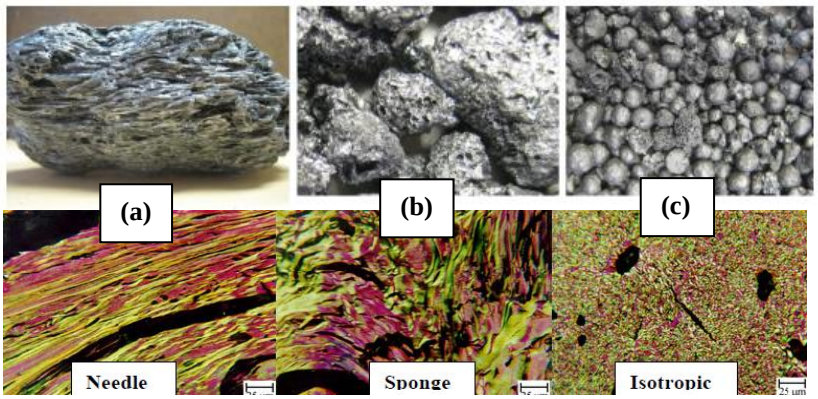

Figure 2.1 Physical structure (by digital camera) and optical micrographs of different kinds of coke: (a) needle coke (b) sponge coke and (c) shot coke [23, 25]

Optical and scanning electron microscopes are useful tools to study coke morphology. During the morphological study with optical microscopy, the material often exhibits optical anisotropy. When coke samples are observed under polarized light, the coke surface looks like a collection of units of varying sizes and colors. This arises due to interaction between the structure and the incident light. The different interfaces between colors probably appear from the grain boundaries [26, 27]. SEM (Scanning Electron Microscopy) can be used as a quick method to examine the coke morphology as it can provide information on the texture of unpolished samples. Detailed structural analysis can be done with SEM because it has large depth of focus, which cannot be done with optical microscope due to its small focus depth [26, 28]. Petroleum coke is composed of mosaic/granular structure, lamella, termed flat or intermediate structure [26, 28]. In 2005, Neyrey *et al.* [29] studied the effects of coke structure (mostly isotropic coke) on anode properties where this coke was added in varying quantities in the blend and reported that it influenced the coefficient of thermal expansion, reactivity, and density.

2.1.1.1 Effect of calcination on different coke properties

Based on earlier discussions, a wide range of publications are devoted to the experimental work aimed at understanding the effect of calcination on different coke properties which is relevant to anode properties.

Numerous researchers reported a clear decrease in electrical resistivity of coke with increasing calcination temperature [22, 30-32]. The specific electrical resistivity of anode-grade calcined coke is around 1000 μΩ·m [33].

Calcination also has an effect on bulk density and real density of coke particles. Calcined coke has a bulk density in the order of 0.8-0.9 g/cm^3. Belitskus (1991) [22] has measured the vibrated bulk densities (VBD) of three different cokes calcined at three different temperatures and have found that coke VBD increases with increasing calcination temperature except at intermediate temperatures.

Calcination temperature and heating rate influence the porosity. Fast volatile evolution due to fast heating rates increases the porosity [34, 35]. Tran and Bhatia (2007) [36] made several important observations on porosity development during calcination and reported that micropore area decreases with increasing calcination temperature. They stated that the the decrease in micro porosity is a result of the increase in the graphitization level of the coke at higher calcination temperatures. They found that laboratory calcined coke has a high graphitized structure with 60-70% organized carbon assembly. They also explained that the reactive micropore volume is the void volume between carbon crystallites and imperfections in crystallites; and due to an increase in calcination temperature, the

imperfections reduce and the crystallite growth takes place. Porosity and specific surface area of cokes increase at a certain temperature when desulfurization occurs. This is accompanied by an increase in reactivity which is directly proportional to the surface area [30, 37, 38]. Hume (1993 and 1999) [17, 34] has suggested that it is important to control the calcination conditions in order to have optimum porosity and, consequently, maintain optimum air and CO_2 reactivity. Fischer and his co-authors [12] have classified the porosities as open and closed. Open pores are interconnected at the surface and closed pores are inaccessible. Good quality coke contains more open pores (around 0.5 μm-15 μm) than closed pores [5].

The average crystalline length (L_c) is an important property for coke in aluminum industry [39]. Crystalline length is a measure of the rearrangement and alignment of the graphite planes and increases with increasing calcination temperature [11, 21, 22, 32, 39-43]. The effect of calcination temperature and soaking time is shown in Figure 2.2. It can be clearly seen that with increasing temperature, both crystalline length (Lc) and crystalline diameter increases. Lc is actually the crystallite size, but is called the crystalline length in industry; thus, the terminology ‘crystalline length’ is used in this thesis. Lc is equal to the space between two hexagonal sheets of carbon rings (C/2) multiplied by the number of such spaces (number of sheets - 1, m in Figure 2.2). The crystalline diameter is the size of the carbon ring groups in each plane.

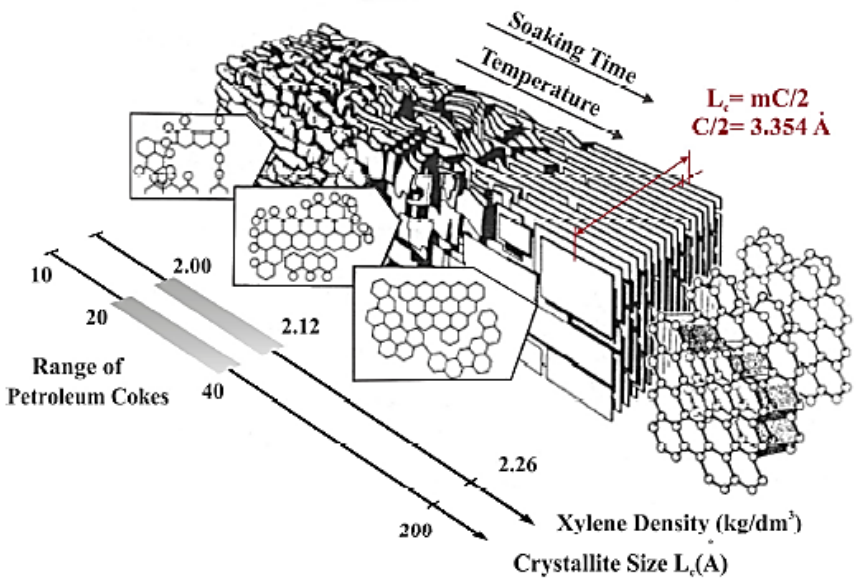

Figure 2.2 Crystalline length based on calcination temperature and soaking time [21, 44]

As reviewed by Rørvik *et al.* [39] and Tran[45], Franklin's model about the structure of disordered carbon by XRD is the most adequate and popular model for petroleum coke (Figure 2.3). This model considers that graphitizing carbons are made of hexagonal sheets of carbon rings, formed with cross-linked small individual stacks. Further heat treatment allows these stacks to merge into bigger stacks with a preferential orientation. L_c is the distance along the c-axis, perpendicular to the graphitic planes ("crystalline length") and L_a is the distance parallel to the planes ("crystalline diameter").

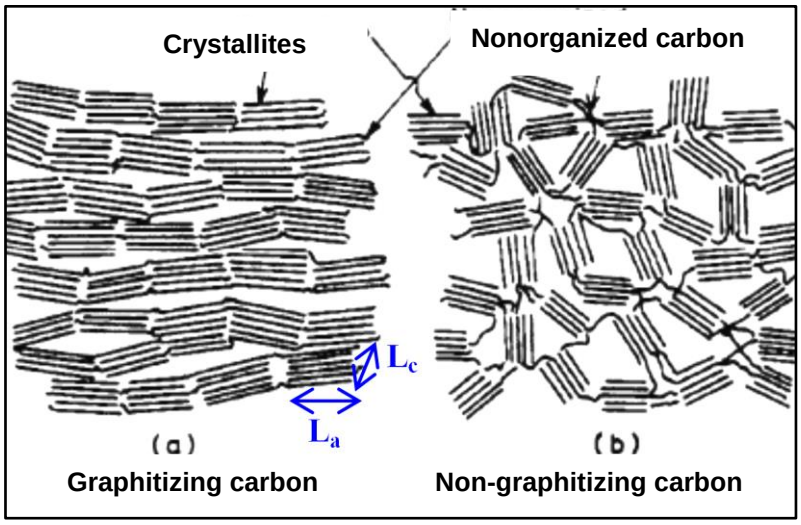

Figure 2.3 Illustration of Franklin's model of a graphitizing and non-graphitizing carbon [45]

L_c is used to characterize the petroleum coke calcination level and also to determine approximately the baking level of anodes [39]. L_c increases with increasing calcination temperature but d-spacing (spacing between the planes in the atomic lattice) shows an opposite trend to that of L_c; thus, it decreases with increasing temperature. These two properties are not affected by desulfurization induced micro-porosity and can be used to predict the calcination temperature [22, 32, 46-48]. Oberlin [49] explained that within the wide temperature range of 700-1300°C, the interlayer defects of the basic structural units of carbon reduce and crystallites start to grow larger. At highest calcination temperature, the crystallites are largest [46]. Tran and Bhatia [36] also obseved a similar trend except for the coke calcined at 1000°C after several repetitions. Coke reactivity decreases with increasing calcination level due to increase in the size of the crystallites [22]. This decrease is due to reduction of the number of highly reactive carbon atoms on the edge with respect to the carbon atoms in the crystal basal plane [30]. Lavigne *et al.* [50] also found that the

reactivity of coke decreases with increasing crystalline length and calcination temperature, probably due to an increase in lattice height and the consequent decrease in highly reactive carbon atoms in the crystal basal plane. Cokes calcined under similar condition attain the same L_c, but different levels of anisotropy; therefore, L_c is not a measure of structural differences between different cokes and their subsequent effect on coke properties [34].

L_c can be measured with an XRD (X-Ray Diffraction) instrument using two standard methods: ASTM D5187 and ISO 20203 based on the modified Scherer formula [39]. The kinetic behavior of coke reactivity is essentially the same whether the carbon is shaped into an anode or it is in granular form. The reactivity of coke is a function of the mass transport of oxygen to the surface of the particle through the gas boundary layer. The chemical reactivity of coke is also a function of the crystallinity and chemical impurities present in the particle that catalyze the oxidation reactions. Mass transport of oxygen to the available surface area of the coke particle is affected by porosity and permeability [51]. Another researcher has explained the importance of porosity on the reactivity considering the type of reaction involved. Air burn is an exothermic reaction and raises the temperature. Increase in temperature increases the reaction rate. As a result, oxidant accessibility into the coke becomes a limiting factor for air burn [17, 34]. In several publications, it is cited that air/CO_2 reactivity of coke is a function of the calcination level [12, 34, 41, 42, 50]. The reaction between coke and air occurs initially on the external surface of the particles and rapidly proceeds into the internal pore structure. The internal reaction develops gradually. Internal reactions are generally concentrated in the narrow pore size range of 1-2 nm [36]. When a certain temperature is reached, desulfurization starts, Consequently, the specific

surface area and the porosity increase, which leads to an increase in reactivity [30]. Air reactivity of calcined coke is generally measured by the ignition temperature. Cutshall and his co-authors [52] have proposed that the coke air reactivity should be measured using a thermogravimetric system at 525°C because the ignition temperature is not a true measure of air reactivity.

2.1.1.2 Effect of various calcined coke properties on anode properties

For a comprehensive view of the impact of coke properties on anode quality, a number of studies are available in the literature.

I. Coke porosity and bulk density

Coke granulometry has a direct impact on the coke porosity and impurities as well as anode strength. To produce good quality (mechanical properties, higher thermal resistance, and higher density) anodes, blending of different particle sizes is important [20, 53, 54]. Studies show that the bulk density of coke considerably improves for those samples which contain a high percentage of -4+6 mesh (3.348-4.75 mm) or -8+14 mesh (2.449-1.295 mm) particles after calcination [55]. Hulse [5] carried out a comprehensive study and proposed that higher fine (50%) and coarse (8-4mm, 20-40%) contents with a lower (10-30%) intermediate particle content tend to increase the vibrated bulk density (VBD). In a recent study, Belitskus [56] reported a similar approach with different butt contents and found an increase in VBD. VBD of discontinuous size distribution gave the highest value at 25% butt content. Coke porosity as indicated by coke bulk density has a direct impact on anode apparent density. In a different study, anodes manufactured with low porosity CPCs

(calcined petroleum cokes) showed lower anode porosity [57]. Paz *et al.* [54, 58, 59] examined the coke density and showed that the anode apparent density increases with higher VBD coke. Samanos and his coworkers [53] found that an increase of 0.12 kg/dm^3 in tapped bulk density (TBD) increased the baked anode apparent density by 0.053 kg/ dm^3. Few authors established linear relation between baked anode density and VBD [60-62]. Correspondingly, Belitskus in 1974 [61] and Khaji *et al.* in 2015 [62] stated that the relation between green and baked anode density is linear. On the contrary, Lossius and his co-workers [63] could not find an obvious correlation between green and baked anode densities and VBD/TBD of the anodes when the anodes were made with different pitch content. They proposed the following correlation between green anode densities and dry aggregate densities:

$$Dry\ Aggregate\ Density = GAD \times (100 - \%\ Pitch)/100 \quad \textbf{(2.1)}$$

II. Coke crystalline length

The average L_c is an important property of carbon materials for aluminum electrolysis. Degree of calcination influences the chemical, physical, and mechanical properties of the anode. Highly calcined coke produces less reactive anode, but poor mechanical and chemical properties. It is necessary to find the optimum baking level, defined by the maximum temperature. The minimum soaking time should be chosen as to avoid the desulfurization [31]. Different authors have shown a strong correlation between grain stability and anode flexural strength, which increases with increasing coke grain stability [64, 65]. Effect of coke calcination temperature on electrolytic consumption has been discussed in various literatures [22, 50, 53]. The results are conflicting. It is reported that an

increase in coke calcination temperature increases the anode density, but also increases the anode reactivity and decreases the thermal shock resistance at low anode baking temperatures. However, the degree of coke calcination has little effect at high baking temperatures [53]. Effect of coke crystalline length on anode reactivity is elaborately discussed in the section 2.1.1.3.

Tran and Berkovitch [66] carried out several carbon anode gasification experiments to comprehend the exact mechanism of the air and CO_2 reactivities and observed that a transformation of crystalline structure takes place in two stages: (a) initially, the removal of disorganized carbon structure; (b) then with further gasification, the reduction in the crystallite width due to preferential consumption of carbon from the edge sites of the graphene layer. As smaller crystallites gasified and merged with the neighbouring crystallites, ordered structure forms leading to increase in crystallite height. They also found that oxygen and CO_2 attack different reactive sites of the crystalline structure. Most reactive sites such as amorphous carbons and carbon atoms at aliphatic side chains react rapidly with air, but CO_2 reacts gradually with all parts of the crystalline structure, and this creates more porosity by air reactivity compared to CO_2 reactivity.

III. Coke electrical resistivity

Electrical resistivity decreases with increasing calcination temperature when the baking temperature is lower than the calcination temperature. When the baking temperature is higher than the calcination temperature, it seems that the calcination level does not affect anode resistivity [22]. Perruchoud has shown that anode specific electrical resistance is a

direct function of coke specific electrical resistance [67]. Later in 2013, Lossius and his coworkers [63] proposed that it is possible to make low electrical resistivity (ER) anodes with high specific electrical resistivity (SER) coke and the anode ER is controlled more by the presence of cracks and pores in the anode rather than by coke SER.

IV. Coke air and CO_2 reactivity

It has been reported by several researchers that coke air reactivity is not an accurate predictor of anode performance [51, 52, 68] as recycled butt has a greater impact in anode reactivity [63]. In several literatures, it is cited that it is possible to manufacture anodes with low anode air reactivity using high air reactivity coke [51, 52, 68]. Also, it is possible to manufacture anodes with high anode air reactivity using low air reactivity coke. On the other hand, Ndjom *et al.* in 2013 claimed that anode CO_2 reactivity reduces with coke CO_2 reactivity [60]. Anode air reactivity is dependent on surface and internal chemical impurities [52, 68, 69]. In 2001 Rolle *et al.* [51] proposed three reasons why the coke reactivity cannot be used in predicting the anode reactivity. Firstly, the preparation of aggregate changes the coke surface area to a higher extent. Secondly, many adsorbed or loosely bonded oxygen molecules are removed during coke grinding. Thirdly, in the green anode fabrication process, any remaining adsorbed oxygen and/or calcined coke surface area is coated with pitch. Adsorbed oxygen and calcined coke surface area is trapped with volatile hydrocarbons. Upon baking or exposure to high temperature for a long period, any available oxygen inside the pores will react during the baking process.

V. Coke granulometry

Calcined coke is available in different particle sizes which vary from a few microns to a few centimetres. The oversized particles are passed through a crusher. This coke is screened and sorted into 3-4 different size fractions. Carbon anodes contain various particle size fractions of calcined coke, recycled anode butts, green and baked rejects, and coal tar pitch. Particle size distribution is important for anode density, mechanical strength, pore size distribution, electrical resistivity, air permeability, reactivity, and even chemical composition of anodes [5, 70-73]. Quantities are taken from a recipe designed to give a dense mix; voids between the coarse particles have to be filled with medium size particles and voids between these to be filled by small size particles. In an anode, coarse coke particles and fine powders are bonded by intermolecular forces and mechanical adhesion [5].

Optimal quantities of coarse, medium, and fine fractions are required for anode formulation to obtain good anode quality [74]. Coke powders, especially the fine powders of anode formulation have a great influence on anode properties [5, 72, 73, 75]. They can fill the open porosity in the distributed system structure, which increases density. Hulse *et al.* (2000) [5, 76] was able to produce highly dense, low resistivity, and mechanically stable anodes using finer dust and optimised process conditions. Electrical resistivity clearly reduced from 94 to 62 μΩm when the amount of particles smaller than 75 μm increased from 10% to 45%. Green density does not improve with the amount of ultrafine particles while baked density is enhanced. Tensile strength, compressive strength and Young's modulus increases with finer particles and reaches their maximum value around the size

range where maximum VBD occurred (60% of ≤ 75μm). Air permeability reduced from 11 to 4 nPm with an increase in the fraction of 75 μm particles from 20 to 60%. This agrees with another publication [77] which disclosed a 2 nPm reduction of permeability with smaller fine fraction. Xiao *et al.* (2011) and Figueiredo *et al.* (2005) also suggested the considerable amount (7 wt% to 28 wt%) of very fine powder (≤ 75 μm) content can improve the anode baked density, electrical resistivity, air permeability, thermal conductivity, air and CO_2 reactivity for the same aggregate formulation, impurity content, and pitch content (17 wt%) [73, 75]. Vitchus *et al.* (2002) indicated that anode air and CO_2 reactivity decrease with a decrease in air permeability [78]. However Xiao *et al.* (2011) [75] witnessed a different trend because ultrafine powder has two effects on anode reactivity. The baked anode with 7 wt% ultrafine powder content shows the lowest CO_2 reactivity. Ultrafine powder can fill the porosity in anode to prevent air and CO_2 infiltration; but, on the other hand, powder, especially ultrafine powder, is easier to react with air and CO_2 [75, 78]. Sulaiman *et al.* (2012) [79] modified the anode recipe and reduced the fine content in recipe from 23% to 21% but ultrafine in ball mill product was increased from 62% to 71% in order to maintain overall ultrafine content in dry aggregate (14.5-15.5%) constant. The changes in recipe resulted in an increase in baked density and a decrease in electrical resistivity, and subsequently a decrease in air permeability. Tkac [80] claimed that finer dust (≤ 63 μm) amount single-handedly does not affect the properties considerably. According to his results, vacuum pressure in vibrocompactor and heating rate along with dust content affect the CO_2 and air reactivity.

In another study by Ndjom *et al.* (2013) [60], +4 mesh particle in recipe was increased from 22.5% to 25.5% which resulted in an increase in the baked density of 0.01 g/cm^3. Several researchers investigated the influence of grain size on thermal shock resistance and found that increased fine particles (≥300µm) to finer particles (between 30µm and 300µm) ratio is important [54, 81]. Fine particles also have a high specific surface area, and the specific surface area of particles increases with decreasing particle size. Higher surface area increases the pitch demand [73] in anode recipe, but the relationship between particle size and surface area is different for coke particles due to variations in shape factors [70, 73]. However, higher fines can cause nonhomogeneous distribution of pitch and cracks during baking [82]. Wharton *et al.* [70] decreased the particle size of finer particles from 150 to 70 µm, and an increase in their surface area by 1 m^2/g and 10 m^2/g, respectively, was observed. The probable reason for the difference in surface area is the exposure of closed pore volumes and resulting increase in the surface area after grinding [64]. Penetration ability and distribution of pitch were also influenced by size distribution of coke fractions. Couderc *et al.* [6] proposed that a particle size below 100 µm is too small and does not allow sufficient penetration of pitch while a particle size above 200 µm is too large to prevent the pitch infiltration. According to Cao *et al.* [83], coke dusts of ≤ 125 µm and ≤ 250 µm had similar penetration behaviour with the same pitch while penetration into ≤ 500 µm coke particles was much faster due to the larger inter-particle spaces. Therefore, the control of ultrafine fine powder (ball mill product and filter dust) is important for the stability of anode quality [75].

All particle sizes are important for anode production. Small particles increase the density, and larger particles give strength to the anode. Green apparent density and packing characteristics of coke increase as dust content increases due to the absence of porosity in the dust. In turn, coarse material is required for anode mechanical properties. The size of porosity also changes with the particle size, and this affects the bulk density. Baked anode properties such as strength and density increases by using a dust fraction with higher specific surface area. It is also found that there is no change in shrinkage during baking. Hulse [5] proposed that for good anode properties, both coarse and fine particles are essential.

2.1.1.3 Anode consumptions

Carbon reactivity is an important factor in the aluminum production industry. Most of the carbon is consumed during the cell operation but there are other losses due to excess consumption which is not economically and environmentally viable. Schematic of specific electrolytic consumption is shown in the Figure 2.4. There are four kinds of carbon consumption:

- Electrolytic Consumption
- Carboxy attack
- Airburn
- Selective oxidation (dusting, sloughing)

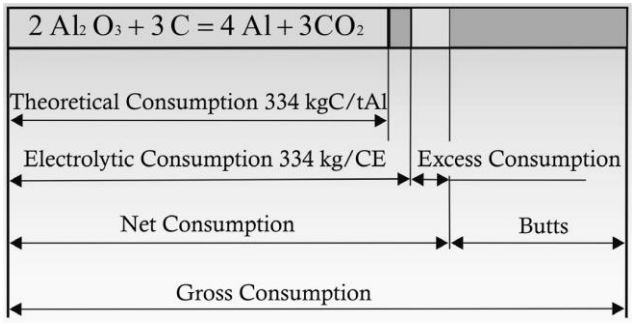

Figure 2.4 Specific anode consumption during electrolysis [84]

I. Electrolytic consumption

Carbon anode is mostly consumed in the electrolytic cell during the reduction of alumina to produce aluminum. The commonly used aluminum reduction process is the Hall-Heroult process in modern aluminum industry where carbon is used as anode material (Figure 2.5). In electrolysis, the current efficiency affects the carbon consumption; the theretical carbon consumption divided by the currect efficiency gives the electrolytic carbon consumption.

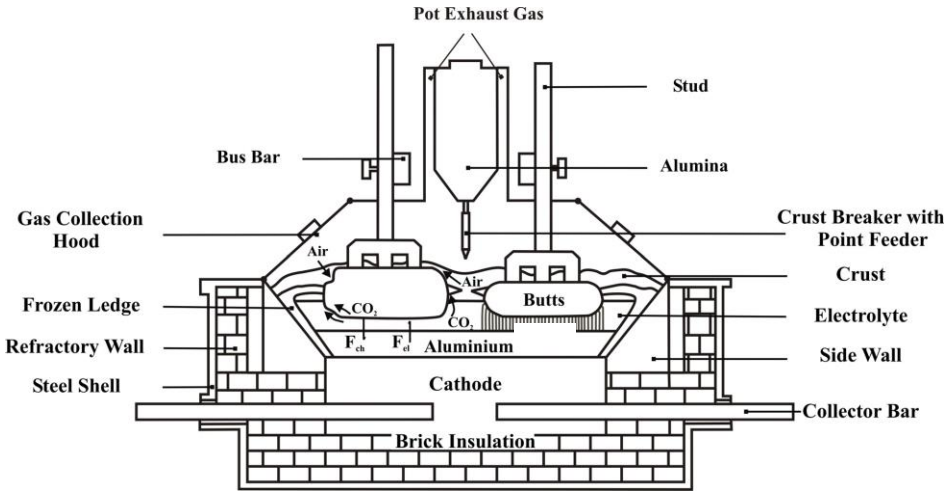

Figure 2.5 Simplified cross-section of a Hall-Heroult cell [21]

II. Carboxy attack (CO_2 reactivity)

Carbon dioxide is produced during the alumina reduction which can react with the anode carbon to produce carbon monoxide. This reaction is endothermic in nature and known as Boudouard reaction or carboxy attack. This reaction generally takes place at the bottom surface of the anode where CO_2 evolves as a result of the electrolytic reaction [17] (Figure 2.6). Carboxy reaction is represented as shown below:

$$CO_2 + C \rightarrow CO \quad \textbf{(2.2)}$$

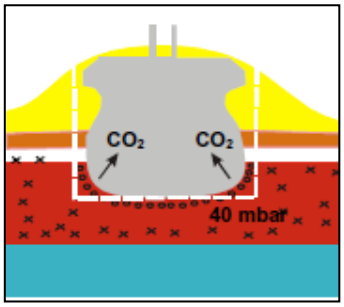

Figure 2.6 Carboxy reaction in the electrolysis cell [85]

Different impurities like sodium, calcium, sulfur have significant effect on carboxy attack. Some such as sodium and calcium act as a catalyst to accelerate the reaction [34] whereas sulfur acts as an inhibitor. It is also found in the literature that carboxy attack is affected by several factors such as raw material properties, green mix formulation, baking and bath temperature, and air permeability [86]. Carboxy attack is dependent on temperature and most favourable at high temperatures (950°C-960°C).

III. Air burn (air reactivity)

Reaction of oxygen near the top surface of the carbon anode is known as airburn. In the temperature region of 300°C to 600°C, anode carbon at the upper part and the sides of the anode is oxidized by air (Figure 2.7).

The following exothermic reaction takes place:

$$C + O_2 \rightarrow CO_2 \quad \textbf{(2.3)}$$

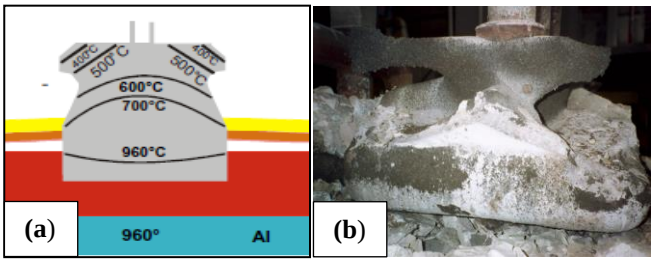

Figure 2.7 (a) Schematic representation of air burn reaction in Hall-Heroult cell [85] (b) severe air burning on anode side [21]

The most important impurities affecting air burn are vanadium, nickel, and sodium. Raw material properties, baking temperature, cover material, cell design parameters, and anode depth in the cell have great influences on the air reactivity of the anode [86].

IV. Selective oxidation (dusting)

Due to reactivity imbalance between binder pitch and anode coke, selective oxidation of the binder phase takes place. This weakens the bond structure, and the physical loss of pitch and coke occurs. This phenomenon is often called dusting. This increases the bath temperature which in turn increases the anode reactivity. Airburn and carboxy attack occurs at the binder matrix if the anode baking temperature is lower than that of the coke

calcination. Hydrostatic pressure of the bath provides the driving force for carbon dioxide to penetrate into the pores of anode, which results in internal reaction. This leads to a massive problem which is not restricted only to the anode surface [17]. Microscopic analysis of anode butts confirms that internal attack is selective, and this mostly takes place in the region of binder and coke fines [17]. Selective oxidation is an influencing factor when coke calcination temperature is significantly higher than the baking temperature [22]. A schematic representation of dusting is shown in the Figure 2.8.

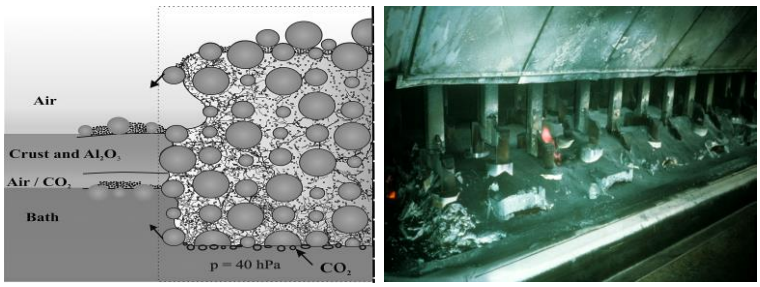

Figure 2.8 Schematical representation of dusting [21]

V. Effect of the degree of calcination on anode reactivity

In recent times, under-calcined coke has become increasingly the center of interest as it appeared in several researches that anode produced from under-calcined coke has less and homogeneous reactivity during electrolysis. This resulted in lower carbon consumption and subsequently less dusting in the electrolysis cell [10, 87]. In general, under-calcined coke has lower real density and crystalline length compared to anode grade standard calcined coke [9-11] (Figure 2.9.). Utilization of under-calcined coke also reduces the fuel consumption of the calciner. However, due to its lower density, the anodes would have to be changed more frequently increasing the operation cost.

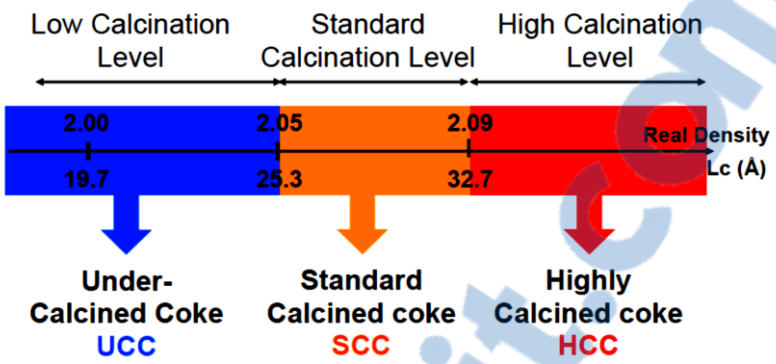

Figure 2.9 Definition of under-calcined, standard calcined, and highly calcined coke [10].

Under-calcined coke (coke calcined at low calcination temperature) decreases the anode air and CO_2 reactivity [9, 11]. This is explained with the fact that pitch is normally more reactive than the calcined coke. Therefore, it is consumed faster than coke when in contact with air or CO_2. Decreasing coke calcination temperature increases the coke reactivity. Thus, the coke and pitch reactivities become comparable. This results in a more homogeneous reactivity within the anode and significantly reduces the dusting problem (Figure 2.10) [9-11, 87]. A similar assessment has been reported earlier by Rodriguez-Mirasol and his co-authors [88] based on their research on carbon-fiber reinforced carbon composites. Additionally, Samanos and Dreyer [53] attributed the improved anode oxidation resistance to the better coke-pitch interaction between under-calcined cokes with the binder pitch.

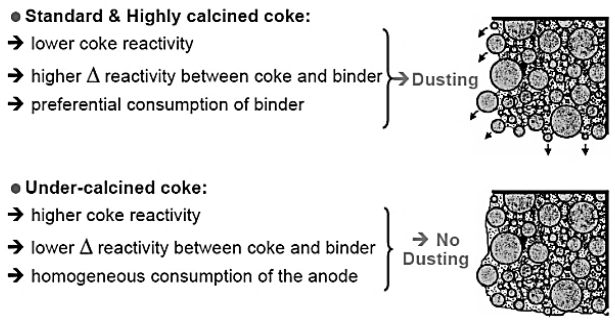

Figure 2.10 Schematic of dusting in standard and under-calcined coke [89].

There have been contradicting reports in the literature regarding effect of under-calcined coke properties on anode properties. The possible reasons could be variations in coke crystalline length, binder level, anode recipe, baking temperatures, impurity content. However, a number of publications are also available in literature about the positive influence of under-calcined coke on anode consumption. Nevertheless, it seems that this influence is dependent on the baking temperature. It is cited in different references that the effect of under-calcined coke is not significant if the baking temperature is high enough. Another study by Lhuissier *et al.* (2009) [9] has shown that baking the anodes above 1100°C virtually eliminates the advantage of using under-calcined coke in anode production on CO_2 reactivity. Similar trend has been supported by Fischer and Perruchoud [11]. Various authors stated that the use of under-calcined coke reduces the baked anode density [9, 10, 53] but the difference between baked and green anode densities are mostly compensated by higher shrinkage rate during baking and the decrease in baked density is relatively small [9, 22, 53].

The properties of anode produced from different calcined cokes studied by several researchers are summarized in Table 2.1.

Table 2.1 Summary of anode properties produced from under-calcined coke

Author(s)	Calcination temperature (°C) [Coke L_c (Å)]	Baking temperature (°C)	Baked anode density (g/cc)	Anode air reactivity	Anode CO_2 reactivity	Dust from CO_2 reactivity
Belitskus 1991[22]	23.6, 29.2, 33	950-1250	Density of anode produced from 23.6Å coke is lower than 33Å coke but higher than 29.2 Å coke. Anode density increases with increasing baking temperature for all cases	Highest for the anodes made with 23.6 Å coke and baked at 950°C	No information	No information
Samanos *et al.*, 2001 [53]	680 (15.3Å), 750(15.4Å), 940 (16.6 Å), 1080 (24Å)	700-1000	Reduced with decreasing L_c and increasing baking temperature	Reduced with decreasing L_c and at lower baking temperatures	Reduced with decreasing L_c and at lower baking temperatures	Reduced with decreasing L_c regardless of baking level
Brym *et al.*, 2009 [11]	1125 ,1270	975, 1050, 1100, 1200	No information	No information	Reduced with decreasing L_c at lower baking temperatures	Reduced with decreasing L_c and increasing baking levels (except 1200°C) They have used baking temperature of 1200°C (Figure 10 and 11
Lhuissier *et al.*, 2009 [9]	800-1000	950, 1000, 1050, 1100, 1150, 1200	Reduced with decreasing L_c and increasing baking temperature	Reduced with decreasing L_c at lower baking temperatures	Reduced with decreasing L_c at lower baking temperatures	Reduced with decreasing L_c. Constant at different baking levels
Tran *et al.*, 2009 [87]	1000, 1100, 1150, 1225, 1300 (Low sulfur coke)	1025, 1150, 1200	No information	Reduced with increasing L_c and increasing baking temperatures	Reduced with decreasing L_c irrespective of baking temperatures	No information
	1000, 1100, 1150, 1225, 1300 (High sulfur coke)	1025, 1150, 1200	No information	Increased with decreasing L_c and increasing baking temperatures	Increased with decreasing L_c and anomalous with baking temperature	No information
Sulaiman *et al.*, 2012 [10]	25.9Å, 28.4Å	1155	Reduced with decreasing L_c	Reduced with decreasing L_c	Increased with decreasing L_c	No information
Fang *et al.*, 2015[90]	800 (17Å), 900(19Å), 1000(22Å), 1100 (27Å) (Three different sulfur content coke)	Baked at same temperature	Reduced with increasing L_c (except at L_c 17Å)	Reduced with decreasing L_c (except at L_c 17Å) Increased with increasing %S	Reduced with decreasing L_c (except at L_c 17Å) Decreased with increasing %S	No information
Cahill *et al.*, [91]	No information	Baked at same temperature	Reduced with increasing L_c	No information	Reduced with decreasing L_c	Reduced with decreasing L_c

VI. Effect of coke sulfur content on anode reactivity

Changes in coke quality available for calcining in aluminium industry are being driven by a range of factors. Two important drivers are: refineries on average are running lower cost, higher sulfur, and heavier crudes which directly impact coke quality; and the significant increase in aluminium production and demand for coke are not being matched by the growth in demand for traditional quality anode-grade cokes. In general, anodes made of low sulfur coke have lower SO_2 emission, but higher CO_2 reactivity [92]. Different authors reported that CO_2 reactivity of anodes is controlled by the sulfur (S) content of the calcined petroleum coke and decreases with increasing sulfur content, but air reactivity shows completely the opposite trend [93-95]. Sorlie *et al.* (1994) [93] reported that the air reactivity of anodes was minimum with around 1.3 wt % S while the CO_2 reactivity decreased with increasing the percentage of S. Thus, they recommended an optimum sulfur content of 1.3 wt % in order to reduce air reactivity. Tran *et al.* (2009) [87] also found that the air reactivity of anode increases with increasing sulfur level but CO_2 reactivity showed completely opposite trend. Tran and his co-authors [87] also proposed a mechanism for air reactivity driven by sulfur. They explained that sulfur weakens the bond of surrounding carbons in a ring structure and lowers the activation energy and oxidation resistance. The possible reason for lower CO_2 reactivity is that sulfur inhibits the metal catalysts by interacting with them to form inactive metal-sulfur compounds. Hume *et al.* (1993) [96] has earlier explained in detail the reaction of sodium with sulfur. It is said that sulfur inhibits the catalytic behavior of sodium and prevents sodium (Na) to migrate during electrolysis. Eidet *et al.* (1997) [97] also found that sulfur causes a reduction in the effectiveness of iron

as a catalyst to the carbon-air reaction by forming iron metal sulfides. Higher sulfur cokes and anodes, therefore, have lower carboxy reactivity and less potential for dusting. Sulfur content also subdues the effect of vanadium on air and carboxy attack [98]. In literature, it has been proposed that ratio of sulfur to vanadium is important but no data was presented on the desired value of this ratio [20, 85]. In contrast, Jones *et al.* (1979) mentioned that the reactivity of anodes is controlled more by the oxidant accessible surface than by S content [95]. Increasing anode sulfur content also lowers the current efficiency [99]. Fisher (1993) [86] stated that, for high sulfur anodes, baking temperatures below thermal desulfurization are required. Once the desulfurization begins to take place at a significant rate, the carboxy reactivity of the anode begins to increase.

2.1.2 Recycled anode butt

In Hall-Héroult cells, carbon anodes are used to reduce alumina for the production of aluminium. The unused part of carbon anode is known as anode butt. Prebaked anodes consist of about 65-68% petroleum coke, 15-25% anode butts, and 13-15% coal tar pitch. [100, 101]. Because of the fact that anode butts are reused, their quality features are also as important as petroleum coke and coal tar pitch. The quality of butt essentially determines the quality of the anode produced. Poor quality of butt increases the reactivity due to their high Na content and deteriorates the mechanical properties of the anodes. Anode butts can be categorized as hard and soft butt. The quality of hard butts is similar to that of the original anodes whereas the soft butts are more severely attacked during electrolysis. Soft butts have higher porosity and permeability which in turn increases the reactivity and

decreases density and mechanical strength of anodes. Influence of butt quality on anode properties is shown in Figure 2.11. The amount of anode butts is important to anode properties. Belitskus [100] showed the increase in baked apparent density with increasing butt content up to 40%. The findings of Fischer and Perruchoud are well correlated with this result [102]. Weng and Vera [103] studied the effect of size and quantity of butt fractions. For pilot scale laboratory anodes, the baked density increased, electrical resistivity and air reactivity slightly decreased with reducing the maximum butt particle size from 38 mm to 19 mm at a constant butt fraction of 25%. However, the results for baked anode cores did not show the same trend.

INFLUENCE OF BUTT QUALITY ON ANODE PROPERTIES	Butt Categories: Hard Clean	Hard Dirty	Soft Clean	Soft Dirty	
APPARENT DENSITY	++	++	+	+	INFLUENCE
MECHANICAL STRENGTH	++	++	+	+	++ *Very Positive*
PERMEABILITY	++	++	×	×	+ *Positive*
CO_2 REACTIVITY RESIDUE	×	–	–	– –	× *Neutral*
AIR REACTIVITY RESIDUE	×	–	– –	– – –	– *Negetive*
INGNITION TEMPERATURE	×	–	– –	– – –	– – *Very Negetive*
PURITY	–	– –	–	– –	– – – *Catastrophic*

Figure 2.11 Effect of butt properties on anode properties [102]

2.1.3 Coal tar pitch

Coal tar pitch is obtained as a by-product of coal pyrolysis and is a complex mixture of hydrocarbon compounds. It is mainly used as a binder in the production of carbon electrodes. During subsequent heat treatment, pitch carbonizes and forms a coke that bridges the filler particles [11]. Typical properties of anode-grade coal tar pitch is reviewed

by Suriyapraphadilok [104] from the book written by Grjotheim and Welch (1988) [105] (listed in Table 2.2). Detailed pitch properties are discussed in the section 2.2.2.

Table 2.2 Typical anode-grade coal tar pitch properties [104, 105]

Properties	
Softening Point (°C)	107-113
Quinoline Insoluble (wt%)	5-20
Toluene Insoluble (wt%)	16-35
β Resin (wt%)	11-22
Mesophase (wt%)	0-10
Coking Value	54-61
Ash (wt%)	0.1-0.5
Distillate at 360°C (wt%)	0.5-5.0
Specific Gravity (25/25°C)	1.31
Flash Point (°C)	-250
Viscosity (cps)	
140 °C	7,000
160 °C	1,600
180 °C	400
Carbon (wt%)	~ 92
Hydrogen (wt%)	~ 1.5
Sulfur (wt%)	~ 0.6
Nitrogen (wt%)	~ 1
Oxygen (wt%)	~ 2
Sodium (ppm)	20 - < 500
Potassium (ppm)	2-100
Silicon (ppm)	100-500
Iron (ppm)	50-500
Calcium (ppm)	10-250
Lead (ppm)	40-500
Specific Heat (cal g^{-1} s^{-1}°C^{-1})	
25 °C	0.27 (1.13 kJ $kg^{-1}K^{-1}$)
100 °C	0.34 (1.42 kJ $kg^{-1}K^{-1}$)
Surface Tension (dyne cm^{-1})	
160 °C	~ 44 (0.146 W m^{-1} s^{-1} K^{-1})
Thermal Conductivity (cal cm^{-2} s^{-1}°C^{-1})	~ 0.00035 (4.184× 10^{2} W m^{-1} s^{-1} $K^{-1)}$

2.2 Wetting Study

The wetting behavior, which depends on the surface properties of coke and pitch, help assess the adhesion of pitch and the suitability of coke-pitch pairs which are necessary to make good quality anodes. The wettability of calcined coke by a molten pitch drop can be characterized with the contact angle formed between the molten pitch drop and the coke

bed. The first widely accepted correlation between interfacial tension and contact angle for a liquid drop on a solid surface is expressed by the Young Equation, which was proposed by Young in 1805 [106]:

$$\gamma_{SV} = \gamma_{SL} + \gamma_{LV} \cos\theta \qquad \textbf{(2.4)}$$

where γ_{SV} is the interfacial tension of the solid-vapor interface, γ_{SL} is the interfacial tension of the solid-liquid interface, γ_{LV} is the interfacial tension of the liquid-vapor interface, and θ is the contact angle. γ_{LV} is also known as surface tension. These phases meet at a point called the triple point. The force balance given by the Young Equation [106] at the triple point (Equation 2.4) determines the wettability of the solid phase by the liquid phase in the presence of vapor phase. Figure 2.12 shows the contact angle and the wettability of liquid/solid systems.

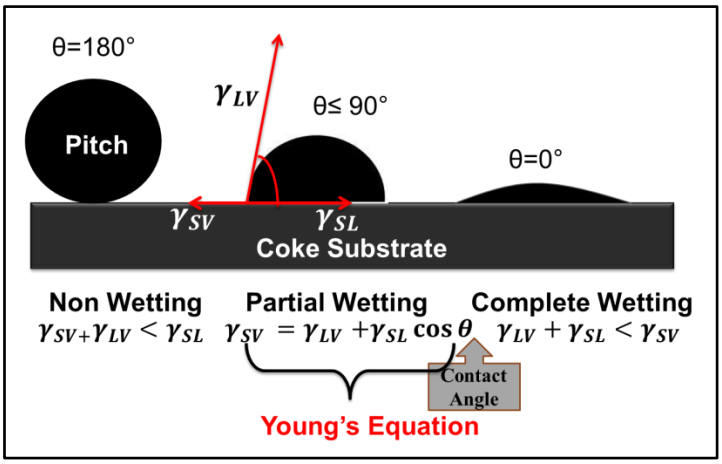

Figure 2.12 Schematic representation of wetting

If θ > 90°, the liquid-solid system is said to be non-wetting; and if θ < 90°, the system is considered wetting (Figure 2.12). The wettability of cokes by pitches is one of the main interests of this study. The sessile-drop technique which is a goniometric method is a

widely used method for characterizing the wettability. The work of adhesion (W_a) of coke-pitch systems is calculated as a function of the contact angle (θ) and the surface tension (γ_{LV}) using the following Equation [106]:-

$$W_a = \gamma_{LV}(1 + \cos\theta) \quad \textbf{(2.5)}$$

Since the work of adhesion is the work per unit area of interface that must be performed to separate reversibly the two phases, it is a measure of the strength of binding between the phases. The condition for perfect wetting is given by $W_a = 2\gamma_{LV}$. This means that the adhesion energy between the solid (coke) and the liquid (pitch) should be equal to twice the surface tension of the liquid.

Different chemical and physical properties of raw materials (such as coke porosity and bulk density, surface chemical composition, pitch surface tension and viscosity) can influence the wetting behavior. Good wettability of coke by pitch directly affects the final anode properties. Good wetting indicates the penetration of binder pitch into the pores and inter particle voids, which directly affects the density and flexural strength of the anodes. Adequate distribution of binder pitch among particles and into the pores of the particles provides homogeneous anode properties. For optimum pitch content, the particles should be covered with a thin layer of pitch. There shouldn't be space between the pitch layer and particle surface (good wettability). If the pitch is less than optimum, it is said that the anode is under-pitched. If the pitch layer is too thick, which separates the particles and weakens the mechanical properties, the anode is overpitched (Figure 2.13).

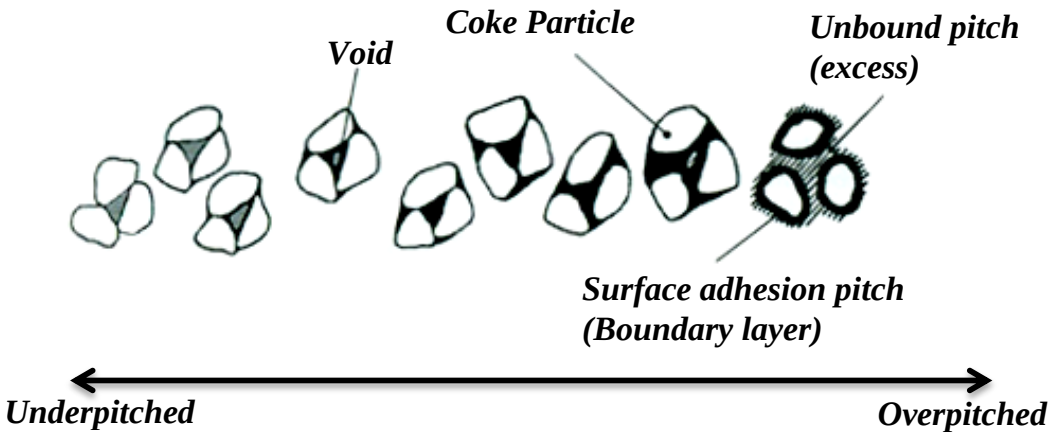

Figure 2.13 Binder–aggregate system [5]

Several investigations are carried out to determine the wettability of coke by pitch using the sessile-drop analysis method. The sessile-drop technique involves placing a drop of liquid pitch on a coke bed or positioning a solid pitch sample on a coke bed and heating the furnace to the desired temperature under inert gas atmosphere. The change of contact angle with time is recorded with a video camera for further analysis [6, 8, 107-110].

Coke/pitch wetting is important because it provides information about the interactions between them during the mixing stage of anode manufacturing. Wettability of coke by pitch is a function of temperature and time as reported in the literature by different researchers. With increasing time and temperature, wetting is improved. The summary of wetting studies using various cokes and pitches conducted by numerous researchers are tabulated in Table 2.3.

Table 2.3 Summary of pitch-coke wettability studies by various researchers

Substrate (s)	Binder(s)	Test	Controlling Parameters	Measuring Parameter(s)	Authors
Artificial graphite; petroleum coke; calcined thermoanthracite	Coal tar pitch and oleic acid as a surface dopant	Penetration test (molded pitch drop)	Temperature	Contact angle	Dmitrieva *et al.*, 1967 [111]
Graphite-grade cokes; pitch-bond carbon black cokes	Coal tar pitch	Penetration test	Temperature	Contact angle	Greenhalgh and Moyse, 1970 [112]
Different types of petroleum cokes	Coal tar pitch	Elongation test	Types of cokes	Elongation	Dell *et al.*, 1970 [113]
Coke (particle size of 147-235 μm)	Coal tar pitch	Penetration test	Size and density of α-resin; β-resin	Complete wetting temperature	Pinoir and and Hyvernat, 1980[114]
Petroleum coke (particle size of 100-150 μm)	Coal tar pitch	Penetration test	Temperature	Geometry and contact angle	Ehrburger and Lahaye, 1984 [115]
Petroleum coke	Coal tar pitch	Penetration test	Temperature, Size and density of α-resin, ΔTg	Length of the tail T_e-T_f*	Saint-Romain *et al.*, 1986 [116]
Different degree of calcined petroleum cokes	Coal tar pitch	Penetration test	Degree of calcinations	Geometry and contact angle	Heintz, 1986 [117]
Petroleum Coke (particle size of 100-150 μm)	Coal tar and petroleum pitches	Penetration test	Size and density of α-resin; β resin	Length of the tail T_e-T_f*	Saint-Romain *et al.*, 1987 [118]
Coke, graphite, glass beads and other materials (200x400 mesh size)	Coal tar pitch and other organic liquids	Capillary rise	Types of binders and fillers	Surface tension	Wolfrom, 2002 [119]
Calcined petroleum coke	Coal tar pitch	Sessile drop	Temperature	Geometry and contact angle	Mirchi *et al.*, 2002 [107]
Calcined petroleum coke (-125μm, -250 μm, or -500 μm)	Coal tar pitch	Penetration test (molded pitch drop)	Temperature, Time, Particle size of coke	Contact angle	Cao *et al.*, 2002 [83]
Petroleum coke, recycled anode butts	Coal tar pitch	Agglomeration test	Coke, recycled anode butts	Ratio of weight of agglomerated coke held by pitch and initial weight of pitch	Adams, 2004 [7]

Substrate (s)	Binder(s)	Test	Controlling Parameters	Measuring Parameter(s)	Authors
Petroleum coke, recycled anode butts	Coal tar pitch	Penetration of pitch into the pores	Coke, recycled anode butts	Volume of pitch penetrated into pores	Adams, 2004 [7]
Calcined petroleum coke (particle size of -100 to -125 μm)	Coal tar and petroleum pitches	Spreading drop test	Completely wetting temperature	Geometry and contact angle	Rocha *et al.*, 2005 [8]
Calcined petroleum coke (particle size of -100 to -125 μm)	Petroleum pitch with three additives	Spreading drop test	Temperature, Heating rate	Geometry and contact angle	Rocha *et al.*, 2005 [120]
Thermally treated petroleum pitch (<0.4 mm particles)	Coal tar and petroleum pitches	Spreading drop test	Degree of heat treatment of petroleum pitch	Geometry and contact angle	Rocha *et al.*, 2007 [108]
Petroleum coke, carbon black, graphite, magnesia, treated alumina, corundum	Coal tar and petroleum pitches, modified petroleum pitch	Spreading drop test	Completely wetting temperature	Geometry and contact angle	Rocha *et al.*, 2010 [109]

*Note:

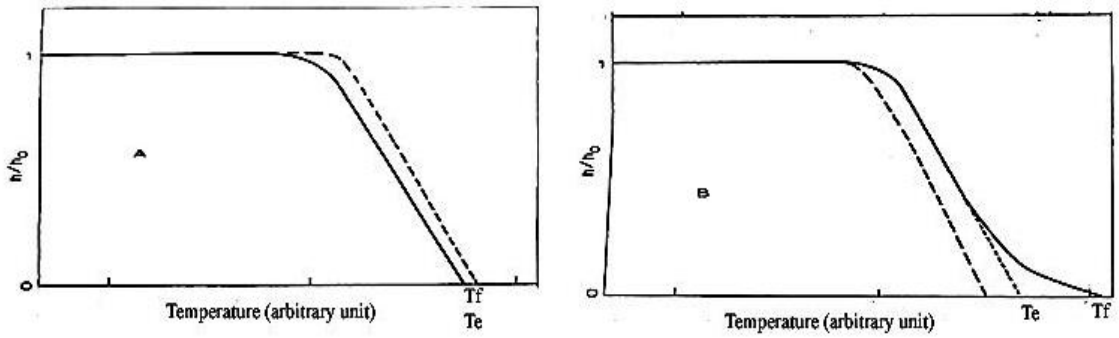

T_f and T_e are defined as the temperature at the end of the penetration and the extrapolated temperature from the linear part of the curve respectively. h/h_0 is the relative droplet height.

2.2.1. Role of petroleum coke in wetting

Petroleum coke is one of the major raw materials used for production of carbon anodes, which contains 65-75% fresh petroleum coke. The ability of pitch to wet the coke surface

depends mainly on the pitch and coke chemistry as well as coke porosity. Coke and pitch should have complimentary surface functional groups for better wetting. It is reported in the literature that petroleum coke surface contains mostly oxygen, nitrogen, and sulfur (other than carbon) [19, 121]. Impurities found on the surfaces of cokes include sodium, potassium, silicon, iron, nickel, vanadium, etc. Effect of different coke properties on wetting is discussed below.

2.2.1.1 Porosity and bulk density

Coke structure and porosity play a key role in coke wettability. High coke wettability might signify high porosity. Penetration of coal tar pitches into petroleum coke is dependent on the mixing conditions and pore size for large coke particles. At lower mixing temperatures, high pitch viscosity creates a hindrance to penetration of binder material through the pores of coke [5]. Wettability might be determined by the largest pores, but micro-porosity is considered as important as macro-porosity and plays an important role in the kinetics of penetration. Change of 0.1 kg/dm^3 in coke bulk density changes the binder demand 1.25% due to change in available surface area in the aggregate structure. It is also found in the literature that the relation between coke bulk density and optimum binder level is not considerable unless there is a significant difference between coke densities [40]. Vanvoren (1987) reported that higher binder demand does not necessarily signify higher penetration through pores. It might be simply due to an increase in the pitch film thickness on coke particles. This might also lead to overpitching [122]. The wettability test can also give an indication of the effect of pore structure on coke/pitch interactions [113].

Microstructural analysis revealed that under-calcined coke is wetted more by the pitch and coke particles are well bonded with the surrounding pitch [11].

2.2.1.2 Particle shape factor

Powder packing and bulk density, porosity, permeability, cohesion, flowability, attrition, interaction of solids with fluids can be affected by particle shape which is an important physical property of powders, but the effect of particle shape on wetting is not studied extensively. In literature, it was found that naturally occurring particles have a higher VBD due to closer packing properties than crushed particles with the same size [123]. Shape parameters are generally used to express some particle characteristics, such as elongation, compactness, roughness, roundness, aspect ratio, etc. The different features of the particles could be associated with the packing behavior of the particles. The compactness is a ratio of area over convex perimeter. The roughness of the particle is a measure of the unevenness or irregularity of a particle surface. Both parameters are directly related to flow performance of particles during packing [74]. Aspect ratio is the ratio of the longest dimension to the shortest dimension of the particle. Circular particle has lower aspect ratio and higher values for compactness and roundness. Lower values of aspect ratio, lower porosity, and higher values of compactness, roughness, sphericity, and roundness help improve the vibrated bulk density of the coke particles [124]. The roundness of the particle is a measure of the roundness of the particle edges and sphericity is the measure of how spherical an object is. The difference between sphericity and roundness is illustrated in Figure 2.14.

Definitions of all the shape factors are given in the Table 2.4. It is cited in the literature that more spherical particles are expected to display better packing behavior and higher bulk density values than plate like or needle like particles [124].

Table 2.4 Particle shape measured by using optical microscope

Shape factor	Definition
Sphericity	$(\frac{4 \times \pi \times Area}{perimeter^2})$ It is the measure of the compactness of the particle. Sphericity of a spherical particle is 1.
Roughness	$\frac{Convex\ Perimeter}{Perimeter}$ The roughness of the particle is a measure of the unevenness or irregularity of a particle.
Roundness	$\frac{4 \times \pi \times Particle\ Area}{(diameter)^2}$ The roundness of the particle is a measure of the roundness of the particle edges.
Compactness	$\frac{4 \times \pi \times Area}{(convex\ perimeter)^2}$
Aspect ratio	longest dimension/shortest dimension

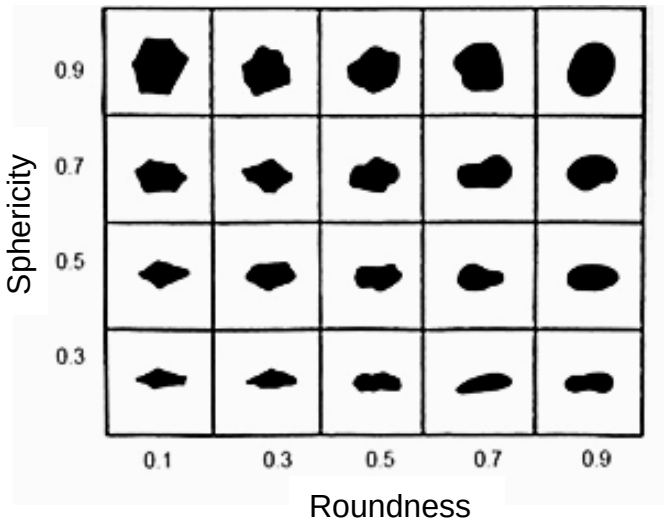

Figure 2.14 Illustration of difference between sphericity and roundness of particles [125].

2.2.1.3 Coke surface chemistry

A wide range of studies are reported in literature on the petroleum coke surface chemistry. Lahaye *et al.* (1985) studied the correlation between surface chemical functional groups of calcined coke and the wettability of coke by coal-tar pitch. He found that coke/pitch interactions depend on the hydrogen bonding between the raw materials; and above a critical value, surface chemical functional group content does not influence coke/pitch wettability [110]. In contrast, Suriyapraphadilok (2004) mentioned in his thesis that calcined coke surface contains a limited amount of hydrogen (less than 0.1 wt.%) and oxygen, thus the possibility of forming the hydrogen bonds with pitch is less [104, 126]. Adams *et al.* (2004) found that the carboxyl, lactonic, and phenolic functional groups are predominant in sponge (calcined) coke surface by performing a selective neutralization technique using different bases [71]. The surface oxygen groups are by far the most significant surface functional groups in terms of influencing most the physico-chemical properties such as wetting, ionic and covalent bonding to other groups [127]. A schematic representation of surface oxygen functional groups that are believed to be present on the carbon surface are given in Figure 2.15.

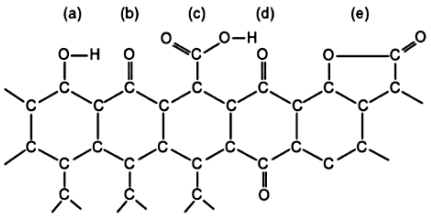

Figure 2.15 Schematic representation of the oxygen functional groups on the carbon surface (a) hydroxyl (b) carbonyl (c) carboxyl (d) quinone and (e) lactone [127]

The inverse gas chromatography (IGC) experiments were also conducted by Adam [7] to determine the dispersive and acid-base surface tensions using alkenes, halogenated and other solvents as a mobile phase, and he concluded that the dispersive component is found to be the greatest contributor to the sponge calcined coke surface. Adams' conclusion is consistent with a separate study by Wolfrom (2002). Wolfrom [7, 71, 119] calculated the dispersive and acid-base surface tensions of the sponge calcined cokes using capillary rise technique. This study showed that the dispersive component pre-dominates the overall surface tension of the coke materials.

Different authors studied the chemical structures of green petroleum cokes by different analytical methods which include NMR (Nuclear magnetic resonance spectroscopy), FT-IR (Fourier transform infrared spectroscopy) and XPS (X-ray photoelectron spectroscopy) for different reasons. No significant literature is found on the utilisation of FT-IR on calcined coke as calcined coke has lower absorption characteristic to baseline levels (no absorption of light) [128]. The presence of aromatic hydrocarbons in petroleum cokes may be responsible for the chemical activity during the coking process. As reported by Michel *et al.* (1994) and Pruski *et al.* (1994), green petroleum cokes are composed of polynuclear aromatic hydrogen-deficient structures with few alkyl side chains as substituents and naphthenic groups such as napthalene, phenanthrene, anthracene, try-phynylene, benzo-pyrene, coronene, pyrene etc. [129, 130]. Jiang *et al.* (2008) performed FT-IR studies on green petroleum coke and mentioned that the surface functional groups such as C–OH, COOH and some alkyl groups of petroleum cokes play a key role in the chemical activation

process [131]. The available literatures on FT-IR peaks of petroleum coke is listed in Table 2.5.

Table 2.5 List of functional groups in different green petroleum cokes from FT-IR study

No	Wavenumber (cm^{-1})	Functional groups
1	750	Ortho-substitution of the aromatic ring [128, 132-134]
2	830	Aromatic CH out-of-plane vibration frequencies [128, 132]
3	1126	Esters C-O [131, 132]
4	1250	C-O-C Vibrations in esters or ether [131, 135]
5	1431,1442,1600	C=C Stretching vibrations [128, 135, 136]
6	1505	C=C Stretching vibrations [136]
7	1720,1700,1654,1648	C=O [133, 136]
8	2701	Aliphatic C-H [134, 136]
9	2800-2980	Aliphatic C-H [134-136]
10	2863	Aliphatic C-H[136]
11	3022	C-H Stretching vibration [136]
12	3000-3100	Aromatic C-H [128, 131, 134]
13	3466-3455	N-H groups in carbazole/ secondary amine/OH stretching [131, 133]
14	3450	OH stretching [135]

Different authors studied XPS spectra of green petroleum coke and carbonaceous material and found that the petroleum coke and carbonaceous material contain mostly carbon. Other than carbon, it contains oxygen, nitrogen, sulfur, calcium, and sodium. The most prominent peak at 284.5 eV is designated as C1s. Other notable peaks include the O1s peak at 532 eV as well as Na1s, S2p, and C KLL [87, 137-140]. The relative positions of these peaks are used to determine the chemical nature of these elements which is listed in Table 2.6. FT-IR and XPS techniques are complementary to each other. FT-IR helps to know the presence of different functional groups, whereas XPS helps quantify them [141].

Table 2.6 List of functional groups and their corresponding binding energy for XPS study

Element	Peak	BE (eV)	Compound
C	1s	284.6	C-C/C-H [87, 142]
C	1s	285	C-O [87, 142]
C	1s	286	C-N [87]
C	1s	286.1-286.5	C-OH/C-O-C [87, 138]
C	1s	287.6-287.7	C=O [87, 138, 142]
C	1s	288.6-289.1	COOH/COOR [87, 138]
O	1s	531	C=O [51, 87]
O	1s	532	C-OH/phenolic [87]
O	1s	533.2	COOH/COOR [87]
O	1s	535.5	Sulfate or metal oxides [87]
S	2p	163.8	Elemental sulfur [87]
S	2p	164.8	Elemental sulfur [87]
S	2p	169.1	Metal sulfate [87]

2.2.2. Role of coal tar pitch

Coal tar pitch is obtained as a by-product of coal pyrolysis and is a complex mixture of hydrocarbon compounds. It is mainly used as a binder in the production of carbon electrodes. The role of pitch is to bind the filler cokes together by entering the pores and filling the voids between them. The ability of pitch to fill the coke pores depends on the viscosity and penetration ability of the pitch. The good binding properties of the pitch can be defined by its penetration ability, viscosity, surface tension and the physico-chemical interaction between the pitch and the coke surface. Chemical properties of coal tar pitch are essential for anode quality. Coal tar pitch contains aromatic hydrocarbons, which accelerate thermal polycondensation reaction resulting in the formation of high-molecular compounds

in the structure of anode material during baking. Good wettability of coke by pitch is very important for the production of good quality anodes.

2.2.2.1 Pitch surface tension

Surface tension of molten pitches has a linear relationship with temperatures ranging from 120-250°C despite of their origins and processes [143]. Surface tension is a property of the surface of a liquid that allows it to resist an external force. Pitch surface tension is a function of pitch density. Pitch wetting is controlled by the pitch surface tension; and if the pitch surface tension is too high, pitch cannot spread through coke particles even at low viscosity [8]. Another author has found a correlation between surface tension and pitch density in the range of 120°C to 220°C [5]. The correlation between surface tension and density is given as follows:

$$\sigma = 18.4\rho^4 \quad \textbf{(2.6)}$$

where $\sigma =$ surface tension N/m and $\rho =$ pitch density in kg/dm^3

Density of pitches has a great influence on the wettability. Generally, high density pitches show poor wetting. If the contact angle is greater than 90°, then there is no obvious penetration. If the surface tension of a liquid is less than the critical surface tension of wetting, then pitch will spread spontaneously on the coke bed [5].

2.2.2.2 Pitch surface chemistry

Pitch is a very complex organic material containing different compounds in a range of ~200 to 2500 amu [104]. Coal tar pitch has a higher value of aromaticity index, lower

atomic H/C ratio, and lower heteroatomic content compared to petroleum pitches [104]. The pitch structure and composition play a major role in pitch wetting behavior. Polycyclic aromatic hydrocarbons (PAH) are predominant in pitch. Also, following compounds are found in coal tar pitch [104, 136, 144].

- ✓ alkylated PAH,
- ✓ PAH with cyclopenteno moieties
- ✓ partially hydrogenated PAH,
- ✓ oligo-aryl methanes,
- ✓ hetero-substituted PAH: NH2, OH,
- ✓ carbonyl derivatives of PAH,
- ✓ polycyclic hetero-aromatic compounds

It has been also perceived in a separate study that pitch comprises of nitrogen-containing functional groups. Concentration of basic nitrogen containing constituents in pitch fractions increases with increasing molecular weight. Different authors used different surface characterization techniques to study the surface functional groups on the pitch surface [133, 134].

2.2.2.3 Other factors

Pitch wetting behavior is dependent on many factors other than surface tension and chemical compositions. A detailed literature review has not been done as it is not a part of this study.

Viscosity of the pitch has an effect on the wetting. Pitch is observed to have a rheology like a Bingham plastic at low temperatures (up to about 300°C) and like a Newtonian fluid

at high temperatures (above 300°C). Viscosity of pitch varies with temperature. Choice of right temperature gives an appropriate viscosity, hence, a good flowing property, which is essential to have good wetting between pitch and coke. The influence of viscosity on wetting can be a function of pitch quinoline insolubles (QI) content. Quinoline insolubles (QI) are produced in the metallurgical coke oven or formed from incomplete combustion of coal volatiles. These particles are spherically shaped and in solid state. Lower QI pitches penetrate better through the coke particles and show better wetting than higher QI pitches [6]. Couderc *et al.* (1986) [6] have found that low C/H ratio of the QI content is considered a good quality for a pitch for better wetting. During the heat treatment of the liquid pitch, crystal spheres known as secondary QI content or mesophase forms. Couderc *et al.* (1986) [6] have also observed that mesophase content has an impact on wetting and high mesophase content slows down the wetting phenomena by hindering the pitch penetration into the pores.

It is also found in the literature that β resins improve the wettability of the coke by pitch. β fraction of resin is the difference between toluene insolubles (TI) and quinoline insoluble (QI) matter. β resins contribute to the coking value and the bond formation between filler particles as β resins indicates the aromatic content of the pitches.

2.2.3 Role of recycled anode butt

The butt surface chemistry may differ significantly from that of petroleum coke because it is already mixed with pitch and has undergone physical and chemical modifications during baking and electrolysis. The surface chemistry of butt may be changed as the bottom

part is exposed to cryolite in the cell and subjected to CO_2 reactivity. In addition, the top portion is affected because of the oxidation due to air reactivity [101].

Wide ranges of studies cited that the wettability and the penetration characteristics of pitch with coke are different than those with anode butt [7, 71, 145]. Prouix (1993) [145] noticed that the optimal binder demand increases about 1% due to the absence of recycled anode butts. The average pitch film thickness on the butt surface is found to be smaller than that found on coke surface [7, 146]. These show that liquid pitch penetrates more easily through accessible porosity due to lower surface energy which results in a thinner film thickness on the surface of the butt [7]. The characterization of the surface properties of the raw materials can help explain this behavior. Adams et al. (2004) found that the carboxyl, lactonic, and phenolic functional groups are present in higher amounts on recycled butt surface than on petroleum coke surface by performing a selective neutralization technique using different bases [71]. Different authors studied the chemical structures of green petroleum cokes by different analytical methods which include SEM, optical microscope, FT-IR, and XPS [26, 27, 87, 128, 138, 139, 147]. However, there isn't any published work on the utilisation of these techniques on recycled anode butts.

2.3 Effect of process parameters on the pitch distribution in anode

Baked anode quality is important for primary aluminum production. Baked anode properties are affected by various process parameters and the quality of green anodes. They are affected by raw material quality, mixing and compaction of raw materials, and finally baking parameters.

Mixing and compaction have an influence on the homogeneity of the green anodes. During mixing, cokes are embedded by binder pitch which also starts to fill the pores of the coke particles. During vibro-compaction, pitch continues to fill the pores between the particles and the internal pores of the particles. The vibro-compaction causes the deformation of anode paste and the rearrangement of coke particles and binder pitch. Coke is considered to be a non-deformable phase and therefore binder pitch is the principle component which might influence the green density of the anodes during vibro-compaction. Proper distribution of pitch can reduce the air gap between the coke aggregates in green anodes which consequently increases green density. This can reduce electrical resistivity and air permeability and anode reactivity. Homogeneous anode pastes reduce the pitch consumption and high local volatile evolution leading to lower internal pressure and cracking rate throughout anode baking [148].

There are few researchers who investigated the influence of compaction properties on anode paste [149, 150]. Their studies revealed that compaction of anode paste with standard composition used during this study is not a time dependent process. Also, viscous behavior of paste does not significantly influence the compaction of the material [149]. Contradictory to the findings of the above study, different authors mentioned that the density of green anodes are related to both mixing and vibration time [80, 150]. Green anode density increases with increasing mixing and vibration time.

2.4 Worldwide anode properties

Table 2.7 represents the worldwide anode properties published by Perruchoud *et al.* (2004) [85] established by a survey from 60 worldwide anode plants.

Table 2.7 Worldwide anode properties [85]

Properties	Unit	Standard	Worldwide Range		Worldwide Mode	
			Mean	2 σ	Mean	2 σ
Apparent Density	kg/dm^3	ISO 12985	1.50 - 1.62	0.015 - 0.060	1.57	0.03
Specific El. Resistance	μΩm	ISO 11713	51 - 74	2 - 20	56	5
Flexural Strength	MPa	ISO 12986-1	4 - 14	2 - 7	11	4
Compressive Strength	MPa	ISO 18515	30 - 65	8 - 20	51	12
Static Elasticity Modulus	GPa	RDC - 144*	3.0 - 6.5	1 - 2	5.1	1.2
Thermal Expansion	$10^{-6}K^{-1}$	ISO 14420	3.6 - 4.6	0.2 - 0.6	4.1	0.4
Fracture Energy	J/m^2	RDC - 184*	100 - 260	40 - 80	210	70
Weibull Modulus	(-)	(-)	2 - 12	(-)	8	(-)
Thermal Conductivity	W/mK	ISO 12987	3 - 5	0.4 - 2.0	3.8	0.8
Density in Xylene	kg/dm^3	ISO 9088	2.05 - 2.10	0.012 - 0.040	2.075	0.022
Crystallite Size	Å	ISO 20203	25 - 32	1 - 4	28	2
Air Permeability	nPm	ISO 15906	0.3 - 4.0	0.3 - 8.0	1.0	1.4
CO_2 Reactivity Residue	%	ISO 12988-1	75 - 96	1 - 20	92	4
Dust	%		0 - 10	0 - 10	2	3
Loss	%		4 - 15	2 - 8	6	4
Air Reactivity Residue	%	ISO 12989-1	55 - 95	4 - 18	68	12
Dust	%		1 -12	1 - 12	6	5
Loss	%		4 - 35	4 - 15	26	9
S	%	ISO 12980	0.8 - 3.0	0.1 - 0.6	2.2	0.3
V	ppm	ISO 12980	30 - 350	5 - 60	220	20
Ni	ppm	ISO 12980	70 - 220	5 - 20	130	10
Na	ppm	ISO 12980	100 - 1000	50 - 800	250	200
Fe	ppm	ISO 12980	100 - 800	50 - 1000	400	200
Si	ppm	ISO 12980	50 - 300	50 - 300	150	150
P	ppm	ISO 12980	1 - 30	1 - 10	5	2

CHAPTER 3

EXPERIMENTAL

In this chapter, the techniques used for preparing and characterizing the materials will be discussed along with the experimental procedures used.

The experimental section consists of several subsections. In section 3.1, the characterizations of calcined cokes including chemical, physical and structural characterization are described. The chemical surface functional groups of raw materials were evaluated by Diffuse Reflectance Infrared Fourier Transform Spectroscopy (DRIFTS) and XPS whereas structural analysis of coke and interface of coke/pitch were carried out using optical microscope and SEM. In addition, the shape factors of the coke particles were investigated by using optical microscope and image analysis. The contact angle tests of different coke/pitch pairs were carried out to evaluate the wetting behavior of the different pitches on different cokes using the sessile-drop method. The tapped bulk density (TBD) tests were carried out to measure the density of the different blends of dry aggregate fractions to predict the final anode recipe. The porosity of the coke particles were measured by water pycnometer technique.

In section 3.2, the preparation of green anodes and their baking procedure are illustrated. Production of green anode is a complex process, and this procedure includes various equipment. A detailed description of different production steps are discussed in this section. The current section also covers the description of different anode characterization methods which include the measurements of apparent green and baked anode densities, electrical

resistivity, mechanical properties, air and CO_2 reactivities. The extraction of the pitch from industrial anode paste is reported in section 3.3.

Section 3.3 comprises of detailed characterization of industrial anodes. Distribution of pitch in anode is very important for homogeneous anode properties. Two different optical methods were used to capture the images for the analysis of the percentage of pitch in the anode sections. In the first method, optical microscope was used to take pictures of anodes sections, and the second method involves a set-up with a normal digital camera. Then, the image analysis was used to analyze these images which are explained later in Chapter 6.

The crystalline length of anodes gives an idea about the baking profile of the anodes. The detailed measurement techniques of crystalline length of baked anodes by XRD technique is also discussed in Section 3.3.

Section 3.4 gives the descriptions of different statistical methods (Artificial neural network, ANOVA, etc.) which were used to analyse different results of industrial anode sections. A detailed organogram of the methodology is illustrated in Figure 3.1.

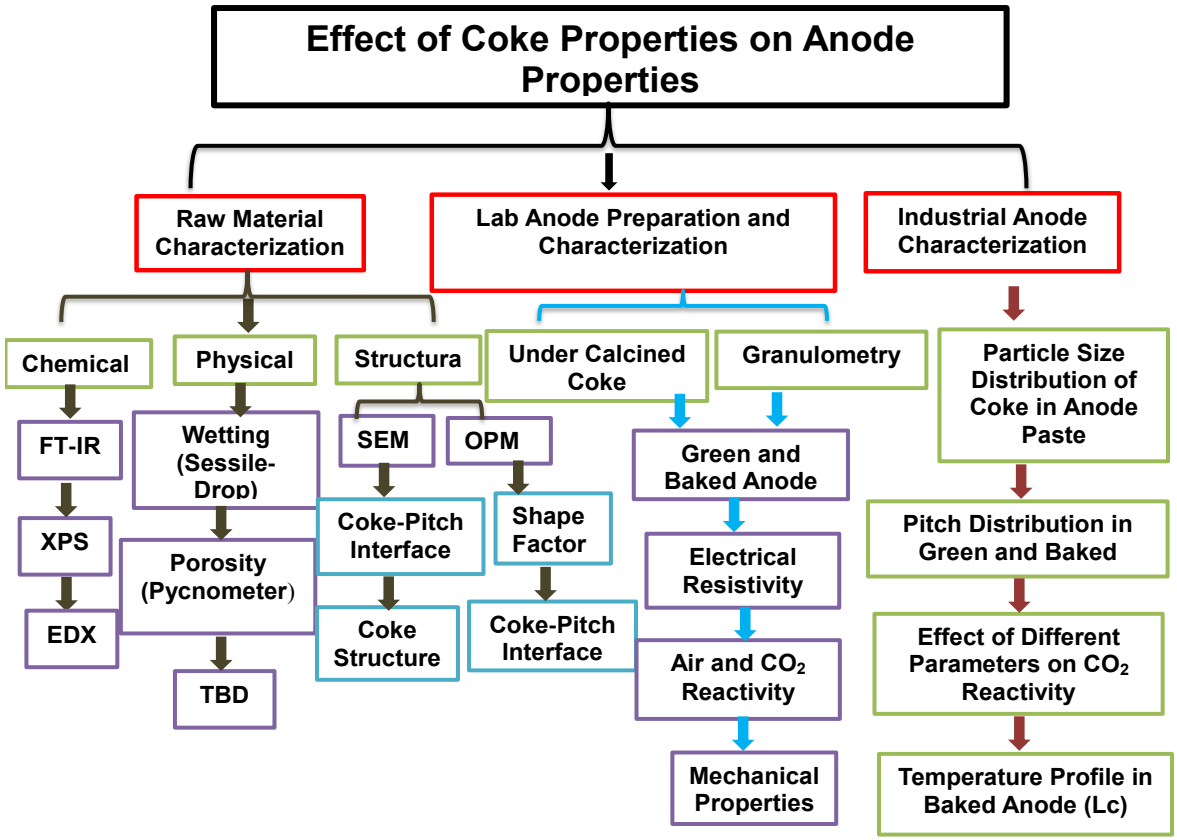

Figure 3.1 Organogram of methodology

3.1 Characterizations of raw materials

3.1.1 Chemical analysis

Different surface characterization techniques such as FT-IR, XPS, SEM and optical microscope were used to characterize petroleum cokes and coal tar pitches. In addition, coke and pitch interface was studied using SEM and optical microscope.

3.1.1.1 FT-IR analysis

Petroleum cokes and coal tar pitches have considerable importance in anode industry since raw material properties contribute significantly to the final anode properties. A dependable characterization method is essential in order to determine the suitable coke-pitch pairs. This characterization is difficult as coke and pitch are complex materials containing a large number of constituent compounds with different chemical functional groups and molecular structure. FT-IR is one of the most versatile techniques to study the complex organic compounds such as coal, pitch, and green petroleum coke. It provides information on surface functional groups based on their bond energies and orientation of atoms in space. The chemical structure of the calcined coke and the pitch samples were examined by Fourier Transform Infrared (FT-IR) spectroscopy at room temperature (Figure 3.2).

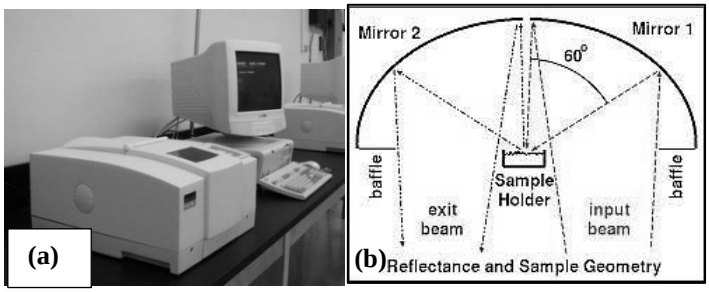

Figure 3.2 (a) Perkin Elmer Fourier Transform Infrared Spectroscopy, Spectrum one and (b) schematic of FT-IR-DRIFTS technique [151]

The main objective was to identify the new bond formation in the coke-pitch mixture which is used in anode production. The IR spectra were collected in the wavenumber range of 500–4000 cm^{-1}, and all the spectra were recorded at 4 cm^{-1} resolution. Each time, 20

scans were carried out prior to the Fourier transformation. All spectra were collected using DRIFTS technique using a FT-IR spectrophotometer Spectrum one, manufactured by Perkin Elmer Instrument. The working principle is shown in Figure 3.3. Equation 3.1 shows the Kubelka-Munk Equation.

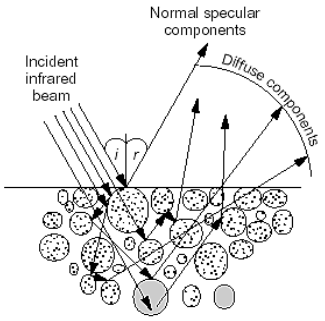

$$f(R) = \frac{(1-R)^2}{2R} = \frac{k}{s} \qquad \textbf{(3.1)}$$

R is the absolute reflectance of the sampled layer, k is the absorption coefficient and s is the scattering coefficient

Figure 3.3 Working mechanism of diffused reflectance infrared technique [152]

Each result was the average of four experiments. Calcined coke has lower absorption characteristics with respect to baseline levels [128] in KBr technique. DRIFTS technique was used with an aperture mask of 2 mm diameter and a reflector angle of 16°. DRIFTS technique is commonly used for rough particles. The diffused reflectance is produced by the sample's rough surfaces' reflection of the light in all directions and is collected by use of an ellipsoid mirror. The specular reflectance component in diffuse reflectance spectra causes changes in band shapes, their relative intensity, and, in some cases, it is responsible for complete band inversions. A Kubelka-Munk conversion was applied to a diffuse reflectance spectrum to compensate for these differences. All spectra were analyzed using the Spectrum version 5.0.1 software. The effective depth of the surface scanning was 0.5-5 μm. In this study, all the FT-IR spectra are presented in transmittance mode.

3.1.1.2 XPS analysis

The coke and pitch samples were studied by AXIS Ultra XPS spectrometer (Kratos Analytical) using Mono-chromate Al K[α] (hε== 1486.6 eV) source at a power of 210 W at the Alberta Centre for Surface Engineering and Science (ACSES), University of Alberta (Figure 3.4). The sample was irradiated with mono-energetic x-rays causing photoelectrons to be emitted from the sample surface. An electron energy analyzer determines the binding energy of the photoelectrons. From the binding energy and intensity of a photoelectron peak, the elemental identity, chemical state, and quantity of an element were determined. The working pressure in the analytical chamber was lower than 2×10^{-8} Pa. The resolution function of the instrument for the source in hybrid lens mode was calibrated at 0.55 eV for Ag 3d and 0.70 eV for Au 4f peaks. The photoelectron exit was along the normal of the sample surface with an analysis spot of 400 × 700 μm^2. During the analysis, a separate charge neutralizer was used to compensate sample charging. Survey spectra were scanned from binding energy 1100 to 0 eV and collected with an analyzer, pass energy (PE) of 160 eV and a step of 0.35 eV. For the high-resolution spectra, the PE of 20 eV with a step of 0.1 eV was used. The XP-spectra fitting was performed using the CasaXPS software at the UQAC/AAI Chair laboratory. The peak area was evaluated and scaled to the instrument's sensitivity factors after a linear background was subtracted from each peak. The composition was calculated from the survey spectra by taking the sum of all peaks after scaling to 100%. High-resolution spectra were used to carry out the spectra fitting and component analysis. The analysed surface depth of the sample was 2-5 nm.

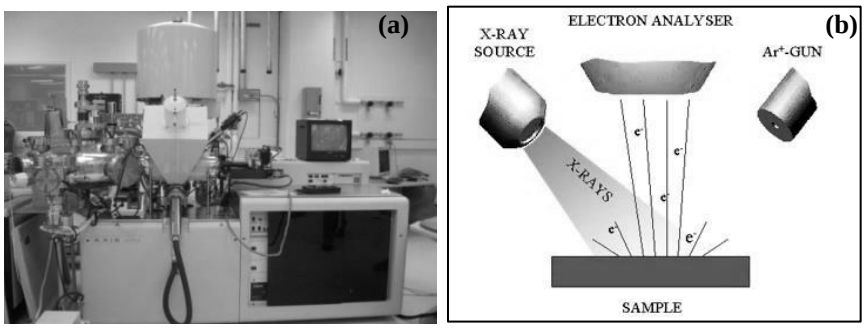

Figure 3.4 (a) AXIS Ultra XPS spectrometer (b) schematic of working principle of XPS [153]

3.1.1.3 Proximate analysis of coke

Proximate analysis was used to determine volatile components, fixed carbon, and inert components in the petroleum coke and the coal tar pitch. All samples were analysed at G.G. Hatch Isotope Laboratories, University of Ottawa, Faculty of Science (Earth Sciences). Samples were weighed into tin capsules. The capsules were loaded with standards into an isotope cube elemental analyser made by "Elementar", Germany (Figure 3.5). Sample was flash combusted with oxygen at about 1800℃ and carried by helium through columns of reducing/oxidizing chemicals to get N_2, CO_2, and SO_2. The gases were separated by "trap and purge" of specific adsorption columns so that the TCD (thermal conductivity detector) could detect each gas separately. The routine analytical precision (2sigma) was +/-0.1%.

Figure 3.5 Isotope cube elemental analyser from ‘Elementar’

3.1.2 Physical analysis

3.1.2.1 Wettability

Wettability can be defined as the ability of a liquid to spread on a solid surface and represents the extent of intimate contact between a liquid and solid. It can be described by the angle of contact between a drop of liquid resting on a solid substrate. The contact angle at equilibrium 'θ' was determined by the Young-Dupre Equation [106]. In this project, the sessile-drop method was used to measure the wettability of different petroleum cokes (under-calcined coke, cokes from different suppliers, cokes with different S content, shot coke, coke with different particle size) by coal tar pitches from different sources. Details about the experimental set-up and procedure are given below.

The sessile-drop system consists of a tube furnace (Thermolyne 21100), an inconel tube with a pitch injection system, a graphite sample crucible, a digital video camera (B/W) (APPRO, model KC), and a secondary rotary vacuum pump (GE, Precision Vacuum Pump, Model D25) (see Figure 3.6).

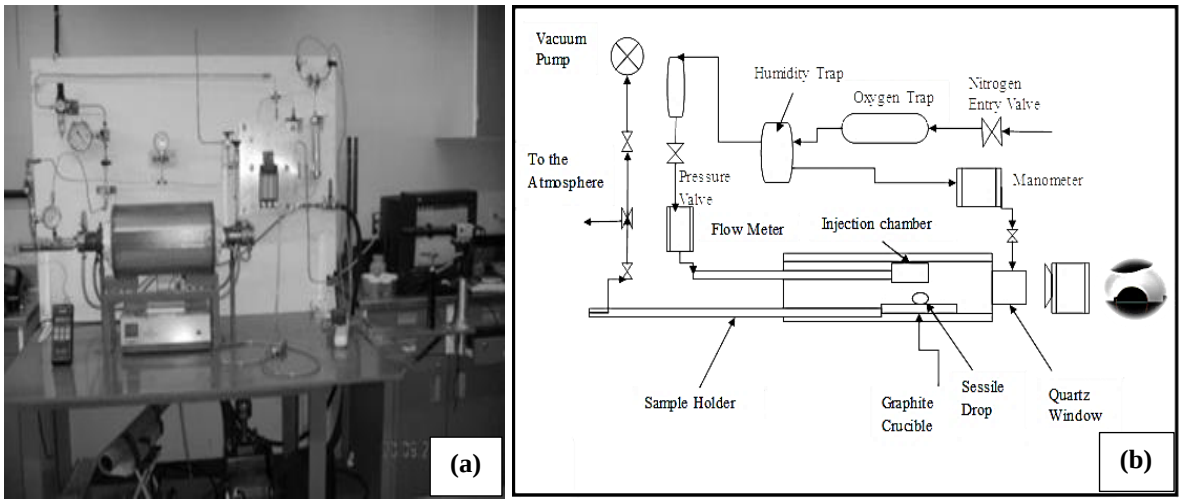

Figure 3.6 (a) Sessile-drop experimental set-up at UQAC (b) schematic diagram of sessile-drop system

The substrate coke powder was placed in the sample crucible. The injection chamber held the solid pitch sample. This chamber had a small hole at the bottom and is located just above the coke sample during the experiment. Coke particles were grounded, and particle size of -125µm was used. This particle size was also used by other researchers [7, 108]. The methodology was standardized and the particles were compacted in the sample crucible in order to have a smooth coke-bed surface using always the same procedure. The experiments were conducted under nitrogen (N_2) atmosphere. In order to decrease the O_2 and humidity content of N_2, it was passed through O_2 (Chromatographic Specialties, Oxygen Trap C36084) and humidity traps (Chromatographic Specialties, Glass Moisture Trap - C36150) before it entered the system. There were two entry lines for nitrogen. The main line was directly connected to the inconel tube to maintain an inert atmosphere inside this tube. The other line, connecting the injection chamber to the inert gas supply, carried

the N_2 gas to slightly pressurize this chamber in order to force the liquid pitch out through the hole and onto the coke bed. Pitch was placed in the injection chamber above the sample. The molten pitch droplet was directly deposited on the coke substrate by arranging the position of the injection chamber hole. The drop size could be changed by adjusting the hole size of the chamber. The sample holder could be removed from the hot region of the furnace by using a specially designed mechanism, and the sample could be quenched for further analysis. A video of the drop was captured for 25 minutes. The system could capture both static and dynamic images. To measure the contact angle, the FTA 32 software was used. The sessile-drop experiments were carried out at 170°C and 190°C. For each experiment, the contact angle was calculated as the average of the angles measured at two sides of drop. Each experiment was repeated twice.

3.1.2.2 Tapped bulk density (ISO 10236)

The anode recipe was characterized by measuring their bulk volume after tapping 1500 strokes of 3 mm amplitude, using the equipment shown in Figure 3.7. A representative sample of 100 ± 5 g, was taken and tapped in a graduated cylinder of 250 ml. Samples were simultaneously transferred to the feeder during tapping within the time frame of 45±15 s. The tapped bulk density (TBD) was calculated by the ratio of mass to volume of the sample in g/cm^3. This operation was carried out for 45 different recipes. The results were used as the input parameter to predict green density of anodes for various recipes by artificial neural network.

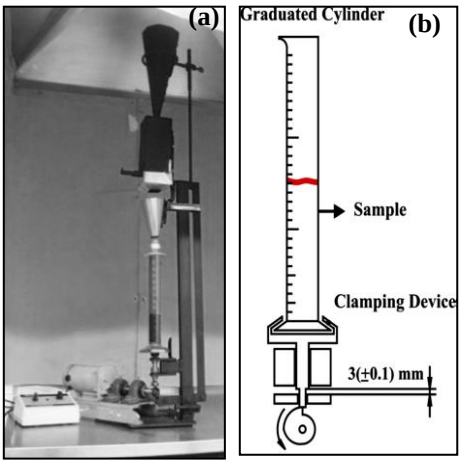

Figure 3.7 (a) Tapped bulk density equipment at UQAC (b) schematic of tapped bulk density equipment (ISO 10236)

3.1.2.3 Measurement of porosity

The porosity of the -125 µm particles were measured using water pycnometer (shown in Figure 3.8). Pycnometer can be also used to determine the density of a solid object that does not dissolve in the working liquid (water). At first, weight of empty, dry pycnometer was measured as m_1. Then the pycnometer was filled with distilled water and the stopper was fitted. The excess water that came out of the capillary of the stopper was dried with filter paper. The pycnometer filled with water was weighed and the weight was noted as M_{w+p}. The water from the pycnometer was removed. A sample weight of (5 ± 0.1g) M_2 was measured and pycnometer was filled with distilled water about 1/3 rd of its volume. It was stirred to get rid of any bubble. Then, the pycnometer was filled with distilled water in such a way that pycnometer as well as capillary hole in the stopper was filled. The spare water that leaks through the capillary hole was dried with a filter paper and total weight of the

pycnometer along with water and sample was measured and noted as m_3. The calculation of density and porosity is given below.

$$V_p = \frac{M_{w+p} - M_1}{D_w} \quad \textbf{(3.2)}$$

$V_p = volume\ of\ the\ pycnometer, D_w = density\ of\ the\ water$

$$M_w = M_3 - M_1 - M_2 \quad \textbf{(3.3)}$$

$M_w = mass\ of\ the\ water\ in\ presence\ of\ sample$

$$V_w = m_w / D_w \quad \textbf{(3.4)}$$

$V_w = Volume\ of\ the\ water\ in\ presence\ of\ sample$

$$V_{sample} = V_p - V_w \quad \textbf{(3.5)}$$

$V_{sample} = Volume\ of\ the\ sample$

$$D_{apparent} = M_2 / V_{sample} \quad \textbf{(3.6)}$$

$D_{apparent} = Apparent\ density\ of\ the\ sample$

$$Total\ porosity\ (\%) = \frac{D_{real} - D_{apparent}}{D_{real}} \quad \textbf{(3.7)}$$

$D_{apparent} = Real\ density\ of\ the\ sample\ from\ supplier's\ data$

Figure 3.8 Schematic diagram of pycnometer

3.1.3 Structural analysis

3.1.3.1 SEM analysis

A normal scanning electron microscope (SEM) operates at a high vacuum. The basic principle is that a beam of electrons is generated by an electron cathode, typically a tungsten filament or a field emission gun. The electron beam is accelerated through a high voltage (e.g.:20 kV) and pass through a system of apertures and electromagnetic lenses to produce a thin beam of electrons, then the beam scans across the surface of a sample. Electrons are emitted from the specimen by the action of the scanning beam and collected by a suitably-positioned detector.

Coke, pitch, and anode samples without polishing were mounted on an aluminum plate with a dimension of 20×30 mm using electrically conducting copper strips. Samples were cleaned using a high-pressure dust-removing air spray in order to remove surface dust and to have strong attachment with the copper strips. The SEM was also used to study the interface of the coke pitch (section of sessile-drop and green anode). For this analysis, samples were grounded and polished using a variable speed grinder-polisher (Buehler, Ecomet 4 with Automet 2 Power Head assembly). Initially 340 and 500 grains of silicon carbide per square inch papers and then 3 μm and 1 μm diamond polishes were used.

The samples were vacuum dried for one day at room temperature prior to SEM analysis. Each sample was then sputtered with gold-platinum coating with a plasma current of 10 mA, a chamber pressure of 6×10^{-2} mbar, and a sputtering time of 140 s using a Polaron Range sputter coater. The SEM analysis was done by using JEOL-JSM-6480LV (Figure

3.9) with secondary electron scattering and back scattering with a voltage of 20 kV and a work distance (WD) of around 10 mm. Energy-dispersive X-ray microanalysis (EDX) enables to determine the composition of the specimens. The principle of EDX is that the electron beam generates X-rays within the specimen. Many of these X-rays have energies characteristic of the elements that emitted them. Therefore, by measuring the energy of the X-rays, elements are identified in the specimen. EDX was used to identify the impurities in the calcined petroleum coke and green anode samples. A SEM can analyze samples sizes from of 15 nm to 100 µm.

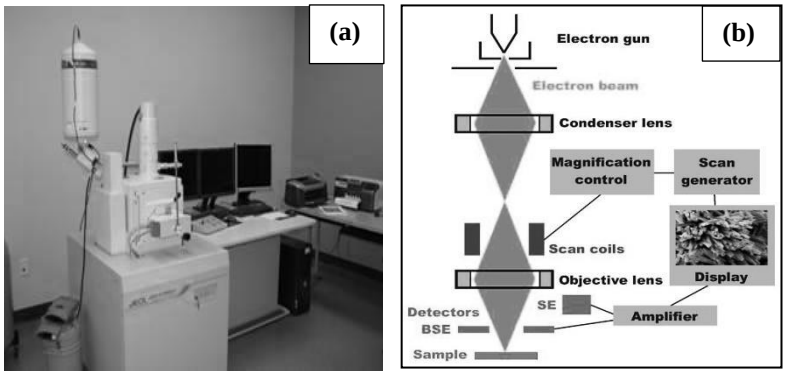

Figure 3.9 (a) Jeol scanning electron microscope (JSM 6480LV) (b) schematic diagram of SEM

Rough nature of cracks found on calcined petroleum coke surfaces make their examination difficult by the optical microscopy at high magnification. A SEM with its large depth of focus is appropriate for studies at higher magnifications. In this work, SEM was used to study the structural differences between coke particles. SEM can be used to examine unpolished coke samples.

3.1.3.2 Optical microscope analysis

The optical microscope uses visible light and a system of lenses to magnify images of small samples. Optical microscopy is an efficient technique to analyze larger surfaces compared to those used with SEM. Optical microscope can analyze samples up to few hundred micrometers. By mosaic technique, it is possible to analyze around 2 cm × 2 cm sample. The digital image from an optical microscope is captured by cameras to generate a micrograph. The utilization of polarized light allows the analysis of pores in coke, and the distribution of pitch into the pores of the coke can also be studied. The optical microscope (Nikon Eclipse ME600P and image analysis software (Clemex Vision 4.0) (Figure 3.10) was used to study the interface of coke pitch (section of sessile-drop and green anode). Samples were ground and polished using a variable speed grinder-polisher (Buehler, Ecomet 4 with Automet 2 Power Head assembly). Initially 340 and 500 grains of silicon carbide per square inch papers and then 3 µm and 1 µm diamond polishes were used. Particle shape analysis is often accomplished with the help of image analysis of micrographs. Optical microscope gives two dimensional projections of the particles which are used to study the particle morphology. A mosaic technique was used to analyze the green anode sample to cover a larger surface area.

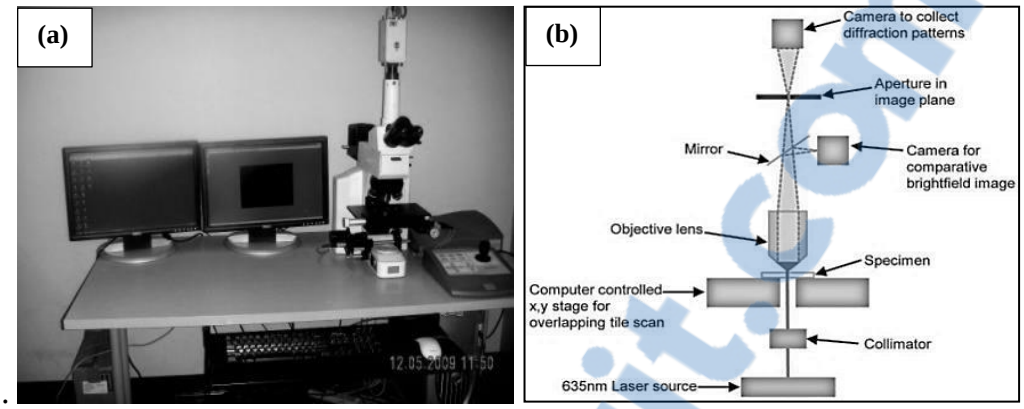

Figure 3.10 (a) Nikon eclipse ME600P microscope at UQAC (b) schematic diagram of optical microscope

3.2 Preparation and characterizations of laboratory anodes

3.2.1 State of the art of anode production

Anode production is a challenging task to perform and includes various complex production steps and parameters. The anode paste recipe has a considerable impact on anode quality. Since this project focused on the coke and its characteristics, different granulometry levels and types of cokes were used to make anodes at UQAC's pilot-scale anode production laboratory. Initially, different fractions of cokes and recycled butts were blended and mixed with molten coal tar pitch to produce anode paste. Thereafter, an anode paste was moulded using vibrocompactor to produce laboratory scale green anode. The baking was done according to similar conditions used in industry. Laboratory scale anode production method is presented in Figure 3.11

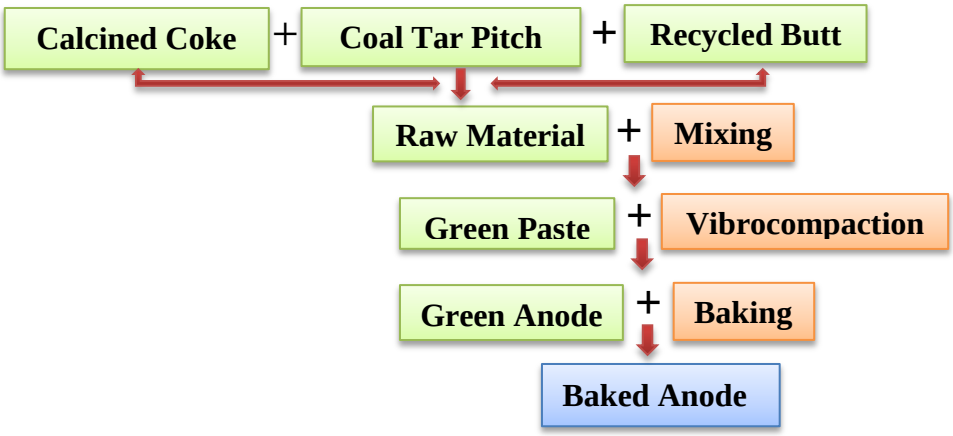

Figure 3.11 Raw materials, process, and products in the manufacturing of carbon anodes

3.2.1.1 Dry aggregate preparation

Anodes were made from four different cokes. Two of these were standard industrial calcined cokes from different sources. Two others were prepared from two specially calcined cokes with crystalline lengths of 24Å and 30Å. A predefined recipe was used for all pilot scale laboratories. Different fractions of coarse, medium, and fine coke particles were sieved using the sieve shaker at UQAC shown in Figure 3.12. The prepared coke fractions were weighed according to the specified recipe.

Figure 3.12 Sieve shaker for the preparation of dry aggregate

3.2.1.2 Mixing

For pilot scale anode production, an intensive mixer was used (Figure 3.13). The prepared coke fractions were preheated and blended with pitch using a predetermined mixing time for all cases. Molten coal tar pitch was added to the dry aggregate after preheating the coke. The mixing parameters were adjusted from control panel, and mixing was started. The paste temperature was maintained at 170°C during mixing. Intensive mixer is a high speed and multiple impeller system. The intensive mixer is comprised of a rotating mixing tank and an eccentrically arranged mixing tool. The mixer is also equipped with a frequency controller.

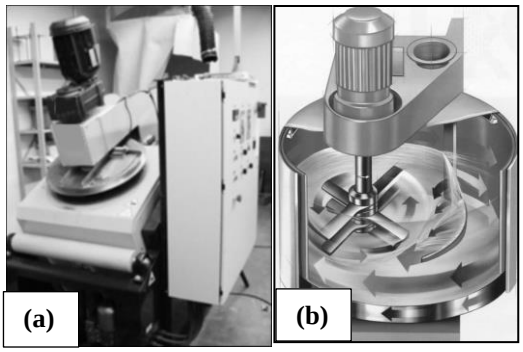

Figure 3.13 (a) Intensive mixer at UQAC (b) schematic of intensive mixer [21]

3.2.1.3 Forming

Anode forming was carried out in a pilot scale vibrocompactor (Figure 3.14). The compactor operates with an optimal load, placed on top of the cover and with optimum amplitude. The vibration frequency can be controlled with a frequency inverter. Two sensors (accelerometer) were attached to the vibrocompactor, so that the vibrocompaction

process can be monitored. It was important that vertical displacements of the cover weight and the table be exactly synchronized to obtain an efficient forming process. The following procedure was used for the production of compacted green anodes. Prior to transfer the paste to the mould, the interior of the heated mould was lubricated by oil to reduce friction and sticking as well as to improve the sample discharge after formation. The mould was filled with paste manually, and then the cover load was lowered and allowed to rest freely on the paste. The forming parameters were adjusted from control panel and the compaction was started. When the desired compaction level was reached, the cover weight was raised and the formed anode block was removed from the mould. The green anode was allowed to cool down using natural convection air cooling before further measurements and experiments were performed.

Figure 3.14 UQAC vibrocompactor

3.2.1.4 Baking

Anode baking is an important step to produce a mechanically-stable and electrically-current-conducting anode for electrolysis, which takes place in a baking furnace. Green anodes were baked under controlled conditions and then characterized. The green anodes

were baked in an electrically heated furnace manufactured by Pyradia (Model No-B07D02029021SVCCH), illustrated in Figure 3.15. The furnace dimension allowed baking of four anodes simultaneously. The baking was done using the conditions (temperature and heating rate) similar to those used in industry. When baking temperature was reached, anodes were subjected to soaking for 8 h. The heating rate should be maintained at a certain level as the devolatilization of tar, methane, and hydrogen from the pitch generates pressure tensions resulting in crack propagation if the heating rate is too high. The anode can be subjected to significant stresses during baking, mainly due to thermal expansion, shrinkage, and inherent temperature gradients, which can affect critical properties of the anode. Hence, several thermocouples were placed in different positions of the furnace to monitor the baking cycle and temperature distribution in the furnace.

Figure 3.15 Baking furnace used to bake green anodes at UQAC

3.2.2 Characterizations of anodes and anode samples

The anode properties were measured to ensure that they conform to general specifications, especially to produce high density, low resistivity, and low reactivity anodes. The following tests and measurements were carried out: air/CO_2 reactivities using the thermogravimetric (TGA) analysis (ASTM D6559 - 00a (2010) and ASTM D6558 -

00a (2010)), density and electrical resistivity of whole anode using the device/method developed at UQAC, density and electrical resistivity of anode samples measured by ASTM D6120-97 (resistivity) and ASTM D5502-00 (density) standards. A long term CO_2 reactivity test was performed for better understanding of dusting and CO_2 reactivity in the electrolysis cell.

3.2.2.1 Sample preparation

Most anode characterization tests require core samples. In order to prepare the anodes for testing, four cores of 50 mm diameter were drilled out of the center of the baked anode blocks. The ends were cut off the block leaving a 130 mm long core. This process removed the surface layer of the anode leaving a more homogeneous material. The anode coring plan is shown Figure 3.16.

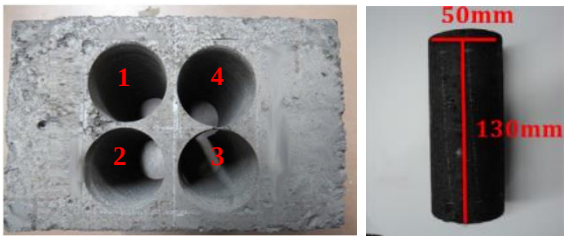

Figure 3.16 Anode coring plan for experimental anodes

Core 1 was used for CO_2 reactivity tests where the top part of the core was used for 21h (long duration) CO_2 reactivity test and the bottom part (50 mm in length) was used for 7h (standard) CO_2 reactivity test. Similarly, the top part (50 mm in length) of the core 3 was used for the air reactivity test. Cores 2 and 4 (130 mm in length) were used for compression and flexural strength tests respectively. Due to the limited amount of undercalcined coke

available, only a certain number of anodes could be produced for this case. Therefore, cores 2 and 4 were used to test the effect of baking temperature. In this case, core 2 was used for CO_2 reactivity and core 4 was used for air reactivity tests in a similar way.

3.2.2.2 Apparent density of anode (UQAC)

The apparent density of a material is defined as the ratio of its dry mass to its volume. Volume of the laboratory made anodes was determined using solid works and the anode measurements taken. The top and bottom width and length were measured using digital slide caliper. An average of eight measurements of height was taken to calculate the volume (Equation 3.8). Corner of the anodes were measured using tri-meter square. All the measurements were taken at room temperature. The density was calculated based on the ratio of weight to volume (Equation 3.9).

$$\boldsymbol{V = l \times w \times h} \quad \textbf{(3.8)}$$

w=width (cm); l= Length (cm); h=height; V=Volume(cm^3)

$$\boldsymbol{D = {M}/{V}} \quad \textbf{(3.9)}$$

M=Mass (g); V=Volume (cm^3); D=Density (g /cm^3)

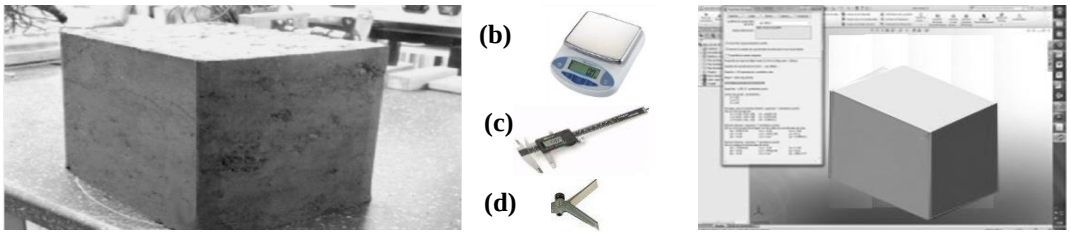

Figure 3.17 Measurement of anode density: (a) anode, (b) balance, (c) slide caliper, (d) trimeter square, (e) calculation of volume in 3-D design software SOLIDWORKS

3.2.2.3 Apparent density of anode sample [ASTM 5502-00 (2005)]

Anode samples (Φ50 mm × 130 mm) were dried, and the prepared samples were weighed in a balance to an accuracy of 0.01g. The lengths at 4 points, 90º apart from the periphery of the circular end faces were measured (Figure 3.18(a)). Four sets of diameter measurements were done. Each set consisted of four measurements, one at each end and two at intermediate point along an axial line (Figure 3.18(b)). Instruments used in this method are displayed in Figure 3.19.

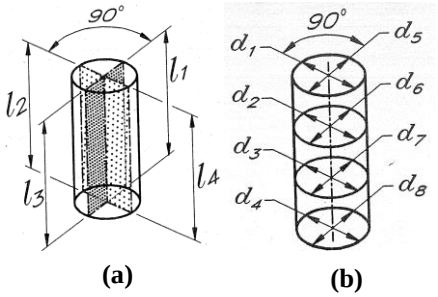

Figure 3.18 (a) Mean of the four length measurements (b) mean of the eight diameter measurements [ASTM 5502-00 (Reapproved 2005)].

Volume was calculated based on average of 4 lengths and 8 diameters (Equation 3.10). Density was calculated based on calculated volume and measured weight (Equation 3.11).

$$V = \pi\left(d^2/_4\right)l \tag{3.10}$$

d=diameter (cm); l= Length (cm); V=Volume (cm^3)

$$D = M/_V \tag{3.11}$$

M=Mass (g); D=Density (g/ cm^3)

(a) **(b)** **(c)**

Figure 3.19 Measurement of anode sample density (a) anode core (b) balance (c) slide caliper

3.2.2.4 Electrical resistivity of anode (UQAC)

Electrical resistivity of the laboratory anodes (green and baked) were measured with a custom made equipment in UQAC shown in Figure 3.20. An electrical current of 5 A was passed through the anode block and the voltage drop or electrical resistance was measured between two points along its lengths. The resistivity was calculated based on voltage drop, distance between the two points and cross sectional area of the anode (Equation 3.12). For laboratory anodes, a number of contact points were used to measure the voltage drop (Figure 3.20). Average of two measurements for length was taken for each measurement to

calculate voltage drop/length (Equation 3.13).

$$\boldsymbol{A = l \times w} \tag{3.12}$$

$$A = area\ (mm^2);\ w = width\ (mm);\ l = \ length\ (mm)$$

$$\boldsymbol{ER = \frac{v \times A}{I \times l}} \tag{3.13}$$

*ER=electrical resistivity (*μΩm); *v=average voltage drop (mV); I=current (A); l=length (mm)*

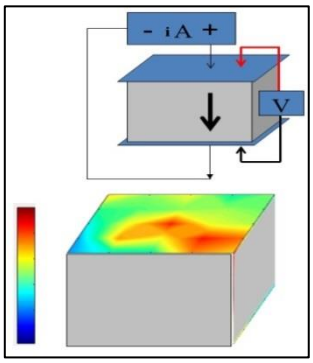

Figure 3.20 Schematic diagram of the set-up for electrical resistivity measurement of anode

3.2.2.5 Electrical resistivity of anode sample [ASTM D6120-97(2007)]

Electrical resistivity of the laboratory anode sample was measured with custom made equipment according to ASTM standard at UQAC. An electrical current of 1 A was passed through the anode samples of 50 mm in diameter and 130 mm in length, and the voltage drop or electrical resistance was measured between two points, which are 100 mm apart, along its length. The electrical resistivity was calculated based on voltage drop, distance between the two points and cross sectional area of the anode sample (Equations 3.14 and

3.15). Four sets of diameter measurements were done. Each set consisted of four measurements, one at each end and two at intermediate point along an axial line (Figure 3.21 (a) and (b)).

$$A = \pi\left(d^2/_4\right) \tag{3.14}$$

$$A = area\ (mm^2);\ d = diameter\ (mm)$$

$$ER = \frac{v \times A}{I \times l} \tag{3.15}$$

*ER=electrical resistivity (*μΩm); *v=average voltage drop (mV); I=current (A); l=length (mm)=100 mm*

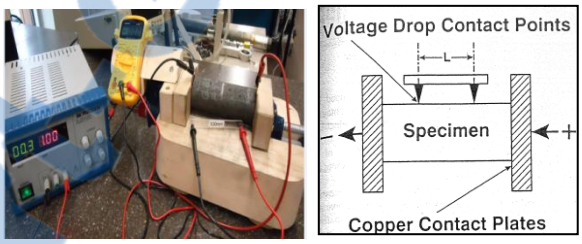

(a) **(b)**

Figure 3.21 (a) Set-up for electrical resistivity measurement of anode core (b) schematic diagram of the specimen holder for electrical resistivity measurement of anode core

3.2.2.6 Determination of air (ASTM D6559-00a) and CO_2 (ASTM D6558-00a) reactivities

This method consists of a thermogravimetric (TGA) determination of both air and CO_2 reactivities and dusting of anode sample (Φ50 mm × 50 mm). A TGA (TVS 12/600), which

is made of 'Carbolite' furnace and a balance (Mettler toledo model XS2002S), was used for all the reactivity tests (Figure 3.22). Exposed surface area of the sample was calculated using Equation 3.16. The samples were preheated to the desired temperature for 30 minutes in nitrogen gas before the reaction gas was introduced. The initial weight of the sample refers to the weight of the sample as soon as the reaction gas is introduced. The reactivity was determined by monitoring continuous weight loss of the sample (Equations 3.17, 3.18, and 3.19).

$$\boldsymbol{A = \left\{\pi dh + \frac{2\pi d^2}{4}\right\}/100} \quad \textbf{(3.16)}$$

A= *exposed surface area (cm^2); d=sample diameter (mm); h=sample height (mm)*

$$\textbf{\textit{Total reactivity Rate: }}\boldsymbol{TR = \frac{1000(W_0 - W_t)}{t.A}} \quad \textbf{(3.17)}$$

TR= total reactivity ($mg/cm^2.h$); W_0=initial weight of the sample (g);

W_t= final weight of the sample (g);.t=total time of the experiment

$$\textbf{\textit{Initial reactivity Rate: }}\boldsymbol{TR_i = \frac{2000(W_0 - W_{30})}{A}} \quad \textbf{(3.18)}$$

TR_i=initial reactivity ($mg/cm^2.h$); W_0=initial weight of the sample (g);

W_{30}= weight of the sample after 30 min (g).

$$\textbf{\textit{Final reactivity Rate: }}\boldsymbol{TR_f = \frac{2000(W_{t-30} - W_t)}{A}} \quad \textbf{(3.19)}$$

TR_f= final reactivity ($mg/cm^2.h$); W_t= final weight of the sample (g).

W_{t-30}= weight of the sample 30 min before the final time (g)

For air reactivity: W_{t-30}= Weight of the sample after 150 min

For 7h CO_2 reactivity: W_{t-30}= Weight of the sample after 390 min

For 21h CO_2 reactivity: W_{t-30}= Weight of the sample after 1230 min

The dusting was determined by collecting the mass of carbon particles that fall off the sample during reaction (Equation 3.20).

$$\textbf{Dusting Rate: } DR = \frac{1000 W_d}{t.A} \qquad \textbf{(3.20)}$$

DR= dusting rate for reactivity test (mg/cm^2.h); W_d= weight of the dust collected during test (g); t=total time of the experiment

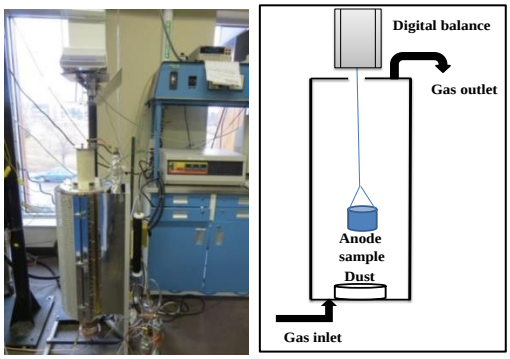

Figure 3.22 (a) Thermogravimetric (TGA) analysis for air reactivity of anode sample at UQAC (b) schematic diagram of TGA (ASTM D6559-00a)

Initial, final, and total air reactivity and dusting were determined by passing the air flow of 2.2 l/min for 3h at 525°C. Initial, final, and total CO_2 reactivity and dusting were determined by passing the CO_2 flow of 2.2 l/min for 7h or 21h at 960°C.

3.2.2.7 Uniaxial compressive strength of anode samples [C695-91 (2005)]

A compression test determines the behavior of materials under crushing loads. The hydraulic press for measuring compressive strength is shown in the Figure 3.23. The sample dimensions were based on the ASTM standard which proposes a diameter of 50 mm and length of 130 mm. A load was applied continuously at a constant rate of 0.1 KN without a shock until ultimate failure. The rate should be chosen in order to get an average rupture time over 30s.

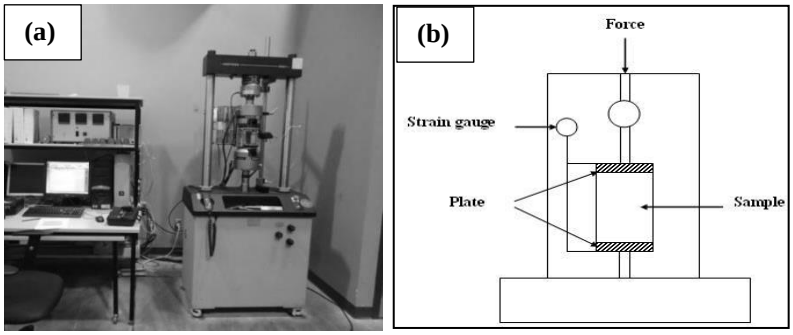

Figure 3.23 (a) Uniaxial compressive strength test equipment at UQAC, (b) a schematic diagram of compressive strength test

The compressive strength of the sample is given by Equation 3.21.

$$C = \frac{W}{A} \tag{3.21}$$

C: compressive strength (MPa)

W: total load on the sample at failure (N)

$A = \pi r^2$: cross sectional area of the sample (m^2)

The modulus of elasticity (Young's modulus) was determined experimentally from the

slope of the stress-strain curve obtained during compression test. A high Young's modulus means a high slope and therefore represents a material with low elasticity and high rigidity.

3.2.2.8 Flexural strength of anode samples (ISO CD 12986)

The three-point bending test is a method to measure the mechanical strength of the anode materials. The equipment is shown in the Figure 3.24. The three-point bending flexural test provides values for the flexural strain, and the flexural stress-strain response of the material. The main advantage of a three-point flexural test is the ease of the sample preparation and testing. This test arrangement creates maximum tensile stress in the middle of the support span, opposite of the load bar. An anode sample of 50 mm diameter and 130 mm of length was taken as per the proposed standard. This equipment applies a steady and linearly increasing load to the sample until a failure occurs. The applied load should be high enough to prevent the slow propagation of cracks and to get the actual mechanical strength of the material. The maximum applied force was registered to calculate the flexural strength. The bending stress of the sample core is:

$$\sigma_{max} = \frac{8.F_{max}L}{\pi d^3} \quad \textbf{(3.22)}$$

$$\sigma_{max} = bending\ stress\ (\frac{N}{m^2}); F_{max} = maximum\ applied\ load(N\ );$$

$$L = support\ span\ length(m);\ d = diameter\ of\ the\ sample\ (m)$$

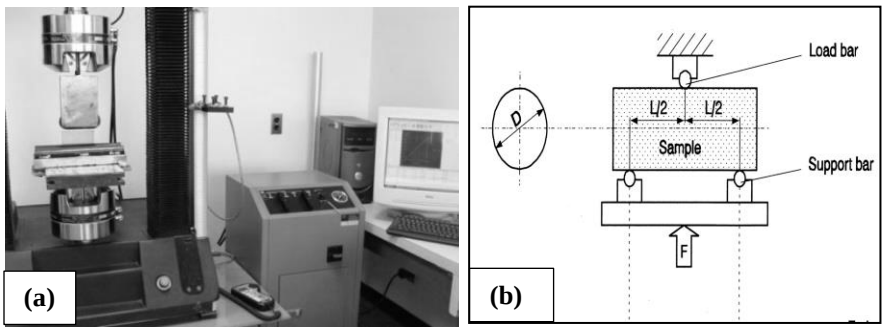

Figure 3.24 (a) Three-point bending test equipment at UQAC (b) a schematic diagram of three-point bending test

3.2.2.9 Sulfur analysis of anode

This method is performed for the determination of total sulfur in anodes before and after baking. In this study, a LECO carbon/sulfur analyser (Model: SC632 620-700-100; series: 3387) was used (Figure 3.25). Initially the anode samples were pulverized (98%-100% <106 μm and 85% <75 μm) in UQAC laboratory. About 2-3 g of pulverized samples were placed in a LECO capsule and then introduced into the furnace (1380°C) under an atmosphere of oxygen. Sulfur was oxidized to SO_2. After the removal of moisture, SO_2 gas was measured by an infrared detector. A computerized system calculated and displayed the concentration of the total sulfur present in the sample.

Figure 3.25 LECO carbon/sulfur analyser

3.3 Characterizations of industrial anodes

This section describes the characterization of different industrial anodes and anode paste. The manufacturing of anodes in industry is a complex process and subjected to continuous monitoring of the process to maintain desired anode quality. Industrial kneader is one of the major steps of the anode manufacturing where dry aggregates and pitch is exposed to kneading action which can break particles during the process resulting in the modification of particle size distribution used in the anode recipe. Similarly, pitch distribution in green anodes is related to mixing and forming conditions of the anodes, and pitch distribution in baked anodes is affected by the baking process as well. Furthermore, temperature profile of the baking furnace has a direct effect on anode properties and hence on crystalline length and anode reactivity.

3.3.1 Paste analysis

The main objective of this test is to analyze the dry aggregate and the anode paste to ensure that coarser fraction is not breaking during the kneading step. Initially, the kneader and the preheater residence times were calculated, and the samples were collected before the preheater (dry aggregate) and after the kneader. Weight of each fraction of the dry aggregate was measured after sieving. There are different industrial pitch extraction methods which are available, but each method includes toxic solvents and long experimental time. A simple, fast, cheap, and eventually environmentally viable method was developed to extract pitch from the anode paste. In this method, acetone was used as the solvent which is comparatively much less toxic than aromatic solvent as well as easily

available in the market. Initially, a filter paper was placed on a sieve, and paste samples were put on the filter paper. Then, samples were treated with acetone for 10 minutes at room temperature and separated with spoon by rubbing. When pitch was extracted, samples were taken out for drying at room temperature. Finally, coke (after extraction) was sieved, and each fraction was weighed using a balance for future analysis. The experimental procedure is given in the Figure 3.26.

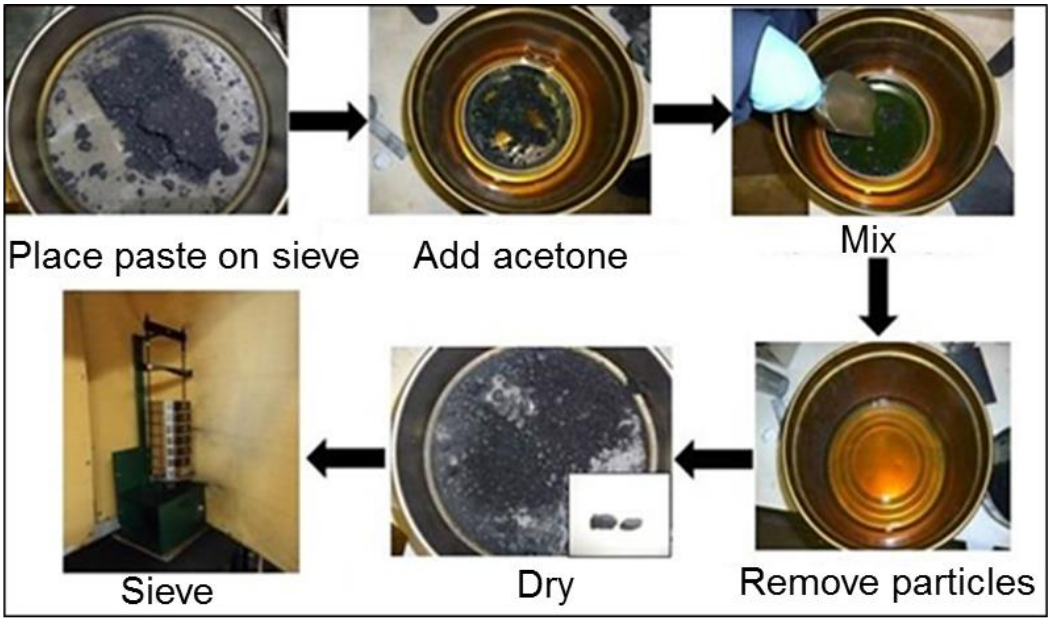

Figure 3.26 Extraction of pitch from anode paste

3.3.2 Pitch and pore analysis in green and baked anodes

Initially, the pitch distribution was measured for four green anodes. Samples were examined by using an optical microscope with linear polarized light. The digital images were acquired using the mosaic technique so that a possibly larger area of analysis can be taken into account. Prior to microscopy examination, the samples required special

preparation. Each 1×1 cm samples were mounted in epoxy resin and were polished in several steps using Struers Tegrapol-35. Subsequently, the samples were polished using silicon carbide (SiC) paper with water and on polishing discs sprayed by diamond spray and continuously wetted by ethanol. The samples were polished in three consecutive steps. In the first and second steps, 6 and 3 μm polishing cloth discs were used with an applied force of 50 N for 5 minutes. The third polishing step was performed using a cloth disc of 1 μm with a force of 20 N. In this case, the sample preparation was a tedious job and only a small surface area could be analysed. A simple optical image analysis method was developed to measure the distribution of pitch in 8 green and 24 baked industrial anodes. The anode cores were polished using 200 and 320 grid SiC paper for 10 minutes to have a smooth surface. A digital camera was used to capture images.

Green and baked anodes are composed of coke, pitch, and pores/ cracks. They all appear gray/black under the white light. Therefore, it was very difficult to differentiate the three constituents. Moreover, the conventional methods rely on the analysis of the equivalent gray image of a colored image. Any color can be expressed in terms of its primary constituents, namely red (R), green (G), and blue (B). The color scales can be expressed as integer values in the range of 0 to 255 for red, green, and blue separately. An example for the image analysis of an anode section is shown in Figure 3.27. Pores/cracks were identified using the shadow created by a light incident at an angle on the sample surface; then, pitch was detected by identifying the particle boundary using the differences in texture.

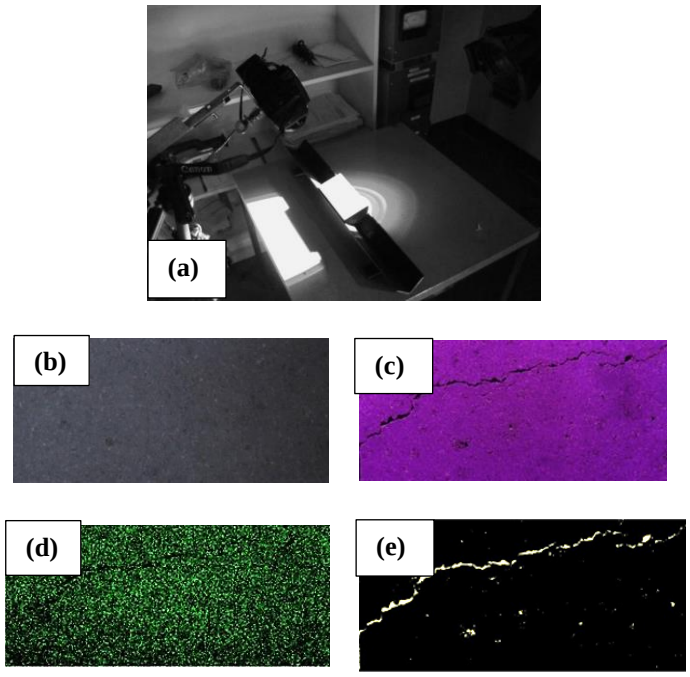

Figure 3.27 Image analysis of carbon anodes (a) image analysis set-up (b) polished sample (c) image of an anode section with polarized light (d) pitch distribution (e) macro pore and crack distribution

Calculation of pitch coke percentage:

The wt % of pitch coke (carbonized pitch) was calculated as follows after subtracting the area percentage of cracks:

- wt % of pitch in green anode by image analysis
- wt % of coke in green anode =(100-wt% of pitch)
- The carbonized pitch was calculated using the industrial weight loss data for each baked anode, and then wt % of pitch and coke were calculated.

3.3.3 Measurement of the crystalline length of baked anode samples by XRD (ASTM D-5187)

The crystalline length measurements of baked anode samples at different positions were measured using the XRD analysis with ASTM D-5187 standard based on the modified Scherrer formula given below (Equation 3.23, see Figure 3.28).

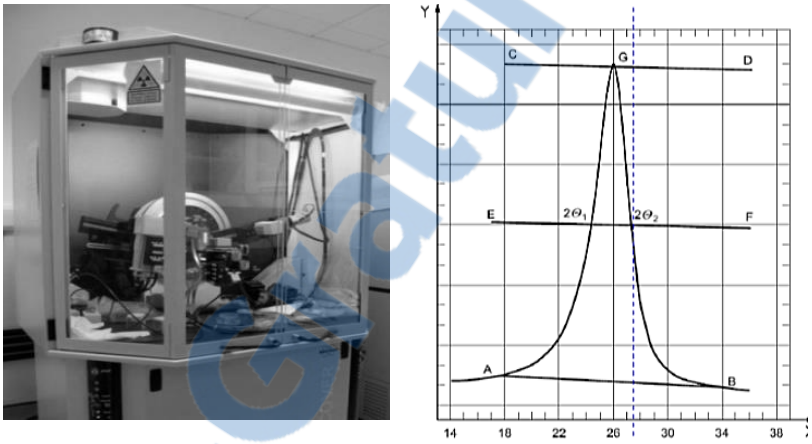

(a) **(b)**

Figure 3.28 (a) XRD equipment at UQAC; (b) parameters necessary for the calculation of the graphite peak broadness by the ASTM D5187-91/ISO 20203 method using modified Scherrer Equation (Y axis is intensity and X axis is $2\theta_i$ angle).

The base line of the peak, the peak height and the half-peak height (intersecting the peak at half of its maximum value), were determined in order to obtain the half peak-height angles $2\theta_1$ and $2\theta_2$. The mean crystallite length was calculated using Equation 3.23:

$$L_C = \frac{0.89\lambda}{2(\sin\theta_2 - \sin\theta_1)} \quad \textbf{(3.23)}$$

where λ is the wavelength and θ_i is the angle of incidence. In this technique, a sample pulverized to less than ≤65µm was exposed to monochromatic X-ray beam and rotated to

produce a diffraction pattern under specific conditions. The location and the shape of the peak with 'hkl' = (002) at d= 3.35Å was used to calculate the L_c. The crystalline length of the baked anodes was used to determine the distribution of the L_c in an anode and effect of L_c on other anode properties.

3.4 Statistical analysis

Various statistical tools were used for different types of analysis of raw materials and anodes. Effect of coke and pitch chemistry on contact angle was studied using linear multivariable analysis and artificial neural network. Artificial neural network was also used to predict the anode recipe from the coke bulk density. Both the analyses of variance (ANOVA) and the artificial neural network (ANN) analysis were used to understand the effect of different parameters on distribution of pitch in anodes.

3.4.1 Linear multivariable analysis

Multiple linear regression analysis is a generalization of linear regression analysis by considering more than one independent variable. A linear multivariable analysis was performed to identify the effect of individual properties of raw materials on wetting characteristics of the liquid (pitch) and the solid (coke) pairs. The basic concept behind the analysis is to express a property θ (contact angle) as a linear function of different independent parameters (X_1, X_2……X_N), i.e.

$$\theta = \sum_{i=1}^{N} A_i X_i \qquad \textbf{(3.24)}$$

where A_i represents the coefficient associated with the value of an independent parameter i. If the sign of the coefficient A_i is positive, then it may be assumed that an increase in property 'i' will increase the contact angle of coke/pitch (θ). On the other hand, if the coefficient A_i is negative, then it may be assumed that an increase in property 'i' will decrease the contact angle of coke/pitch (θ). The absolute value of the coefficient gives an idea about the extent of contribution of the property 'i' to the contact angle (θ). If N is the total number of independent variables and M is the total number of experimental observations, then the input matrix B will be:

$$B = \begin{bmatrix} Z_{1,1} & Z_{2,1} & \ldots\ldots & Z_{N,1} \\ Z_{1,2} & Z_{2,2} & \ldots\ldots & Z_{N,2} \\ \ldots & \ldots & \ldots\ldots & \ldots \\ Z_{1,M} & Z_{2,M} & \ldots\ldots & Z_{N,M} \end{bmatrix} \quad \textbf{(3.25)}$$

where, $Z_{i,j}$ denotes the value of input parameter 'i' for observation number j. For M observations, the matrix for the output property θ (contact angle) is represented as:

$$C = \begin{bmatrix} K_1 \\ K_2 \\ \ldots \\ \ldots \\ K_M \end{bmatrix} \quad \textbf{(3.26)}$$

where K_j denotes the value of contact angle θ at observation number j. If P is the matrix of coefficients defined as:

$$P = \begin{bmatrix} A_1 \\ A_2 \\ \dots \\ \dots \\ A_N \end{bmatrix} \quad \textbf{(3.27)}$$

and it is calculated as:

$$P = (B^T B)^{-1} (B^T C) \quad \textbf{(3.28)}$$

Though the method may not be highly accurate for all cases as there may not always be a linear relationship between the dependent variable and the independent variables, it can still give an indication of the influence of a single independent parameter on the value of a dependent parameter. MATLAB 2014 was used to solve the matrices.

3.4.2 Artificial neural network analysis (ANN)

Analytical mathematical tools are often used to predict values of dependent parameters if there is an existing mathematical relationship between the dependent and the independent parameters. Artificial neural network is an important tool in predicting the values of dependent parameters where no mathematical model is available [154] or even though some mathematical relationship is available, it is hard to find numerical parameters [155].

Neural networks are inspired by biological nervous systems [156]. They are used as a mathematical tool:

1) to find patterns and classify data,

2) to express output parameter as a function of a number of input parameters, and

3) to predict the value of an output parameter for a set of input parameters.

It basically contains different interconnected layers such as input layer, hidden layers and the output layer. The input variables are connected to the input layer, the output layer is connected to the output variable and the hidden layers stay in between the input and the output layers. There may be one or more hidden layers and the connections between the hidden layers may be in series, in parallel or a combination of series and parallel.

The steps involved in the development of an artificial neural network model are:

1) Modelling of artificial neural network

2) Training

3) Validation

4) Prediction of output for a new set of values of input parameters

1) Modelling an artificial neural network: It involves

a) Association of a transfer functions to each layer

b) Setting up connections between different layers

c) Finding the contribution (weight and bias) of the connections.

2) Training: It involves the use of training data set to find appropriate weight and bias values for all the connections.

3) Validation: It involves

a) Prediction of values of output parameters using input data for which output values are known.

b) Plotting of the predicted values of output variable against known values.

c) Finding the Equation of the best-fit straight line [156]. For best fitting, the equation of the straight line would ideally be of the form y = 1.x + 0, R^2 =1, where y is the predicted value corresponding to the known value x.

4) Prediction of output for a new set of values of input parameters.

Each layer can be schematically represented (in a simplified way) as shown in Figure 3.29

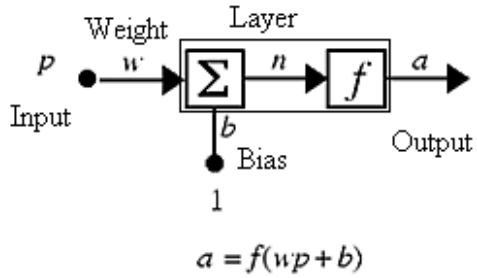

Figure 3.29 An abstract neuron

The key part of a layer is the transfer function (*f*) associated with it. While developing a neural network, the transfer functions are chosen usually by trial-and-error method. The input p is transmitted through a connection that multiplies its strength by the weight w, to form the product w_p. The bias b is simply added to the product w_p at the summing junction to manipulate the input.

In this study, a statistical method (ANN) was developed to study various complex phenomenon related to anode production. ANN was used for adjusting the granulometry of the raw material for anode production, studying the effect of raw material properties on contact angle, understanding the effect of different parameters on reactivity and also

studying the effect of different parameters on pitch distribution in anode.Two customized feed-forward neural network models with back-propagation training were tried using MATLAB 2014. They were the feed-forward back-propagation and cascade feed-forward back-propagation networks. For networks, one input layer, two hidden layers connected in series, and one output layer were selected.

Various transfer functions such as logsig, tansig, purelin are associated with the hidden layers. The logsig function can be represented as logsig(n) = 1/(1 + exp(-n)). Similarly, tansig function can be represented as tansig(n) = 2/(1+exp(-2*n))-1. Purelin is a linear function represented as purelin(n) = n. The transfer functions process the input to a layer such that the output can be easily classified into groups of similar data, which is important for an efficient prediction. The networks were trained based on the measurement of error in prediction. The errors were measured in terms of mean squared error (mse) and mean average error (mae). A flow chart below shows the working mechanism of artificial neural network in Figure 3.30.

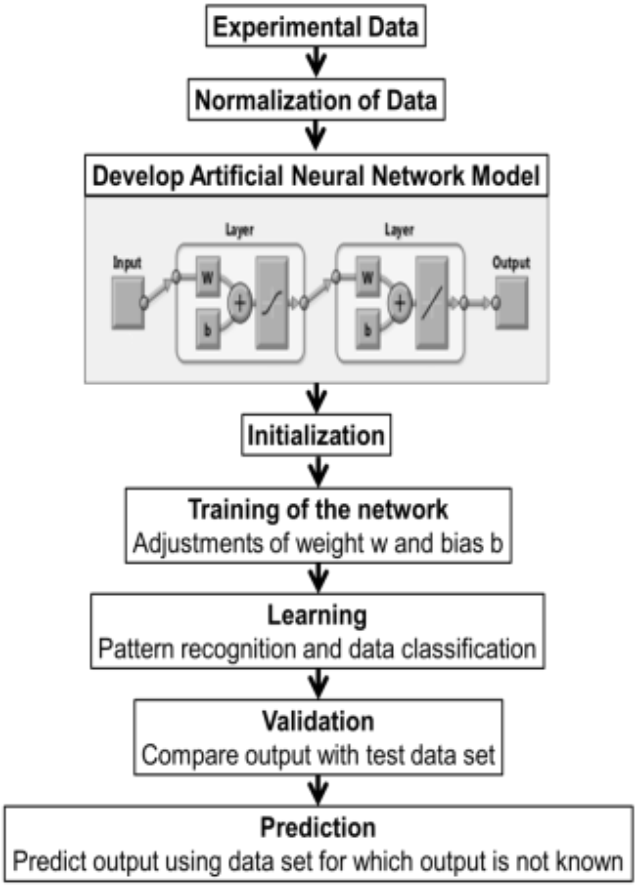

Figure 3.30 Flow chart of artificial neural network (ANN) [157]

3.4.3 Analysis of variance (ANOVA)

The ANOVA test was used to determine the impact of independent variables on dependent variables in a regression analysis. A factorial ANOVA allows to measure interaction between two (or more) sets of conditions that influence the response. The ANOVA test is the primary step in identifying factors that are statistically contributing to the data set's variability for a given data set. ANOVA is a statistical model used in order to analyze the differences between the group means for normally distributed population.

ANOVA test results can then be used in an F-test (test of equality of variances) on the significance of the regression formula overall. The larger the value of F is, the more significant the difference is. Also, if the probability is less than 5% (if p value is < 0.05), the correlation is usually considered significant. The basic concept behind the analysis is expressed in Table 3.1. The observations considered are 'y_i' where i=1,…, k, and 'k' is the number of treatments. Total number of cases is denoted as 'n'. The overall mean is symbolized as 'm', and 'm_i' signifies the mean within the group 'i'.

Table 3.1 Concepts of ANOVA

Source	**Degree of freedom (*df*)**	**Sum of squares (*SS*)**	**Mean square (*MS*)**	**F test**
Total (T)	n-1	$SST = \sum (y_i - m)^2$	MST=SST/(n-k)	
Treatment	k-1	$\sum (m_i - m)^2$	$\frac{SST}{(k-1)}$	$\frac{MST}{MSE}$
Error (E)	n-k	$SSE = \sum (y_i - m_i)^2$	$MSE = \frac{SSE}{(n-k)}$	

When the experiment includes observations of all possible combinations for all factors, it is termed as factorial. The factorial model includes the term for the main factors such as x, y, z and also the terms for the interactions such as xy, yz, xz and xyz.

CHAPTER 4

WETTABILITY

In this chapter, the results obtained during the wettability study are discussed. This chapter is divided into different sections and each section contains several sub sections. In the first section, the wettability of calcined petroleum coke by coal tar pitches from different suppliers was studied (three cokes and two pitches). The surface characterization results of raw materials were compared to comprehend the interaction mechanism between them when they are brought into contact. In the following section, the effect of coke crystallinity on wetting is discussed. Wettability of recycled anode material by coal tar pitches were studied in the subsequent section. In the last section, the results of two models developed using the linear multivariable analysis and the artificial neural network were compared. Due to the space limitations, rest of the wettability (for different combination of Coke 3 to Coke 6, high and low sulfur coke, shot coke and Pitch 3 to Pitch 8) results are given in Appendix 1 along with the wettability and characterization of shot coke and the effect of sulfur in coke on wettability.

4.1. Wettability of petroleum coke from different suppliers by coal tar pitch

4.1.1 General

The information on the coke and pitch interactions is very valuable for the aluminium industry. This information can be used in choosing the types of coke and pitch as well as the appropriate mixing parameters to be used in anode production. In this study, the

interaction mechanisms of pitch and coke during the mixing stage were studied by the sessile-drop test using two coal-tar pitches as binder and three petroleum cokes as substrate. The results showed that coke-pitch interaction behavior was related to both pitch and coke chemical compositions. The contact angle of different coke-pitch systems decreased with increasing time and temperature. At high temperatures, decreasing pitch viscosity facilitated pitch spreading and penetration into the coke bed. The chemical nature of petroleum cokes and coal tar pitches were studied using FT-IR spectroscopy and XPS. The present study has shown that the coke particle shape, structure, and interfacial reaction played an important role in coke-pitch interaction during wetting. It was observed that high values of sphericity, roundness, and compactness improved wetting. It was also found that a given pitch penetrates at different rates through beds made of different coke particles due to differences in particle shape (consequently, packing and bed porosity) along with other physical, chemical, and structural properties. The results showed that the wettability behavior of cokes by pitches is dependent on their physical properties as well as the presence of surface functional groups of coke and pitch which could form chemical bonds.

4.1.2 Materials

The physical and chemical properties of the three calcined petroleum cokes and two coal tar pitches (from commercially available sources) used in this study are given in Tables 4.1 and 4.2.

Table 4.1 Physical and chemical properties of coke

Properties	Calcined Petroleum Coke [158]		
	Coke 1	Coke 2	Coke 3
Bulk Density[1] (g/cc)	0.87	0.82	0.92
Sp. Electrical Resistance (µ ohm-m)	990	1070	940
CO_2 Reactivity (%)	14.5	6.8	3.9
Air Reactivity(% per min)	0.23	0.14	0.1
Porosity of Coarse Particles[2] (%)	21.5	18.1	13.7
Porosity of -125µm Particles[2] (%)	6.2	5.85	5.13
Crystalline length(Å)	28.5	29.7	28.2

[1]Measured by ASTM D4292-10, [2]Measured by ISO 1014:1985

Table 4.2 Physical and chemical properties of pitch

Properties	Coal-Tar Pitch [158]	
	Pitch 1	Pitch 2
Ash at 900°C (%m/m)	0.12	0.14
β Resin (%m/m)	22.3	23.2
Density at 20°C (g/ml)	1.320	1.320
Quinoline insoluble (%m/m)	8.5	5.7
Toluene insoluble (%m/m)	30.8	28.9
Coking Value (%m/m)	60.4	57.7
Softening Point (°C)	118.2	120.5
Dynamic Viscosity 170°C (mPa.s)	1710	1210

4.1.3 Contact angle test

Numerous wetting studies were carried out for different coke pitch systems. Due to the space limitations, the wetting results for all the pairs cannot be discussed in this chapter. Results are presented in Appendix 1 in tabulated format. This project focuses on the effect of calcined coke properties on the anode properties. The effect of pitch properties on the anode properties is the subject of another project. To study the wettability of calcined coke, two pitches were chosen based on their wetting properties. Pitch 1 showed the lowest

wettability (highest contact angle) and Pitch 2 showed the highest wettability (lowest contact angle) within the range of study.

The change of contact angle with time was found to be nonlinear for all the coke/pitch combinations. Figure 4.1 and Figure 4.2 demonstrate the change in contact angle of different coke/pitch combinations as a function of time at 170°C and 190°C. Typical industrial mixing temperatures of coke and pitch vary around 170°C. 190°C was also tried in order to see if there is any advantage of mixing at higher temperatures. Also, wetting study was conducted for 25 min since it was found that pitch penetration in anode continues even after kneading operation. SEM micrographs of anode sections cooled after different time intervals are presented in Chapter 5 (see Section 5.3).

The contact angle for different coke/ pitch systems decreased with increasing time. The initial and final contact angles observed with Coke 1 were the lowest among all the cokes studied. Coke 3 had the highest final contact angle. All three cokes had almost similar initial contact angles. For this system, the contact angles for both Coke 2 and Coke 3 decreased up to 600s, but after that the contact angle of Coke 2 decreased relatively faster compared to that of Coke 3. The final contact angle of the Coke 1, Coke 2, and Coke 3 were 23°, 33°, and 49°, respectively (Figure 4.1(a)).

Similar trend was observed for Pitch 2 with the same cokes as shown in Figure 4.1(b) with the exception that the contact angles of Coke 2 and Coke 3 started to differ after 200s. Coke 1 had the lowest whereas Coke 3 had the highest initial and final contact angles. It can be clearly seen from this figure that the initial contact angle of Pitch 2 is nearly same for Coke 1 and Coke 2, but then, the contact angle of Coke 1 further decreases;

consequently, it is wetted more by this pitch compared to Coke 2. The final contact angles of the Coke 1, Coke 2 and Coke 3 were 18°, 28°, and 47°, respectively.

The results indicated (Figures 4.1 (a) and (b)) that all coke/pitch systems studied show similar trends at this temperature (170°C). Coke 3 has the highest contact angle and Coke 1 has the lowest contact angle at all times. If the physical properties of the cokes (Table 4.1) were compared, it can be seen that the porosity of Coke 1 was the highest and that of Coke 3 was the lowest. Therefore, this might be one of the parameters affecting the wettability since the highest porosity coke was wetted the most and the lowest porosity coke was wetted the least by both pitches. Pitch 2 had lower viscosity than that of Pitch 1 at this temperature (Table 4.2). However, the final contact angles were not very different, those of Pitch 2 being slightly lower. To be able to understand their behavior, the chemical surface analysis was carried out. The results of FT-IR and XPS analysis for cokes and pitches and their relationship to wettability of coke by pitch are discussed in the following sections.

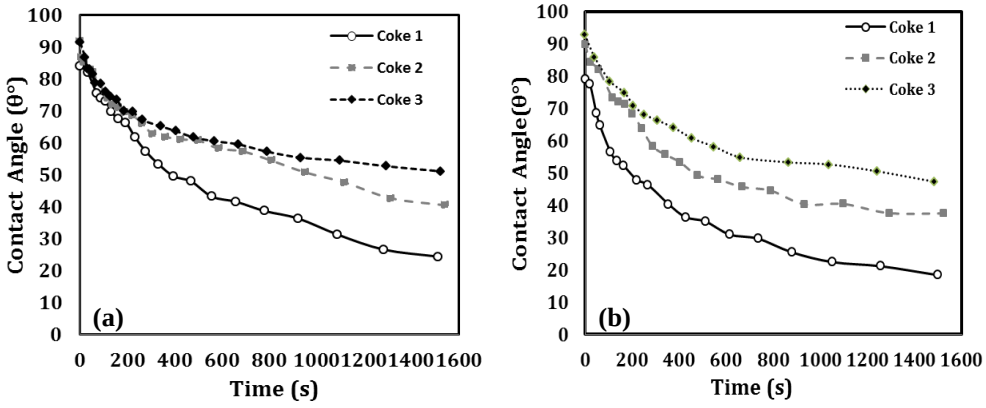

Figure 4.1 Dynamic contact angles of (a) Pitch 1 (b) Pitch 2 on three different cokes at 170°C

Figures 4.2 (a) and 4.2(b) represent the results of the wetting experiments carried out with two pitches, which had different viscosities, at a higher temperature (190°C). For Coke 1, the contact angle changed rapidly during the initial 500 s and reaches 0° within 1244 s at the higher temperature (Figure 4.2 (a)). In the case of Coke 3, the contact angle changed gradually with time; even after 1500 s, and its value was 32° (Figure 4.2 (a)). The change of contact angle with time was found to be very rapid with Pitch 2; and Coke 1 and Coke 2 were completely wetted by this pitch (Figure 4.2(b)). For Coke 1, the contact angle change was very fast and reached 0° within 591 s whereas, for Coke 2, the contact angle approached 0° within 1030s (Figure 4.2(b)). For Coke 3, the contact angles were found to be the highest (least wetting) at all times; but, considerable decrease in dynamic contact angle was observed with increasing temperature. Coke 1 with the highest particle porosity (-125 μm particle, see Table 4.1) had the lowest contact angle while Coke 3, the lowest porosity coke, had the highest contact angle as it was the case at 170°C. The lower viscosity pitch (Pitch 2) completely wetted both Cokes 1 and 2 during the experiment whereas the higher viscosity pitch (Pitch 1) completely wetted only the highest porosity coke (Coke 1).

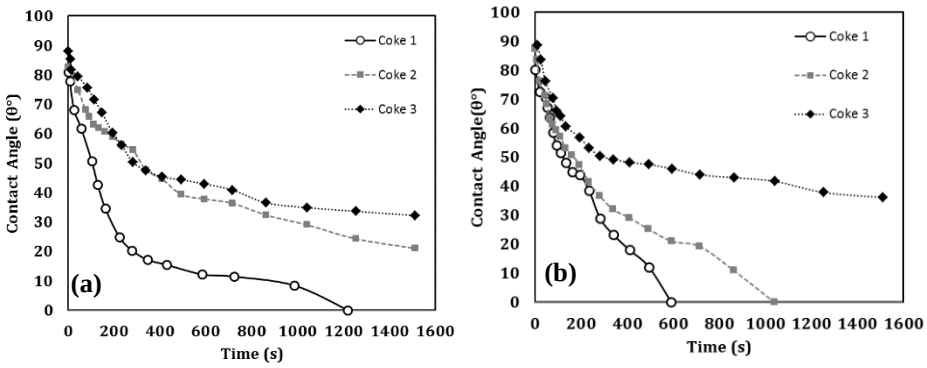

Figure 4.2. Dynamic contact angle: (a) Pitch 1 and (b) Pitch 2 on three cokes at 190°C

The initial and final contact angles are shown in Figure 4.3 for three cokes and two pitches at the temperatures studied. The initial contact angles of Coke 1 at lower and at higher temperatures were almost the same for Pitch 1; but for all the other cokes, the initial contact angles were slightly lower at higher temperature (190°C) compared to those measured at lower temperature (170°C). The initial contact angle of Coke 3 was the highest for Pitch 1 at both temperatures (Figure 4.3).

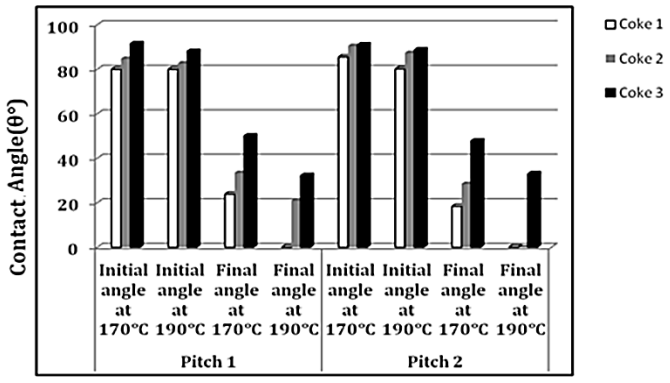

Figure 4.3. Intial and final contact angles of Pitch 1 and Pitch 2 on three cokes at two different temperatures

The work of adhesion of pitch-coke systems was calculated using the value of surface tension and contact angle. The condition for perfect wetting is given as $W_a = 2\gamma_{lv}$ [150]. This means that the adhesion energy between the coke and the pitch should be twice of the surface tension of the liquid which is mainly due to cohesive forces. The surface tension of Pitch 2 at 170ºC calculated using the FTA32 software was 39.33 dyne/cm. The work of adhesion for Pitch 2 and Coke 1, Coke 2, and Coke after 1500 s was 74.94, 73.66, 64.36 dyne/cm, respectively. These values indicate that pitch-coke system exhibits a strong interface, and Coke 1 (with a value slightly higher than coke 2) had the strongest interface among all the cokes studied. This was in agreement with the contact angle results since Coke 1 was wetted most by the both pitches.

In this study, -125 µm particles were used to study the wettability of coke by pitch. This particle size was chosen by many researchers as reported in the literature [7, 105]. To study the effect of particle size, a number of contact angle measurements were performed using -40 µm particles. As the particle size decreases, the effect of bed and particle porosities decrease. Also, smaller particle size helps reduce the surface roughness, and the substrate (coke bed) surface becomes smoother. Figure 4.4 shows that the trend observed for wettability with -125 µm particles and -40 µm particles was same. The contact angle with -40 µm particles was found to be higher (less wetted) than that for -125 µm particles for the same coke. Initially, the contact angles for -40 µm particles and -125 µm particles were similar but after 100s, -125 µm particles cokes were more wetted by the pitch. The results clearly indicated that increase in porosity increases wetting and decreases contact angle. However, this shows that the chemical as well as physical nature of the coke surfaces plays

an important role in wettability of coke by pitch. This test is useful for comparing the wettability of different coke and pitch pairs on relative basis regardless of the particle size used (-40 µm or -125 µm) since the trend remains the same.

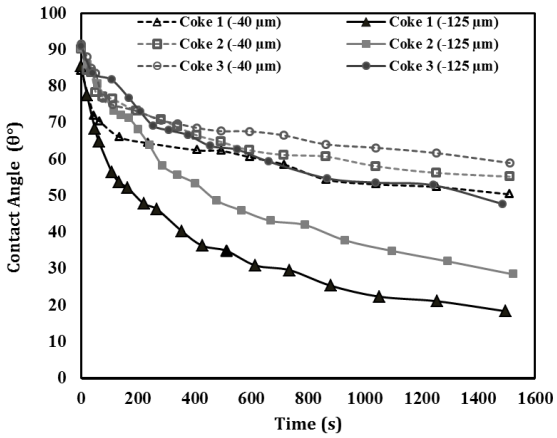

Figure 4.4 Comparative wetting studies of -40 µm and -125 µm particles with time at 170ºC for three different calcined cokes (for Pitch 2)

As seen from the contact angle tests, increasing temperature had a beneficial effect on the wetting behavior of pitch due to change in viscosity, which leads to better spreading and penetration of pitch through coke porosity. However, the change in pitch viscosity with temperature seems to affect the wettability of some cokes more than the others. This might be due to the difference in structure of coke (porosity) as explained above or their chemical nature. It is possible that an increase in temperature impel chemical reactions (thus, bonding) to take place at coke-pitch interface since the reaction rate increases with temperature. The initial contact angles of all coke/pitch systems were found to be very high; however, they decrease with time. Therefore, it is possible that the interfacial reactions might facilitate the wetting of cokes by pitch at prolonged times by modifying the

surface properties. However, the confirmation of whether there were any interfacial reactions or not required further investigation. In order to study the effect of chemical surface characteristics of both pitch and coke on wettability of coke by pitch, FT-IR and XPS were used for analysis of coke and pitch; and the results are presented below. First, a qualitative FT-IR analysis was carried out to determine which bonds are possibly present on the surface of a given material. Then, a quantitative XPS analysis was performed. The information required for the detailed XPS analysis on the bonds present at the surface was obtained from FT-IR analysis results (see Section 4.1.6). Therefore, these two analyses were complimentary to each other.

4.1.4 Structural analysis

Particle shape had an effect on the wettability of coke by pitch. The shape analysis of coke particles and the effect of shape factors on wetting were studied using optical microscope and image analysis. The different shape factors determined for three cokes are given in Table 4.3. The values of each of the parameters were determined based on average of a number of randomly chosen particles. The results indicated that a slight increase in sphericity, roughness, roundness, and compactness of the coke particles increased the wettability by pitch. Moreover, the present results seem to show that the wettability decreases with increasing particle aspect ratio. It is clearly seen from Table 4.3 that Coke 1 which was wetted most has highest sphericity and compactness compared to those of other two cokes. On other hand, Coke 3 contains particles with highest aspect ratio and lowest

sphericity, roundness, roughness, and compactness and therefore had the most elongated and irregular particles. The characteristics of Coke 2 were in between Coke 1 and Coke 3.

Table 4.3 Shape factors of -125 μm calcined petroleum coke particles studied

Shape Factors	Coke 1	Coke 2	Coke 3
Sphericity	0.869	0.85	0.842
Roughness	0.968	0.961	0.953
Roundness	0.673	0.629	0.56
Aspect ratio	1.63	1.66	2.07
Compactness	0.819	0.801	0.764

Particle shape is associated with the packing behavior of the powder, and it is believed that the beds made of spherical particles have lower bed porosity as packing density increases with sphericity [159]. It is also known that the spherical particle had lower aspect ratio and high value of compactness and roundness. The results of this study are in good agreement with those reported in the literature [124, 160]. As Coke 1 contained more spherical particles, its bed porosity was lower compared to that for other cokes. Lower bed porosity reduces pitch penetration, but contrarily by Coke 1 contained higher particle porosity which led to higher wetting. As can be seen from its definition, higher roughness values designated smoother surface (Table 2.4). Equally, smaller sized particles with smooth surface and lower bed porosity acted like a flat plate, facilitating the spread of pitch drops on coke bed. As it is well-known that wetting is a combined phenomenon of spreading and penetration, Coke 1 showed lower contact angle due to higher spreading and pitch penetration through particle pores.

Physical and chemical properties of cokes presented in Table 4.1 together with wetting results (Figures 4.1 to 4.3) give a clear evidence of the effect of the different particle shapes

on wetting and support the wetting results presented in this section. Nevertheless, beside the shape factors, chemical and structural properties of the materials need to be taken into consideration as possible factors affecting the wettability.

The morphology of the three different calcined petroleum cokes (particle size of -125 μm) are assessed using the optical microscope. The optical images (Figure 4.5) of three different cokes show that there were significant differences in the surface structure of the cokes. There were two types of porosity, open and closed. Open pores were inter connected at the surface and closed pores were inaccessible. Good quality coke contains more open pores around 0.5 μm-15 μm than closed pores [12]. Cokes containing high closed porosity resulted in low density anodes since these pores were not accessible to pitch. Shi [5] found that petroleum coke has a mixed microstructure of anisotropic, isotropic, and flat plate grains which consist of randomly oriented aromatic structure. Figure 4.5 (a) shows that Coke 1 surface contained lot of small and big pores. Some pores were quite small and some pores were interconnected. Coke 2 contains big round pores; smaller microspores as well as macrospores which were mainly inter crystallites spaces (Figure 4.5 (b)). Figure 4.5 (c) represents optical micrograph images of Coke 3. Coke 3 contained some elongated pores along with some small pores and void volume between carbon crystallites. It is possible that larger and interconnected pores of Coke 1 improved the pitch wetting which resulted in lower contact angle value. The aspect ratio of a pore may also play a role.

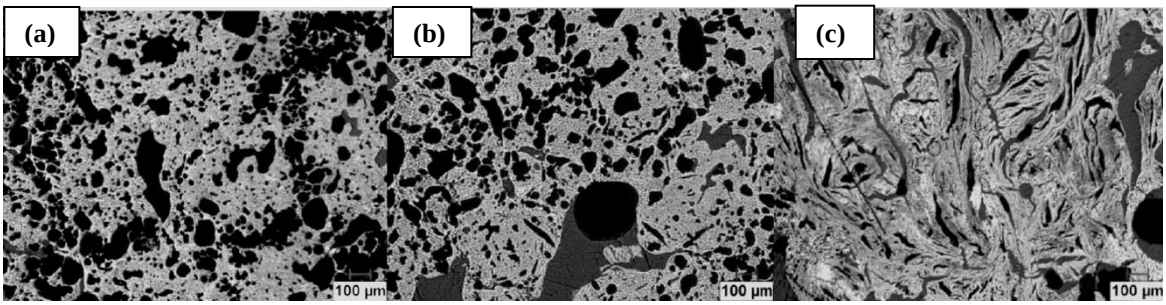

Figure 4.5 .Optical micrograph of three different petroleum cokes (a) Coke 1 (b) Coke 2 (c) Coke 3

The structural differences between three different cokes of particle size of -2 +1 mm were studied using SEM. Figures 4.6-4.8 showed the micrographs obtained at different magnifications using SEM for the three different calcined petroleum coke samples.

Coke is a nonhomogeneous material, and it's difficult to classify whether the carbon textural components in petroleum coke have been categorized into lamellar, intermediate, and granular structures [26]. Figures 4.6-4.8 indicate that the SEM images of three cokes appeare to be structurally different. As shown in Figure 4.6,Coke 1 contained mostly granular structures as well as a mostly random basal plane. It was observed that after crushing to -125 µm, Coke 1 contained mostly smaller particles and size distribution was quite uniform (Figure 4.6 (a)). Figure 4.6 (b) shows presence of many large cavities on the surface while Figure 4.6 (c) shows altered mosaic and granullar structure of coke and typical size of the mosaics was around 20 µm. Figure 4.9 (d) show random crytalline basal layer of carbon. It can be said that irregular structure of Coke 1 created more surface area for pitch wetting.

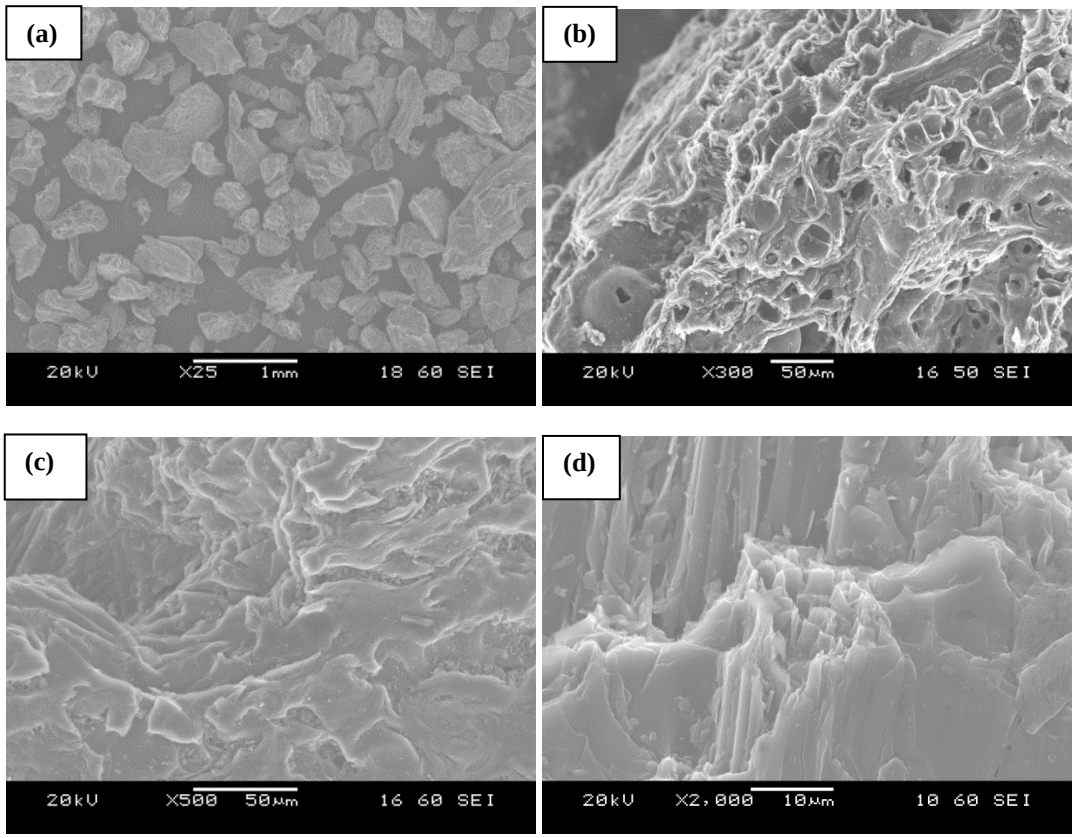

Figure 4.6 . Structural analysis of Coke 1 using SEM at different magnifications (a) 25X, (b) 300X, (c) 500X, and (d) 2000X

Coke 2 mainly contained lamella structure and a well aligned basal plane. Figure 4.7(a) shows that after crushing to -125 µm, Coke 2 contained a mix of small and large particles and the size distribution was non-uniform. Ground mass of Coke 2 displays mosaic and large devolatization pores in Figure 4.7 (b) and (c) respectively. Well allignment of carbon basal layers or lamella structure was depicted in Figure 4.7 (d).

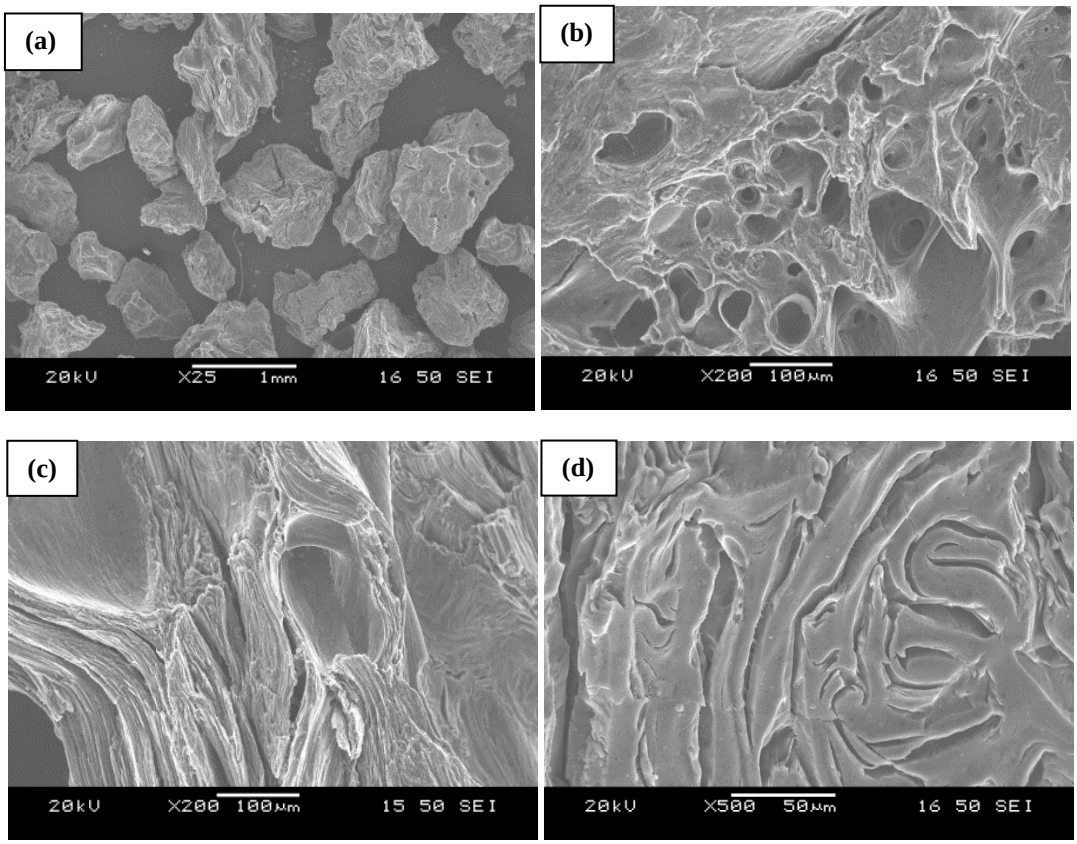

Figure 4.7 Structural analysis of Coke 2 using SEM at different magnifications (a) 25X, (b) 200X, (c) 200X, and (d) 500X

Coke 3 was mostly lamellar and the basal layer alignment was good. Ground mass of Coke 3 contained mixture of large and small particles and size distribution was mostly non homogeneous (Figure 4.8 (a)). The prominent exsistance of mosaic structure and their association with pores and other structure can be clearly seen from the Figure 4.8 (b). Presence of sound lamella structure and presence of coarse mosaic can also be observed (Figure 4.8 (c) and (d)). It can be observed that as intercrystallite defects reduced, carbon basal layer alignment improved. It was observed that the coke with the lamellar structure

was wetted less by pitch compared to the other cokes. It seems that the lamellar structure prevented the penetration of pitch.

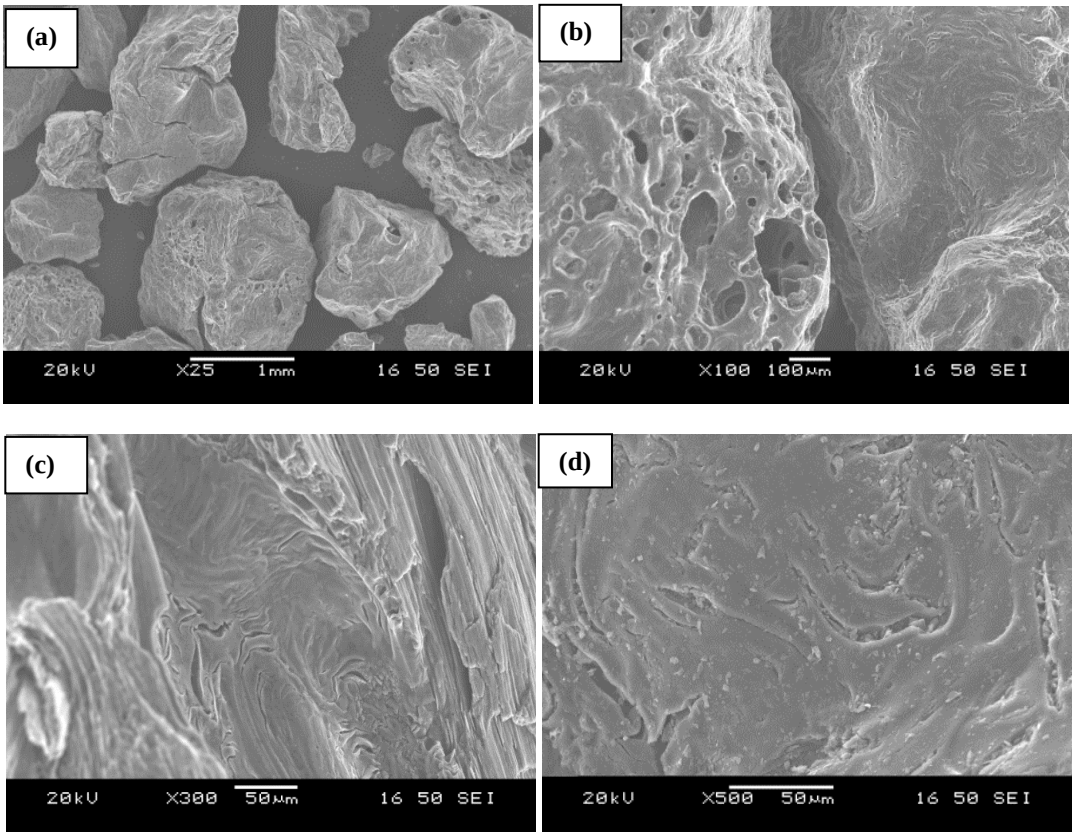

Figure 4.8 Structural analysis of Coke 3 using SEM at different magnifications (a) 25X, (b) 100X, (c) 300X, and (d) 500X

The pore structure and size were characterized by using a custom made software previously developed at UQAC. The average pore sizes of Coke 1 is between 25-30 µm. There is also presence of micropores of size 8-10 µm and large pores of size 60 µm. Figure 4.9 displays the working mechanism of custom made software to measure pore sizes of Coke 1. Intially, the pixels of the two different points in the image was measured using the custom made software. Later, the pixels were converted to µm using the scale generated

during the SEM microghaph. It is clear from the Figure 4.9 that 110 pixel is equivalent to 50 µm. Similarly, the pore size distribution of other two cokes were measured. Coke 2 contained average pores of 20-25 µm and small pores of size 5-6 µm. The average pore sizes of coke 3 was measured as~10-15 µm but the presence of very few large pores of 70-90 µm was also noticed.

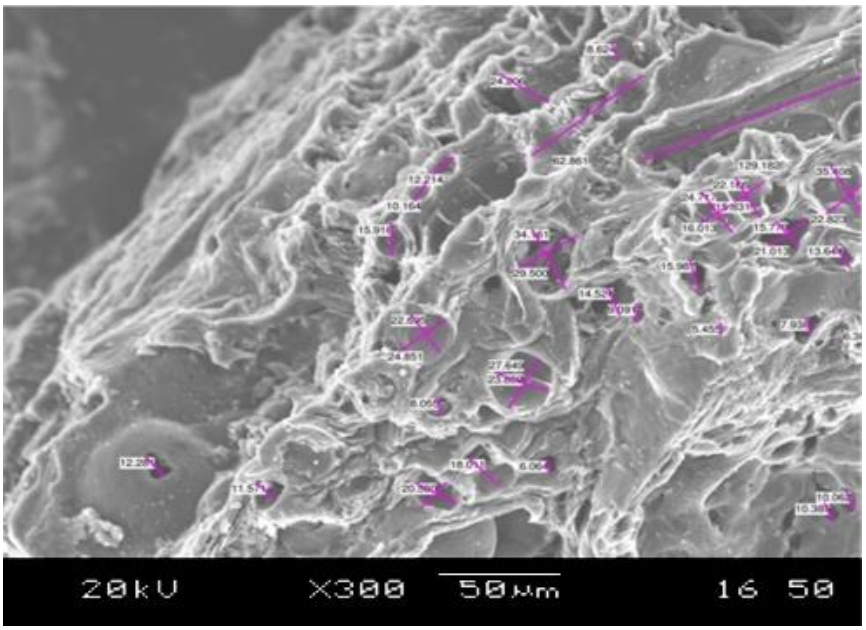

Figure 4.9 Measurement of pore sizes of Coke 1 using custom made software developed at UQAC

It can be seen from the SEM images that all calcined petroleum coke surfaces contained pores and cracks. The dimensions of some pores were quite small, but there were also larger pores. It is reported in the literature that the existence of very small pores prevents the pitch penetration into coke particles [40] and controls the wettability of pitch. It was evident that the structural differences affected the wetting behavior of pitch into pores. Analysis with custom made software revealed that the average pore size of Coke 1 was

higher compared to those of other two cokes. This result was in agreement with wettability results as Coke 1 contained higher particle porosity (Table 4.1) and higher average pore size distribution, consequently, it was wetted best by the pitch.

During the measurement of contact angle by sessile-drop method, -125 µm coke particles were used. This particle size was chosen so that the effect of bed porosity can be minimized [7, 108]. Also, the particles were compacted to ensure negligible bed porosity.

To study the effect of porosity on the wetting, the porosity of the -125 µm coke particles were measured by water pycnometer according to ISO 1014:1985. Due to crushing, porosity may change. The porosity of the bulk material (coke before crushing) and porosity of the crushed -125 µm coke particles were plotted, and it was observed that there existed a good correlation (Figure 4.10). For the particles of bulk material having the highest porosity, the porosity remained the highest after crushing. Similarly, for samples prepared by crushing the coke with lowest porosity, the porosity was also found to be lowest.

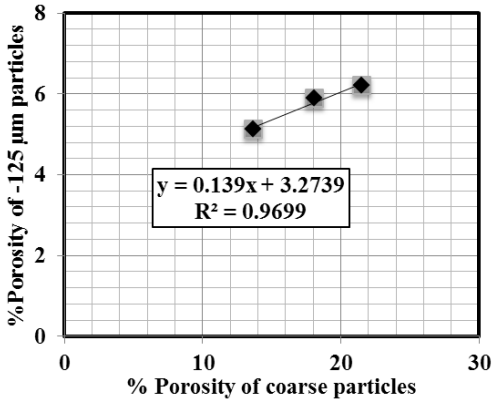

Figure 4.10 Correlation between percentage porosity of crushed and coarse particle of calcined petroleum cokes

4.1.5 Chemical analysis

The surface functional groups of the samples were identified by FT-IR. Figure 4.11 shows the FT-IR spectra of the three different calcined petroleum cokes. The calcined petroleum coke has very low transmission characteristics to baseline levels [7]. The assignments of the bands were performed (Table 4.4) based on the literature FT-IR data for green coke because no FT-IR study of calcined coke was documented in the literature. Before the detailed analysis, each sample was tested four times, and each spectrum was the average of four spectra (Figure 4.11).

Table 4.4 List of functional groups in different petroleum cokes from FT-IR study

Wavenumber (cm^{-1})	**Functional group**	**Type of Coke**		
		Coke 1	**Coke 2**	**Coke3**
670	Alkyne C-H bend/CH-CH_2 metallicalic impurities	**X**		
750	Ortho-substitution of the aromatic ring [128, 133, 134, 147]		**X**	**X**
832	Aromatic CH out-of-plane vibration frequencies.[128, 147]	**X**		
983	Aromatic CH		**X**	**X**
1006	Cyclic hydrocarbon ring vibrations	**X**		
1090	C-N amines		**X**	**X**
1126	Esters C-O, ether, COOH[147]	**X**		
1250	C-O-C Vibrations in Esters or ether[147]		**X**	**X**
1431	C=C Stretching Vibrations[131, 135]		**X**	**X**

Wavenumber (cm^{-1})	Functional group	Type of Coke		
		Coke 1	Coke 2	Coke3
1505	C=C Stretching Vibrations[131, 135]	**X**	**X**	**X**
1799	C=O[133]	**X**	**X**	**X**
2701	Aliphatic C-H stretching mode in aldehyde [136]	**X**		
2751	Aliphatic C-H stretching mode[136]	**X**	**X**	**X**
2863	Aliphatic C-H in sp^2		**X**	**X**
2950	Aliphatic C-H [136]		**X**	**X**
3022	C-H Stretching vibration in sp^2[136]	**X**		
3040	Aromatic C-H in sp^2[131, 134]		**X**	**X**
3337	Free NH/OH	**X**	**X**	**X**
3452	N-H groups in carbazole/secondary amine/OH stretching [131, 133]	**X**		
3527	OH /COOH from phenol or carboxylic acid	**X**	**X**	**X**
3610-3645	Free moisture or low concentration of phenol		**X**	**X**

FT-IR spectra of three cokes show the presence of similar peaks; however the peaks of Coke 1 are more diffused compared to those of Cokes 2 and 3 (Figure 4.11). It typically displayed a transmittance band near 3000-3050 cm^{-1} for all cokes due to aromatic C-H stretching vibrations; the pattern of transmittance bands between 900 and 700 cm^{-1} which arose from the out-of-plane vibration of aromatic C-H bonds, and bands corresponding to aromatic C=C bond near 1500 cm^{-1} for all three coke particles. Carbonyl and C=C bond stretching exhibited transmission close to each other; certainly, they were sometimes difficult to assign because of the overlap with each other. C-O (acid, hydroxyl,carboxylic,ester)/C-N (amines) and ortho-substitution of the aromatic rings found

at transmittance frequency around 1100 cm^{-1} and around 729 cm^{-1}, respectively. On the aliphatic side, the spectra consisted of a pattern of transmittance bands corresponding to saturated C-H stretching vibrations of alkyl substituents and methylene groups in hydro aromatic compounds (region between 3000 and 2700 cm^{-1}) and those corresponding to the C-H bending vibrations of C=C stretching vibrations for aromatics or alkane CH stretching (1431 cm^{-1}) and C-O-C vibrations in ester or ether (1250 cm^{-1}) groups as petroleum cokes contained carboxylic acid [16]. It can also be noted that phenolic functionalities or (hydrogen-bonded) OH or moisture were related to the transmittance band at 3610-3645 cm^{-1}.

Coke 1 contained diffused broad peaks for aliphatic hydrocarbons as well as functional groups containing heteroatoms (such as O, N). This indicates the presence of smaller chains (of different lengths) of aliphatic C-H as well as similar chains with different functional groups in Coke 1 when compared with two other cokes. This reduces the steric hinderance of Coke 1 during bond formation with pitch functional groups.

In general, the FT-IR spectra of Cokes 2 and Coke 3 were similar with regard to functionality although there were some qualitative (presence of different functional groups) as well as quantitative (ratio of peak areas for different functional groups such as aromaticity index) differences. As reported by Michel *et al.* [17] and Pruski *et al.* [18], petroleum cokes were composed of polynuclear aromatic hydrogen-deficient structures with few alkyl side chains as substituents and aromatic or naphthenic groups such as naphthalene, phenanthrene, anthracene, tri-phenylene, benzo-pyrene, coronene, pyrene etc., which are in relevant with the FT-IR result of the present work. For Coke 2 and Coke 3,

cyclic hydrocarbons ring vibration was observed. The presence of methylene (C=C) group could be seen from the FT-IR spectra corresponding to the peaks at 2865 cm^{-1} and 1431 cm^{-1}. It was assumed that most of the methyl groups are present in long chains and α-position in aromatic rings. Aliphatic chains in α-positions (such as the ortho-position in an aromatic ring) can easily undergo cyclisation [7]. At 750 cm^{-1}, ortho-substitution groups were noticed. However, no direct information on the exact structure of the coke can be derived from the available FT-IR results.

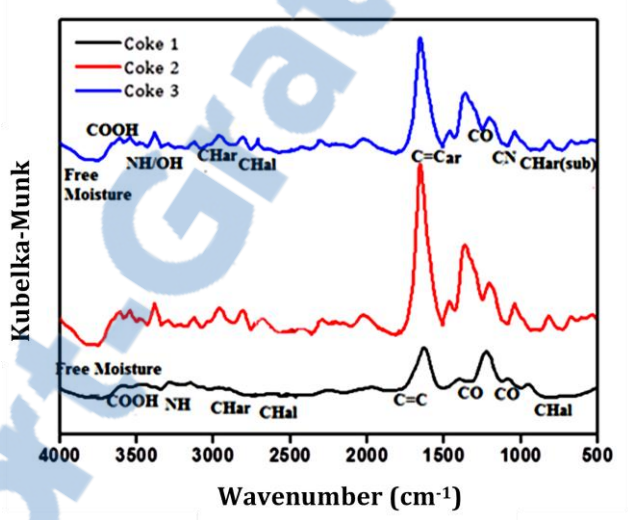

Figure 4.11. FT-IR analysis of calcined petroleum cokes by DRIFTS method at room temperature

Since the petroleum coke and coal tar pitch contained complimentary functional groups, it might be possible that the functional groups on the coke surfaces may interact with those present in pitches. Polycyclic aromatic hydrocarbons (PAH) were predominant in pitch. Also, alkylated PAH, PAH with cyclopenteno moieties, partially hydrogenated PAH, oligo-

aryl methanes, hetero-substituted PAH: NH_2, OH, carbonyl derivatives of PAH, polycyclic hetero-aromatic compounds were found in pitch [14, 19, 20].

Carbonyl and small amounts of phenolic/carboxylic as well as amine (NH) groups were determined on the surface of Coke 1. These groups can form covalent bonds with oxygen- or nitrogen-containing functional groups in pitch; therefore, their presence in small quantities was desirable. They could also assist hydrogen bonding with oxygen and nitrogen atoms of other groups. The phenolic/carboxylic/alcoholic/amine functional groups in coke and pitch could form hydrogen bonds; also, they could react to form ester or ether. FT-IR analysis of cokes, presented in Figure 4.11, showed that there was a formation of broad transmission band at 1114 cm^{-1} for C-O stretching vibration in ester or ether and a broad transmission peak (805 cm^{-1}) for aromatic CH out-of-plane vibration. It was also possible that aromatic compounds of the coke could react with aliphatic compounds of the pitch and vice-versa which might result in an increase in transmittance band at 1505 cm^{-1} for C=C bond. CN groups of the coke and pitch can form a new (pyridine) structure as a result of a reaction with aromatic hydrocarbons of the coke and pitch. Compounds with a nitrogen atom (free NH) in cokes might attach to a carbonyl structure to form amides or hydrogen bonds. Jiang (2007) performed FT-IR studies on green petroleum coke and mentioned that the surface functional groups such as C–OH, COOH, and some alkyl groups of petroleum cokes play a key role in the chemical activation process [12].

FT-IR of Pitch 1 and Pitch 2 are given in Figure 4.12. FT-IR spectra of both pitches showed the presence of similar chemical functionalities. Pitch 1 and Pitch 2 displayed a broad peak around 3428 cm^{-1} for free moisture. Around 3038 cm^{-1}, a peak was observed

due to aromatic CH stretching vibrations and other peaks were perceived due to aliphatic CH stretching vibrations on pitch surfaces around 2903 cm^{-1} and 2837 cm^{-1}. Various bands related to aromatic CH out-of-plane bending with different degrees of substitution were observed in the region of 700-900 cm^{-1}. A very sharp peak at 742cm^{-1} was spotted due to ortho-substituted aromatic ring vibrations. A weak peak at 1725 cm^{-1} was noticed due to carbonyl group. It is possible due to CO_2 in air also. As background correction was done for air, the effect of CO_2 in air may be neglected. The band at 1595 cm^{-1} was attributed to aromatic C=C stretching. Multiple peaks were detected in the region of 1200-1300 cm^{-1} due to C-O (acid)/CN vibrations and in the range of 1050-1150 cm^{-1} due to C-O stretching of acid/alcohol/ether/ester. Peaks around 1438 and 1374 cm^{-1} were found to be due to methyl substitution of aromatic rings [11].

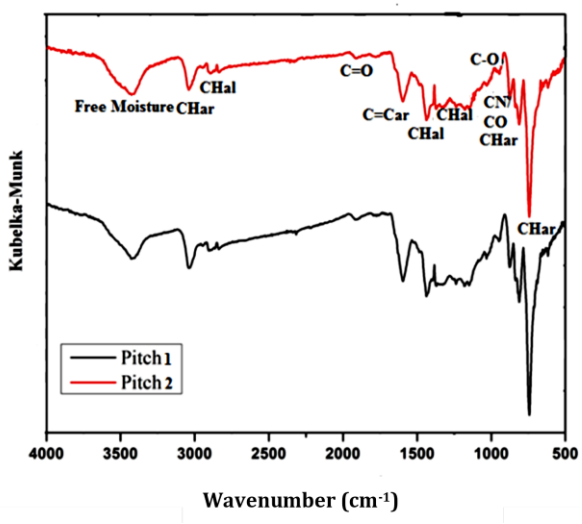

Figure 4.12. FT-IR analysis of pitches by DRIFTS method at room temperature.

In order to see the effect of mixing pitch and coke on the surface functional groups, they were mixed at two different temperatures (170°C and 190°C), cooled down, and FT-IR

analyses of the mixtures were carried out. The results for all three cokes with Pitch 1 are shown in Figure 4.13 at 170°C. As it can be seen from Figures 4.11, 4.12, and 4.13, the individual spectra of cokes and pitches were different than those of their mixture.

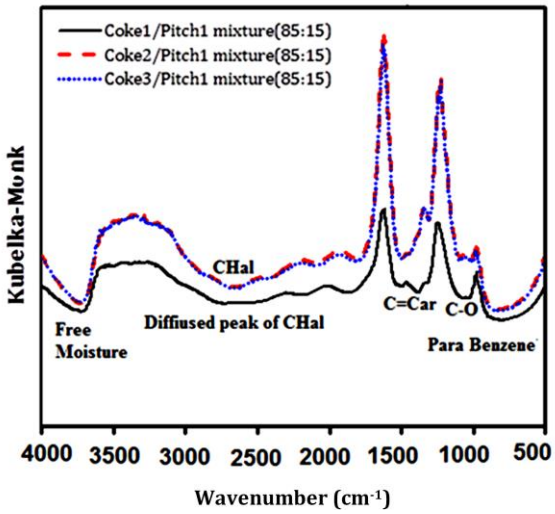

Figure 4.13. FT-IR analysis of the mixtures of calcined petroleum cokes and Pitch 1 (in a ratio of 85:15 wt % and maintained at 170°C for 1 hr in N_2 atm) by DRIFTS method at room temperature.

The mixtures exhibited the formation of similar functional groups, i.e., broad transmission peaks for C-O stretching in ester or ether (1116 cm^{-1}), C-H outer plane vibration (836 cm^{-1}) and C=C (1506 cm^{-1}) stretching vibration (Figure 4.13). In the spectral region of 2700-2900 cm^{-1}, a clear difference could be seen in the FT-IR spectra when different cokes were used. A diffused peak was formed due to chemical reactions. In addition, Coke 1 showed further diffused peak for aliphatic hydrocarbons. This phenomenon could be elucidated by smaller aliphatic chains which create less stearic hindrance to the cyclisation or condensation reactions for Coke 1. This might explain the

reason for better wettability of this coke by the pitches investigated compared to those of the other two cokes.

FT-IR analysis of the mixtures showed that the chemical interactions occurred between pitch and coke when they were mixed. The results of the FT-IR analysis at 190°C were similar to those obtained at 170°C. This indicated that increasing the temperature within the range studied did not affect the nature of the chemical interactions. Thus, the differences in wetting (contact angles) can be attributed to the difference in physical properties of cokes and pitches.

FT-IR analysis was used to identify the chemical functionality of coke and pitch surfaces. During XPS analysis, the information obtained from FT-IR analysis was used to carry out the de-convolution of C1s peak. Atomic percentages of different components of three different calcined coke samples are presented in Table 4.5 for the survey spectra and de-convoluted C1s spectrum. The de-convoluted C1s spectra of calcined cokes were presented in Figure 4.14. It was evident from the XPS results that all the coke samples contained greater amounts C=C and C-C bonds and trace amounts of oxygen, nitrogen, and sulfur components. Also, it can be seen from Table 4.5 that Coke 1 had the highest oxygen percentage whereas the Coke 3 had the lowest. The greater the oxygen percentage is, the higher is the possibility of forming bonds between coke and pitch functional groups, consequently, the wettability increased with increasing oxygen percentage. As it is well-known, bonds containing oxygen and nitrogen are more reactive. Also, the presence of COOH might play a key role in chemical reactions. Coke 1 and Coke 2 contained COOH functional groups but Coke 3 did not contain any. Therefore, it is possible that fewer

chemical bonds were formed between Coke 3 and the different pitch samples compared to the other two cokes both at 170°C and 190°C resulting in lower wettability of this coke. The lower nitrogen concentration in Coke 3 could be attributed to the presence of lower concentration of amine (C-N) groups. This probably acted against the interaction between pitch and coke and, consequently, decreased the wettability (higher contact angles) of Coke 3 by both pitches. CN, C-O, C=O, COOH functional groups are very reactive and form new chemical bonds with the CN, C-O, C=O, COOH components of the pitch, therefore, their presence resulted in better wetting. Also C=C groups help in wetting as it can undergo addition reaction. Furthermore, results obtained at both temperatures agree well with the trends found (Figures 4.1 and 4.2). In addition, Coke 3 had the highest sulfur percentage compared to those of the other two cokes. The presence of sulfur containing functional groups might increase the possibility of intra-molecular bonds and therefore reduce the wettability. This is also in accordance with the wettability results which indicated that Coke 3 was the least wettable.

Also, Coke 1 contained more C=C bonds than Coke 2 and Coke 3. Double bonds are more restrictive to movement compared to the single bond. The reason the double bonds are reactive is that they contain both sigma and pi bonds. Pi bonds are not as strong as sigma bonds and therefore easier to decompose and to react. Thus, the reactivity of pi bond is the reason for the reactivity of C=C bond. C=C can help in wetting as it can undergo addition reactions. This might be one of the reasons for the better wettability of Coke 1 by the pitches.

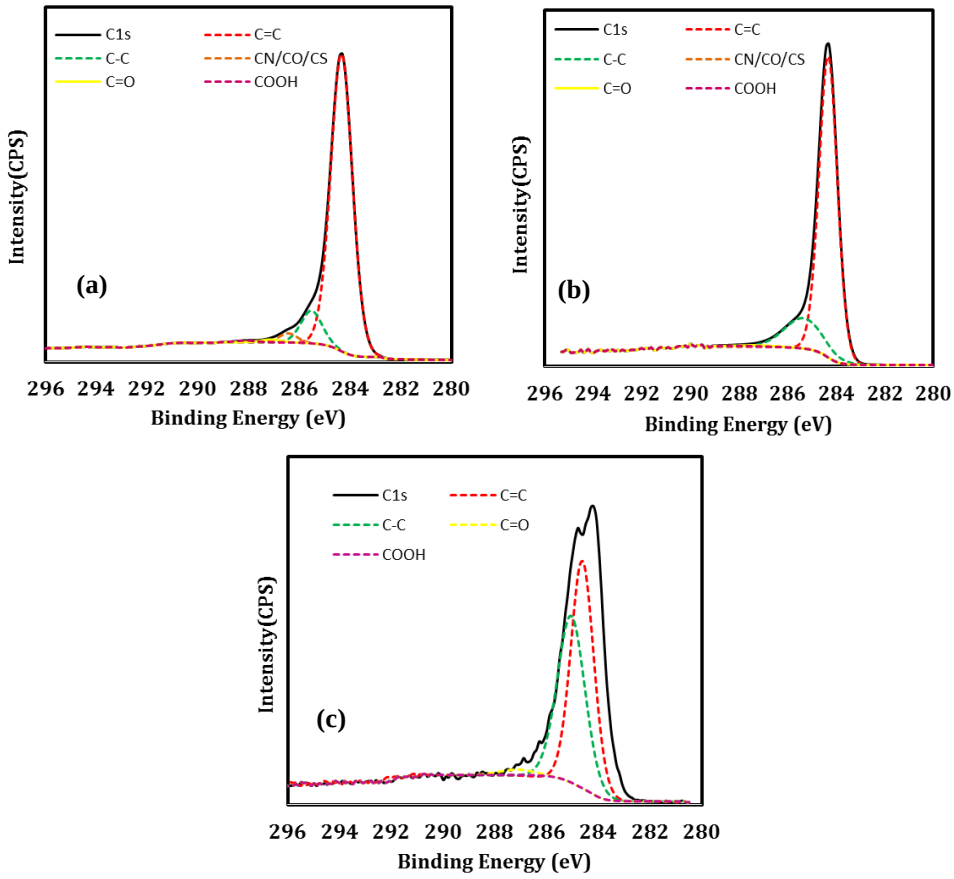

Figure 4.14. De-convoluted C1s peak of three cokes (a) Coke 1 (b) Coke 2 (c) Coke 3

Table 4.5.Atomic percentages of different components of three different industrial cokes

Coke Type	***C(%)***	***Carbon components***					***O(%)***	***N(%)***	***S(%)***
		C=C	**C-C**	**CN/CO/CS**	**C=O**	**COO**			
Coke 1	95.4	87.22	9.73	2.23	0.75	0.43	2.95	0.95	0.68
Coke 2	96.57	81.23	17.13	0.49	0.76	0.34	2.43	0.30	0.70
Coke 3	97.30	78.99	19.04	0.12	0.84	-	1.35	0.06	1.29

Atomic percentages of different components of two different coal tar pitch samples were tabulated in Table 4.6 for de-convoluted C1s spectrum. The de-convoluted C1s spectrum of coal tar pitches were presented in Figure 4.15.

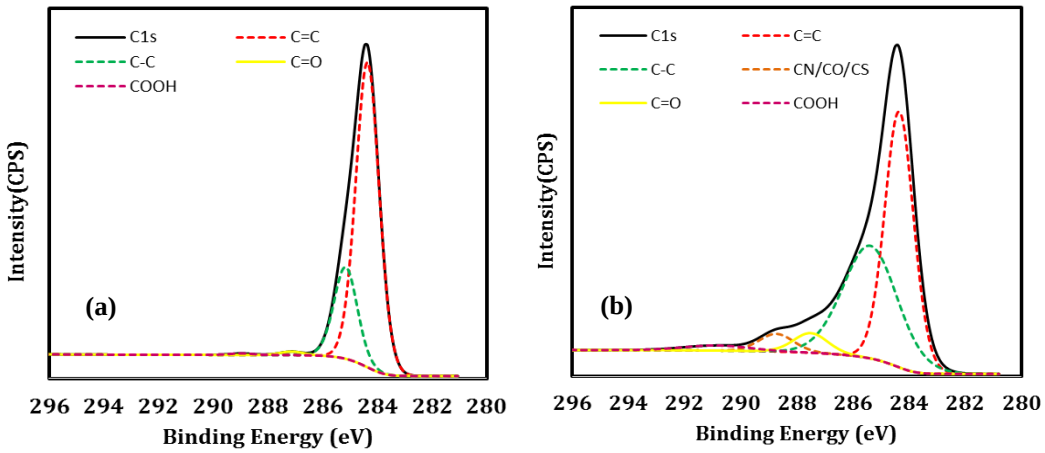

Figure 4.15. Deconvoluted C1s peak of two pitches (a) Pitch 1 (b) Pitch 2

Table 4.6. Atomic percentages of different components of two different industrial pitches

Pitch Type	***C(%)***	***Carbon components***					***O(%)***	***N(%)***	***S(%)***
		C=C	**C-C**	**CN/CO/CS**	**C=O**	**COO**			
Pitch 1	98.52	75.91	22.84	0.0	0.87	0.39	1.58	0.03	0.03
Pitch 2	92.40	48.62	40.63	4.46	4.06	2.23	4.15	3.21	0.26

The high resolution C1s spectrum of pitches shows that Pitch 2 contains high amounts of oxygen and nitrogen, which made it more reactive compared to Pitch 1. Therefore, in general, Pitch 2 wets the coke better than Pitch 1. This is also supported by the wettability test results. Usually, C=C bond in aromatic compounds helped in wetting by electrostatic bond. Thus, C=C bond in aromatic compounds need compounds with positive centres (such as $NH4^{+}$) for interaction. However, these kind of positive-centre compounds were not

present in any notable quantity in calcined petroleum coke. Thus, the low amount of C=C in Pitch 2 was not affected the wettability.

4.1.6 Analysis of coke-pitch interface

As can be seen from Figure 4.16, the optical microscopy of the sessile-drop sections provided useful information on the distribution of Pitch 2 within three different petroleum cokes since it was possible to observe relatively large areas at lower magnification. The drop sections for Pitch 2 with all three cokes were studied as it showed better wetting characteristic compared to Pitch 1 with the same cokes. This made the comparison of three different coke-pitch pairs' interfaces possible from the samples obtained after the wettability tests were carried out at 170ºC. Optical microscopy images showed good adhesion for all cases, but Pitch 2 penetrated better through Coke 1 compared to the other two cokes, which is in accordance with the wetting test results (Figure 4.16). As can be seen from this figure, the particles of Coke 1 are completely covered with pitch whereas there were void spaces between the particles of Cokes 2 and 3. The penetration behavior of Pitch 2 was relatively similar in Cokes 2 and 3. It was not possible to see if there is any reaction at the petroleum coke-coal tar pitch interface from the optical microscope images. SEM image analysis was conducted to detect the reaction zone at the interface using higher magnifications.

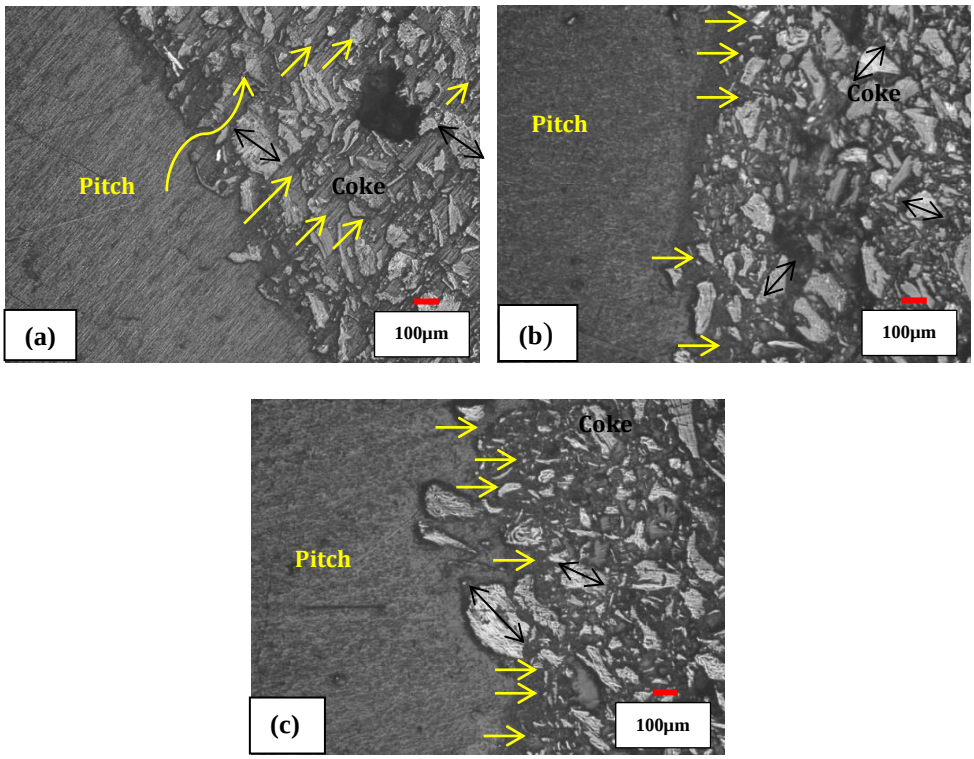

Figure 4.16. Optical microscopy analysis of the sessile-drop interface for (a) Coke 1, (b) Coke 2, (c) Coke 3 with Pitch 2 (Arrows indicate direction of pitch penetration)

It is also difficult to conclude from SEM image with certainty if any reaction has taken place at the coke-pitch interface but appearance of regions with different intensity and texture can suggest presence of reaction zones. In a reactive system, wetting frequently takes place as a result of the chemical reactions occurring at the interface (chemical wetting) due to formation of a new surface (reaction products) which is more favorable for wetting compared to the original surface. It is shown in Figure 4.17 (a) for Coke 1 that a white line was created around the coke particle which could indicate a reaction or accumulation of electron (due to the presence of sharp edges or poor conducting surfaces). To eliminate the possibility of electron accumulation, the samples were polished (to remove

sharp edges) and coated with gold-platinum layer (to have a good conducting surface). Also copper strips were used to facilitate the removal of charge from the sample. Therefore, it is quite likely that the white boundaries represent reaction zones. The SEM image at higher magnification (Figure 4.17 (b)) shows the deformation of the surface in the direction of pitch penetration. The same trend was displayed by Coke 2 and Coke 3 (Figures 4.18 and 4.19).

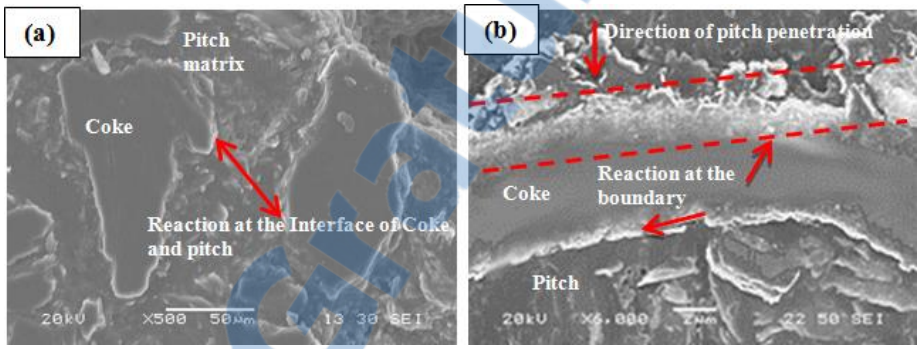

Figure 4.17. Scanning electron microscopy analysis of Coke 1/Pitch 2 interface after 1500s: (a) 500X magnification (b) 6000X magnification.

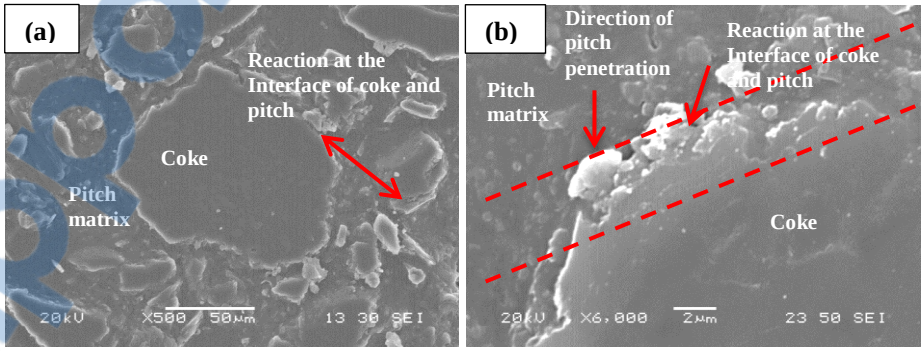

Figure 4.18. Scanning electron microscopy analysis of Coke 2/Pitch 2 interface after 1500s: (a) 500X magnification (b) 6000X magnification.

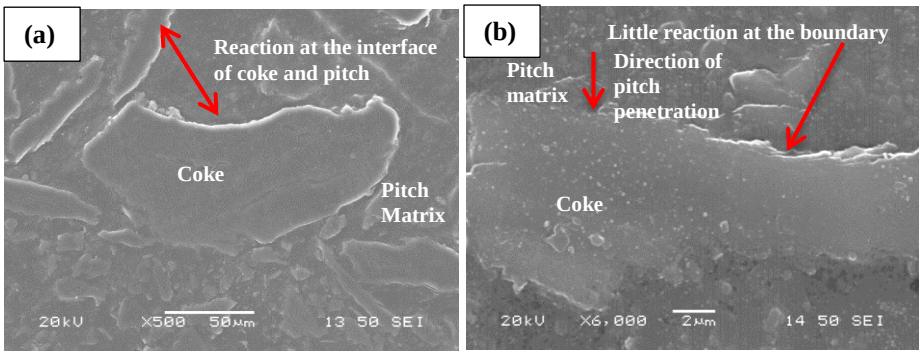

Figure 4.19. Scanning electron microscopy analysis of Coke 3/Pitch 2 interface after 1500s: (a) 500X magnification (b) 6000X magnification

It was evident from the SEM images that the degree of reaction was different for each coke. Coke 1 showed most reaction in the direction of pitch penetration than Coke 2 and Coke 3 (Figures 4.18 and 4.19). These results are well supported by wetting results. It is important to note that the reaction layer around the particles is not necessarily continuous and homogeneous.

4.1.7 Concluding remarks

The results showed that there was a significant difference between the final contact angle of Coke 1 and Coke 3 for both pitches at both temperatures studied. In general, the contact angle decreased with increasing time and temperature. This might be due to the fact that both the extent of the reaction between coke and pitch and the penetration of the pitch through pores increased as the temperature and time increased. The wetting results revealed that Pitch 2 wetted all three cokes somewhat better than Pitch 1, and both Pitch 1 and Pitch 2 penetrated better into Coke 1 compared to Coke 2 and Coke 3.

The effect of structural differences also seems to be important for wetting as per SEM and optical micrograph. Presence of higher porosity and higher average pore size also appears to be a contributing factor for better wettability of Coke 1. The results indicate that the regular texture and lowest porosity of Coke 3 affected its wettability which resulted in highest contact angle values (lowest wetting). Also Coke 1was more porous (see Table 4.1) which could lead to better penetration of pitches into the pores. Optical micrograph of Coke 1 revealed that it is wetted better by the pitch compared to the other cokes studied. The SEM analysis of the microstructure at the pitch-coke interface indicated formation of new phases. This implies that the wetting is chemical in nature. Coke 1 showed highest degree of reaction at the interface compared to other cokes, which facilitated the wetting.

The influence of the coke particle shape seems to be significant in such a way that the irregular non spherical structure of the Coke 3 particles resulted in highest values of contact angle (lowest wettability) compared to the spherical Coke 1 particles.

The FT-IR analysis of coke and pitch mixtures indicated the presence of chemical interaction between them shown by pronounced growth of carbonyl (C-O), aromatic hydrocarbon (C-H), and alkene or olefin (C=C) bonds for all three mixtures due to chain reaction between hydrocarbons and addition reactions between C-C bonds to form C=C (alkene) or to form ester (RCOOR) after reaction with the carbonyl group. The formation of these new functional groups can be explained using FT-IR spectra of the individual coke and pitch samples. The functional groups present in coke and pitch can react easily if there is less steric hindrance between the reacting molecules.

The FT-IR spectroscopy results showed that there was a difference in the chemical nature of cokes. The peaks in the range of 2800-2950 cm^{-1} were diffused for Coke 1 which had smaller lengths of aliphatic chains. This created less steric hindrance for wetting in the case of Coke 1, which might facilitate the formation of hydrogen bonds that improves its wettability. Cokes 2 and 3 had similar functional groups, but Coke 3 had lower porosity. This was probably another reason for the low wettability of Coke 3. The SEM images of coke-pitch interfaces illustrated the presence of reaction in the direction of penetration.

XPS results showed that Coke 3 was significantly different from the other two cokes in terms of chemical composition. Coke 1 had more oxygen and nitrogen groups which might be the reason for its better wettability as these two surface functional groups are easy to decompose and interact with those of pitch. Also Coke 1 contained more carbon double bonds which were reactive. However, Coke 3 contained high amount of C-S bonds on the surface which resulted in its low wettability of this coke by two pitches studied compared to the wettability of other cokes. This might be due to the possibility that S atoms on the surface of the coke might form intra or inter molecular hydrogen bonds which make them unavailable for hydrogen bonding with pitch.

Pitch 2 penetrated better into the coke due to its lower viscosity (Table 4.2) and higher nitrogen and oxygen functional groups compared to Pitch 1. The exact mechanism of pitch/coke interactions is still not clearly known and further work is needed to understand this mechanism.

4.2 Effect of coke crystallinity on the wettability of cokes by pitch

4.2.1 General

Under-calcined coke gained interest in anode production technology as it is reported that anode produced from under-calcined coke has lower reactivity and undergoes more homogeneous consumption during electrolysis. It is also important to have good bonding between the coke and coal tar pitch to produce dense anode. Wettability of calcined petroleum coke by molten pitch gives an idea about the quality of bonding between these two and affects significantly the final anode properties. In this study, effect of coke crystalline length on coke wettability by pitch was studied by means of sessile-drop test at 170°C (mixing temperature used in industry). Coke calcination temperature directly influences the coke crystalline length and coke crystalline length increases with increasing calcination temperature. It was found that final physical and chemical properties of coke are dependent on its calcination temperature, thereby, this temperature greatly effects the wetting properties. The chemical and physical properties of the coke calcined at different temperatures and pitch were studied using FT-IR and XPS and SEM.

4.2.2 Materials

In this study, four calcined petroleum cokes with different L_c and one coal tar pitch have been used for all the tests. The physical and chemical properties of the cokes and pitch are given in Table 4.7 and 4.8.

Table 4.7 Physical and chemical properties of coke

Properties	Calcined Petroleum Coke			
	Coke 24L_c	**Coke 28 L_c**	**Coke 30 L_c**	**Coke 34 L_c**
Bulk Density[1] (g/cc)	0.893	0.901	0.909	0.893
Sp. Electrical Resistance (μohm-m)	1117	1005	932	911
Real Density(g/cc)	2.038	2.058	2.075	2.070
CO_2 Reactivity (%)	9.6	5.2	7.0	3.6
Porosity for -125μm particle[2] (%)	8.1	6.5	6.1	4.9
Crystalline length(Å)	24.14	28.14	30.73	34.14
Ash Content[3] (%)	0.2	0.2	0.13	0.2
Moisture Content (%)	0.1	0.045	0.03	0.013
C[4] (wt%)	85.55	92.23	90.53	88.25
N[4] (wt%)	0.95	0.83	0.76	0.75
H[4] (wt%)	2.19	1.66	1.05	0.9
S[4] (wt%)	2.84	2.78	2.81	3.21

[1]Measured by ASTM D4292-10, [2]Measured by ISO 1014:1985, [3]Measured on dry basis. [3]Measured by proximate analysis.

Table 4.8 Physical and chemical properties of Pitch 8

Properties	**Pitch 8**
Ash at 900°C (%m/m)	0.12
β Resin (%m/m)	22.2
Density at 20°C (g/ml)	1.320
Quinoline insoluble (%m/m)	6.9
Toluene insoluble (%m/m)	29.1
Coking Value (%m/m)	59.1
Softening Point (°C)	119.6
Dynamic Viscosity 170°C (mPa.s)	1390
Surface Tension (dyne/cm) at 170°C	39.33

4.2.3 Contact angle test

The contact angle measurements of a pitch on a coke substrate are essential for understanding the spreading and penetration characteristics of that pitch, which indicates the degree of interaction between them and consequently the potential impact on anode quality. Figure 4.20 (a) compares the dynamic contact angles of the coal tar pitch and the four coke samples from the same source with different crystalline lengths. Coke 34L_c (over-calcined coke with the highest crystalline length) had a higher contact angle at all times

compared to Coke 24L_c (under-calcined coke with the lowest crystalline length). Coke 28L_c and Coke 30 L_c had contact angles in between Coke 24L_c and Coke 34L_c. The contact angles measured for Coke 28L_c and Coke 30L_c were similar up to 80 s; and then Coke 28L_c wetted slightly better and the pitch completely penetrated at around 120 s whereas a complete penetration was achieved around 140 s for Coke 30L_c. It is also clear from Figure 4.20 (b) that there was almost 9° difference in initial contact angles of these two cokes, but after the initial few seconds, the contact angles approached together. For all cases, the dynamic contact angles of coke-pitch pairs reduced rapidly and penetrated completely between 110 s and 160 s. Figure 4.20 (b) shows initial contact angle data for four cokes studied. It is noticeably seen that Coke 24L_c showed the lowest initial contact angle. Coke 30L_c and Coke 34L_c exhibited the highest and similar value for the initial contact angle.

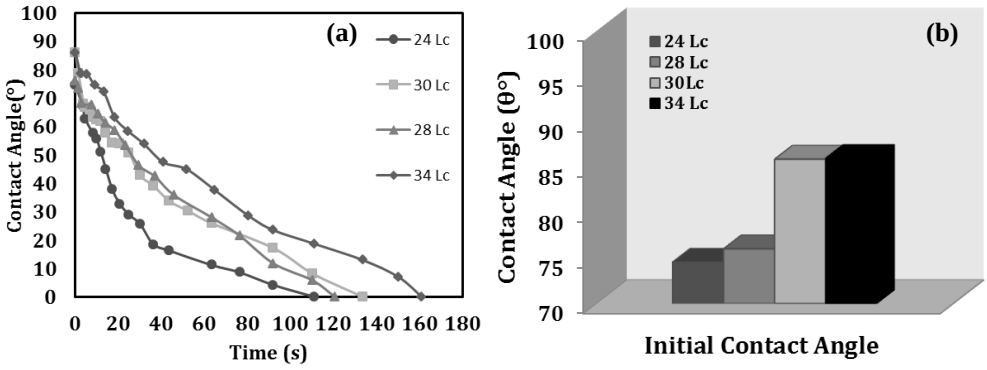

Figure 4.20 (a) Dynamic contact angles and (b) initial contact angles of Pitch 8 on four calcined cokes with different L_c

The work of adhesion of pitch-coke systems was calculated using the surface tension of pitch at 170ºC and the contact angles measured at 80s. These conditions correspond approximately to the temperature and the residence time of an industrial kneader in which

pitch and coke are mixed. The condition for perfect wetting is given by $W_a = 2\gamma_{lv}$ [161]. This means that the adhesion energy between the coke and the pitch should be twice the surface tension of the liquid which is mainly due to cohesive forces. The surface tension of pitch at 170ºC was calculated using the FTA32 software as 39.33 dyne/cm. The work of adhesion of pitch with Coke $24L_c$, Coke $28L_c$, Coke $30L_c$, and Coke $34L_c$ after 80s was 78.2, 75.91, 75.79, and 73.84 dyne/cm, respectively. These values indicated that the pitch-coke system exhibited a strong interface since work of adhesion calculated for all cokes are close to twice the value of the surface tension. Coke $24L_c$ had the strongest interface (strongest adhesion force, strongest pitch-coke interaction, hence best wetting) among all the cokes studied which were calcined at different temperatures. These trends are consistent with the contact angle results since Coke $24L_c$ was wetted most by the pitch as indicated by the lowest contact angle.

Anode-grade cokes used in industry have a crystalline length of around 30 Å, similar to Coke $30L_c$ here. This coke with the pitch used in this part of the study has displayed a different wetting behavior compared to the previous ones. Such differences could occur for different coke-pitch pairs due to the differences in their properties (source of the raw material, coke structure, chemical and physical properties, etc.).

4.2.4 Structural analysis

The structure of the coke plays an important role in wetting as well as in final anode quality. Structurally, sponge coke is preferred for anode production because it has a combination of low impurity levels, low air and CO_2 reactivity, a moderate coefficient of

thermal expansion (CTE), desired density, and enough open porosity to allow good interlocking and bonding with a binder pitch. The sponge coke structure is intermediate between the isotropic (fine grains and similar structure in all directions) and anisotropic (coarse grains) coke [24, 48].

SEM micrographs of the longitudinal surfaces at a high magnification are presented in Figure 4.21. This structure in calcined coke is commonly known as the lamella or flow structure. Figure 4.21 illustrates how the aligment of the lamella/flow structure improves with the calcination level (L_c values). It can be seen that the lamella structure was rearranged with increasing calcination temperature up to a certain level (up to Coke 30Lc). Above this level, it is difficult to distinguish the change in structure from the images. Coke 30Lc and Coke 34Lc show a better organized structure (see Figure 4.28 (c) and (d)). A possible reason could be that the interlayer defects of the basic structural unit of carbon reduced, and the crystallites started to grow larger with increasing calcination temperature.

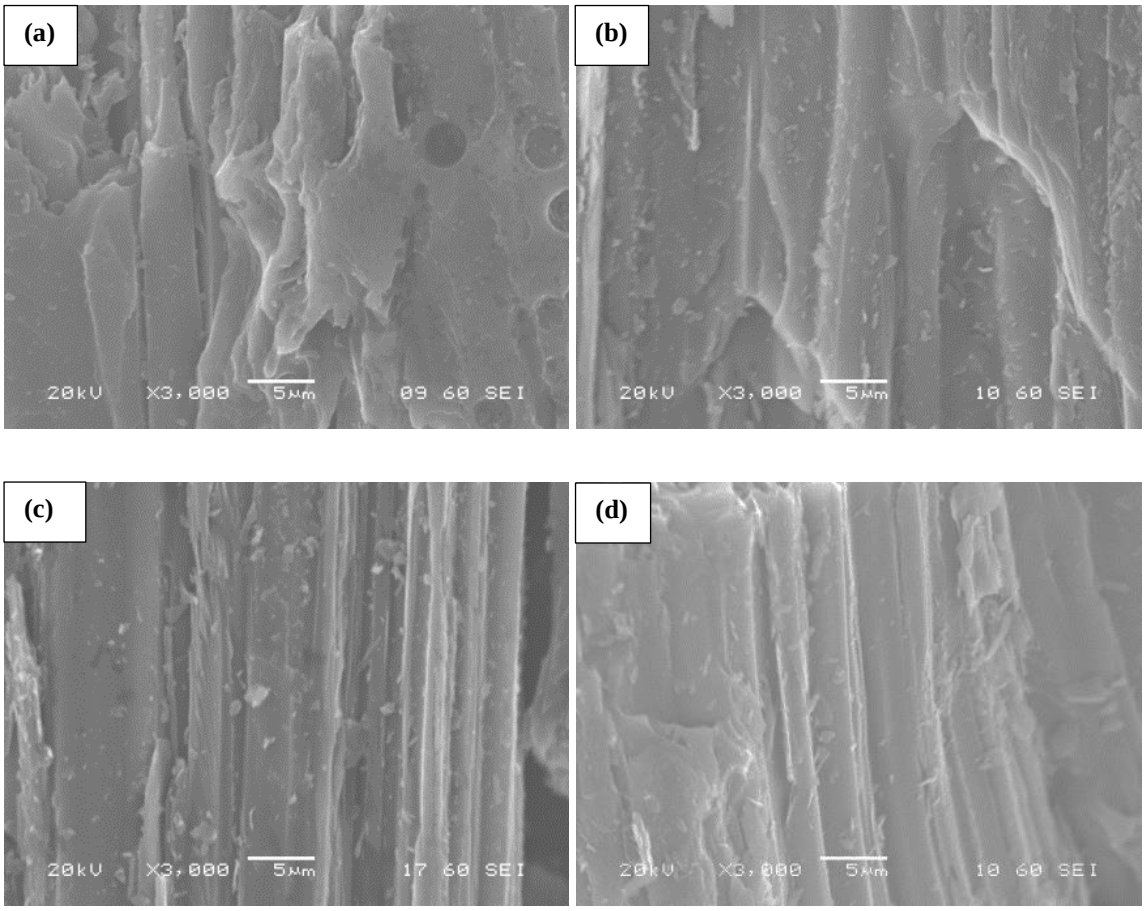

Figure 4.21 SEM images of the longitudinal surfaces of the four coke samples with different L_c values: (a) Coke 24L_c (b) Coke 28L_c (c) Coke 30L_c (d) Coke 34L_c

As seen in Figure 4.22, the transverse surfaces of the coke samples give an impression about their mosaic/granular structure and their association with pores. The figure shows the formation of coarse grains with increasing crystalline length which was directly related to the calcination level. At the highest calcination level studied (L_c of 34Å), the crystallites were largest, and as the interlayer defects reduced [11, 21, 22, 32, 39-43]. Due to that, probably less amount of pitch could enter into spaces. This resulted in higher contact angle and lower wettability.

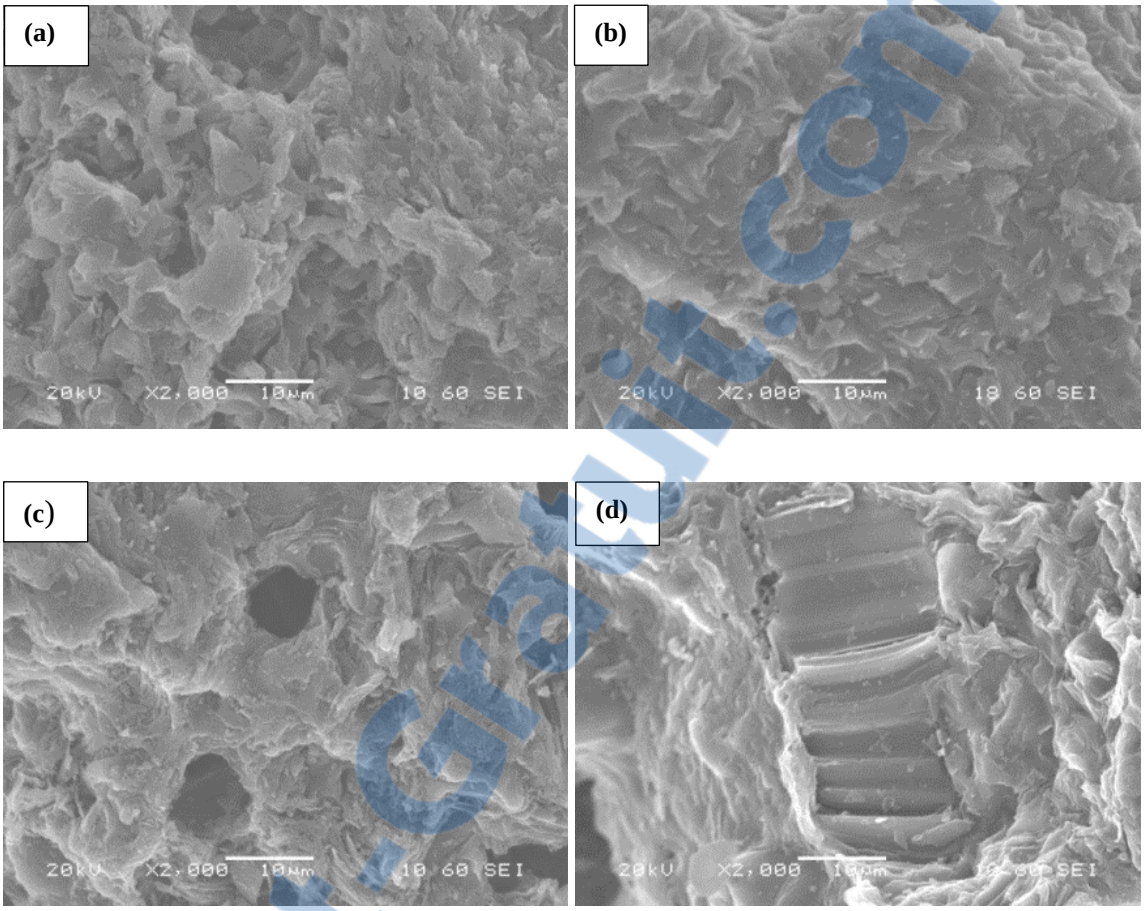

Figure 4.22 SEM images of transverse surface of the four coke samples with different Lc values: (a) 24 L_c (b) 28 L_c (c) 30 L_c (d) 34 L_c

Figure 4.23 displays the surface porosity for the four coke samples studied. This figure indicates that, the formation of micropores or inaccesible pores increased due further devolatilization with increasing calcination level. It is possible that larger dimension of pores helped pitch to penetrate better, consequently contributing to a better wettability for coke 24L_c, 28L_c, and 30L_c by pitch. On the contrary, micropores and microcracks were entrapped with air, and the presence of too many micropores created hindrance to the wettability of coke by pitch. This became evident during the coke apparent density

measurements since water could not enter these pores. It seems that the stucture strongly influenced the wettability of coke and affected the strength of coke-pitch bonding at the interface, hence the anode quality. However, scanning electron microscopy (SEM) can be used to visualize the surface texture of coke particles at nano-scale. SEM has a limitation to analyze large coke surfaces. Coke is highly nonhomogeneous and SEM images may not represent the actual pore distribution in the bulk of the coke sample.

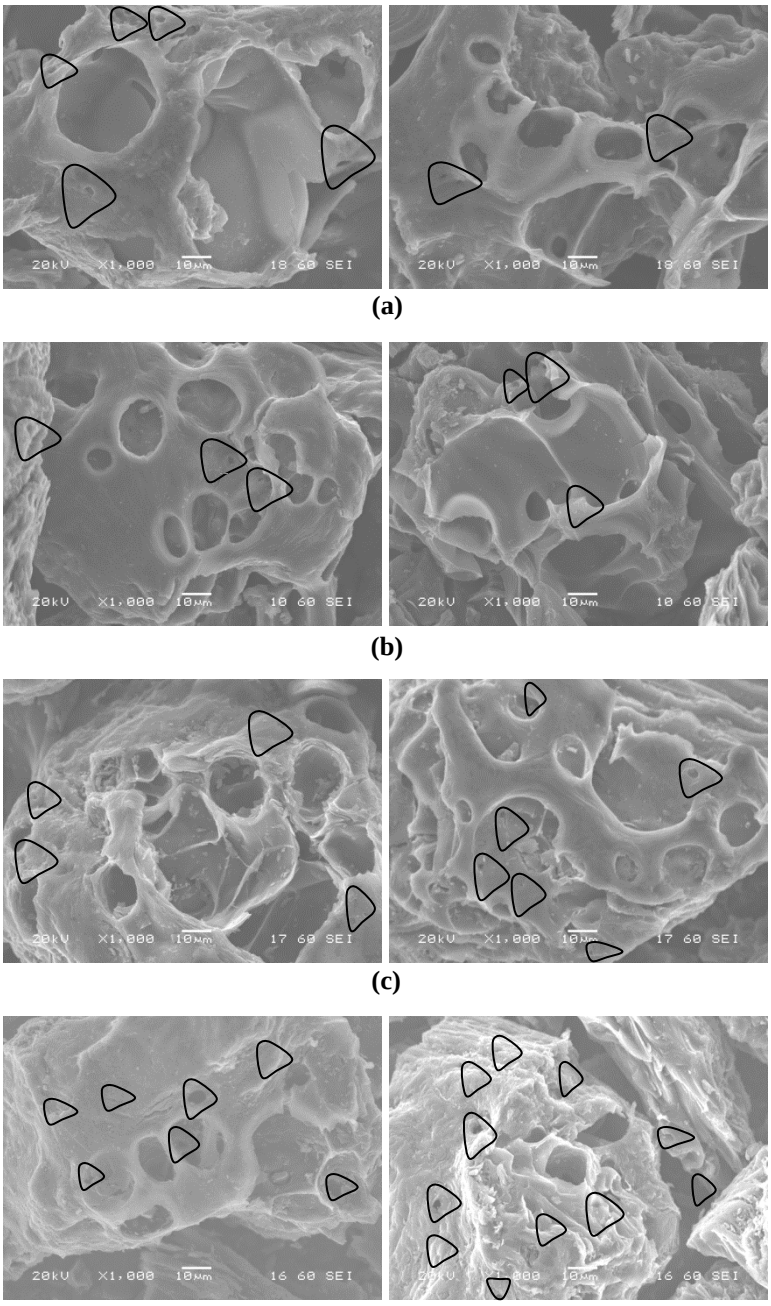

Figure 4.23. SEM images of the surface porosity distribution of the four coke samples with different L_c values: (a) Coke $24L_c$ (b) Coke $28L_c$ (c) Coke $30L_c$ (d) Coke $34L_c$

4.2.5 Chemical analysis

A qualitative analysis was performed to identify surface functional compounds using FT-IR. Usually infrared spectroscopy is sensitive to the presence of functional groups of organic compounds. The spectra of four cokes with different crystalline lengths (calcined at different temperatures) showed the following regions of interest (Figure 4.24): NH/OH stretching mode near 3200-3400 cm^{-1}, aromatic C-H stretching region near 3000-3100 cm^{-1} (C-Har), aliphatic C-H stretching modes between 2700 and 3000 cm^{-1} (C-Hal). Shoulders could be seen between 2100-2200 cm^{-1} from C=C stretching vibration, C-O-C vibrations from esters/ethers at 1100-1300 cm^{-1}, peaks around 1600 cm^{-1} from carbonyl groups. All of the four cokes showed a peak at 980 cm^{-1} which corresponds to C=C bending. The C=C vibrations can be attributed to the presence of aromatic rings as well as other organic compounds which have double bonds between carbon atoms. Substituted aromatic ring vibration in 700-900 cm^{-1} was observed for three cokes except for Coke $24L_c$. It was also found that Coke $30L_c$ had an overall lower intensity than other three cokes. For all the cokes, the sharp strong band near 3000 cm^{-1} was due to C-H stretching vibration in aromatics [27], and a clear peak around 2950 cm^{-1} was from aliphatic (sp^3 C) C-H asymmetric stretching vibration of alkyl substituents [27-29]. The broad weak band at 3254 cm^{-1} might not be only from the H bonded NH, but also from the OH stretching [27, 28]. Spectra corresponding to the band 2870 cm^{-1} was due to aliphatic C-H symmetric vibration [30, 31], and the band near 2750 cm^{-1} was from aliphatic CH stretching mode vibration [28, 29]. C-O (in plane C-OH bending) vibrations for ester/alcohol/acid was observed at 1343 cm^{-1} [32]. As it is known that coke contains carboxylic acid, C-O and C=O vibrations were

observed at around 1188 cm^{-1} and 1630cm^{-1} respectively. The peak around 1630cm^{-1} could be due to presence of carbonyl compounds. A C-O-C vibration of ether/ester and substituted aromatic ring vibration were detected around 1100 cm^{-1} and 790 cm^{-1}, respectively, for all the cokes with different L_c

In general, the FT-IR spectra of four cokes calcined at different temperatures were almost similar with regard to functionality although there were some qualitative and quantitative differences. It can be noted that the functionalities identified using the IR spectra for calcined coke are in accordance with the compounds found using NMR technique by other researchers for green petroleum coke. As calcined petroleum coke has a very low percentage of H, no signal (other than the background) can be detected by the NMR study [33]. The FT-IR and NMR studies demonstrated that the green petroleum coke consists of polynuclear aromatic hydrogen-deficient structures with few alkyl side chains as substituents and aromatic or naphthenic molecules such as naphthalene, phenanthrene, anthracene, tri-phenylene, benzo-pyrene, coronene, and pyrene [29, 30]. Thus, the presence of aliphatic and aromatic functional groups in calcined coke may be the result of the presence of the polynuclear aromatic and natphthenic molecules in the green coke.

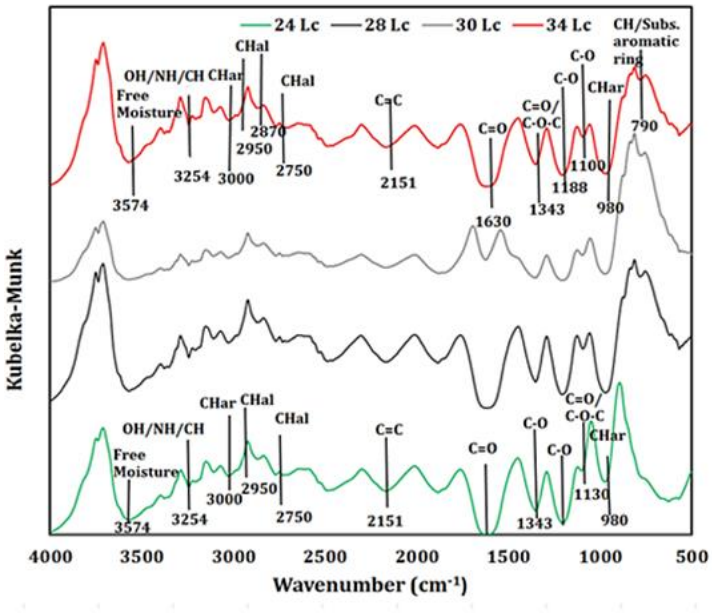

Figure 4.24. FT-IR spectra of four calcined cokes with different L_c.

Figure 4.25 shows the IR spectra of coal tar pitch used. Coal tar pitch is composed of poly aromatic hydrocarbons (PAH), polycyclic hetero aromatic compounds and their alkyl derivatives. Also, alkylated PAH, PAH with cyclopenteno moieties, partially hydrogenated PAH, oligo-aryl methanes, hetero-substituted PAH:NH_2, OH, carbonyl derivatives of PAH are present [104, 136, 144]. Nevertheless, CN, CO, CS, bond from compounds such as pyridine, furan, and thiophene, respectively, were not detected by FT-IR because peaks corresponding to these chemical functions overlapped. Pitch displayed a broad peak around 3452 cm^{-1} for moisture or free OH. Around 3048 cm^{-1}, a peak was observed due to aromatic CH stretching vibrations, and other peaks were detected due to aliphatic CH stretching vibrations on pitch surfaces around 2881 cm^{-1}. Numerous bands related to aromatic CH out-of-plane bending with different degrees of substitution were detected in the region of 700–900 cm^{-1}. A very sharp peak at 741 cm^{-1} was noticed due to o-substituted

aromatic ring vibrations [162]. A weak peak at 1910 cm^{-1} may be originated from carbonyl. The band at 1591 cm^{-1} was ascribed to aromatic C=C stretching. Multiple peaks were identified in the region of 1200–1300 cm^{-1} due to C-O (acid/alcohol)/CN vibrations, and those in the range of 1050–1150 cm^{-1} were due to the C-O stretching of acid/alcohol/ether/ester. Peaks around 1426 cm^{-1} and 1360 cm^{-1} appeared due to methyl substitution of aromatic rings [133, 158]. Petroleum coke and coal tar pitch contain complimentary functionalities which could lead to a number of reactions during mixing. The possibility of reactions between complementary groups could be explained with the following two examples. FT-IR study revealed that OH and O/N are present in coke and pitch. H of OH in coke can form hydrogen bond with strongly electronegative O/N atoms of pitch. Similar reaction can happen for the OH group present in pitch. Pi-electron cloud of the aromatic ring can form electrostatic bond with electron deficient centres such as N^{+} of quarternary ammonium group. The above information suggested that reactions may take place between pitch and coke during mixing.

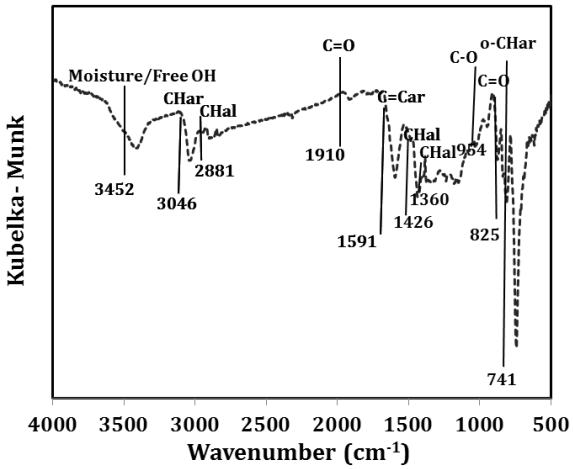

Figure 4.25. FT-IR spectra of Pitch 8

The chemical functionality of coke and pitch surfaces was identified by the FT-IR technique. During the XPS analysis, the information acquired from the FT-IR analysis was used to de-convolute the C1s peak. Atomic percentages of different components of the four calcined coke samples studied are presented in Table 4.9 for the survey spectra and de-convoluted C1s spectrum. The de-convoluted C1s spectra of these cokes are presented in Figure 4.26. It is evident from the XPS results that all the coke samples contained high amount of C=C and C-C bonds and trace amounts of oxygen, nitrogen, and sulfur components. Also, it can be seen from Table 4.9 that Coke $24L_c$ had the highest oxygen percentage whereas Coke $34L_c$ had the lowest. The greater the oxygen percentage is, the higher is the possibility of forming bonds between coke and pitch functional groups; consequently, the wettability increased with increasing oxygen percentage. It is also clear from Table 4.9 that an increase in the crystalline length of the coke consequently decreased the presence of oxygen- and nitrogen-containing functional groups; this was due to further devolatization at higher temperatures. Depending on the binding energy of C-O and C-N bonds in different organic molecules, the extent of the loss of O and N from coke might vary during the calcination process. For example, nitrogen could exist as amine or pyridine, but it is easier to remove nitrogen if it existed as amine. This might explain why 30Lc coke had a lower nitrogen percentage than that in 34Lc. It also suggests that there may be differences in functional groups of the green cokes. Oxygen and nitrogen atoms in an organic molecule usually pull the electron cloud of a bond towards themselves because of their high electronegativity. Also, the presence of COOH might play a key role in chemical reactions because this functional group could form hydrogen bonds and also undergo acid-

base reaction. Three of the four coke samples contained COOH functional groups; Coke $34L_c$ lacked them due to its calcination at much higher temperature. Therefore, it is possible that Coke $34L_c$ was able to form fewer chemical links with the pitch compared to the other three cokes at 170°C. The lower nitrogen concentration in Coke $34L_c$ could be attributed to the presence of lower concentration of amine (C-N) groups. This probably acted against the interaction between pitch and coke and consequently decreased the wettability (higher contact angles) of Coke $34L_c$ by the pitch. CN, C-O, C=O, COOH functional groups could form new chemical bonds with the functional groups attached to C-C/C=C components of the pitch; therefore, their presence resulted in better wetting. They could also help condensation reactions. These results were in agreement with the results of wetting tests (Figure 4.20). In addition, Coke $34L_c$ had the highest sulfur percentage compared to those of Coke 30Lc and Coke $28L_c$. However, Coke $34L_c$ shows less wetting. As such, sulfur also has high electronegativity. Regarding the chemical aspect of wetting, the percentage of electronegative heteroatoms may not always necessarily indicate better wetting through the formation of bonds. The structure of the compound containing the heteroatoms and the neighboring molecules may reduce the availability of heteroatoms through the formation of intra or inter-molecular bond. The sulfur-containing functional groups might have undergone intra or inter-molecular bonding and reduce the wettability. Coke $24L_c$ contains high amount of oxygen- and nitrogen-containing functional groups, which might supersede the effect of the presence of high sulfur concentration on wetting. It may be noted that nitrogen and oxygen have higher electronegativity compared to sulfur due to their small atomic size. Also, Coke 24Lc contains more C=C bonds than the other three cokes. While

double bonds are resilient than single bonds, they are also more preventive to movement. The reason the double bonds are more sensitive is that they contain both sigma-bond and pi-bond. Pi-bonds are not as resilient as sigma-bonds and therefore easier to decompose; thus a pi-bond is the one which increases the reactivity of C=C bonds. C=C can endure addition reactions whereas C-C has limited ability. The pi electron cloud of C=C can also help the formation of electrostatic bonds. This might explain why Coke 24Lc was wetted best by the pitch.

The de-convoluted C1s spectrum of the coal tar pitch is presented in Figure 4.27.The high resolution C1s spectrum of the pitch shows that it contained notable amounts of oxygen and nitrogen, which made it reactive towards calcined cokes. Often coal tar pitches contain high amount of C-C bonds. Usually, C=C in aromatic compounds helps in wetting by electrostatic bonding. Thus, C=C in aromatic compounds need compounds having a positive center (such as NH^{4+}) for interaction. However, these kinds of positive-centered compounds are not present in any notable quantity in calcined petroleum coke. Consequently, the low amount of C=C in pitch did not really affect the wettability.

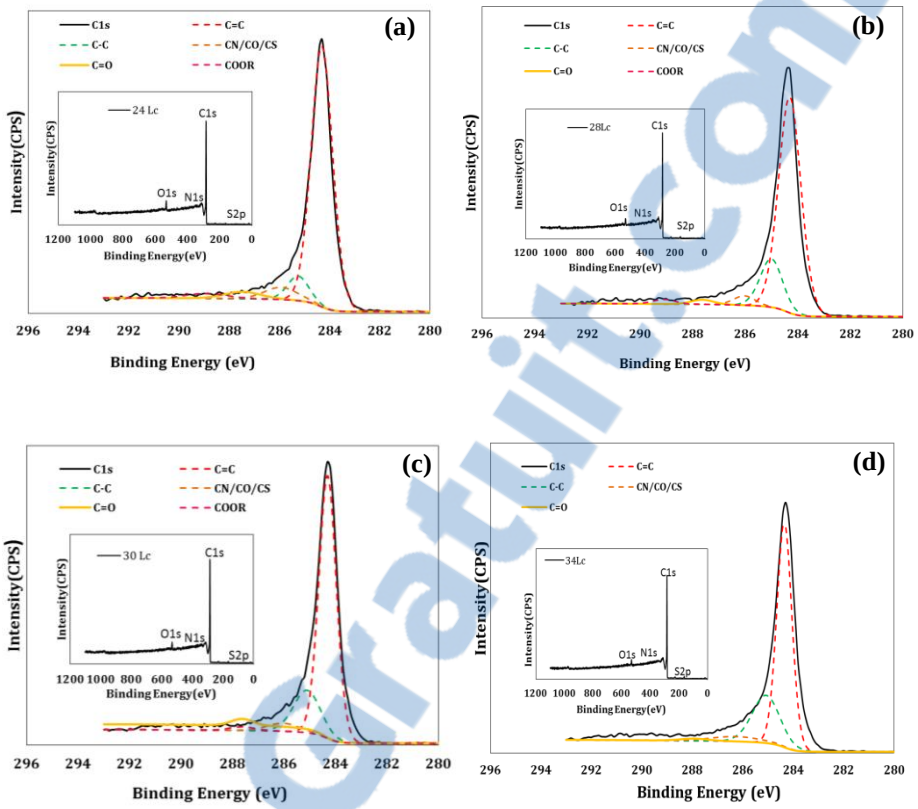

Figure 4.26 De-convoluted C1s peak of four different cokes (a) Coke 24Lc (b) Coke 28Lc (c) Coke 30Lc (d) 34Lc

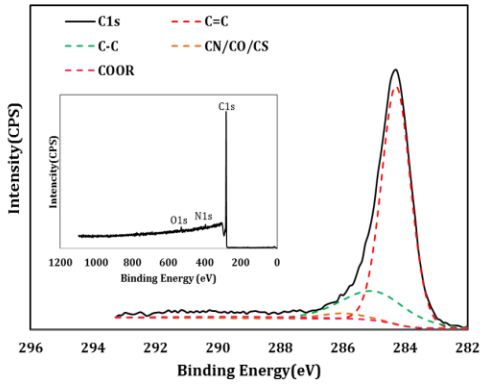

Figure 4.27 De- convoluted C1s peak of Pitch 8

Table 4.9.Atomic percentages of different components of four different calcined cokes and coal tar pitch

Coke Type	*C (%)*	*Carbon components*					*O (%)*	*N (%)*	*S (%)*
		C=C	**C-C**	**CN/CO/CS**	**C=O**	**COO**			
Coke 24L$_c$	94.2	79.99	7.57	5.84	3.66	2.94	3.23	1.86	0.7
Coke 28L$_c$	95.52	76.43	17.14	3.18	1.63	1.62	2.85	1.3	0.63
Coke 30L$_c$	96.69	74.50	18.68	4.10	1.26	1.46	2.43	0.06	0.36
Coke 34L$_c$	96.94	67.44	26.43	4.92	1.21	-	1.99	0.43	0.72
Pitch 8	97.77	74.48	20.72	2.74	-	2.06	1.16	1.07	-

4.2.6 Analysis of coke-pitch interface

Scanning electron micrographs of pitch-coke interface, which are taken from the cross-sections of the pitch sessile-drops placed on coke beds of -125 μm particles, are presented in Figure 4.28. It is evident from the FT-IR and XPS results that coke and pitch had complementary functional groups which could lead to reactions at the coke/pitch interface [158]. The amounts of functional groups present at the surfaces of four cokes studied were different, and thus it was expected that the degree of reaction at the interface would also be different. The SEM images at higher magnification show the possibility of formation of a new phase (reaction products) at the interface. The difference in the texture of material at the coke-pitch interface compared to those in the bulk of coke or pitch could be interpreted as the formation of reaction products. Also, the difference in composition at the interface, measured using EDX, suggested the possibility of presence of reaction products. As can be seen from Figure 4.28 (a) and (b), interphase of Coke 24L$_c$ and Coke 28L$_c$ with pitch seems

to have the highest amount of reaction products. These results are in agreement with those of the wetting tests and XPS results as Coke 24L_c exhibited the lowest contact angle and higher amount of chemical functional groups at the surface. This figure also indicates that an increase in the crystalline length reduced the reaction at the interface as the increasing calcination temperature decreased the surface functional groups, inter crystallites defects, and size distribution of the porosity. Figure 4.28 (d) shows almost no reaction products at the interface for Coke 34Lc (highly calcined coke).

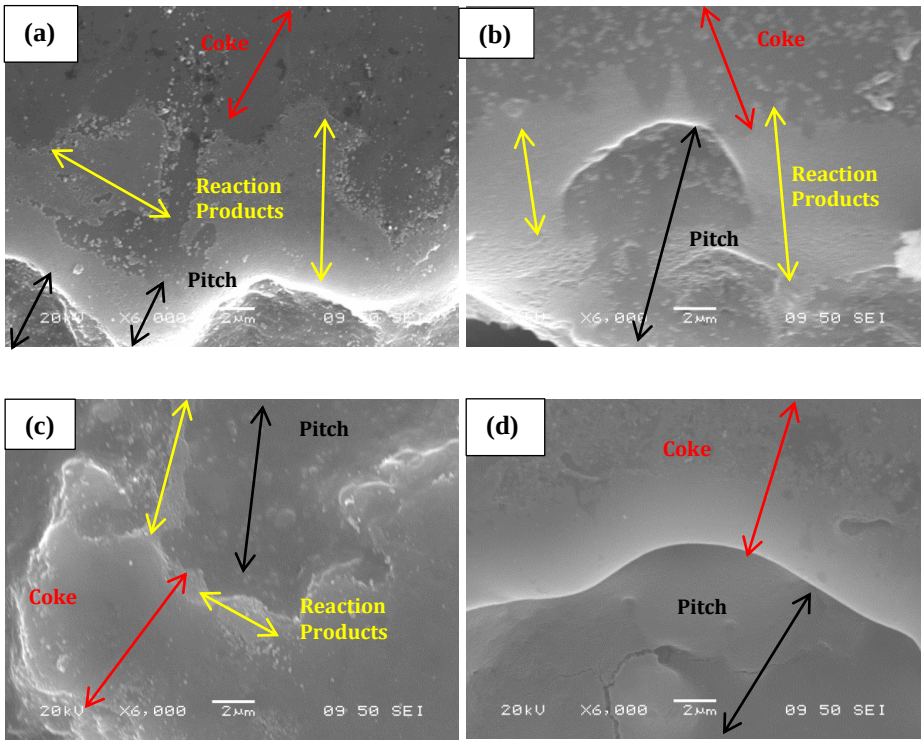

Figure 4.28 SEM images of coke/pitch interface (a) Coke 24L_c (b) Coke 28L_c (c) Coke 30L_c (d) Coke 34L_c

It should be noted that, EDX analysis gives an idea about the elements present in that reaction-induced zone (Figure 4.29). The EDX and XPS analysis of the pure 24L_c coke and

pitch (Figure 4.29(a) and (b); Table 4.9 and 4.10) indicates the presence of higher amount of carbon and lower amount of heteroatoms (oxygen, sulfur) compared to reaction-induced phase of Coke 24L_c/pitch interface. Therefore, this information indicates that there was a possibility of the formation of molecular species due to the interaction between the oxygen/sulfur-containing functional groups of the coke particles and pitch (Table 4.10).

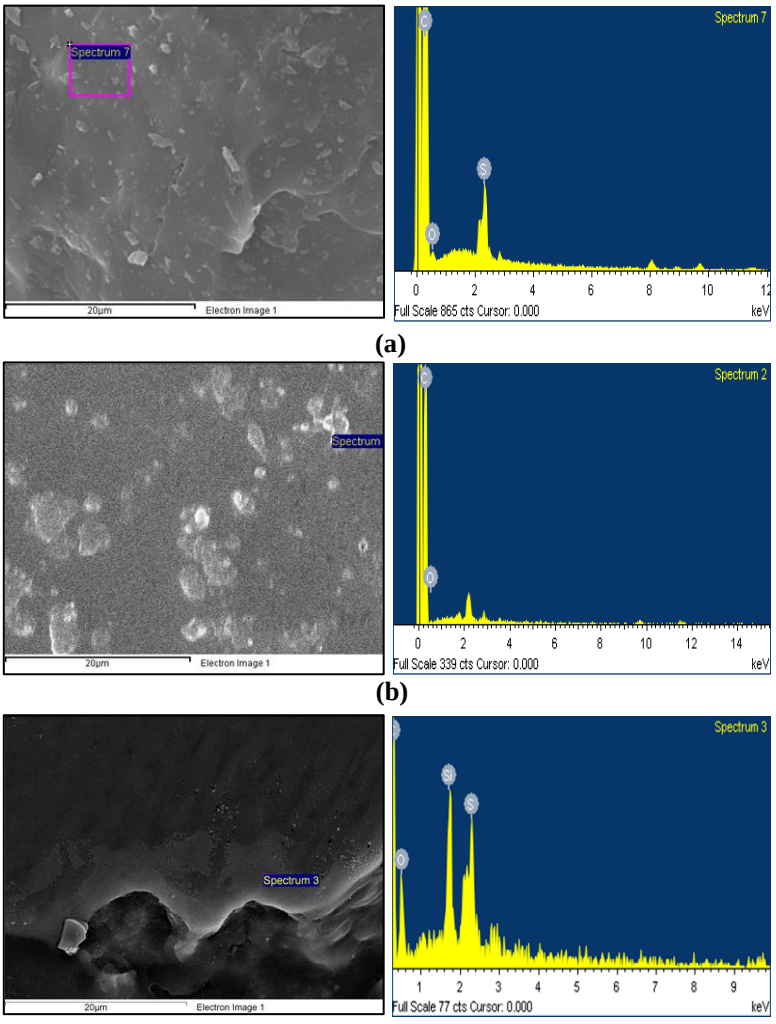

Figure 4.29 EDX analysis of (a) Coke 24L_c (b) Pitch 8 and (c) reaction products at the Coke 24L_c/pitch interface

Table 4.10 Atomic percentages of reaction products formed at the Coke $24L_c$/pitch interface, pitch and 24Lc coke

	Coke $24L_c$	**Pitch 8**	**Coke $24L_c$ /Pitch8**
Element	**Atomic %**	**Atomic %**	**Atomic %**
C	97.27	95.61	81.04
O	2.29	4.39	16.04
Si	-	-	1.59
S	0.44	-	0.72

4.2.7 Concluding remarks

There was a substantial difference between the final and initial contact angles of Coke $24L_c$ and Coke $34L_c$. In general, all the cokes were wetted by the pitch, and all the coke/pitch pairs can be stated as wetting. In this study, the results show that the contact angle decreased with increasing time for a given coke-pitch pair. This might be due to the fact that both the extent of reactions between coke and pitch and the penetration of pitch through the pores increased with time. The FT-IR spectroscopy results did not detect significant difference in the chemical nature of the cokes despite a few variations. Coke $24L_c$ was slightly different from the other three cokes. It was difficult to conclude the exact chemical structure of the coke and the pitch by this method, but the results indicated the presence of different complementary functional groups in coke and pitch. The presence of these complementary functional groups suggested the possibility for the occurrence of reactions at the coke/pitch interface.

XPS results show that all the cokes were significantly different from each other in terms of their chemical composition. Oxygen content in coke reduces as the crystalline length

increases. Oxygen and nitrogen containing functional groups in calcined cokes might be the reason for better wettability they can easily interact with those of pitch. Similarly, Coke $24L_c$ contained more carbon double bonds which are reactive. The C=C decreased with increasing calcination temperature. Coke $34L_c$ contained high quantities of carbon and sulfur bonds on the surface which might decrease wettability by pitch compared to the wettability of other cokes. This might be due to the possibility that sulfur atoms on the surface of the coke might have form intra or inter-molecular hydrogen bonds, which made them unavailable for hydrogen bonding with pitch. Coke $24L_c$ contained the same amount of sulfur as Coke 34Lc, but higher amounts of C=C, COOH, CN, CO bonds. The presence of higher amounts of oxygen and nitrogen atoms might have played a greater role than that of S content. It is possible that Coke $34L_c$ was less reactive compared to other three cokes. The porosity of the cokes gradually decreases with increasing crystalline length. This was probably another reason for the lower wettability of Coke $34L_c$. In general, further devolatization at higher temperatures created additional porosity; but, probably most of them were micro pores or inaccessible pores. The porosities of Coke $28L_c$ and Coke $30L_c$ were very close, and this might be the reason for their similar wettabilities by pitch. Also, the SEM analysis showed that inter-crystallite defects decreased as the crystalline length increased, and this acted against wettability. The SEM image of a coke, which is highly nonhomogeneous, cannot show the actual pore distribution of the bulk of the coke sample due to small sample size, but it showed the structural rearrangements which occurred as the calcination temperature increased. The SEM images indicated the presence of reaction at the coke/pitch interface, and the degree of reaction seems to decrease with increasing

crystalline length. This study showed that under-calcined coke was most wetted by pitch and had a strong interface. Thus, the presence of porosity, C=C bonds, and oxygen were important factors for better wetting of coke by pitch. However, under-calcined coke has low real density which probably decreases the anode density. To understand the effect of using under-calcined coke on anode properties, anodes should be made from under-calcined coke, and properties should be compared with those of the anodes produced from standard calcined coke.

4.3 Wetting characteristic of recycled anode butts

4.3.1 General

Prebaked anodes are produced from aggregates (calcined coke, recycled butts and anodes) and binder pitch. Good binding between aggregates and pitch results in dense anodes and has a direct impact on the anode electrical resistivity. The quality of coke and butts has a strong influence on anode properties. A comprehensive study of the physical and chemical interactions taking place during mixing allows a better understanding of the important factors and helps determine conditions that will lead to improved anode properties. The objective of this part was to characterize the surface properties of a calcined petroleum coke and recycled anode butt and then relate them to their wettability by pitch. The wetting tests were carried out using the sessile-drop method. Further investigations were carried out using SEM, FT-IR, and XPS.

4.3.2 Materials

In this study, Coke 1 and industrially recycled anode butt were compared. Pitch 2 was used for all the tests. The physical and chemical properties of the cokes and pitches are given in Tables 4.1 and 4.2.

4.3.3 Contact angle test

The contact angle measurements of coal tar pitch on the dry aggregate (petroleum coke and recycled anode butt) are valuable for having an idea about their compatibility. In this section, the wettability results of Coke 1/Pitch 2 pair (best standard calcined coke-pitch pair with lowest contact angle, hence, highest wettability of this study) was chosen for comparison with those of the recycled anode butt. Figure 4.30 compares Coke 1 and recycled anode butt dynamic contact angles obtained with Pitch 2. The initial contact angle of calcined petroleum coke and recycled anode butt differed by 9º. The wettability increases (contact angle decreases) with time for both coke and butt. Recycled anode butt had a lower contact angle compared to petroleum coke at all times, showing that the butt was wetted better than the coke by pitch. It is observed that the contact angle for recycled anode butt decreased very rapidly and pitch completely penetrated through the butt surface and particle bed within 133 s (0º contact angle). On the other hand, the final contact angle was found to be 18º for calcined petroleum coke even after 1500 s. The wettability tests gave information not only on the penetration of the liquid into the solid substrate but also on the spreading of the liquid on the substrate. The spreading of pitch on the recycled anode butt was found to be faster than the spreading on the petroleum coke. In order to investigate

the penetration characteristic of coal tar pitch, the images of the pitch drop as well as the sections of the anode butt and petroleum coke samples were taken using an optical microscope after the wettability tests.

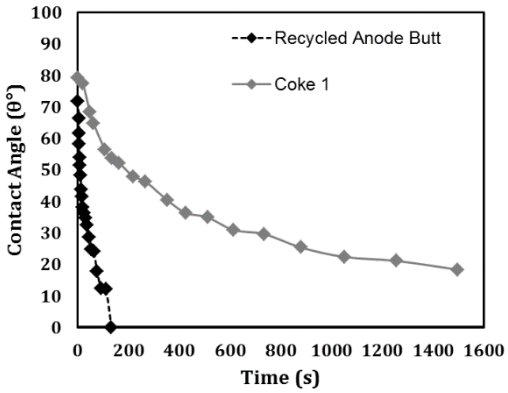

Figure 4.30 Comparison of the wettability of butt and calcined petroleum coke by coal tar pitch

4.3.4 Structural analysis

Figures 4.31 (a) and (b) demonstrate the structural integrity and differences between Coke 1 and recycled anode butt samples, respectively. As discussed before, Coke 1 surface contained pores and cracks, and the presence of well-aligned basal layers of carbon was evident (Figure 4.6 and 4.31 (a)). The dimensions of some pores were very small although there were also larger pores. Earlier it was mentioned that the presence of very small pores prevent the penetration of pitch into coke particles [40] and reduces the wetting of coke by pitch due to air entrapment into pores. Recycled anode butt surface also contained different size pores. The results of this study also indicated that surface irregularity is higher on the butt surface containing sharp edges. Tran and Bhatia [36] stated that the total pore area

decreases with heat treatment at higher temperature as a result of increase in the graphitization level of coke. Also, the butt particles already contain pitch carbonized previously during baking in some of its pores. Therefore, anode butt might contain less micro-pores and different surface characteristics which might lead to higher wetting compared to coke.

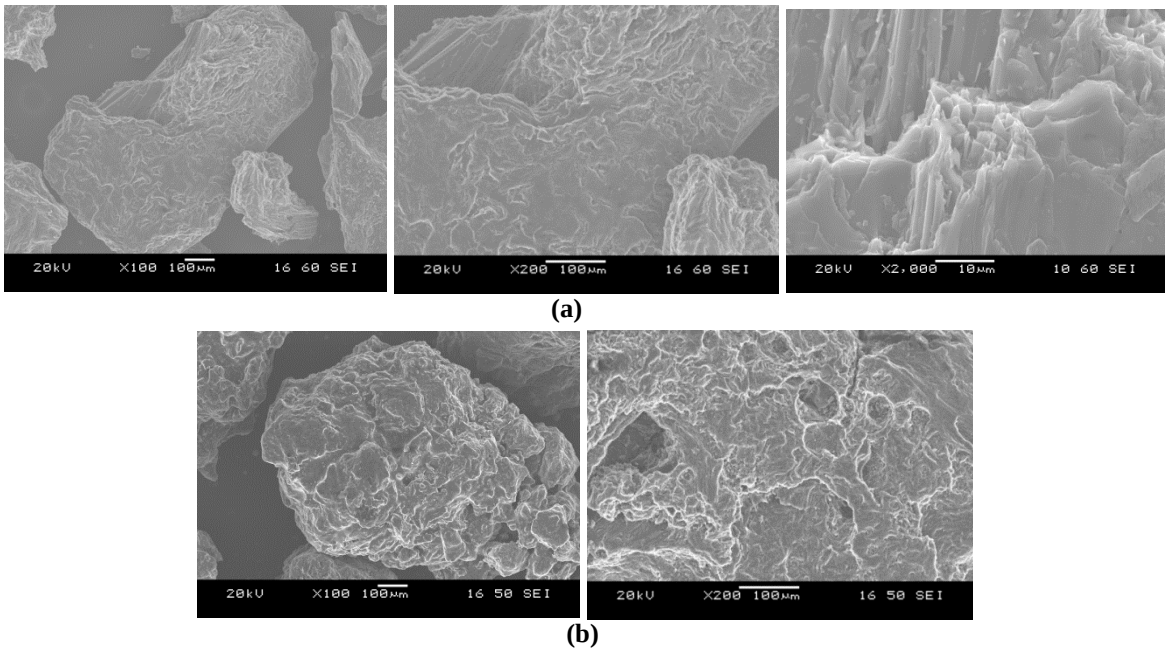

Figure 4.31 SEM image analysis of (a) Coke 1 and (b) recycled anode butt

4.3.5 Chemical analysis

SEM/EDX analysis was performed to study the surface chemistry of the coke and the butt. The presence of sodium on butt surface confirmed the sodium penetration into the anode during electrolysis. The analysis also displays presence of higher oxygen since anode was subjected to electrolysis. It is also possible that the presence of different impurities and greater amount of oxygen on butt surface might enhance the chemical wetting and lower

the contact angle compared to that of coke. The results of EDX analysis of anode butt and Coke 1 are given in Table 4.11.

Table 4.11 Chemical composition of recycled anode butt and petroleum coke by EDX analysis

Elements	Recycled Anode Butt (wt%)	Coke 1(wt%)
C	87.21	92.47
O	8.76	4.73
Na	0.28	-
S	3.14	2.78
K	0.60	-
Total	100.00	100.00

FT-IR analysis of recycled anode butt was carried out to identify different surface functional groups and also to compare with those of calcined petroleum coke. The assignments of the bands were performed based on the literature of FT-IR data for green coke [128] and pitch [134]. Figure 4.32 shows the DRIFTS analysis of the anode butt and coke samples. It is evident from Figure 4.32 that FT-IR spectra of calcined petroleum coke and recycled anode butt were distinctly different from each other. FT-IR analysis shows the presence of aliphatic (2850-3000 cm^{-1}) and aromatic (3000-3100 cm^{-1}) hydrocarbons, C-N/C-O (1200-1300 cm^{-1}), C-O stretch for ester/ether/alcohol (950-1150 cm^{-1}), substituted aromatic C-H (700-900 cm^{-1}), CN (2100-2160 cm^{-1}) in both coke and anode butt.

Anode butt and petroleum coke both might contain COOH functional group as appeared from the transmittance bands around 3530 $cm^{-1}$and 1126 cm^{-1}. At around 3040 cm^{-1} transmittance band, petroleum coke showed the presence of aromatic CH in which carbon is in sp^2 hybridized state whereas this bond was missing in recycled anode butt. Peak around 2100-2160 cm^{-1} for anode butts appeared to be mainly due to presence of nitrile

groups. There was also a possibility of a presence of small peak for C≡C (2130-2150 cm^{-1}) in this region [163]. This peak was not significant in the case of calcined petroleum coke. Peak at 2349 cm^{-1} transmittance band was due to CO_2 which was not considered for analysis. Since Coke 1, anode butt, and Pitch 2 (Figure 4.12) contain complimentary functional groups, there is a possibility that the functional groups on the coke and butt surfaces might interact with those present in pitch. Pitch contains mostly polycyclic aromatic hydrocarbons (PAH) [134]. This shows that there is a possibility of the formation of electrostatic as well as hydrogen bonds between coke or butt and pitch during wetting.

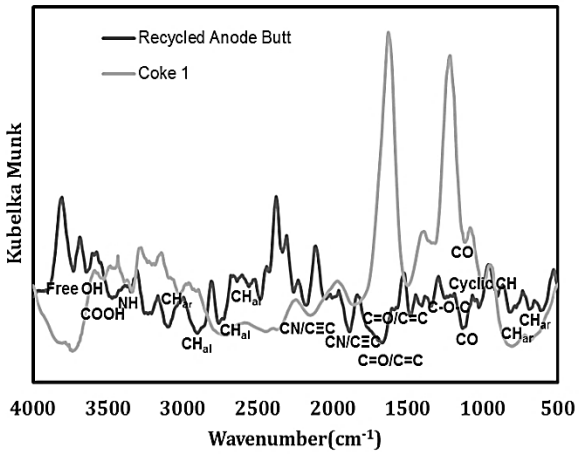

Figure 4.32 FT-IR spectra of calcined petroleum coke and recycled anode butt by DRIFTS technique

FT-IR analysis was used to identify the chemical functionality of the calcined petroleum coke and the recycled anode butt. Data acquired from FT-IR analysis were used to execute the de-convolution of C1s peak for the XPS data for a given coke or pitch. The de-convoluted C1s spectrum for anode butt was very different than that for petroleum coke. XPS spectra of anode butt comprises of a separate large peak for C-C at 285.5 eV. Atomic

percentages of different components of calcined petroleum coke and recycled anode were presented in Table 4.12 for the survey spectra and de-convoluted C1s spectrum. The de-convoluted C1s spectra of calcined petroleum coke and recycled anode butt were illustrated in Figure 4.33. It could be observed from this figure that butts had a significant amount of C-C because it was exposed to high temperature during baking which may have modified its properties. For this reason, coke and butt properties differed. However, butts contained less amount of C=C compared to that of calcined coke. Usually C=C in aromatic compounds helped wetting through electrostatic bond formation. Thus, C=C bonds in aromatic compounds needed compounds with positive centres (such as $NH4^{+}$) to establish an interaction. However, these kinds of electron-deficient functional groups were not present in notable quantity in pitch. Thus, the low amount of C=C in butts did not significantly affected its wettability. It was evident from the XPS results that recycled anode butts contained higher amounts of heteroatoms (O, N) and sodium (Na) compared to those in calcined petroleum coke (Table 4.12). The functional groups with heteroatoms might form covalent/ hydrogen bonds with conjugate functional groups and assisted wetting. Thus, the difference in the amount of heteroatoms in coke/butts might explain the difference in their wettability by pitch.

Table 4.12 Atomic percentages of different components of calcined petroleum coke and recycled anode butt

Sample	C (%)	Carbon components					O (%)	N (%)	S (%)	Na (%)
		C=C	C-C	CN/CO/CS	C=O	COO				
Coke 1	95.4	87.22	9.73	2.23	0.75	0.43	2.95	0.95	0.68	-
Butt	90	50.69	29.57	5.60	8.34	4.60	7.46	1.15	0.40	0.99

The greater the oxygen percentage is, the higher is the possibility of bond formation between recycled anode butt and pitch functional groups; consequently, the wettability increased with increasing oxygen percentage. As it is well-known, bonds containing oxygen and nitrogen are more prone to reactions which increase its interaction with coke. Also, the presence of greater amount of COOH in butt (see Table 4.12) seemed to play a role in the initiation of chemical reactions. The acidic COOH group in butt could react with the basic NH_2 group in pitch. Consequently, it was possible that presence of lower amount of heteroatoms on the surface of Coke 1 compared to those on butt surface resulted in formation of fewer chemical bonds between this coke and Pitch 2 than the number of bonds formed between the recycled anode butt with the same pitch. It was also possible that the presence of lower concentration of amine groups on coke surface due to lower nitrogen concentration in coke resulted in lower wettability of coke compared to the wettability of butt.

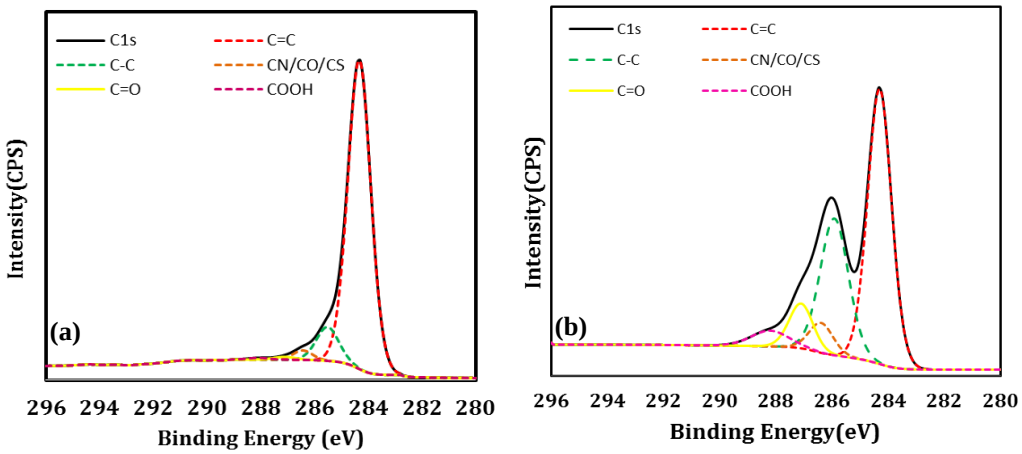

Figure 4.33 De-convoluted C1s peaks of (a) Coke 1 (b) recycled anode butt

4.3.6 Analysis of coke-pitch and butt-pitch interfaces

The optical microscopy of the sessile-drop sections provided useful information on the distribution of the coal tar pitch within the butt and the petroleum coke beds since it was possible to observe relatively larger areas at low magnification. This made the comparison of coke-pitch and anode butt-pitch interfaces possible from the samples obtained after the wettability tests carried out at 170ºC. Optical microscopy images showed good adhesion for both cases, and pitch penetrated completely through the recycled anode butt particles (Figure 4.34). It was hard to conclude from the optical microscope images if there was a presence of interfacial reaction. The presence of reaction at Coke 1/Pitch 2 interfaces is already discussed in section 4.1.1.6 (Figure 4.17)

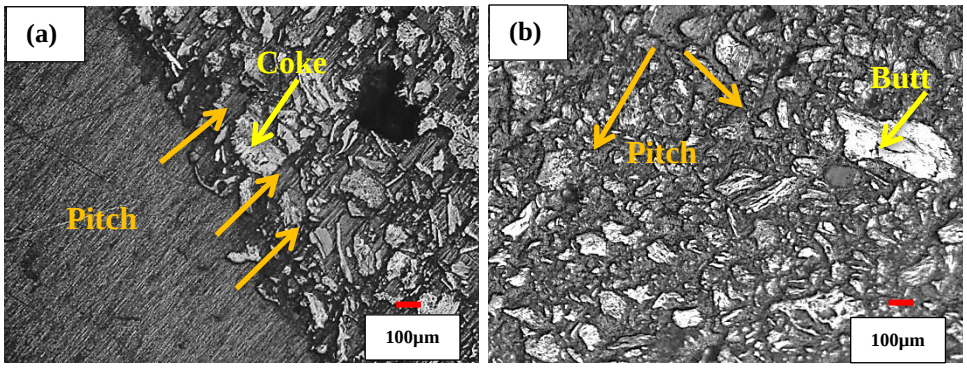

Figure 4.34 Optical microscopy analysis of the sessile-drop interface: (a) Coke 1/Pitch 2 (b) Butt/Pitch 2

It was difficult to directly confirm the presence of a reaction phase at a butt-pitch interface using an SEM image at lower magnification but the white lines around the particles were possibly reaction products (Figure 4.35 (a)). The SEM images at higher magnification (Figure 4.35 (b)) seemed to better illustrate the formation of a new reaction phase at the interface. It was found in the previous analysis that recycled anode butt contained higher quantity of hetero atoms which could lead to reaction at the interface and improve the wetting. The EDX analysis results revealed that presence of higher amount of carbon, nitrogen, oxygen and insignificant amount of sodium, sulfur and vanadium in butts (see Figures 4.11, 4.36 and Table 4.13).

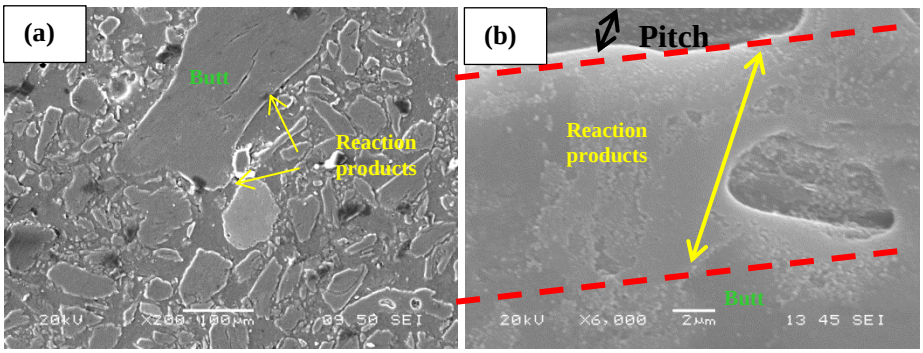

Figure 4.35 SEM images of the sessile-drop interface of Butt/Pitch 2 (a) 200X (b) 1000X

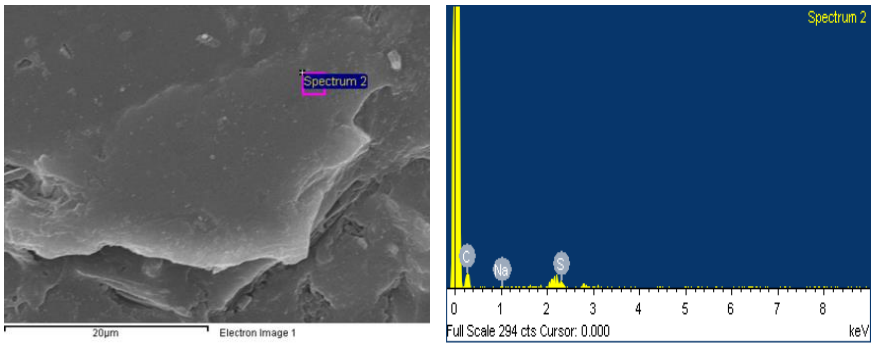

Figure 4.36 EDX analysis of reaction products at the Butt/Pitch 2 interface

Table 4.13 Atomic percentages of reaction products formed at the Butt/Pitch 2 interface measured by EDX

Elements	Atomic %
C	57.54
N	37.24
O	4.80
Na	0.20
S	0.17
V	0.05

4.3.7 Concluding remarks

The results showed that the butt particles had a lower contact angle; consequently, they were better wetted by pitch than the coke particles for the samples studied. Optical microscopy revealed the higher penetration of pitch through the butt particles compared to that of petroleum coke. The SEM analysis revealed appearance of reaction induced phase at interface of butt and Pitch 2. These behavior might be the result of the presence of more oxygen containing functional groups in the anode butt compared to the coke. FT-IR analysis indicated the presence of surface functional groups in both coke and anode butt which could lead to chemical bonding with coal tar pitch , hence, wetting. EDX results showed the presence of Na which was probably due to anode's exposure to cryolite. Also EDX of butt sample indicated high concentration of oxygen containing functional groups which were likely due to air and CO_2 reactivities in anode [71].

4.4 Utilization of different statistical tools to analyze and predict the influence of raw material composition and impurities on contact angle

4.4.1 General

As it was already discussed, good interaction between coke and pitch is essential for the generation of a satisfactory bond between them, and the contact angle is a measure of this interaction. A program was developed using the linear multivariable analysis to predict the contact angle for a given coke/pitch pair at different times. Normalized coke and pitch properties and their corresponding contact angles were used to determine the coefficients.

Normalization means adjusting values measured on different scales to a notionally common scale to present data with similar significance. In this study, a normalization technique was used to bring all values into the range 0 to1 (Equation 4.1). The precision of the model depends on the amount of data available for training and the linear dependency of the input and output variables. The value and the sign of the coefficients indicated the effect of the input parameters on the contact angle. The model gave information on the effect of raw material properties such as composition and impurities on the contact angle.

Multivariable analysis techniques such as linear multivariable analysis and regression analysis are some of the commonly used techniques to study the effect of input parameters on the output properties. Linear multivariable and regression analyses require the assumption of well-defined mathematical relationships between the dependent and independent variables. Thus, its predictions may not be accurate for the cases which do not have such a relation.

As there is usually no well-defined mathematical relationship between the composition and impurities of the raw materials and the contact angle, it is hard to accurately predict changes in contact angle as a function of their concentrations using these analytical tools.

In these cases, the artificial neural network (ANN) could be a useful predictive tool to analyze the effect of composition as well as impurities of pitch and coke on a contact angle. ANN processes information in a similar way the human brain does. The network is composed of a large number of highly interconnected processing elements, called neurons. Neural networks learn by example. The requirements for the implementation of ANN are a

large set of experimental data, choice of the most suitable ANN model, proper training and learning algorithms.

The analysis provided an insight into the effect of raw material composition and impurities (input data) on contact angle (wettability of coke by pitch, output). Consequently, the information obtained might help improve the quality of bonding between coke-pitch and finally anode properties by setting the limits to the impurity content of raw materials acceptable to be used. Normalized input data and their corresponding contact angles were used to train the program.

4.4.2 Materials

Eight different calcined petroleum cokes and seven different pitches were used as raw material. Contact angle data were obtained experimentally for each coke and pitch pair at 170°C. Surface chemical compositions of raw materials were measured by XPS which is a quantitative technique to measure the elemental composition of the material surface (section 3.1.1). Data for raw material impurities were taken from suppliers certificates. All the data were normalized before analysis. Chemical composition and impurities of coke and pitch are shown in Table 4.14 and Table 4.15, respectively.

Table 4.14 Surface chemical compositions and impurities of calcined petroleum cokes used

Comp.	Coke 1	Coke 2	Coke 3	Coke 4	Coke 5	Coke 6	Coke 7	Coke 8
Supplier (wt%)								
Si	0.01	0.0055	0.0046	0.01	0.012	0.0192	0.02	0.002
V	0.03	0.0348	0.0296	0.024	0.03	0.0303	0.04	0.01
Na	0.01	0.0012	0.0012	0.008	0.006	0.0052	0.2	0.001
Ca	0.01	0.0026	0.0027	0.011	0.007	0.0149	0.02	0.001
Fe	0.02	0.0121	0.0092	0.02	0.028	0.0292	0.035	0.009
Ni	0.02	0.018	0.0159	0.02	0.019	0.0182	0.03	0.009
XPS (At%)								
C	95.4	97.3	96.96	95.78	96.57	97.12	95.0	99.0
O	2.95	1.35	1.87	2.66	2.43	1.81	3.0	1.0
N	0.95	0.06	0.19	0.89	0.3	0.21	1.0	0
S	0.68	1.29	0.99	0.67	0.7	0.85	1.0	0

Table 4.15 Surface chemical compositions and impurities of coal tar pitches used

Comp(%)	Pitch 1	Pitch 2	Pitch 3	Pitch 4	Pitch 5	Pitch 6	Pitch 7
Supplier (wt%)							
Si	0.0113	0.0091	0.0127	0.0099	0.0085	0.0094	0.0250
V	0.0000	0.0000	0.0000	0.0000	0.0000	0.0000	0.0000
Na	0.0105	0.0108	0.0111	0.0108	0.0094	0.0130	0.0100
Ca	0.0044	0.0029	0.0028	0.0028	0.0037	0.0027	0.0096
Fe	0.0112	0.0122	0.0124	0.0120	0.0109	0.0101	0.0153
Ni	0.0000	0.0000	0.0000	0.0000	0.0000	0.0000	0.0000
Pb	0.0172	0.0134	0.0126	0.0157	0.0141	0.0176	0.0147
Zn	0.0233	0.0192	0.0183	0.0200	0.0191	0.0202	0.0197
XPS (At%)							
C	98.52	93.02	96.78	97.32	97.12	98.73	98.49
O	1.58	3.95	1.59	1.44	1.89	0.19	0.68
N	0.03	3.2	1.46	1.19	0.86	0.95	0.69
S	0.03	0.26	0.17	0.06	0.13	0.13	0.14

4.4.3 Linear multivariable analysis

A model was developed based on the solution of Equations (LMV model) given in section 3.4.1. It was applied to two cases: the prediction of contact angles measured at 80 s and contact angles measured at 1500 s for the same coke-pitch pairs. In each case, some of the data sets (called the training sets) were used to determine the coefficients (weighting factors for input variables); and using these coefficients, the contact angles were calculated with the LMV model for the same pairs to determine the quality and the predictive power of the model by comparing with the experimental data. Then, the remaining data sets (called the test sets) were used to test again the quality as well as the predictive power of the model since these data have not been used in determining the coefficients. Raw material chemical compositions and impurities were taken as input parameters. Several calcined petroleum cokes and coal tar pitches were considered in the training of the model. The full dataset for each case was divided into two groups: 40 data sets for training and 2 data sets for testing. The relationship between the experimental contact angle and the chemical compositions were determined.

4.4.3.1 Contact angle at 80 s

The calculated vs. experimental contact angles at 80 s for the training and test sets are illustrated in Figure 4.37. The predictions of the contact angle at 80 s by the LMV model were quite satisfactory for both training and test sets (Figure 4.37). The standard deviation of predicted errors (SDPE) was 11.64°. In the ideal case, the R^2 value should be 1 and the

intercept should be 0. Use of more data for training could improve the accuracy of the predictions.

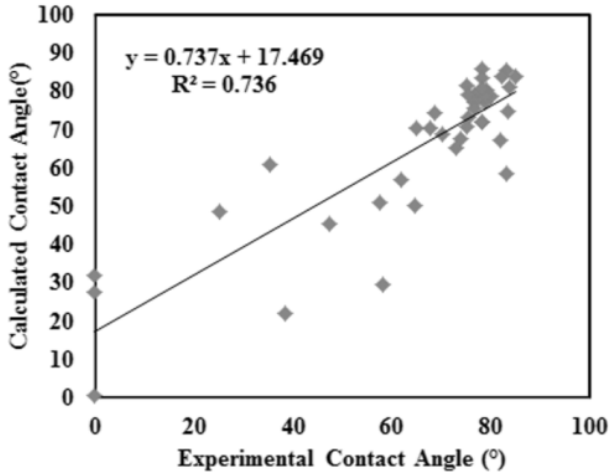

Figure 4.37 Experimental vs. calculated values for the coke-pitch contact angles at 80 s

The weighting factors (coefficients) obtained for the material properties included in the training sets for the contact angle at 80 s are given in Figure 4.38. The results in Figure 4.38 illustrate that the following chemical compositions and impurity contents with large negative coefficients are: coke oxygen (O) content, pitch calcium (Ca) content, pitch lead (Pb) content, and coke silicon (Si) content. The negative coefficients indicate that increase in these properties will reduce the contact angle and improve wetting. The chemical components of raw materials that had large positive coefficients and thus increased the calculated/predicted contact angle values were: coke sulfur (S) content, coke nitrogen (N) content, coke sodium (Na) content, transition metal impurities of coke (Ni, V, Fe), and pitch oxygen (O) content. In addition, higher coke carbon content seems to increase the value of the contact angle at 80 s (lower the wettability). In this case, some results are in

conflict with XPS (Table 4.5 and 4.6) and ANN results (Figure 4.48). LMV sometimes can make false predictions since it assumes a linear relationship between the independent and the dependent variables.

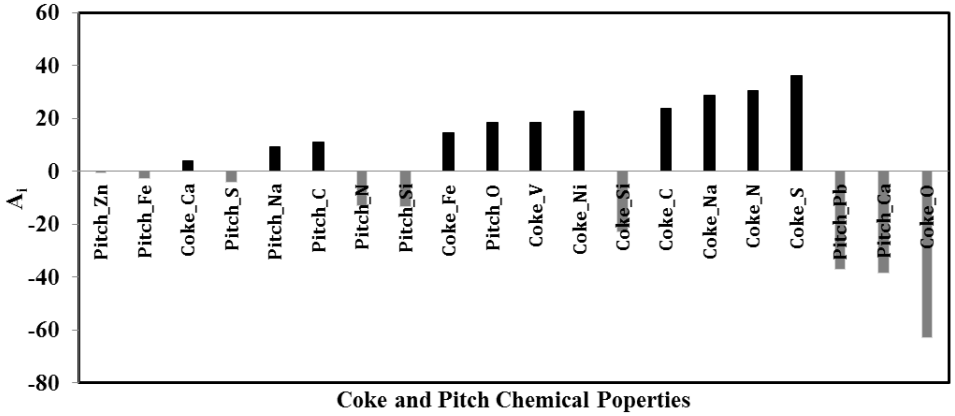

Figure 4.38 Weighting factors for the correlation of coke and pitch chemical chemical compositions and impurity contents with the contact angle at 80 s

4.4.3.2 Contact angle at 1500 s

Similarly, the contact angles at 1500 s were predicted with the same model. The calculated and experimental contact angle at 1500 s values for both training and test sets are given in Figure 4.39. The R^2 value was higher and the intercept value was much lower (much closer to 0) than those of contact angle at 80 s predictions as can be seen from the Figures 4.37 and 4.39. The standard deviation of predicted errors (SDPE) for this case was 6.47°. Thus, the predictions for the contact angle at 1500 s were somewhat better compared to those at 80 s. The negative values of contact angles seen in Figure 4.39 were due to the error in prediction of low contact angles.

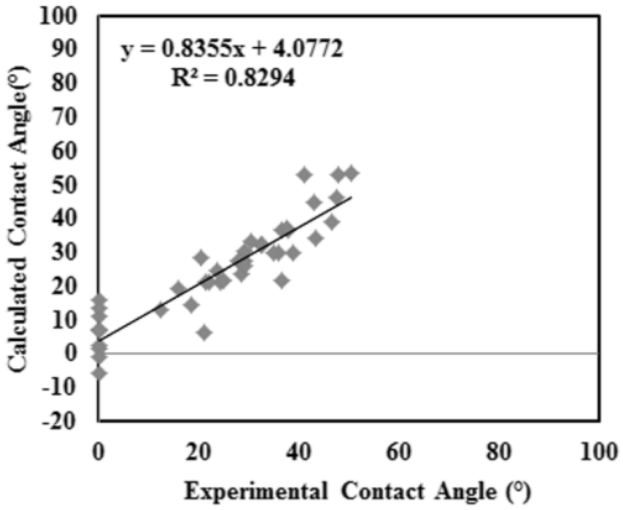

Figure 4.39 Experimental versus calculated values for the coke-pitch contact angle at 1500 s

The weighting factors (coefficients) obtained for the material properties included in the training sets for the contact angles at 1500 s are shown in Figure 4.40. The LMV coefficients indicated that the most significant components had positive coefficients. The contact angles increase with increasing coke sulfur (S) content, coke vanadium (V) content, and coke nitrogen (N) content. Also, increasing coke nickel (Ni) content, coke carbon (C) content, and pitch oxygen (O) content can increase the contact angle at 1500 s. An increase in these components increased the contact angle at 1500 s and reduced the wettability. The components that reduced the contact angle (favors wetting) were coke oxygen (O) content, pitch lead (Pb) content, and pitch calcium (Ca) content. In this case also, some results are in disagreement with XPS (Table 4.5 and 4.6), and ANN results (Figure 4.48) due to the limitations of the LMV model.

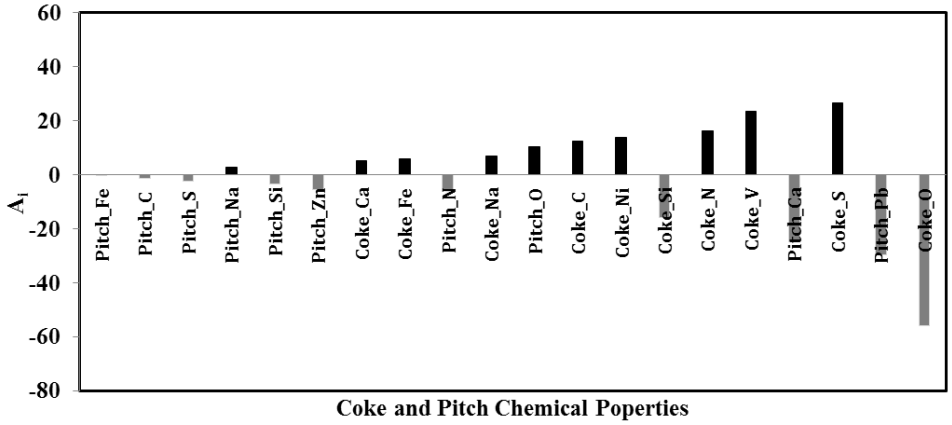

Figure 4.40 LMV weighting factors for the correlation of coke and pitch chemical compositions and impurity contents with contact angle at 1500 s

4.4.3.3 Validation of contact angle predictions

The predictive ability of the LMV model derived from the training sets was validated by using the test sets, which enabled the reliable evaluation and interpretation of the model. Therefore, the results of the test sets were scrutinized in more detail. The contact angles at 80 s and 1500 s for two test sets (one per each case) were calculated, and the results are presented in Figure 4.41 which gives a comparison of the experimental and predicted values.

The prediction for the contact angles at 80 s and 1500 s was quite satisfactory. The percent maximum error for contact angle at 80 s is 4% (3° in contact angle) and for the all contact angle at 1500 s is 14% (5° in contact angle).

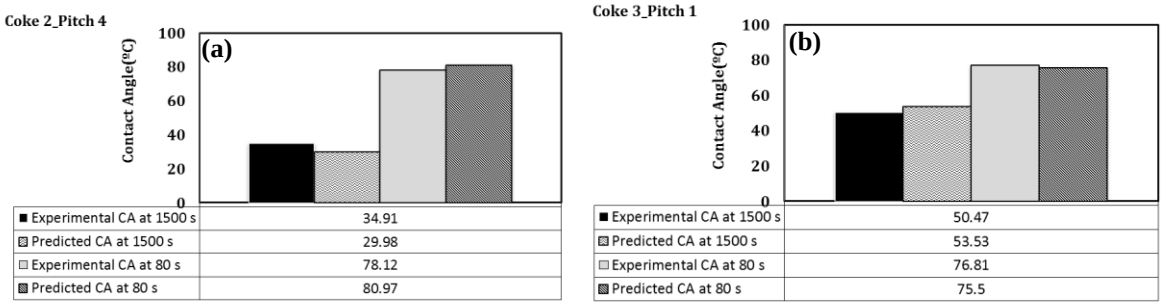

Figure 4.41 Predicted values of (a) Coke 2/Pitch 4 (b) Coke 3/Pitch 1 using the test sets for the two cases (contact angle at 1500 s and contact angle at 80 s)

4.4.4 Artificial neural network

A feed-forward network which consisted of four layers of neurons, namely, an input layer, two hidden layers, and an output layer was developed. The transfer functions associated to the first and second hidden layers were sigmoidal and linear, respectively. As there were few experiments compared to number of input parameters, principal component analysis was used to reduce the number of input parameters. In principal component analysis, a correlation matrix was created with all the input and output parameters. The correlation matrix gives the table of probability values, which is commonly known as ‘p’ value. In principal component analysis, input parameters having p value less than a specified value are chosen as the principal components. Usually the value is chosen as 0.05 for 95% confidence level. It helps reduce the number of input parameters for the ANN model. Initially, all 20 variables were used as input parameters to determine the ‘p’ values for each input variable. A small ‘p’ value (typically ≤ 0.05) indicates that the effect of the input variable on the output variable is statistically significant. Based on the ‘p’ value

results, four input parameters, which affected the contact angle most, were chosen to feed the ANN model to predict the contact angle at 80 s and effect of different impurities and composition of raw materials on contact angle at 80 s were noted. Similarly eight input parameters were chosen to feed the ANN model to predict the contact angle at 1500 s and effect of different impurities and composition of raw materials on contact angle at 1500 s were studied. The final model was validated using a set of data with a known output which was not used in the training phase. The model was selected based on the value of the regression coefficient for the predicted output of the model with respect to the experimental results. The models for which the regression coefficients were close to 1 were considered suitable. To study the effect of one single parameter, the neural network model was applied to a set of input data where only that parameter was changed keeping all other parameters constant.

4.4.4.1 Contact angle at 80s

The following Figure 4.42 demonstrates the ‘p’ value results and indicates that oxygen content of calcined petroleum coke and silicon, iron and sulfur content of pitch was statistically significant for contact angle at 80 s (Figure 4.42).

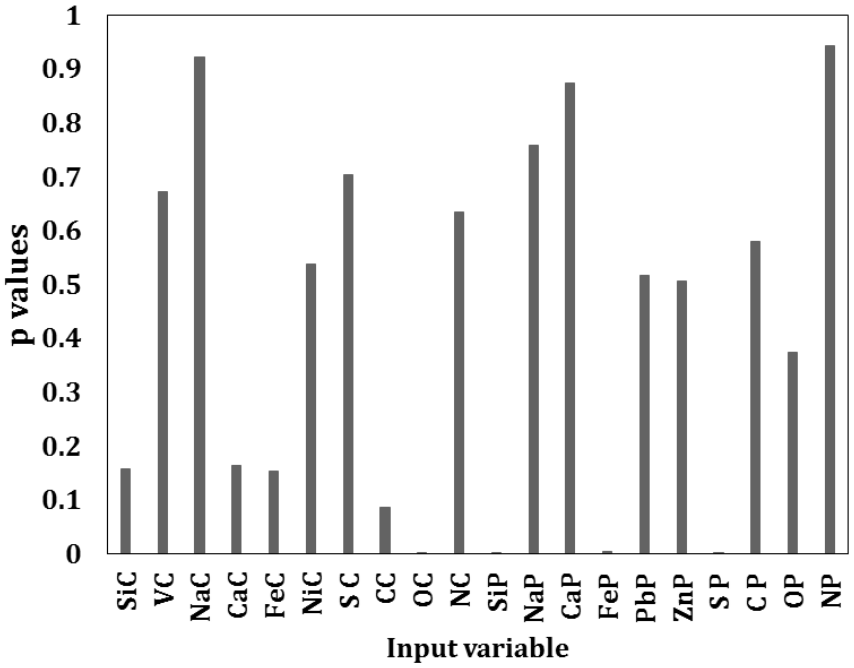

Figure 4.42 "p" value for different input variables (chemical compositions and impurity contents of coke and pitch) for contact angle at 80 s

The ANN model was developed as defined earlier. Trial and error methods were used to initialize all the parameters. Thirty eight points were used to train the model and four points were used for validation (Figure 4.43). The input variables are oxygen content of calcined petroleum coke and silicon, iron and sulfur content of pitch. Due to the small number of data available for this study, the model was chosen based on a correlation coefficient R^2 for all the 38 points and the tolerance of predicted and experimental values which was set to $\pm 5^o$. The R^2 was 0.784. The percentage of points within $\pm 5^o$ was 71%. The prediction of the right trends were found to be better for ANN model compared to that of LMV.

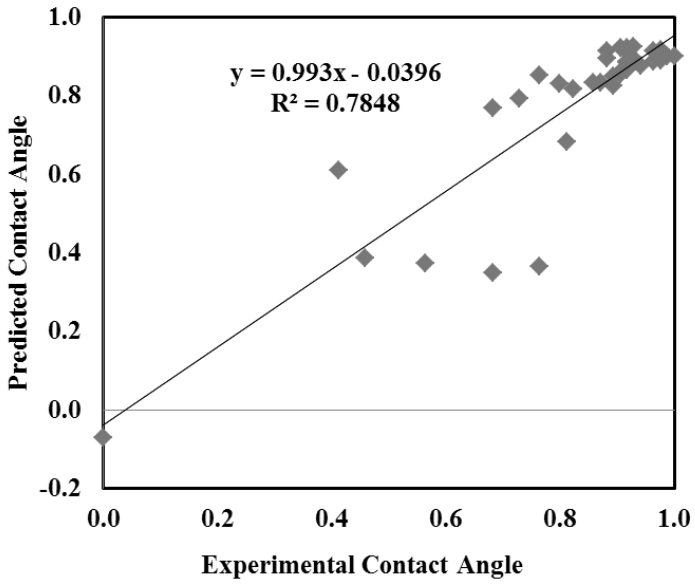

Figure 4.43 Normalized predicted vs. experimental contact angles at 80 s

Similarly the negative values of contact angles seen in Figure 4.43 are due to the error in prediction of low contact angles and lack of enough data for training. The effect of different material properties on contact angles at 80 s obtained by ANN model are shown in Figure 4.44 and Figure 4.45. All the input variable data in Figure 4.43 and Figure 4.44 are normalized based on following Equation.

$$\text{Normalized value} = \frac{\text{Value to be Normalized - Minimum Value}}{\text{Maximum Value - Minimum Value}} \qquad \textbf{(4.1)}$$

The Figure 4.44 shows that presence of oxygen in coke improves wetting at the beginning. Oxygen is highly electronegative and can form covalent/hydrogen bonds with conjugate functional groups and support wetting.

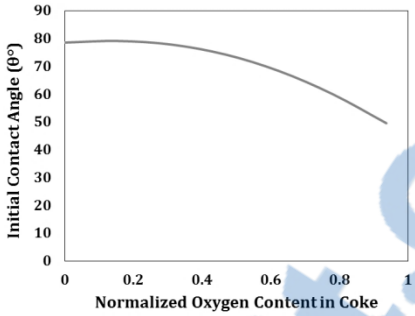

Figure 4.44 Effect normalized oxygen content in coke on contact angle at 80 s

Figure 4.45 (a) displays that contact angle at 80 s reduced with increasing silicon (Si) content. Due to its non-metallic character, silicon could form covalent/Van der Waal's bonds with electronegative components in coke and pitch resulting in increased wettability (lower contact angle). It can be seen from Figure 4.45 (b) that iron had a negative effect on coke-pitch wetting. Iron is mostly present as sulfide form and only activated at higher temperatures [164]. It was possible that presence of sulfur in FeS, might have polarized the electron cloud of Fe. Sulfur is also electronegative, and it was probable that the amount of free sulfur increases at higher total sulfur content, which could help the formation of covalent bonds and improve wetting.

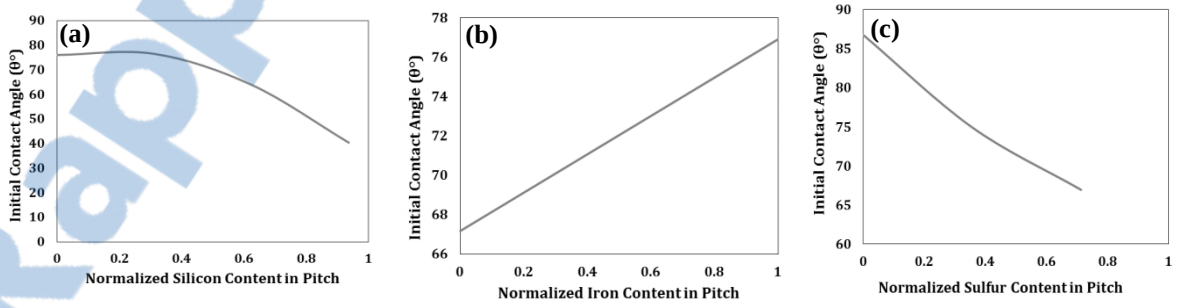

Figure 4.45 Effect normalized pitch impurities on contact angle at 80 s (a) silicon (b) iron (c) sulfur

4.4.4.2 Contact angle at 1500 s

Figure 4.46 illustrates the ‘p’ value results and indicates that vanadium, sodium, nickel, carbon, oxygen, nitrogen content of calcined petroleum coke and silicon and sulfur content of pitch were statistically significant (Figure 4.43).

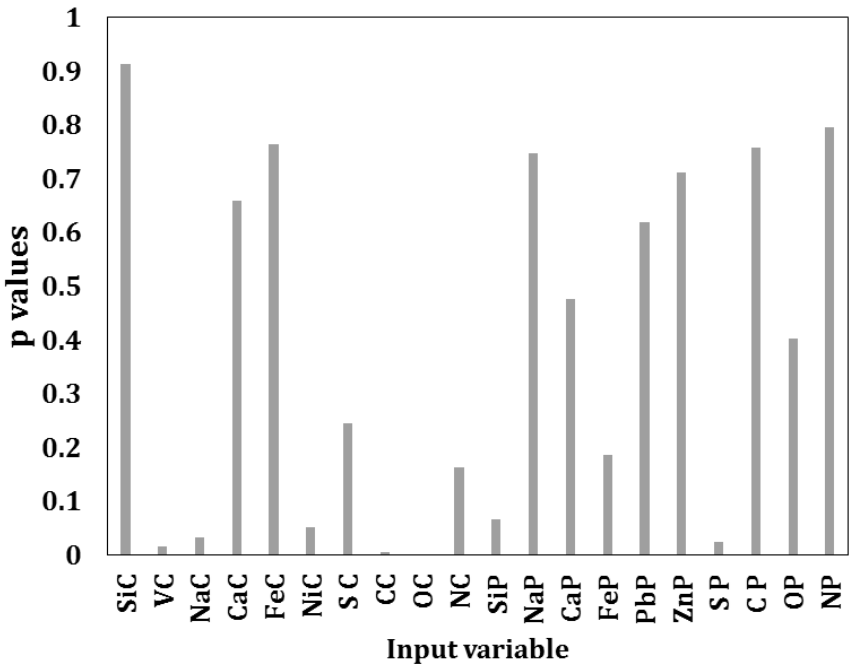

Figure 4.46 ‘p’ value for different input (chemical compositions and impurity contents of coke and pitch) variables (XC denotes element X in coke, XP denotes element X in pitch)

A similar ANN model was developed for contact angle at 1500 s. Trial and error methods were used to adjust all the parameters. Thirty eight points were used to train the model and four points were used for validation (Figure 4.47). The input variables were vanadium, sodium, nickel, carbon, oxygen, and nitrogen content of calcined petroleum coke and silicon and sulfur content of pitch. Due to the small number of data available for

this study, the model was chosen based on a correlation coefficient R^2 for all the 38 points and the tolerance of predicted and experimental values which was set to $\pm 5^o$. The R^2 was 0.902. The percentage of points within $\pm 5^o$ was 85%. The model was validated based on 4 data set.

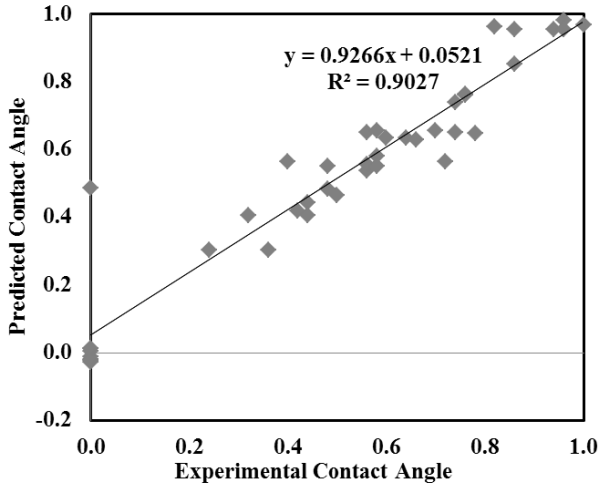

Figure 4.47 Normalized predicted vs. experimental contact angles at 1500 s

Thus, it can be seen that the customized feed-forward neural network model with back-propagation training was able to predict the output (contact angle) for the test data set better than the linear multivariable analyses (Figure 4.43). Similarly the negative values of contact angles seen in Figure 4.47 are due to the error in prediction of low contact angles and lack of data for training. The effect of different material properties on contact angles at 1500 s sobtained by ANN model are shown in Figure 4.48 and Figure 4.49. ANN model allows the study of the variation in each parameter individually while keeping all other parameters constant. All the input variable data in Figure 4.48 and Figure 4.49 were normalized based on Equation 4.1.

Figure 4.48 presents the results of the ANN model showing the effect of vanadium in coke on the contact angle at 1500 s when all other parameters are kept constant. As can be seen from this figure, the wettability decreased (contact angle increased) with increasing vanadium and nickel content of coke, but on the other hand the contact angle decreased to a certain extent when sodium in coke increased. Coke and pitch both contains polycyclic aromatic compounds. Sodium formed additional compounds with naphthalene and other aromatic polycyclic compounds and with aryl alkenes. Sodium could also react with alcohols to produce sodium salts and hydrogen. These reactions in returns could improve the wettability of coke by pitch. Vanadium, which is mostly stable at lower temperatures, needs some activation period before reacting [17]. Vanadium and Nickel are transition metals. They can form coordinate covalent bonds with non-metals having lone pair of electrons. For this they need to be in metallic or ionic form. As a compound their electronic configurations are stable. In solid coke they cannot stay as ionic species. Also they do not stay as pure metal in coke. They usually stay as metal-ligand complexes. So it is difficult for them to react with O/N of pitch at lower temperature. Sufficiently high amount of energy is required to break those bonds. The wettability test was done only at 170°C. It was possible that at this temperature the vanadium compounds were inactive and needed to transfer to an active state or it might not be in a catalytic form which could have sped up the reaction. This may be a reason for lower wettability. The lower wettability in presence of nickel again could be explained with its inactivity at lower temperatures. It can be also seen from this figure that wettability of coke by pitch increased as carbon percentage in coke increased. Coke contains C-C bond and C=C (Table 4.5). In general, presence of

higher amount of C=C indicates presence of higher aromatics. Thus the increase in carbon could correspond to the increase in aromatic content. The presence of aromatics could improve wetting by electrostatic interaction due to their pi electron cloud. Equally Figure 4.48 shows that presence of oxygen and nitrogen improves wetting. Oxygen and nitrogen are hetero atoms and they are highly reactive. Also, these atoms are highly electronegative and might form covalent/hydrogen bonds with conjugate functional groups and support wetting.

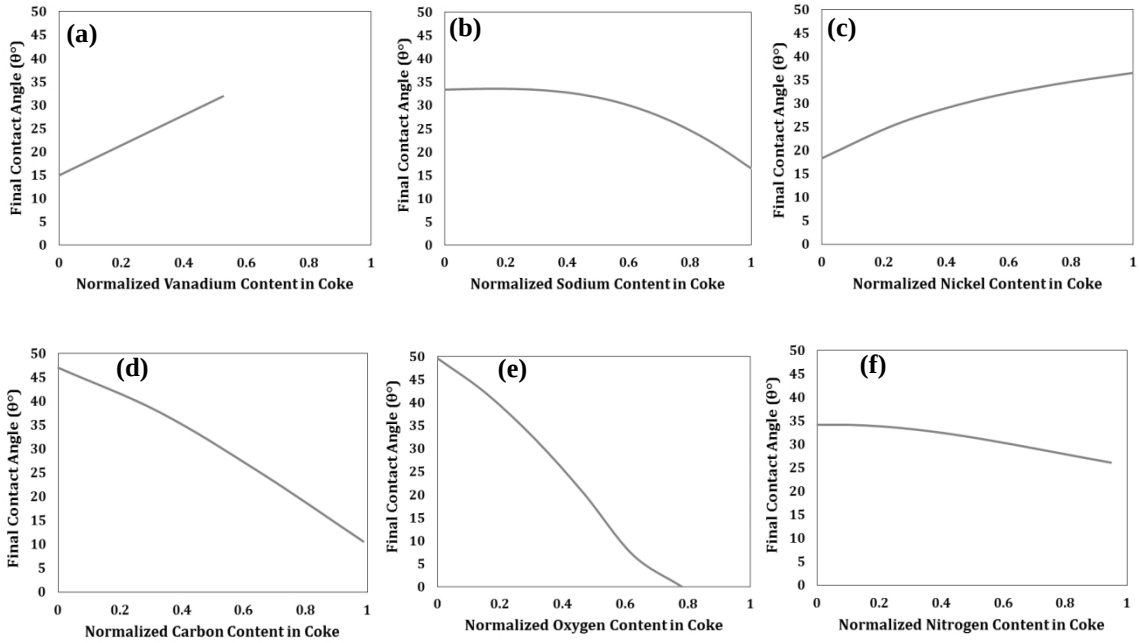

Figure 4.48 Effect of normalized coke chemical compositions and impurities on contact angle at 1500 s (a) vanadium (b) sodium (c) nickel (d) carbon (e) oxygen (f) nitrogen

Figure 4.49 presents the effect of pitch properties on the contact angle at 1500 s, hence, on the wetting capacity of pitch. Figure 4.49 (a) displays that contact angle at 1500 s reduces with increasing silicon content. Similar trend was observed for contact angle at

80 s. The ANN model shows that, an increase in sulfur resulted in a slight increase in the contact angle (lower wetting) up to a certain value of sulfur (S from 0 to 0.4 and contact angle from 30.8° to 32.5°; see Figure 4.49(b)). It is possible that at lower sulfur content, there was not enough free sulfur remaining to form covalent bonds and hence increased the contact angle at 1500 s. Further increase in sulfur seemed to reduce the contact angle at 1500 s (Figure 4.49(b)). At higher sulfur content, it was probable that the amount of free sulfur increased which could aid the formation of covalent bonds and improve wetting. It should be mentioned that the change in contact angle is very small with changing sulfur content and most probably not significant.

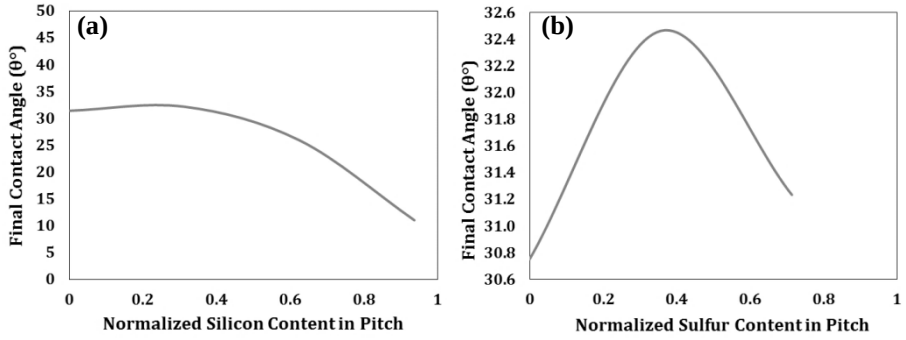

Figure 4.49 Effect normalized pitch impurities on contact angles at 1500 s (a) silicon (b) sulfur

4.4.4.3 Validation of contact angle predictions

The predictive ability of the ANN model derived from the training sets was validated by using the test sets, which enabled the reliable evaluation and interpretation of the model. Therefore, the results of the test sets were scrutinized in more detail. The contact angles at

80 s and 1500 s for four test sets were predicted, and the results are presented in Figure 4.50 which gives a comparison of the experimental and predicted values. The predictions for the contact angles at 80 s and 1500 s were quite satisfactory. The R^2 value for predictive ability for unknown test sets was 0.89 for contact angle at 80 s and 0.98 for contact angle at 1500 s. The average percent errors in prediction were 8 % and 5% for contact angles at 80 s and 1500 s respectively.

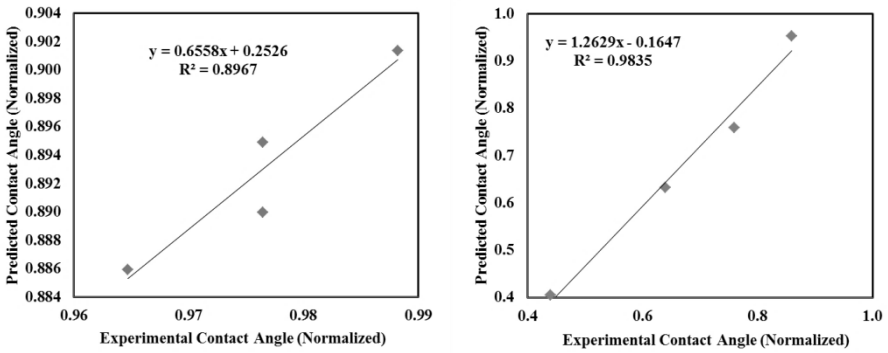

Figure 4.50 Predicted values of (a) normalized contact angle at 80 s (b) normalized contact angle at 1500 s using the test sets for the two cases

During the mixing of coke and pitch, there are several parameters that can influence their interaction. Industries often maintain information about the raw material properties and that can be used as input parameters to predict the best coke/pitch pair. These vast data base of coke and pitch chemical compositions and impurities can be utilized to train ANN. The industrial data is highly nonlinear in nature, and there is no mathematical relation available between those data. In such a situation, ANN has substantial potential for quality control to produce good quality green anodes. In the case of variations in the properties of

raw materials, a trained ANN model can predict the contact angle without performing any additional test.

4.4.5 Concluding remarks

First, principal component analysis was used to identify the parameters which significantly affect the contact angle. Then, those selected parameters were used as inputs in an ANN model. In this study, models based on the linear multivariable analysis and artificial neuron network were developed to predict the contact angles at 80 s and 1500 s for different pitch-coke pairs on the basis of their surface chemical composition and presence of impurities. The LMV model shows that coke O and Si as well as Pb and Ca contents of pitch decreased wetting angle at 80 s whereas S, N, Na and transitions metal contents of coke has a negative impact on initial wetting. It was also found that the presence of higher amounts of S, V, N, Ni, C contents in coke decreased final wetting, and O content of coke as well as Pb, Ca contents of pitch favors final wetting (based on angles at 1500 s). The results showed that the ANN model has better prediction ability and better correlation with input parameters compared to LMV model. This current model also predicted the influence of different chemical functional groups and impurities on contact angle. The ANN results showed that O content of coke and Si, S content of pitch helped in wetting, and Fe content of pitch reduced wetting at the initial stage whereas increasing amount of Na, C, N, O content in coke decreased contact angle at 1500 s and V, Ni content of coke increased contact angle at 1500 s. Increasing Si content in pitch reduced contact angle at 1500 s . The contact angle at 1500 s initially increased with increasing S content in pitch upto a certain

level but later that it decreased. The current predictive ANN model, demonstrated how the suitable coke-pitch pairs to be used for anode paste preparation can be identified based on their surface chemical properties and impurity contents without the need for further experiments. This novel approach can be used as a tool in evaluating the potential of a given pitch to wet the dry aggregate during pre-assessment of various anode recipes. The major advantage of ANN over the other method is that it can efficiently handle highly nonlinear data with fluctuations where there is no existing mathematical relationship.

The predictive ability of both the models can be improved by introducing more training sets of data. Development of ANN model is laborious and challenging because it involves numerous trials and errors. However, once it's developed it gives more accurate results compared to LMV model.

CHAPTER 5

PRODUCTION OF LABORATORY ANODES AND THEIR CHARACTERIZATION

This chapter presents the production of laboratory anodes and their characterizations. The first part of this chapter presents the results of the study on the effect of different coke fractions and recycled anode butt percentage on the green and baked anode properties with the objective of improving the anode properties. This part is divided into two subsections.

In the first subsection of the first part, an artificial neural network model was developed to predict green anode densities for different paste recipes. This model was built in two stages, using experimental tapped aggregate bulk density measurements of different recipes and ratios of tapped bulk density to green anode density as input parameters. The developed ANN model shows the effect of different size fractions and recycled anode butt percentage on dry aggregate density as well as on green anode density.

After a comprehensive survey of the available testing methods to characterize anodes, detailed analysis was conducted to compare the properties of laboratory anodes produced using different recipes in the second subsection. Also, the development of a novel recipe, which increased the density and decreased the electrical resistivity, and the reactivity of laboratory anodes compared to those of the laboratory anodes made with standard recipe, is described.

In the second part, anodes produced from cokes with different crystallinity and sulfur content were studied. Under-calcined coke is known to reduce the selective burning (CO_2 reactivity), consequently, the dusting of the anodes. Also, it was found in the literature that

sulfur in the coke reduces the CO_2 reactivity of the anodes by inhibiting the activity of metal impurities. In this study, anodes were made with cokes calcined to different degrees and their properties were compared. Also, effect of sulfur content of the under-calcined coke and the baking temperature.

The third part of this chapter (section 5.3) contributes to the fundamental understanding of the influence of different natural convection cooling times on pitch penetration, wetting, and distribution in anode.

5.1 Improvement of anode recipe

5.1.1 General

During the anode fabrication, calcined petroleum coke, coal tar pitch and recycled materials (butts, green and baked reject) are blended in certain percentages and mixed. The composition of this mixture is known as “anode recipe” or “anode paste recipe”. Considering the differences in raw material quality, optimizing the anode recipe becomes an important task to ensure good anode quality. All individual fractions of coke are important for the quality of anodes. Fine and dust contents increase the density of the anode by filling the openings between the large particles. This decreases the bed porosity, hence, the air and CO_2 reactivity since the internal structure of anode becomes inaccessible to these gases. However, they are also more reactive when they are in contact with CO_2 or air as they have larger surface area. The coarse material and recycled anode butts increase the mechanical properties of the carbon anodes. Again higher quantity of recycled butt increases the reactivity due to impurities (especially Na). Thus, an optimized recipe is

important for anode properties. The fraction sizing, which affects the porosity and packing, could influence most of the anode properties. Different fractions of coke particles were mixed to optimize the anode recipe; however, it was laborious to find experimentally the suitable percentage of each fraction in anode paste which would give good anode properties. The bulk density of dry aggregates is a good indicator of particle packing and volume occupied by fractions for different recipes. Tapped bulk density of dry aggregates was used to predict the anode paste recipe using the ANN method. In this study, ANN model was developed for adjusting the granulometry of the raw materials for anode production. Consistent correlations were found between different size fractions and dry aggregate bulk density and anode green density. In the field of the current thesis work, a better picture of the impact of recipe parameters on the relevant properties for anode reactivity and dusting was obtained. This is quite significant as in the literature often only anode density data and mechanical properties are reported.

5.1.2 Materials

Two different cokes and one coal tar pitch were used to make anodes. Table 5.1 and Table 4.8 illustrate properties of cokes and pitch, respectively.

Table 5.1 Physical and chemical properties of coke

Properties	CPC 1	CPC 2
Bulk Density[1] (g/cc)	0.89	0.901
Real Density (g/cc)	2.06	2.072
CO_2 Reactivity (%)	9	8
Ash Content[2] (%)	0.2	0.15
Moisture Content (%)	0.1	0.19
Na (wt%)	0.007	0.0059
Si (wt%)	0.01	0.0095
P (wt%)	0.0006	-
S (wt%)	2.75	0.73
Ca (wt%)	0.01	0.004
V (wt%)	0.031	0.024
Fe (wt%)	0.02	0.01
Ni (wt%)	0.02	0.019

[1]Measured by ASTM D4292-10, [2]Measured on dry basis.

Sieved coke fractions, recycled anode butt, ball mill product (BMP) and filter dust (FD) were weighed according to specified recipe and blended in an intensive mixer together with coal tar pitch. A vibrocompactor was used for the production of green anodes. The detailed methodology is given in section 3.2.1.

5.1.3 Development of ANN model

Two customized feed-forward artificial neural network (ANN) models with back-propagation training were developed using Matlab 2014. The detailed methodology is given in section 3.4.2. In the first model, measured tapped bulk density of each fraction and the corresponding granulometry of different dry aggregate recipes were fed to model as input to predict tapped bulk density of the specific recipe. For this model, 46 sets of aggregate bulk density data were used to train the network and five random data, which were not used in training, were used for validation.

Then, 14 laboratory anodes were produced using different recipes. These recipes were chosen using the predictions of the first ANN model which indicated the percentage of each fraction to be used in order to obtain high aggregate density. To see if the high aggregate density will result in high quality anodes, the green densities of these anodes were measured. In the second model, tapped bulk density of an anode recipe and granulometry were used as input to predict the ratio of dry aggregate to green anode density. Ten of the fourteen data were utilized to train the database and four random recipes were chosen for validation. Afterwards, two models were combined to predict the green anode density for a chosen recipe. In order to minimize the errors in training and testing calculations, the values predicted by ANN were plotted against the experimental results for numerous test data sets. The coefficient of determination for linear regression was used as the criteria for the quality of the network predictions. The closer the value of the coefficient of determination to unity is, the better the model's ability for prediction is. It can be seen from the Figure 5.1 that the R^2 value for training and test sets were found as 0.966 and 0.975, respectively, for dry aggregate density (first model).

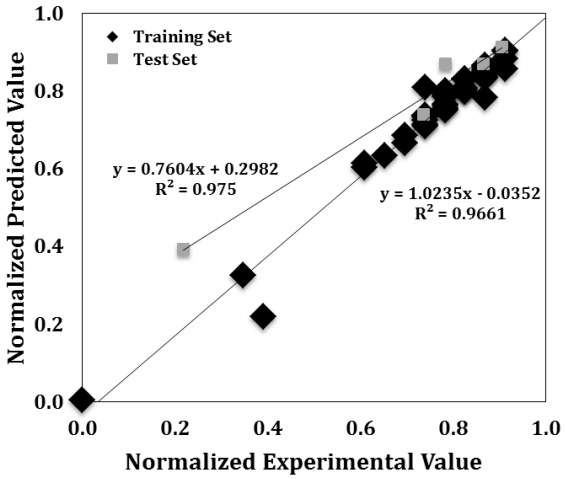

Figure 5.1 Normalized predicted and experimental dry aggregate densities using the first ANN model

Figure 5.2 shows the predicted vs experimental ratios of green anode density to dry aggregate density for the second model. The model had R^2 value of 0.982 for training data set. The accuracy of the prediction is further indicated by the R^2 (0.986) value of the test set.

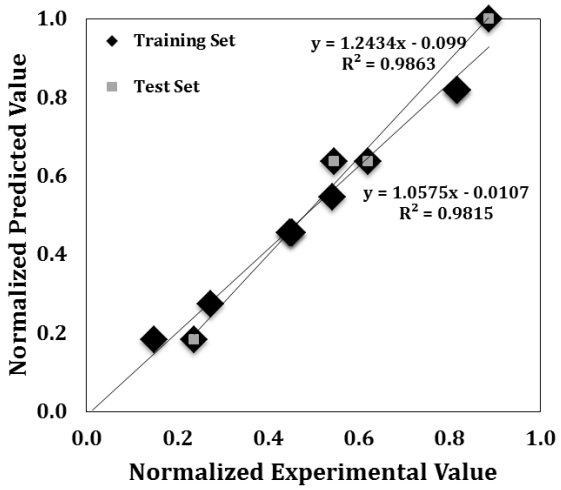

Figure 5.2 Normalized predicted and experimental values of the ratio of green anode density to dry aggregate density using the second ANN model

The ANN model developed could be utilized to determine the granulometry required to obtain a desired tapped density of an aggregate and green anode density which is produced using this aggregate recipe. It was possible to vary the percentages of all the different size fractions which could yield a desired range of dry aggregate or green anode density. However, this might lead to a large number of combinations with different size fractions.

As it was discussed earlier, each fraction has an effect on anode properties. The model was used to demonstrate the effect of medium fractions and recycled anode butt on dry aggregate density and green anode density. To demonstrate the application of the model here, only the percentages of two particle sizes (described as coarse and medium in decreasing order in size) of fresh coke were varied keeping all other parameters constant (Figure 5.3). Then, the aggregate densities and anode densities corresponding to the granulometry used were predicted. This model was trained for one type of coke only. Also the pitch percentage was kept constant at 15%. The percentages of all fractions are normalized based on the Equation 4.1. Effect of medium particles on dry aggregate density and green anode density is illustrated in Figure 5.3. The results show that an optimum percentage of medium fractions were required to obtain high green anode density. High green anode density did not necessarily correspond to high dry aggregate density, rather usually low value of dry aggregate density was observed for high values of green anode density. It can be noted that when the coarse fractions were in the lower end of the range and when medium fraction percentage decreased, dry aggregate density increased. The green anode density reached an optimum at a certain medium fraction percentage (Figure 5.3 (a)). When the coarse fractions were in medium range, it can be seen from Figure 5.3 (b) that there was an optimum composition for maximum green anode density, even if the variation in dry aggregate density was not very large. For the anode with a high amount of coarse fraction, the green anode density increased with decreasing medium fraction percentage whereas dry aggregate density showed the completely opposite trend (Figure 5.3 (c)). Another interesting result was noticed that, at a higher level of medium fraction

percentage and at a certain point, the dry aggregate and green anode densities were the same and showed opposite trend on both sides of this point.

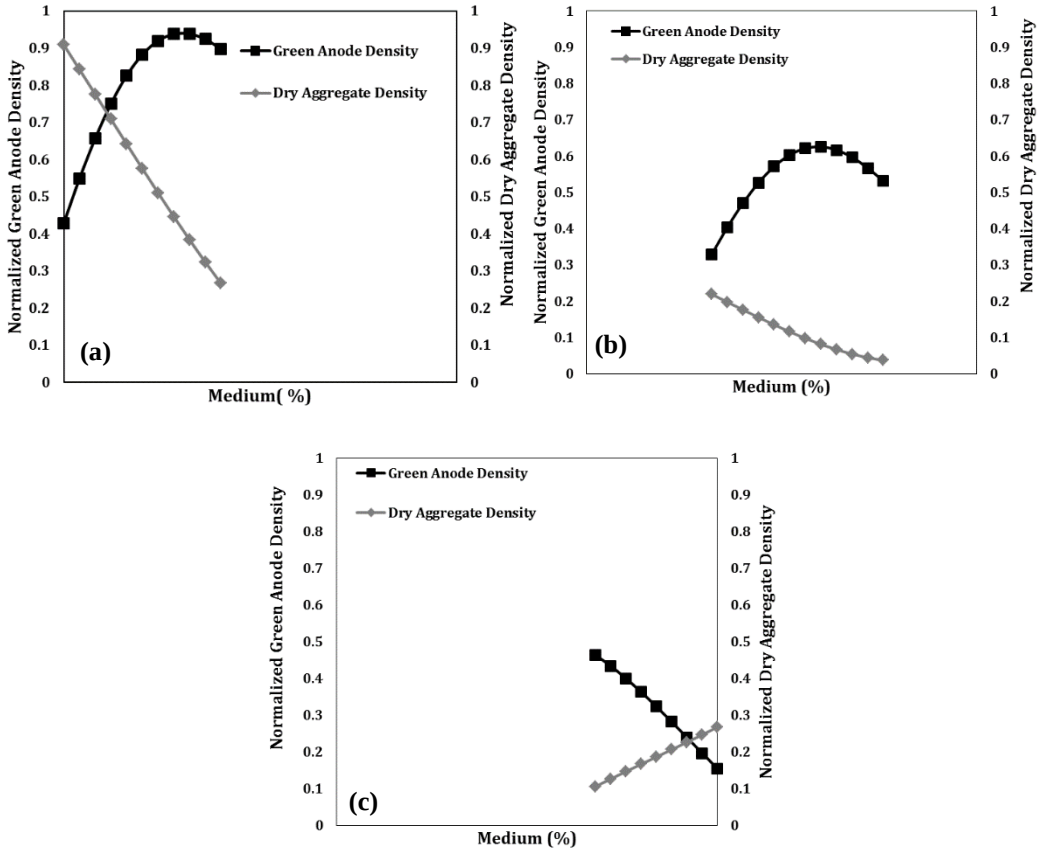

Figure 5.3 Effect of medium fractions on normalized dry aggregate density and normalized green anode density (a) low amount of coarse fraction (b) medium amount of coarse fraction (c) high amount of coarse fraction

Similar approach was taken to analyze the effect of recycled anode butt percentage on dry aggregate and green anode density. It could be seen from Figure 5.4 that predicted dry aggregate density and green anode density increased with increasing butt content up to certain level. Afterwards, it decreased. These results indicate that it is important to select an optimum range for each fraction to improve the anode density.

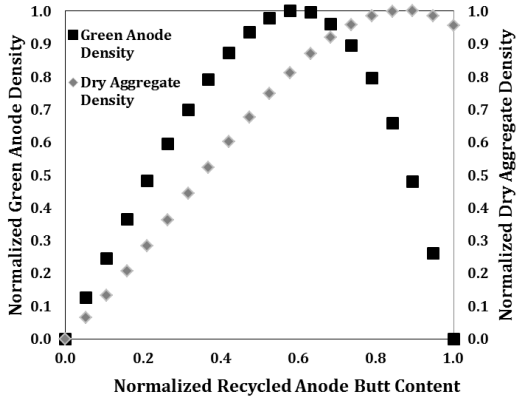

Figure 5.4 Effect of normalized recycled butt on normalized dry aggregate density and normalized green anode density

Information obtained from the ANN analysis is a useful tool for plants since controlling the recipe line is not an easy task. The ANN model developed might be used to improve the anode density by readjusting the granulometry when there is a change in recipe line during operation.

5.1.4 Characterizations of anodes

To establish the impact of particle size distribution on green anode density, two sets of experiments were made. Several recipes were prepared using various combinations of recycled anode butt, coarse, medium, and fine fractions of fresh coke. Characterization of anodes produced from different recipes is discussed in this section. All recipes with their corresponding anode numbers are presented in Table 5.2.

Table 5.2 Anode recipes and their corresponding anode number and properties

Anode No	Butt(%)	Coarse*	Medium*	Fine*	Type of coke	Green Anode Density(g/cc)	Green Elec.Res. (μΩm)	Baked Anode Density(g/cc)	Baked Elec.Res. (μΩm)
1[1]	25	0.0	1.0	0.0	CPC 1	1.587	5566	1.543	59.04
2**	25	0.0	1.0	0.0	CPC 1	1.586	6357	1.528	59.86
3[1]	25	0.3	0.6	0.3	CPC 1	1.638	3837	1.572	54.88
4	25	0.3	0.6	0.3	CPC 1	1.629	3951	1.561	54.29
5	25	0.3	0.6	0.3	CPC 1	1.632	3933	1.563	54.22
6***	25	0.3	0.6	0.3	CPC 1	1.585	6647	1.535	57.93
7	25	0.6	0.0	1.0	CPC 1	1.568	5868	1.478	65.05
8	25	0.3	0.8	0.0	CPC 1	1.603	4539	1.546	60.02
9	25	0.3	0.6	0.4	CPC 1	1.587	6349	NA	NA
10	25	0.3	0.4	0.6	CPC 1	1.593	5090	1.512	65.35
11	25	0.7	0.2	0.6	CPC 1	1.590	4256	NA	NA
12	0	1.0	0.0	0.6	CPC 1	1.574	5840	NA	NA
13	25	1.0	0.0	0.6	CPC 1	1.623	4043	1.546	57.23
14	25	0.3	0.5	0.5	CPC 1	1.625	4487	1.552	58.11
15	0	0.0	1.0	0.0	CPC 1	1.576	4505	1.511	54.01
16	15	0.0	1.0	0.0	CPC 1	1.577	6357	1.506	59.09
17	35	0.0	1.0	0.0	CPC 1	1.568	6409	1.496	59.74
18**	25	0.0	1.0	0.0	CPC 2	1.594	5909	1.546	60.41
19	25	0.3	0.6	0.3	CPC 2	1.626	4258	1.571	55.05

[1] The anodes 1 and 3 were produced earlier, and the vibro speed was not measured.
*All the coke fractions are normalized by column wise using Equation 4.1.
** Standard recipe
***14% pitch was used where the other anodes were made with 15% pitch

5.1.4.1 Green and baked density of anodes

To establish the effect of fraction sizing on green anode density, a total of 19 pilot-scale anodes were prepared from two different sources of petroleum coke using different recipes including a standard recipe (Anode 1 and 2, Table 5.2, Figure 5.6). Aggregate size

distributions, specially medium and coarse fractions, were varied. The anode making conditions were kept the same for all the anodes. Green and baked densities of the anodes were determined according to the method described in section 3.2.2.2.

Green and baked apparent densities are the two of the key quality measures of the anode. Many of the anode properties, which will be discussed in this section, are correlated with the baked anode density (BAD). In general, once the BAD were optimized, overall anode properties followed. In addition to this, the density measurement was relatively simple and non-destructive. Therefore, after the routine BAD measurements on all anode samples, they were subsequently utilized for other tests. It was desired that the value of the BAD to be as high as possible without detriment to other anode properties. Analysis of densities of anodes made of different recipes gave some noteworthy results. The recipes with different recycled butt contents showed consistently higher green and baked densities at 25% butt content (Figure 5.5). In all recipes, 15% pitch was used except for anode 6. The optimum (25%) butt content had a significant impact on green and baked anode densities, more than any other butt content. The result was in accordance with the results in literature [102]. For anode 17, the butt content was increased to 35%, which slightly reduced the anode density. In general, recycled anode butt is more wettable compared to petroleum coke (section 4.3) [7, 71]. Butt also has lower surface porosity. It is possible that the anode was overpitched due to presence of excess butt, hence, pitch layer around the butt particles (as it has less porosity) was thicker compared to that of the petroleum coke. This resulted in an increase in anode volume which in turn decreased the density. In addition, the shape of the recycled butt particles is completely different than that of petroleum coke [165], and it is possible

that this might have affected the packing behavior of the aggregate causing a decrease in green anode density. It is also possible that higher butt content changes the binder demand [145] which, in turn, affects density if the binder content is not adjusted accordingly.

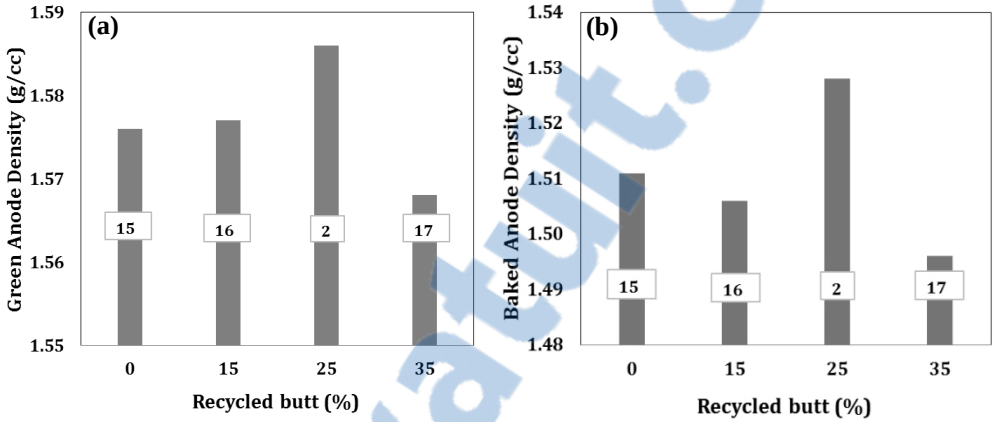

Figure 5.5 Effect of butt content on (a) green and (b) baked anodes densities

Green and baked densities of anodes produced from different recipes with constant butt and pitch contents are illustrated in 3-D plots in Figures 5.6 and 5.7, respectively. In these 3-D plots, symbol sizes increases and color code changes with increasing density values. The axes represents the normalized coarse, medium, and fine fraction amounts used in the recipe. Anode 1 and 2 represent the typical standard recipe. Aiming to improve the anode density, trials were carried out to adjust the medium and coarse fractions in the recipe. Decrease of medium fraction around 40% compared to that of the standard recipe (Figure 5.6, Figure 5.7, and Table 5.2) improved the green and baked anode densities when 25% butt was maintained in the recipe. It is a well-known fact that an increase in fine fractions increases the anode density but it can affect the anode mechanical properties and binder demand. . In this study, the ultra fine fractions (BMP and FD) were kept similar to that of

the standard recipe. Finally, an improved anode recipe (anodes 3, 4, and 5) was found giving higher green and baked anode densities compared to those of the standard recipe. Green density of anode increased from 1.586 g/cc to 1.638 g/cc. Two repetitive measurements were done to confirm the improvement of the anode properties. An increase in density was observed for an anode produced using a different coke with similar recipe (see anode 19 in Table 5.2, Figures 5.6 and 5.7). Recipe corresponding to anode 14 also revealed a promising future. It could be observed from the Table 5.2 and Figure 5.6 that lower amount of the medium fractions in the paste recipe gave comparatively better green anode density. Hulse [5] also found similar trend and mentioned in her thesis that lower intermediate fraction couldn improve the dry aggregate density yielding higher anode density. The results also showed that complete removal of medium fraction sharply reduced the anode quality (anodes 7 and 12) except for anode 13. It can be seen that for anode 7, density was reduced even though it contained high amount of fines. It was possible that density was reduced because inter-particle spaces were not well filled as the medium fraction was completely missing. Also it was possible that higher amount of fine increased the binder demand and coke particles were not wetted sufficiently by pitch due to under-pitching. As it can be seen, the recipe of anode 12 and 13 were similar. The density of anode 12 was lower as this anode did not contain any recycled anode butt. This result was in good agreement with the previous findings of the present study. This showed that suitable amount of recycled anode butt, medium, coarse, and fines fractions were required to have good packing and good anode properties. Thus, it was evident that the presence of lower medium fractions with optimal recycled butt, coarse, and fine particles could

improve the anode density. As it could be observed in Table 5.2, the pitch level had pronounced influence on the green and baked density (anodes 3 and 6). As noted, the anode containing 14% pitch (anode 6) had inferior quality than that with 15% (anode 3) pitch. The baked anode densities also followed the green anode densities.

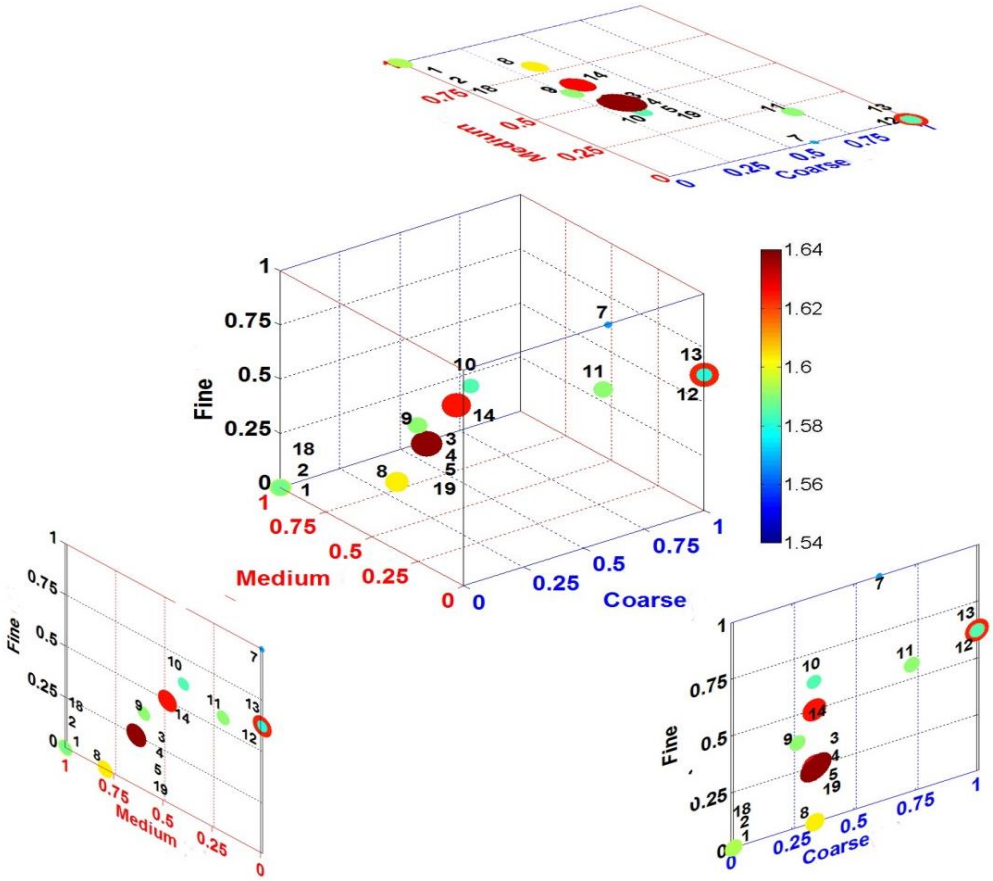

Figure 5.6 Green anode density of different recipes (symbol size increases with increasing density)

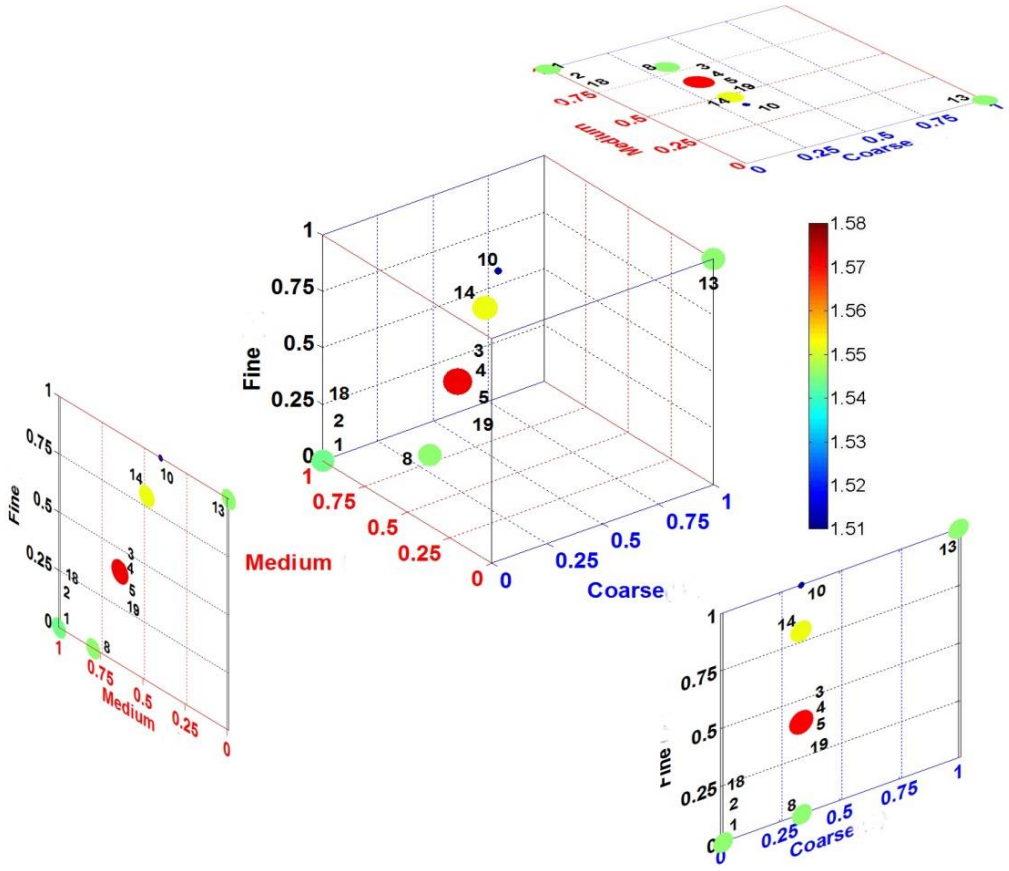

Figure 5.7 Baked anode density of different recipes (symbol size increases with increasing density)

As it can be seen from Figure 5.8 that pilot scale laboratory anodes were homogeneous in nature. The error bars indicated that the differences in density measured from different cores at different position of the anodes was insignificant. The density of the anode samples were measured by standard ASTM method (section 3.2.2.3).

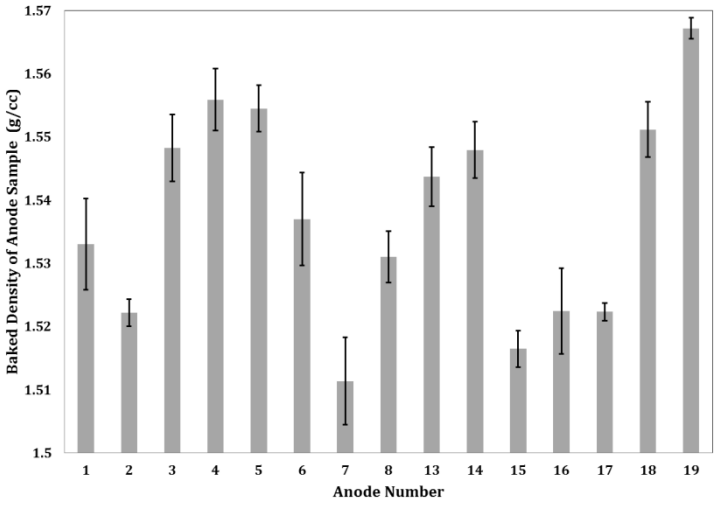

Figure 5.8 Baked density of anode samples

5.1.4.2 Electrical resistivity of green and baked anodes

The electrical resistivity (ER) measurement is essential to determine the anode quality. The ER gives an indication of the structural integrity through the current conducting properties of the anode. Electrical resistivity of anode is closely related to anode density. Generally higher density anodes should yield lower ER as dense anode contains lower porosity. However, this is not always the case as highly dense anodes can have more crack formation during baking which results in higher ER. Several physico-chemical transitions occur in anodes at different stages of heat treatment. Different types of chemical reactions take place and their relative contribution is dependent on the concentration and reactivity of different pitch components. Thermochemistry of reactions taking place during baking is complex. The principal chemical reaction is dehydrogenative polymerization of aromatic compounds. Initially, monomeric PAHs undergo addition reaction to produce biaryls and

oligo-aryls. Afterwards, bi- and oligo-aryls go through intramolecular dehydrocyclization reactions to form pericondenzed aromatic systems which continue to grow larger by cross linking [166, 167]. At this stage, evolution of mesophase occurs and these spherical molecules go through polymerization reactions which generate long chains of molecules, consequently, reduce specific electrical resistivity of anodes [166, 168]. On the contrary, production of bigger mesophase spheres in higher quantity could hinder the pitch penetration into pores. In addition, bigger molecules could generate more cracks. Also, this kind of polymerization reactions are reversible in nature and upon reaching to their decomposition temperature, the reversible transition begins. This might lead to an increase in the anode ER. Therefore, it is hard to find a clear-cut relation with baked density and ER. The ER of the green and baked anodes was measured using custom made equipment developed at UQAC (section 3.2.2.4) and results are presented in Figures 5.9, 5.10, and 5.11.

The results showed that anode produced without butt had the lowest electrical resistivity. ER increased if butt was added to the aggregate recipe. However, it slightly changed with further increase in butt content. This result is in contrast with the work reported by Belitkus (1980) [100]. Anode 17 exhibited lowest density that resulted highest value of ER. Anode 2 had somewhat higher ER compared to anode 1 (both were made from the same recipe and butt content). Highest green and baked density of anode 1 (standard recipe) gave lowest ER among all the recipes studied with different butt content. The decrease in baked anode resistivity observed for anode 15 compared to that of the standard anode could be attributed to the absence of butt particles. Since the mechanical properties of butts and fresh coke are

different, the stress created at the positions where butt is present might cause new cracks to form.

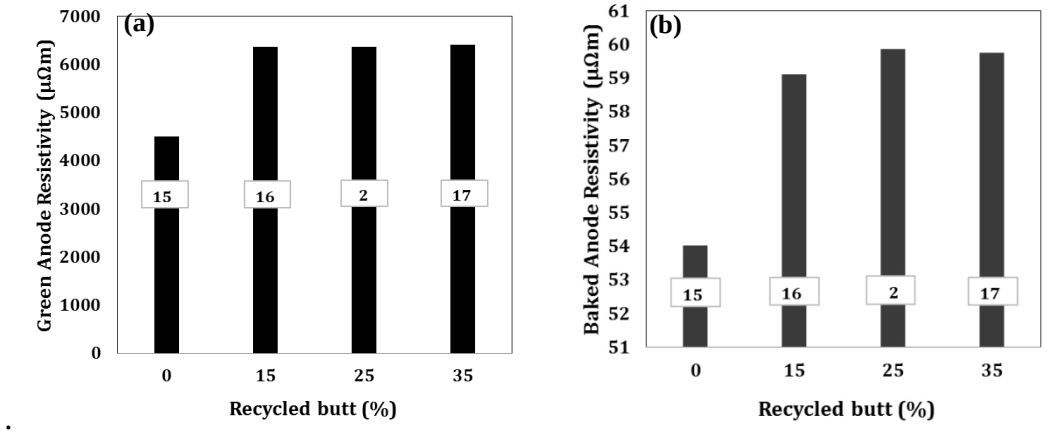

Figure 5.9 Effect of butt content on (a) green and (b) baked anodes electrical resistivity

Table 5.2 showed the ER of the anodes as functions of pitch content in the anodes. The ER was reduced with increased pitch level to 15% from 14%. This result was in good agreement with the findings of Figueiredo *et al.* (2005) [73]. Previous investigation demonstrated (section 5.1.4.1) that for higher pitch content, density was higher which was directly reflected on electrical resistivity results. Of course this is only true if the anodes are not overpitched.

The ER values of the green and baked anodes produced from different paste recipes are plotted similarly as 3-D plot used to describe anode density shown in the Figure 5.10 and 5.11. The changes in ER of anodes with different recipes followed the same trend as the density. In most cases, highly dense green and baked anodes displayed lower ER. For some baked anodes, this trend was not followed. This can be explained with the fact of mesosphere formation which was described earlier. Decrease in medium fraction with

adjusted coarse, fine and butt content led to a general decrease in green ER. Previous investigation in the present study confirmed that the best recipe (anodes 3, 4, and 5) found among the recipes tried during this study had highest density (Figure 5.10, Figure 5.11, and Table 5.2). This trend was consistent for ER and resulted lowest ER for both green and baked anodes. The 3-D plot (Figure 5.10) showed that anode electrical resistivity of baked anodes produced from the best recipe (anodes 3, 4 and 5) reduced significantly from 59 μΩm to 54 μΩm compared to standard recipe (anodes 1 and 2). Anode produced from CPC2 also displayed similar tendency and anode ER of baked anodes formed from the best recipe (anode 19) reduced from 60 μΩm to 55 μΩm compared to standard recipe (anode 18) (Figure 5.11). Anodes 12 and 13 were produced from similar recipe but green ER of anode 12 was higher. Since the recipe of anode 13 resulted in much higher density, its resistivity was lower. Anode 14, which showed a higher density value, exhibited lower ER in unbaked stage; but, after baking, the ER value was just slightly lower than the standard recipe. Similar trend was observed for anode 13. Alternatively anode 7 and 10 which had comparatively lower ER before baking gave higher ER after baking compared to the standard recipe (Figure 5.10, Figure 5.11, and Table 5.2). Thermochemical changes and formation of mesophase during baking could be the probable reason behind this behaviour as described in different literatures [166-168]. Maximum values of ER were measured for anode 2 and 9 before baking (Figure 5.10). Similarly Anode 10 showed the maximum value of ER after baking (Figure 5.11).

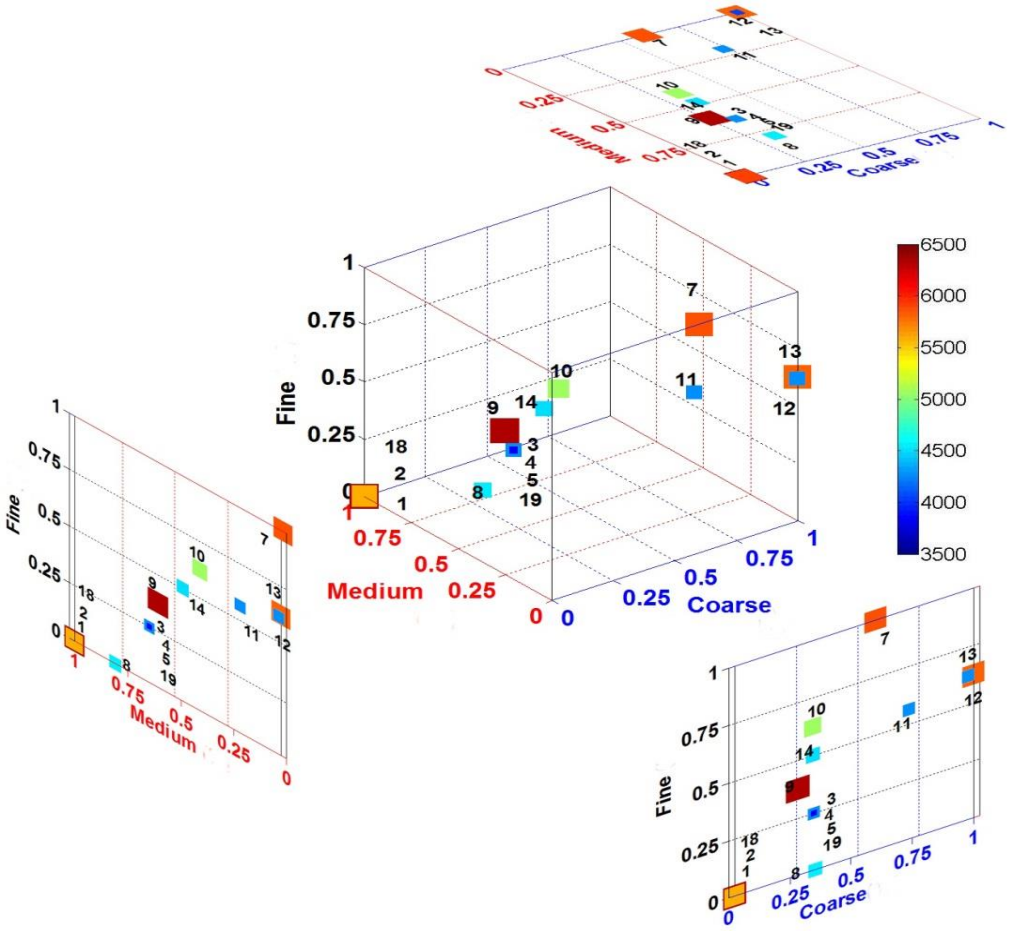

Figure 5.10 Electrical resistivity of green anodes produced from different recipes (symbol size increases with increasing electrical resistivity)

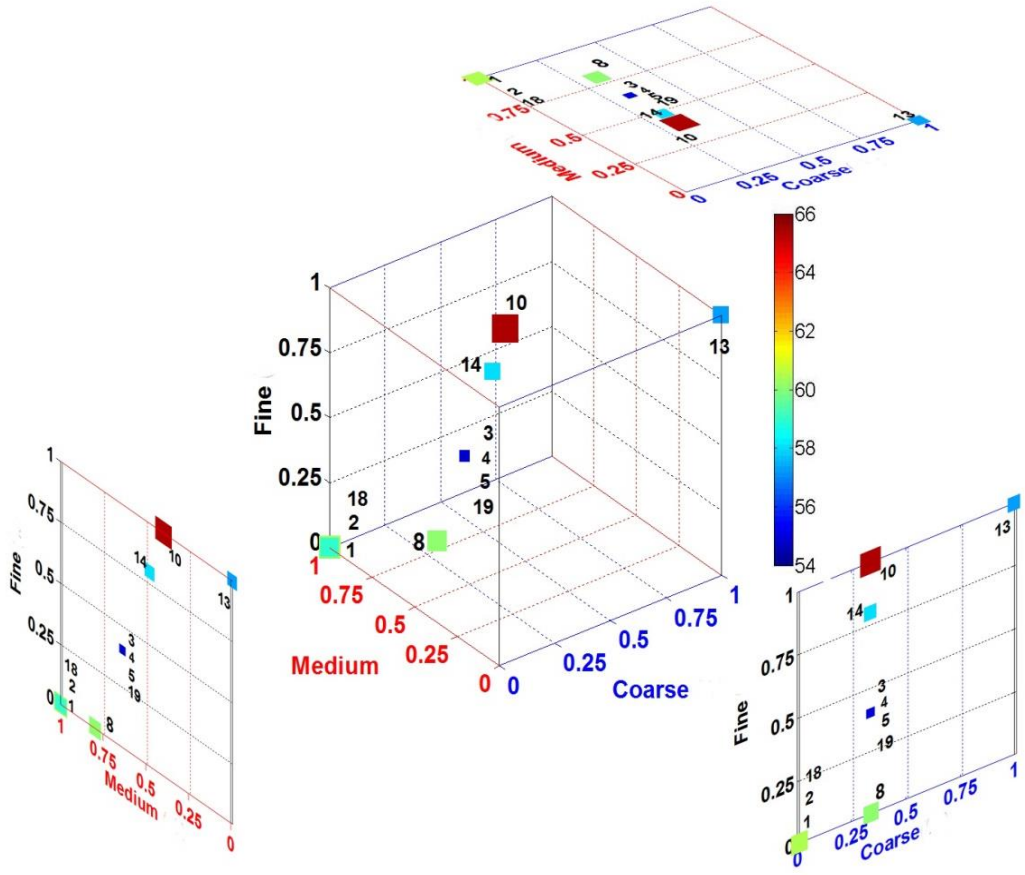

Figure 5.11 Electrical resistivity of baked anodes produced from different recipes (symbol size increases with increasing electrical resistivity)

The ER results of baked anode samples were summarized in Figure 5.12. The standard deviation of anode samples showed that there is small variation in ER measured from the different cores of the same anode. These results indicated that pilot scale laboratory anodes were relatively homogeneous in nature. The ER of baked anode samples for anode 14 is the lowest in Figure 5.12 which is not the case for ER of the baked anode 14 in Table 5.2. Also anode 7 has the highest ER in Table 5.2, but trend was changed for anode samples (Figure 5.12). The variance was due to the difference between the whole anode measurements and

core samples measurements. The differences in results show that cores do not necessarily represent the whole anode.

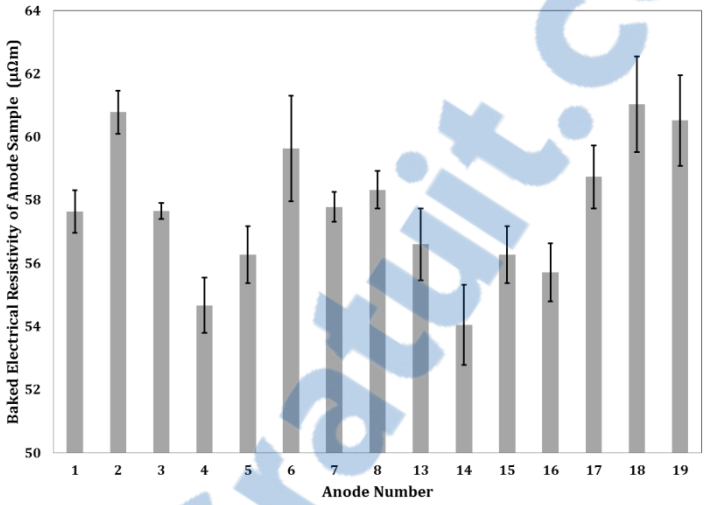

Figure 5.12 Electrical resistivity of baked anode samples

5.1.4.3 Air reactivity

The raw results were given in Table 5.3; Figures 5.13 to 5.15 illustrate the trends observed for air reactivity of anodes, made with two different types of coke and with different recipes including different butt and pitch content. As far as reactivity is concerned, only those of high baked density anodes compared to standard recipe were tested. Table 5.3 showed the air reactivity values obtained by ASTM D6559-00 a method given in section 3.2.2.6.

It could be seen from Table 5.3 and Figure 5.14 that there were differences in reactivity between the anodes produced from the same recipe such as anodes 1 and 2 (both produced from the standard recipe) as well as anodes 3 and 4 (both produced from the best recipe).

Anode 1 and 3 were produced at the very beginning of these studies. Motor speed of the vibrocompactor could not be measured at that time. It was assumed that it could have some effect on the difference in reactivity. Afterwards, the vibrocompactor speed was monitored carefully, and it was ensured that it remains constant during anode production. It could be also noted that air reactivity results followed the same trend with repetitive measurements which meant air reactivity and dusting of the anode produced from the best recipe was always higher than standard recipe. The exact reason of this deviation in reactivity for two replicates was unknown. From this point onwards the properties of anodes 2 and 4 will be used for comparison.

Table 5.3 Air reactivity data of the anodes produced from different recipes

Anode No	Butt (%)	Coarse	Medium	Fine	Pitch (%)	Total Rate (mg/cm^2h)	Dusting Rate (mg/cm^2h)	%/min	Sample Baked Density (g/cc) (core 3)
1	25	0.0	1.0	0.0	15	66.46	5.83	0.088	1.541
2	25	0.0	1.0	0.0	15	97.69	5.81	0.135	1.525
3	25	0.3	0.6	0.3	15	73.70	5.60	0.095	1.543
4	25	0.3	0.6	0.3	15	108.09	3.06	0.142	1.555
6	25	0.3	0.6	0.3	14	62.32	3.38	0.082	1.541
7	25	0.0	0.6	0.0	15	56.53	6.86	0.078	1.502
8	25	0.3	0.8	0.0	15	108.85	4.52	0.146	1.537
13	25	1.0	0.0	0.6	15	70.74	4.47	0.094	1.550
14	25	0.3	0.5	0.5	15	116.28	5.66	0.152	1.553
15	0.0	0.0	1.0	0.0	15	43.44	2.52	0.059	1.517
16	15	0.0	1.0	0.0	15	74.50	4.74	0.100	1.522
17	35	0.0	1.0	0.0	15	77.87	7.56	0.103	1.524
18	25	0.0	1.0	0.0	15	127.33	3.57	0.165	1.553
19	25	0.3	0.6	0.3	15	121.50	3.46	0.157	1.565

Figure 5.13 summarizes the effect of butt content on anode total air reactivity and dusting. The results corresponded well with those reported by Belitskus [100]. The recycled

butt additions seemed to increase the overall anode air reactivity due to its sodium content and the presence of other impurities such as potassium, calcium, aluminum, iron, sulfur, nickel, silicon, fluoride etc. [101, 169, 170]. The reactivity was minimum when anode did not contain any butt. The air reactivity was more affected by butt content than the CO_2 reactivity. The results also showed that at 35% butt content, reactivity suddenly dropped, but dusting increased continuously with increasing butt content. This could be correlated with density of the anodes. Air could react with impurities, aromatic and aliphatic carbon on the surface of the anode. Higher density represents a higher amount of carbon on the surface which in turn increases the air reactivity. As it was previously shown, anode containing 25% of butt exhibited highest green and baked density. Therefore, this could be the possible reason for higher air reactivity.

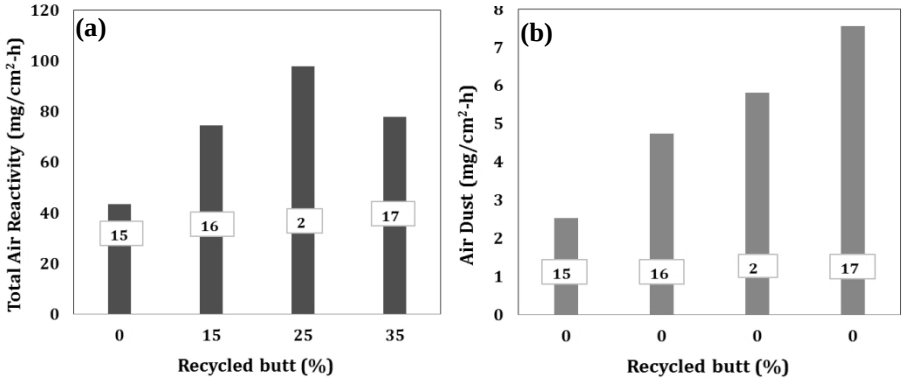

Figure 5.13 (a) Total air reactivity and (b) air dust of anodes prepared with different butt percentages

The air reactivity of the anodes seemed to be strongly affected by the anode recipe including different pitch level (Table 5.3). The anode (anode 6) with lower pitch content (14%) had a lower overall air reactivity and dusting compared with the anode containing

higher amount of pitch (15%) (anode 2). Table 5.3 shows that the amount of dust produced due to air reactivity from the anode was sensitive to the binder pitch level. The higher air reactivity was probably caused by the mechanisms of selective oxidation although the oxidation of coke was also very fast. Binder matrix was more reactive than coke causing selective air burn of the binder matrix. The higher amount of pitch resulted in increased amount of dust and air reactivity.

Figure 5.14 and 5.15 showed the total air reactivity measurement and dusting during air reactivity as a function of the anode paste recipe. The 3-D plot (Figure 5.14) depicted that with decreasing medium particles (anode 4, 8, 14, 19), anode air reactivity increased. This was due to the increase in the density with decreasing medium fractions in the anode paste recipe. As discussed earlier, highly dense anodes led to higher air reactivity due to increased contact surface. The best recipe (anode 4) of this study also indicated that this anode had higher air reactivity but lower dusting compared to the standard recipe (anode 2). In most of the recipes studied, highly dense anodes (anode 14) showed higher overall air reactivity and dusting. Figure 5.14 showes that anode 13 did not contain any medium fraction and gave lowest air reactivity. Figure 5.14 also illustrates that anode prepared from CPC 2 coke (anode 18 and 19) had higher air reactivity compared to anode produced from CPC 1 coke (anode 2 and 4) for the same recipe due to higher sodium content and higher real density for CPC 2 coke (see Table 5.1). It can be also noted from the Figure 5.15 that dusting did not follow any trend with the air reactivity. Anode 4 showed the lowest and anode 14 indicated the highest dusting values within the range of study.

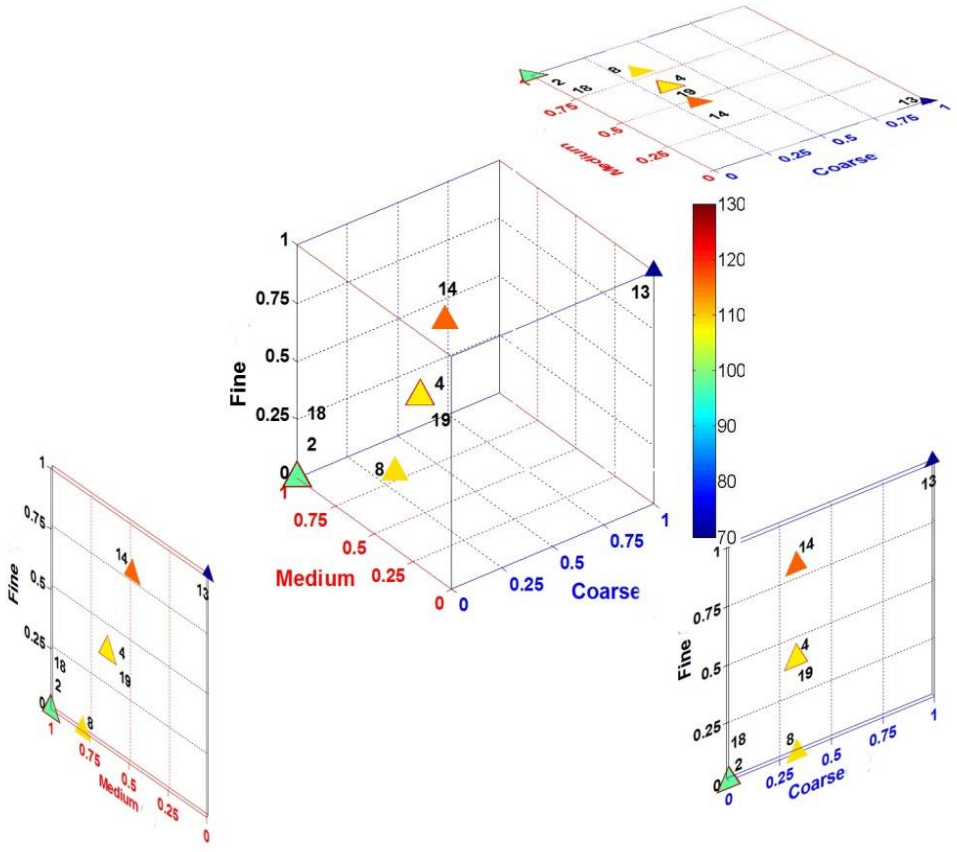

Figure 5.14 Total air reactivity of anodes prepared with different recipes (symbol size increases with increasing air reactivity)

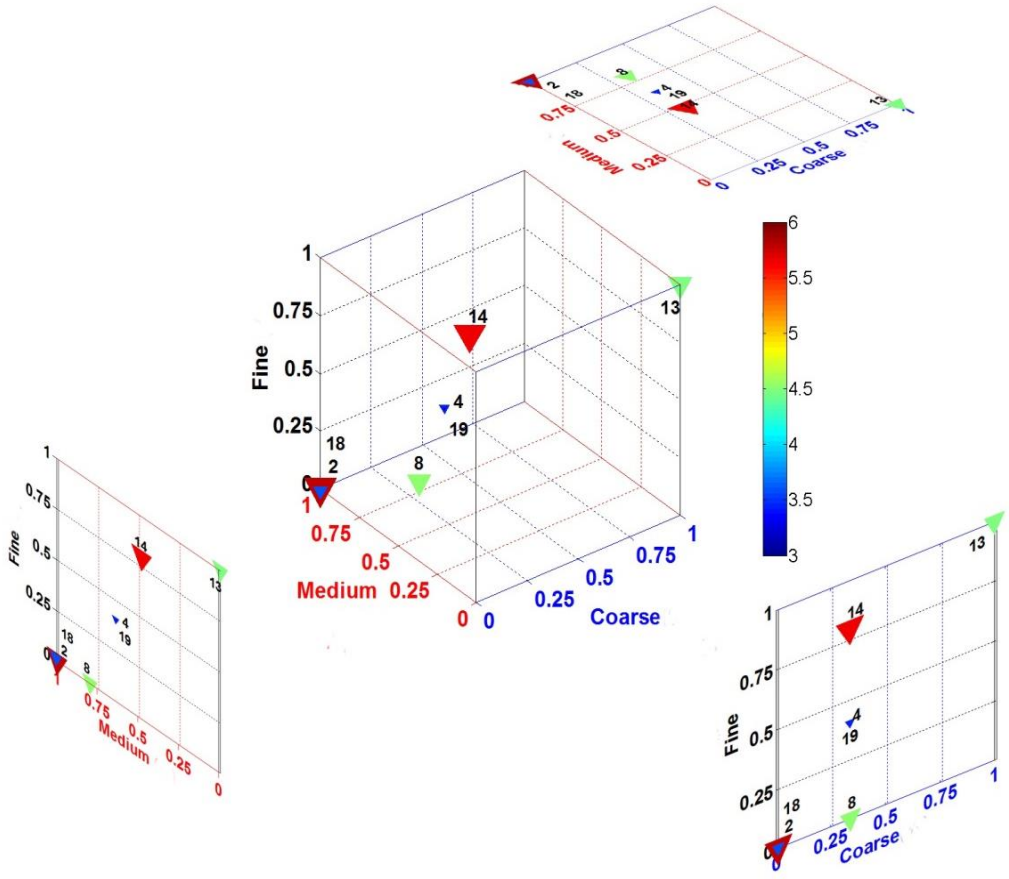

Figure 5.15 Dusting due to air reactivity of anodes prepared with different recipes (symbol size increases with increasing dusting)

5.1.4.4 CO_2 reactivity

Carbon dioxide is produced during the alumina reduction which can react with the anode carbon to produce carbon monoxide. In order to investigate the effect of anode paste recipe on the CO_2 reactivity, anode samples were tested using the method described in section 3.2.2.7.

Table 5.4 CO_2 reactivity data of the anodes produced from different recipes

Anode No	Butt (%)	Coarse	Medium	Fine	Pitch (%)	Total Rate (mg/cm^2h)	Dusting Rate (mg/cm^2h)	%/min	Sample Baked Density (g/cc) (core 1)
1	25	0.0	1.0	0.0	15	20.25	2.24	0.027	1.535
2	25	0.0	1.0	0.0	15	15.10	1.66	0.021	1.521
3	25	0.3	0.6	0.3	15	20.62	1.48	0.026	1.545
4	25	0.3	0.6	0.3	15	15.72	0.59	0.021	1.549
6	25	0.3	0.6	0.3	14	17.95	1.48	0.023	1.536
7	25	0.0	0.6	0.0	15	23.49	3.48	0.031	1.518
8	25	0.3	0.8	0.0	15	17.43	1.23	0.023	1.530
13	25	1.0	0.0	0.6	15	17.75	1.47	0.023	1.539
14	25	0.3	0.5	0.5	15	16.89	0.98	0.022	1.554
15	0.0	0.0	1.0	0.0	15	15.31	0.88	0.021	1.514
16	15	0.0	1.0	0.0	15	16.27	1.22	0.022	1.524
17	35	0.0	1.0	0.0	15	25.13	4.11	0.033	1.517
18	25	0.0	1.0	0.0	15	25.44	4.50	0.035	1.556
19	25	0.3	0.6	0.3	15	24.76	3.22	0.032	1.569

Figure 5.16 (a) displayed effect of butt content on anode CO_2 reactivity. Recycled anode butt contains many impurities. These include sodium, potassium, calcium, aluminum, iron, sulfur, nickel, silicon, fluoride and many more [101, 169, 170]. As expected, anode CO_2 reactivity increased with increasing butt content due to the presence of impurities. However, anode CO_2 reactivity is not only dependent on the level of impurities but also on anode density. All anodes with different butt level displayed a similar trend with respect to density. Higher density of anodes exhibited lower CO_2 reactivity. Though anode 2 has 25% butt content, it exhibited lower CO_2 reactivity due to its higher density. CO_2 reactivity depends on the diffusion where it is solely determined by the ability of this gas to penetrate

though the open pores and react with the carbon body of the anodes. Higher density corresponds to lower porosity which in turn helps reduce the CO_2 reactivity. Figure 5.16 (b) presents that anode dust formation, which increased with increasing butt content due to increased impurity content.

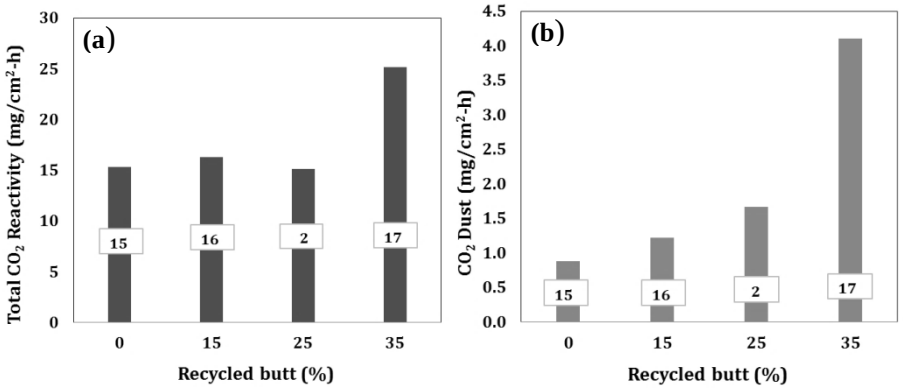

Figure 5.16 (a) Total CO_2 reactivity and (b) dusting due to CO_2 reactivity of anodes prepared with different butt percentages

CO_2 reactivity of anodes depends on several factors such as the type and proportion of raw materials in the anode recipe (amount of pitch, coke and butt), the impurity content of the anode and anode density and graphitization level [17, 50, 80]. CO_2 reactivity and dust also decreased as the level of pitch was raised (anode 4 and 6; Table 5.4). This result is also well associated with the effect of apparent density on CO_2 reactivity. The CO_2 reactivity and dusting results for other recipes are presented in Figures 5.17 and 5.18, respectively. Figure 5.17 shows that anode CO_2 reactivity reduces with the reduction in medium fractions in the paste recipe compared to standard recipe (anode 2). This result is directly related to the anode density. A trend was previously observed that a reduction (anodes 4, 8) or complete elemination (anode 13) of medium fractions from recipe with adjusted amounts

of coarse, fine and butt improved the anode density (Figures 5.6-5.7 and Table 5.2). It can be also noticed from Figures 5.17 and 5.18 that total CO_2 reactivity of anode 4 (best recipe) was similar to anode 2 (standard recipe), but the dust rate was much lower for anode 4 (best recipe) due to higher density of anode 4 compared to anode 2, which helped reduce the CO_2 gas diffusion into anode. Another recipe (anode 14) also exhibited significantly lower dusting compared to that of the standard recipe and displays a promising future. Anode produced from CPC 2 coke (anodes 18 and 19, Figures 5.17 and 5.18), displayed comparatively higher rate of reactivity and dusting due to lower concentration of sulfur. It was found in literature that sulfur inhibited the catalytic activity of metal impurities [17, 87, 96]. Effect of sulfur was discussed in the next section.

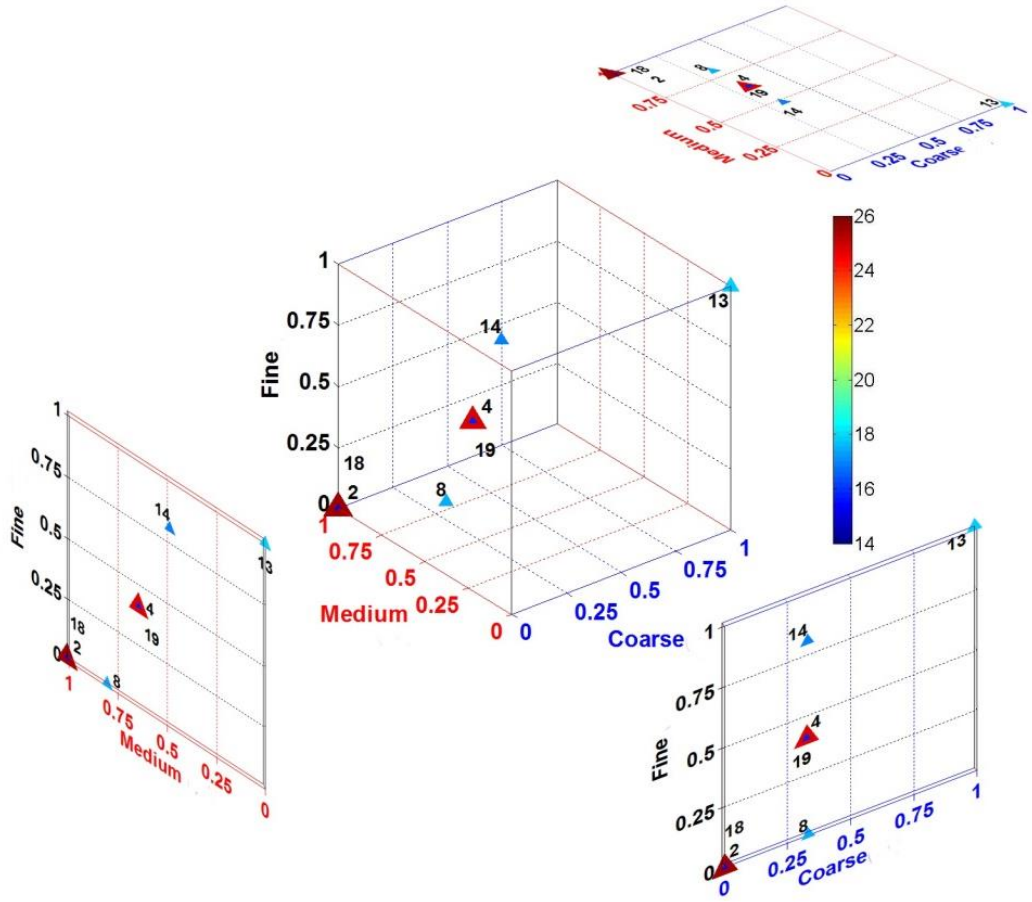

Figure 5.17 Total CO_2 reactivity of anodes prepared with different recipes (symbol size increases with higher values)

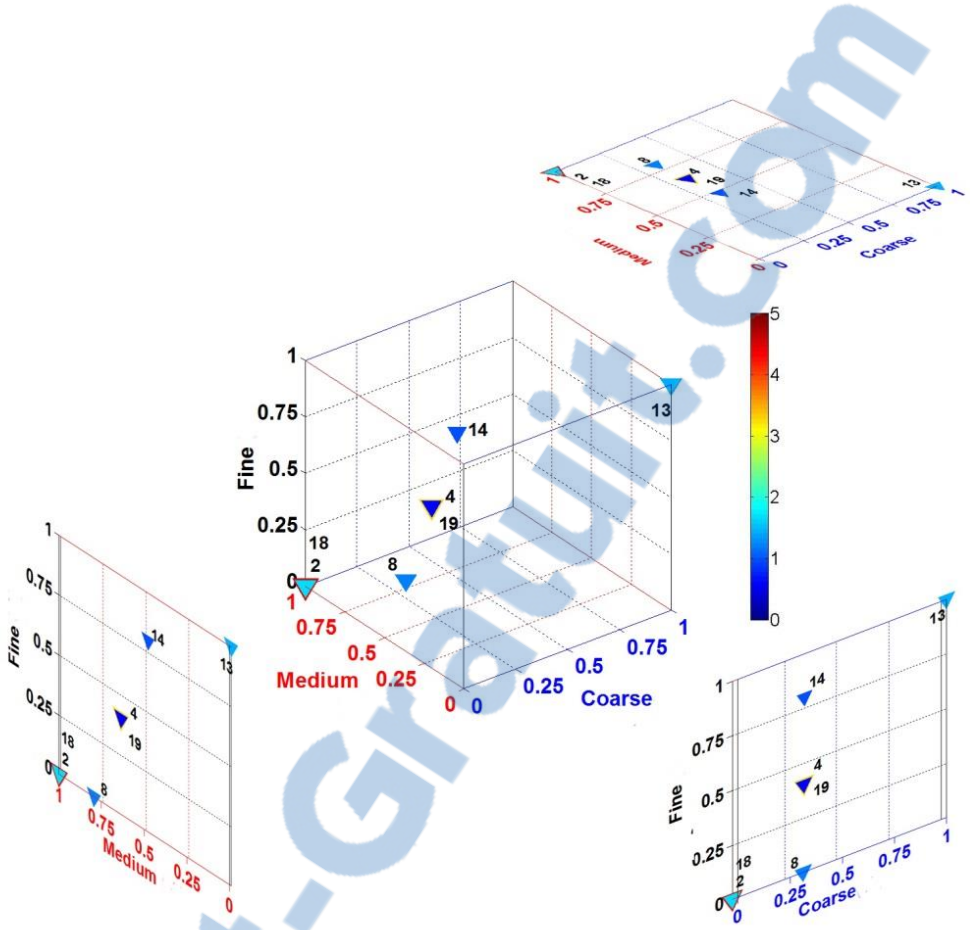

Figure 5.18 CO_2 dust of anodes prepared with different recipes (symbol size increases with higher values)

The carbon anodes are consumed during the electrolysis process and have to be replaced every 2-4 weeks depending on the size and density of the anode and the operating conditions of the electrolytic cell. However 7 h CO_2 test does not represent the actual reactivity and dusting in the electrolysis cell as anodes are exposed to the bath for longer times. For a better understanding, a 21-hour test was carried out for standard (anodes 2 and 18) and best recipes (anodes 4 and 19) for both cokes. Anodes 2 and 4 were produced from

CPC 1 coke and anodes 18 and 19 were produced from CPC 2 coke. The results of the 21-hour CO_2 test were shown in Figure 5.19. Results demonstrate that for best recipe (anodes 4 and 19), total CO_2 rates were reduced and compared to those of the standard recipe (anodes 2 and 18). It could be also seen from Figure 5.19 (a) that the final rate was significantly reduced for best recipe (anodes4 and 19) for both cokes. Dusting rate was always better for adjusted best recipe regardless of the type of cokes (anodes 4 and 19). The reason for this behaviour could be higher density of the best recipe compared to the standard recipe. Also, anode produced from CPC 2 coke exhibited higher CO_2 reactivity and dusting due to lower sulfur content in the coke.

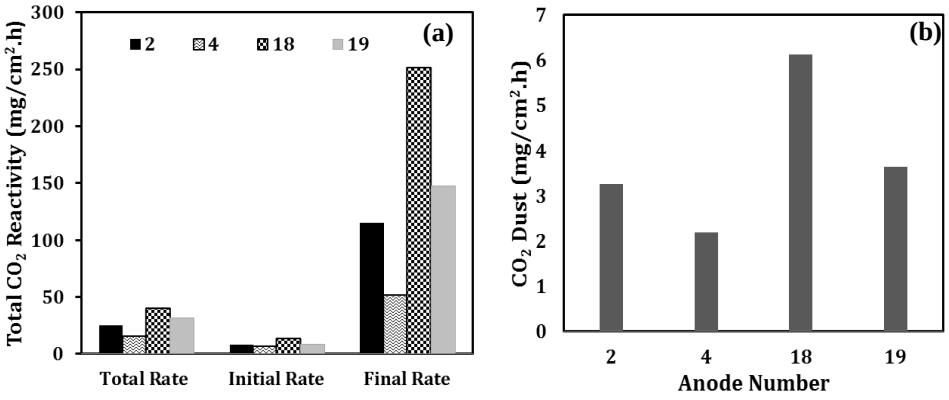

Figure 5.19 (a) Total CO_2 reactivity (21 h) and (b) CO_2 dust (21 h) of standard and best recipes

5.1.4.5 Uniaxial compressive strength

The compressive strength at room temperature is the capacity of a material to withstand axially directed compressive forces. When the limit of the compressive strength is reached, the materials are crushed. The effect of the recipe on physical properties and reactivity was studied and the results are presented in the previous sections. However, the granulometry

also affects the mechanical properties. Therefore, the compressive strength of anodes was measured according to ASTM standard described in section 3.2.2.9. The modulus of elasticity (Young's modulus) was determined experimentally from the slope of the stress-strain curve created during compression experiments. A low Young's modulus means a small slope and therefore represents a material with high elasticity. The evolution of mechanical properties was done to ensure that the recipe proposed in this study was mechanically feasible. The compressive strength and young modulus of the samples were tabulated in Table 5.5. All the young modulus data are put to dimensionless form by dividing the real value by the highest value.

Table 5.5 Compressive strength of anode sample

Sample No (Anode-Core)	Compressive Strength (MPa)	Young Modulus[1]	Specification
1-2	36.7	0.86	Std-CPC1
3-2	30.5	0.82	Best-CPC1
2-2	35.7	0.92	Std-CPC1
4-2	32.6	0.69	Best-CPC1
5-2	42.5	1.00	Best-CPC1
5-4	40.0	-	Best-CPC1
18-2	37.6	0.93	Std-CPC2
19-2	37.4	0.91	Best-CPC2

[1] Dimensionless value

The compressive strength values were found to be within an acceptable range. Anode 3 and 4 showed slightly lower compressive strength compared to that of the standard but anode 5 exhibited higher value. Anode 19 produced from coke CPC 2 showed similar compressive strength with standard recipe anode 18. Similar trend was observed with the lower value of Young modulus. It seemed the pilot scale laboratory anodes were elastic in

nature. A probable cause of this lower value of compressive strength for anode 3 was micro cracks. These results indicated that it was possible to produce anodes using the best recipe found during this study with a compressive strength within a practical limit of 30-65 MPa [85].

5.1.4.6 Flexural strength (Bending)

The flexural strength of anode produced from best and standard recipe was compared (Table 5.6) in order to carry out final screening. The test results showed that the anode from best recipe had quite similar flexural strength with standard recipe and varied within the range of 9-11 MPa. The flexural strength values of optimum best recipe lied within in the practical range of industrially accepted anode flexural strength of 4–14 MPa [85].

Table 5.6 Flexural strength (Bending) of anodes

Anode No. (Anode-Core)	Bending stress (MPa)	Specification
1-4	11.3	Std-CPC1
3-4	8.7	Best-CPC1
2-4	10.7	Std-CPC1
4-4	11.0	Best-CPC1
18-4	10.7	Std-CPC2
19-4	9.8	Best-CPC2

5.1.5 Concluding remarks

The stability of the raw material supply is one of the important issues for the aluminum industry. It is very important to find alternative ways to produce good quality anodes. Extensive pilot scale work on determining the effect of coke properties, particle size

distribution, butt content and binder level on anode properties was done. The characterization test results made the comparison of the anode properties, consequently, endeavoured to understand the relative influences of different factors on the anode quality. A new recipe was developed which possessed better anode properties compared to the standard recipe. The results showed that reducing the medium fraction to a certain level, improved the overall anode quality, but further reduction and/or complete elimination of this fraction deteriorated the quality.

Recycled butt contained impurities such as sodium which increased the reactivity of the anode. Also, recycled butt contained less porosity which could result in overpitching, consequently, increasing the volume of the anodes which, in turn, decreasing the density. Anode resistivity increases as pitch coats the outside of the particle and creates hindrance to the current flow as pitch is nonconductive in green (unbaked) state. Therefore, the overpitching is not desired. Anode produced from CPC 2 coke displayed higher reactivity values due to the presence of low sulfur. Experimental results confirmed the efficiency of new recipe irrespective of type of coke used. The anodes made with the best recipe had reasonable compressive and flexural strengths which were in the industrially accepted range. This study, to our knowledge, is the one of the rare studies which produced and tested anodes with properties similar to those of the industrial anodes. This might make their application possible in industry. An industrial trial is in planning stage to test the best recipe of this study.

5.2 Influence of coke crystallinity and sulfur content on anode reactivity

5.2.1 General

Carbon anodes are produced from the mixture of petroleum coke and coal tar pitches. The reactivity of the carbon anodes are mostly influenced by the coke structure, porosity and impurities. In this study, the effect of two factors, namely, coke crystalline length (L_c) and sulfur content were studied using laboratory scale anodes.

The coke crystalline length, which is a measure of the rearrangement and alignment of the graphite planes, is related to the coke structure as explained in Section 2.1.1.1. In current years under-calcined coke gained attention as raw material for anode production since it is cited in literatures that anodes produced with this type of coke have lower CO_2 reactivity and less dusting in the pot room. Correspondingly, reduction in calcination temperature helps to reduce fuel consumption of the calciner and, hence, the production cost decreases [10].

In addition, temperature also seems to affect the anode reactivity. Furthermore, it is reported in literature that increasing sulfur content of anode decreases CO_2 reactivity. However, sulfur content should be within a certain limit due to the effect of gaseous sulfur compounds on environment.

As explained above, there are studies reported in the literature on the effect of coke crystalline length as well as anode baking temperature and coke/anode sulfur content on anode properties. However, in general, these are studied separately [9-11, 87, 89, 93]. There are some studies on the combined effect of crystalline length and baking temperature on

anode reactivity [9, 11, 53] but the effect of all three (crystalline length, baking temperature, sulfur content) parameters were never studied under the same conditions. Also, most of the literatures available in this topic had incomplete information. In various sources of literature, the information regarding anode baked density, air reactivity and dusting (air and CO_2) was not included [10, 11, 22, 87, 90, 91]. In this study, a systematic approach was taken to investigate the combined effect of these factors on baked anode density, reactivities (air and CO_2) and dusting (air and CO_2) of anodes.

5.2.2 Materials

In the present work, under-calcined coke (UCC) and coke calcined under standard conditions (SCC), which were derived from a single source, were used. Anodes were produced from these cokes with different crystallinity using standard recipe but without any addition of recycled butt (except in ball mill product). The butt addition is avoided since their impurity content is relatively high and butts made with the same cokes were not available. Using butts which are made of cokes with different L_c than the one studied, might prevent to see clearly the effect of degree of calcination. However, the ball mill product was included in the recipe since the fine particles have a substantial effect on the anode properties. The ball mill dust fraction was either taken from another standard calcined coke (CPC1) or prepared in a hammer mill in the laboratory using the pan fraction of the same cokes (two different cokes with different crystalline lengths of 24Å and 30Å). By using the hammer mill, it was possible to avoid the contamination of the dust fraction by iron, which was caused by steel balls in the ball mill as well as butts. Also, in this case,

BMP dust fraction had the same Lc as the other fractions used since it was produced from them. The coke with a crystalline length of 24Å was denoted as under-calcined coke (UCC) whereas coke with a crystalline length of 30Å was designated as standard calcined coke (SCC). First, the effects of coke crystalline length (24Å and 30Å) and baking temperature (1050ºC and 1150ºC) on anode reactivity and dusting were studied.

To study the effect of sulfur content on anode reactivity and dusting, it is necessary to make anodes with different sulfur contents. Pitch used in this study has very low sulfur content (around 0.45%). Therefore, sulfur mainly comes from the coke. If different cokes with different sulfur contents are used to make anodes, it is not possible to compare the results since it is also almost impossible to find two cokes, which differ only in sulfur content. Usually, the contents of all the other impurities change and it is well-known that different impurities also affect the reactivity and dusting. Therefore, it was decided to add sulfur to coke in order to produce anodes with different sulfur contents. Nevertheless, the sulfur has to be added in a form similar to the one naturally present in coke. Sulfur can be present in coke in both organic and inorganic forms such as thiophenes, pyrite and sulfates. According to literature, the majority of the sulfur in coke is in thiophene form. Thus referring to the work of Sorlie and Engvoll [93, 166], sulfur containing organic compound dibenzothiophenes (DBT) was chosen as sulfur dopant and added to the finer fraction of the cokes. Dibenzothiophene was chosen due to its stability of sulfur atom in large polymeric structure which can be removed only at high temperatures.

Eight anodes were prepared at UQAC laboratory. Four of the anodes were produced using UCC (L_c=24Å) and the other four anodes were made with SCC (L_c=30Å). All the

anodes were made with the same recipe. Anode samples were baked at two different temperatures, which were within the range used in industry, in the laboratory baking furnace described in section 3.2.1.4. Four of the anodes were made without sulfur addition. These were used to study only the effect of crystalline length and baking temperature.

The other four anodes were prepared with the coke doped with sulfur. These were used to study the combined effect of sulfur content, crystalline length and baking temperature. All the average anode properties (green and baked anode density, resistivity, air an CO_2 reactivity) of the eight anodes were normalized using Equation 4.1. Zero value means the lowest value and 1 denoted the highest value among the range of sample studied.

The coke properties including the coke sulfur contents were given in Table 4.7. The crystalline length of cokes, BMP preparation method and initial sulfur contents of green anodes were given in Table 5.7.

Table 5.7 Information on green anode preparation

Anode No	**Lc of Coke Used (Å)**	**BMP Preparation Method**	**% S (Total S Content of Green Anodes)**
20	24	Crushed in a laboratory hammer mill	2.84
21	30	Crushed in a laboratory hammer mill	2.81
22	24	Industrial BMP	2.79
23	30	Industrial BMP	2.77
24	24	Industrial BMP	2.9
25	30	Industrial BMP	3
26	24	Industrial BMP	2.9
27	30	Industrial BMP	3

5.2.3 Effect of coke crystallinity and baking temperatures on anode properties

All manufacturers of carbon anodes for aluminum industries are continuously seeking to improve the anode properties in order to reduce the aluminum production cost. In this part of the study, the green and baked anodes are characterized by measuring the anode density, electrical resistivity and reactivity (CO_2 and air) and dusting. Anode reactivity and dusting affect the excess carbon consumption in the pots. The electrical resistivity is related to the energy consumption in the pot. The anode density influences both the anode consumption and the reactivity. The properties of anodes made were given in Table 5.8.

Table 5.8 Properties of green and baked anodes made from UCC and SCC

Anode No.	Core No.	Coke L_c (Å)	Baking Temperature (^oC)	Green Anode Density*	Baked Anode Density*	Green Anode Resistivity*	Baked Anode Resistivity*	Type of Reac.
20	1	24	1050	0.60	0.31	0.34	0.89	CO_2
20	2	24	1150	0.33	0.41	0.35	0.82	CO_2
20	3	24	1050	0.36	0.39	0.36	0.90	Air
20	4	24	1150	0.63	0.52	0.12	0.47	Air
21	1	30	1050	0.43	0.52	0.09	0.65	CO_2
21	2	30	1150	0.50	0.63	0.08	0.51	CO_2
21	3	30	1050	0.61	0.51	0.06	0.63	Air
21	4	30	1150	0.63	0.52	0.12	0.47	Air

*Density and resistivity values were normalized by column wise using Equation 4.1(using the data base of all eight anodes).

The influence of coke crystallinity on green anode density and electrical resistivity was shown in Figure 5.20. Anode green density increased slightly with increasing calcination level (L_c). Green anode electrical resistivity showed completely inverse trend and decreased

with increasing density. Also, the wettability results (section 4.2) indicated that UCC had good wetting characteristics. The results presented here are in agreement with the wettability results. Green anode density of anodes made of UCC were found to be lower compared to those of the anodes made with SCC since real density of the UCC was considerably lower than that of SCC [10, 21, 53] (Table 4.7). Also, resistivity of the anodes made with UCC was found to be higher due to its lower density and lower crystalline length as it was well-known and reported in the literature that coke resistivity decreased with increasing calcination level [53].

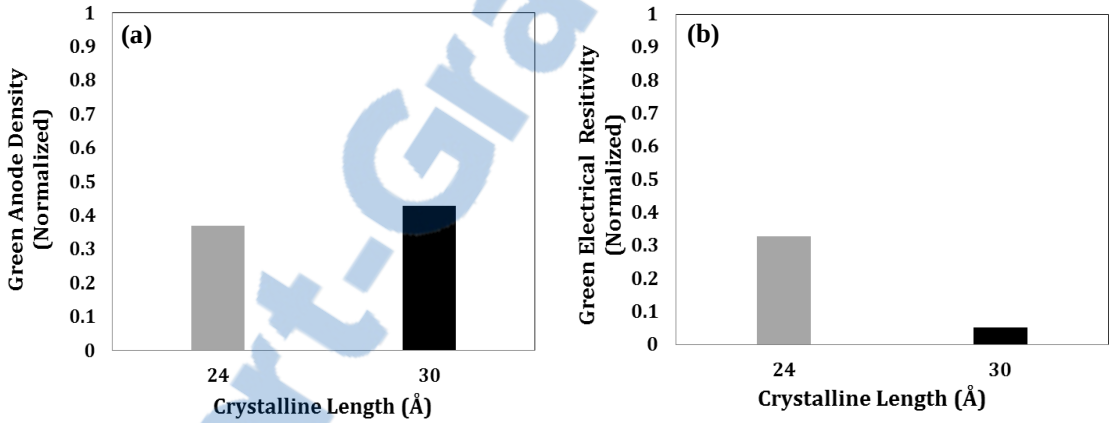

Figure 5.20 Effect of coke crystalline length on green anode properties (a) normalized density (b) normalized electrical resistivity

Figure 5.21 compared the effect of baking temperatures on baked anode properties (density and resistivity) made of UCC and SCC. The results were average of two core sample measurements. The laboratory anodes produced with UCC (lower crystalline length) had a lower baked density and higher electrical resistivity. Baked anode density increased notably as the baking temperature increased.

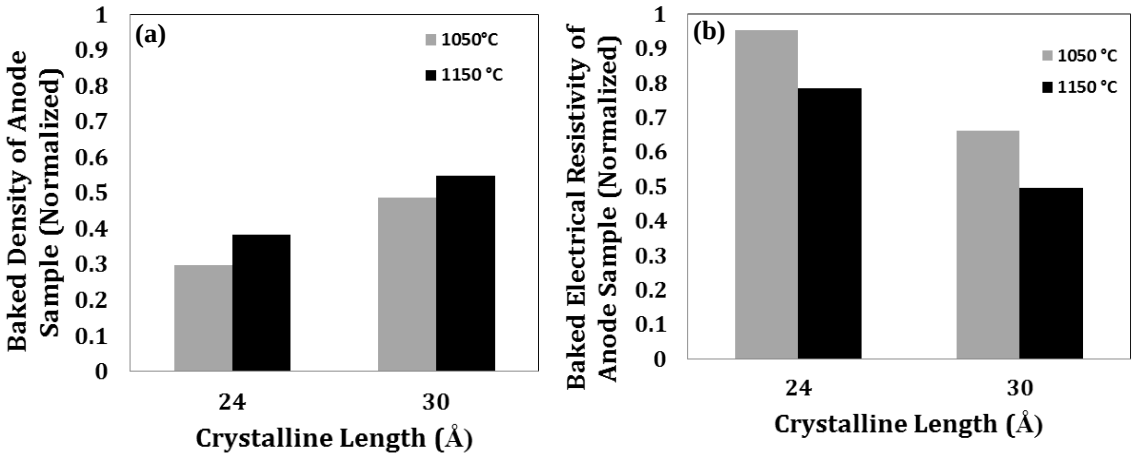

Figure 5.21 Effect of coke crystalline length on baked anode (core sample) properties (a) normalized density (b) normalized electrical resistivity

The electrical resistivity decreased as the baked density of pilot scale anodes increased. It was witnessed by many authors that an overall increase in particles packing improved the coke grain bridging and influenced the electrical contacts between particles [5, 72, 75, 171]. This is valid when there is no crack formation due to the conditions used for obtaining high density anodes such as overcompaction.

Conflicting results were reported in literature regarding the effect of coke calcination level on anode reactivity and dusting [9-11, 50, 53]. The potential reasons could be variation in recipe, source of coke, and essentially the baking level. Figure 5.22 presents air reactivity and dusting rate due to air reactivity of anodes produced from UCC and SCC. A clear correlation was observed with both crystalline length and baking temperature. The results revealed that the air reactivity and dusting were lower for UCC anode compared to those of the SCC anodes. Baking at higher temperature reduced the advantage of using UCC regarding the air reactivity and dusting although UCC anodes were still slightly better

under the conditions used during this study. It is possible that this advantage will disappear completely if baking temperature is further increased.

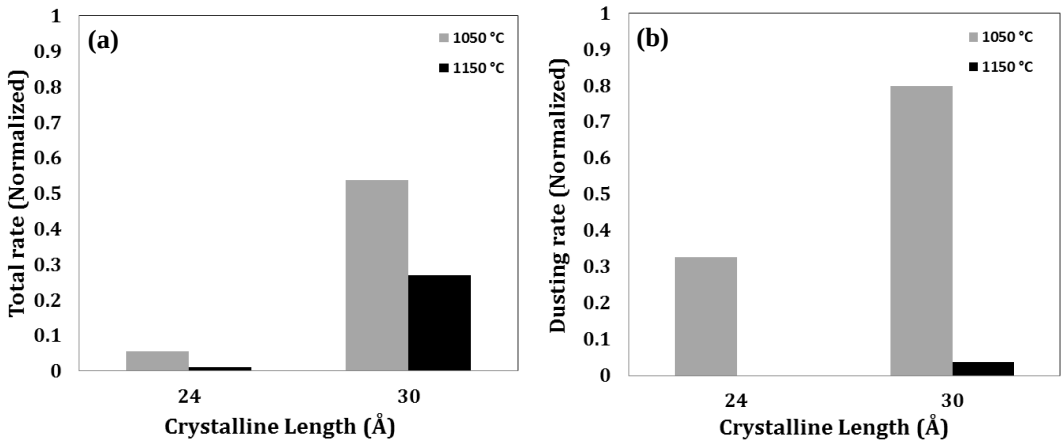

Figure 5.22 (a) Normalized air reactivity and (b) normalized dusting rate as a function of coke crystalline length and anode baking temperature

The CO_2 reactivity and dusting rates of the UCC and SCC anodes are presented in Figure 5.23. The results show that using UCC reduced the dusting at both baking temperatures but the differences were more prominent at lower baking temperature. For UCC anodes, the dusting was significantly reduced compared to SCC anodes for both temperatures. This result shows the importance of the anode baking temperature on dusting. The CO_2 reactivity was reduced with increasing temperature. However, the difference in the reactivity of anodes made of UCC and SCC were not very different. At lower baking temperatures, their CO_2 reactivity was similar. At the higher baking temperature, reactivity of the anode made with UCC was slightly lower.

Above results were well correlated with the results reported by Sulaiman *et al.* (2012) [10]. The CO_2 dust of the anodes made from SCC were always higher than UCC but

variation in dusting rates were reduced at higher baking level. This was due to structural reorientation of both binder and filler phase during baking at higher level. Anode dusting reduced at lower baking temperature for anode prepared with UCC compared to anodes made with SCC due to homogeneous reactivity between coke and binder pitch, similarly as reported in literature [9, 11]. If baking temperature was too high, under-developed coke structure of UCC underwent structural changes (re-calcination), and the overall reactivity increased since the oxidation became selective.

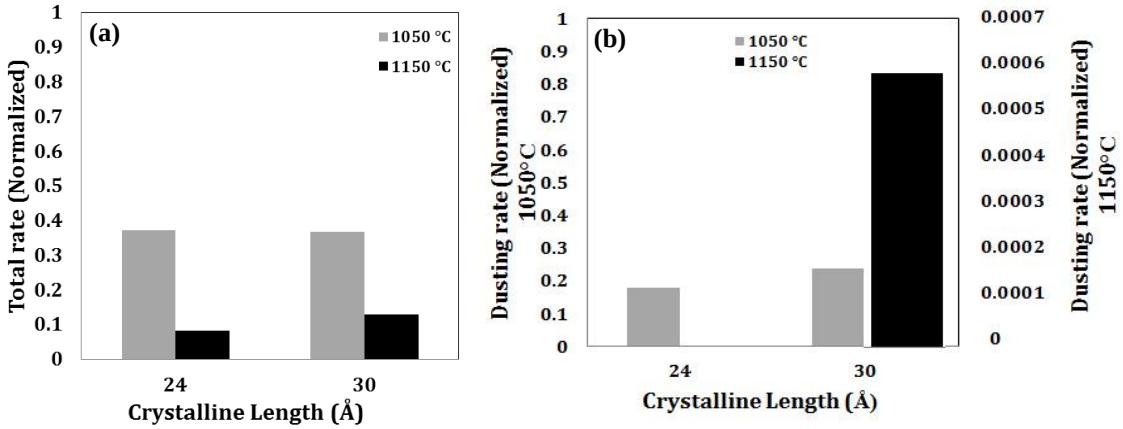

Figure 5.23 (a) Normalized CO_2 reactivity and (b) normalized dusting rate as a function of coke crystalline length and anode baking temperature

Thus, it could be said that the baking temperature influenced significantly both air and CO_2 reactivities.

5.2.4 Combined effect of coke crystallinity, sulfur content and baking temperatures on anode reactivity

Table 5.9 summarized the ranges of sulfur before and after baking, as well as initial sulfur content in coke. There was no additional sulfur in the anodes 22 and 23. Sulfur was added to the finer fractions (ball mill product) of the coke in the paste recipe of the anodes 24 to 27 and they were baked at two different temperatures. Sulfur content of the anodes before and after baking was measured using LECO elemental analyser at COREM research lab in Quebec City. The detailed procedure was discussed in section 3.2.2.11. The loss of sulfur was probably due to early evaporation during anode production (during mixing mainly) and mostly due to baking at higher temperature. The results presented in Table 5.9 showed that sulfur loss was generally more at higher baking level. Also, it could be noted that the overall sulfur content was usually more in case of UCC. UCC contained more hetero atoms which could bind more sulfur by forming covalent bond that might result in slightly greater amount of sulfur in anodes even after baking.

Table 5.9 Sulfur content of anode before and after baking

Anode No	Initial Sulfur Content of Coke (% wt)	Sulfur Before Baking (% wt)	Baking Temperature (°C)	Sulfur After Baking (% wt)	Sulfur loss during baking (% wt)	Crystalline Length (Å)	Naming Convention*
22	2.79	2.79	1050	2.48	0.31	24	LS-24
23	2.77	2.77	1050	2.37	0.4	30	LS-30
24	2.79	2.9	1050	2.46	0.44	24	MS-24
25	2.77	2.9	1050	2.23	0.67	30	MS-30
26	2.79	3.0	1050	2.59	0.41	24	HS-24
27	2.77	3.0	1050	2.56	0.44	30	HS-30
22	2.79	2.79	1150	2.28	0.51	24	LS-24
23	2.77	2.77	1150	2.33	0.44	30	LS-30
24	2.79	2.9	1150	2.55	0.35	24	MS-24
25	2.77	2.9	1150	2.4	0.5	30	MS-30
26	2.79	3	1150	2.49	0.51	24	HS-24
27	2.77	3	1150	2.41	0.59	30	HS-30

*LS:Low sulfur content; MS: Medium sulfur content; HS: High sulfur content

Density and resistivity of green anodes produced with using different cokes with different calcination levels (UCC and SCC) and sulfur contents were presented in Figure 5.24. A naming convention was used to identify the samples : for example, LS-24 stands for low sulfur with crystalline length 24 Å. All the anode properties were given in Table 5.10.

Table 5.10 Properties of anodes produced from under and standard calcined coke with different sulfur content

Anode No	Crystalline Length (Å)	Core No	Baking Temp. (°C)	Green Density*	Baked Density *	Green Elec. Res. *	Baked Elec. Res. *	Type of Reactivity
22	24	1	1050	0.14	0.10	0.94	0.99	CO_2
		2	1150	0.29	0.00	0.90	0.60	CO_2
		3	1050	0.14	0.10	0.90	0.88	Air
		4	1150	0.29	0.30	0.91	0.64	Air
23	30	1	1050	0.43	0.30	0.51	0.46	CO_2
		2	1150	0.43	0.30	0.54	0.46	CO_2
		3	1050	0.14	0.20	0.67	0.50	Air
		4	1150	0.43	0.30	0.61	0.47	Air
24	24	1	1050	0.14	0.10	0.91	1.00	CO_2
		2	1150	0.14	0.30	0.95	0.66	CO_2
		3	1050	0.00	0.30	1.00	0.80	Air
		4	1150	0.14	0.20	0.90	0.82	Air
25	30	1	1050	0.71	0.60	0.33	0.09	CO_2
		2	1150	0.71	0.70	0.31	0.03	CO_2
		3	1050	0.71	0.80	0.21	0.24	Air
		4	1150	0.71	0.70	0.32	0.21	Air
26	24	1	1050	0.14	0.10	0.94	0.98	CO_2
		2	1150	0.29	0.30	0.83	0.76	CO_2
		3	1050	0.14	0.20	0.90	0.64	Air
		4	1150	0.43	0.20	0.74	0.81	Air
27	30	1	1050	0.86	1.00	0.05	0.12	CO_2
		2	1150	1.00	0.90	0.00	0.00	CO_2
		3	1050	0.86	1.00	0.09	0.13	Air
		4	1150	0.86	0.80	0.02	0.11	Air

*Density and resistivity values are normalized by column wise using Equation 4.1(using the data base of all eight anodes). Thus, 0 indicates the minimum and 1.00 the maximum.

In this study, anodes were produced with BMP prepared using industrial ball mill which also contained recycled butt (Table 5.7). Due to higher real density of the SCC itself, anodes made from SCC had higher density compared to the densities of anodes produced from UCC. Another interesting result was that densities of anodes manufactured from the SCC were increased with increasing sulfur content as dibenzothiophene (DBT) reduced the softening point of the pitch [93]. This effect was not evident for under-calcined coke. This might be due to the existence of higher quantity of molecules with hetero-atoms in UCC. Probably these molecules created covalent bonds with free sulfur additives leaving less amount of sulfur available to react with pitch and to reduce its softening point [92]. As a result, this probably led to only a slight increase in density with sulfur addition.

Also distribution of pitch had an important effect on anode density. As it was earlier found that $24L_c$ coke (UCC) was more wetted by the pitch (section 4.2), and it was possible that a decrease in pitch softening point with the remaining sulfur filled only the space between the particles and increased the volume. This increased the density, but only marginally. Due to greater density, electrical resistivity was found to be lower for anodes manufactured from SCC.

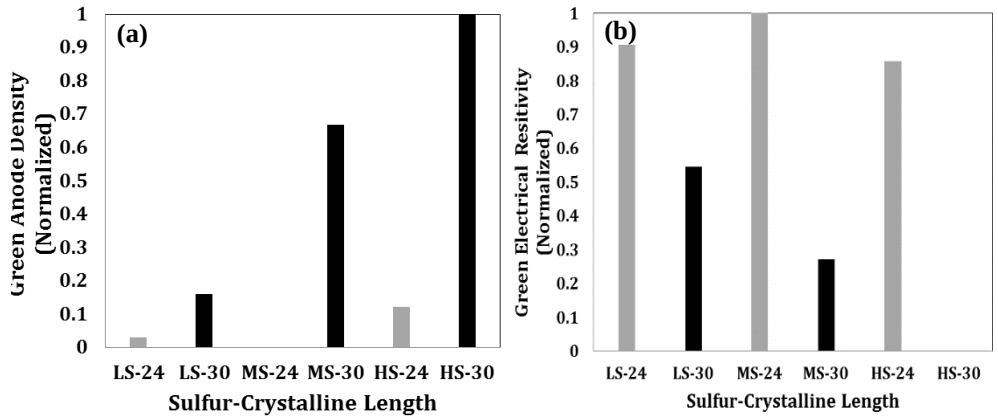

Figure 5.24 Effect of coke crystalline length and sulfur content on green anode properties (a) normalized density (b) normalized electrical resistivity

Similar trend was observed for average baked density and electrical resistivity with regard to utilization of UCC and SCC (Figure 5.25). Anode density slightly increased and the electrical resistivity slightly decreased with increasing baking temperatures. These results were in accordance with the work of previous authors [22, 93]. The results for baked density and electrical resistivity were average of two core samples.

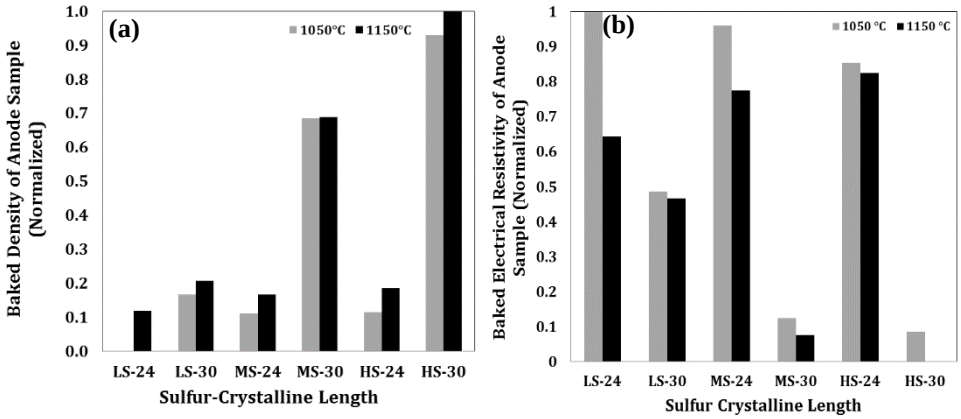

Figure 5.25 Effect of coke crystalline length and sulfur content on baked anode (core sample) properties: (a) normalized density (b) normalized electrical resistivity

Figure 5.26 illustrated the air reactivity results for anodes produced with different coke crystalline length and sulfur levels. A trend was observed that there was a reduction of air reactivity and dusting with an increased baking temperature. An increase in sulfur level increased the air reactivity and dusting for UCC coke. But for SCC coke, this effect was very slight and could be considered as insignificant. Anode produced with UCC showed lower air reactivity compared to anode produced from SCC at lower baking temperature due to homogeneous reactivity. The air reactivity for anode produced from UCC (LS-24) showed slightly greater reactivity at higher baking temperatures compared to anode made from SCC (LS-30). The possible explanation for the change in behavior at higher baking temperatures could be further calcination of coke, which eliminated the influence of UCC coke since the reactivity became selective. This in turn increased the reactivity. In the previous study, a different trend was observed (Figure 5.22) at higher baking temperature where fines (-110 μm) were crushed in a laboratory hammer mill. In this study (Figure 5.26), anodes were produced using industrial ball mill (-75 μm) which contained recycled butt and metallic impurities. Another explanation could be the activation of metal impurities at higher baking temperature which might increase the air reactivity of anodes produced from industrial ball mill product.

The air reactivity of anodes made from UCC coke slightly changed with increasing sulfur content at higher baking temperature, but the change was not significant. Also, the reactivity almost unchanged with increasing sulfur content for SCC (anode samples: LS-30 MS-30, HS-30) at higher baking temperature probably due to the effect of baking temperature and anode density.

It could be also noticed that in general air dusting rate increased with increasing crystalline length and sulfur content except for low sulfur anodes (Anodes LS-24 and LS-30) at higher baking temperature. Tran *et al.* (2009) [87] speculated the reason behind it was that sulfur weakened the bonding of neighbouring carbons in the ring structure and lowered the activation energy. Thus, the oxidation resistance of the carbon constituent decreased with increasing sulfur level. Furthermore, sulfur is very reactive in oxygen atmospheres and produces SO_2 which could lead to increased reactivity and dusting. Also, the density of the anode made from SCC was increased with increasing sulfur content, in turn increasing the air reactivities at the lower baking temperature since a highly dense anode was more prone to air attack. At higher baking level with increasing sulfur content, anode produced from SCC coke showed lower reactivity compared to that of the anode made with UCC. This was probably due to the further calcination of UCC coke at higher temperature and higher sulfur content due to covalent bonds of sulfur with heteroatom present in UCC.

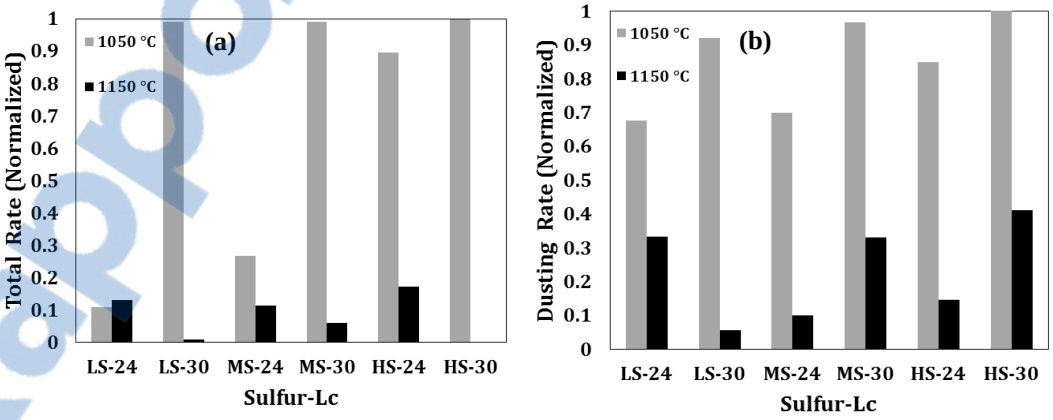

Figure 5.26 (a) Normalized air reactivity and (b) normalized dusting of anodes as a function of sulfur content and baking temperatures.

The CO_2 reactivity pattern was shown in the Figure 5.27. The anode consumption due to CO_2 reactivity generally decreased with increasing baking temperature. The CO_2 reactivity rate was different from the air reactivity rate. The reaction and dusting rate was monotonically reduced with increasing sulfur content, suggesting a different reaction mechanism compared to air. With higher sulfur content, the densities of the anodes made up of SCC were higher which helped to prevent CO_2 gas penetration into the samples and reduced the CO_2 reactivity. Also it was found in the literature that sulfur inhibited the CO_2 reaction by interacting with metal catalyses to form stable sulfur compounds [96, 98]. Addition of sulfur was more effective for anode produced from SCC compared to UCC. This could be elucidated with the fact that higher quantity of heteroatoms is present in UCC compared to SCC. Sulfur probably forms hydrogen bond or covalent bond with other hetero atoms in UCC and may not be available to interact with metal impurities. On the other hand for SCC, sulfur might be able to form more bonds with metal constituents and offset their catalytic impact on reactivity.

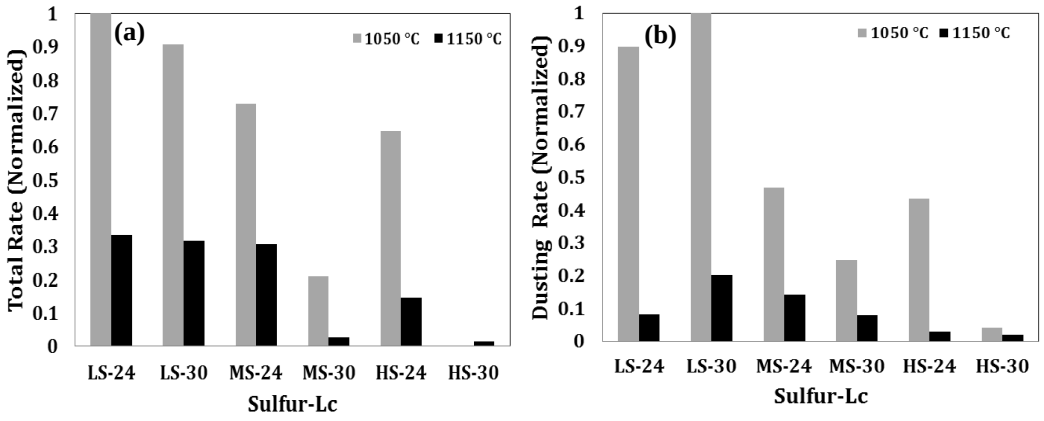

Figure 5.27 (a) Normalized CO_2 reactivity and (b) normalized dusting of anodes as a function of sulfur content and baking temperatures.

5.2.5 Concluding remarks.

The effect of coke crystalline length, coke sulfur content and anode baking temperatures on various anode properties were studied. Conclusions from this study were in agreement with the findings of different literatures available on this subject. A clear relation was found with coke crystalline length and anode baking temperature with carbon consumption. The addition of dibenzothiophene as sulfur additive to the anodes resulted in reduced CO_2 reactivity and dusting but slightly increased air reactivity at both temperatures. It was also found that effect of sulfur was not significant at higher baking temperature due to more sulfur loss at these temperature. At higher baking temperature, density of the anode was the most important factor contributed to the air and CO_2 reactivity. Anode baked density decreased significantly with decreasing coke crystalline length at both baking temperatures. Simultaneously anode electrical resistivity decreased with increasing anode baked density. No significant effect of sulfur addition on reactivity was observed for anode produced from UCC due to its chemical structure.

5.3 Effect of green anode cooling times on pitch redistribution in anodes

5.3.1 General

An anode was produced using a standard recipe to understand the effect of cooling on pitch redistribution in the green anode. After the forming process, anodes are cooled. During the initial part of the cooling period, pitch remains in liquid form and may continue

to flow and redistribute in the anode. To study if such a phenomenon occurs, this work was conducted.

5.3.2 Materials and methodology

A standard anode was made. The properties of coke and pitch as well as the anode recipe were given in Tables 5.1, 4.8 and 5.2, respectively. The detailed production method was given in the section 3.2.1. The standard green anode produced was cut into four blocks immediately after it was removed from the vibrocompactor. Each block was cooled in air for a certain period and then placed in water bath at room temperature to quench it. This was done with 5-minute intervals (5, 10, 15, 20 min). Each block was kept in water until it was completely cold. While in air, the anode block remains relatively hot due to low cooling rate; and this probably allows pitch to continue to penetrate into the coke bed and even probably into the coke particles. Quenching interrupts this process. Samples were then taken from each block and dried in a furnace at 80°C for 17 hrs. These samples were polished using the standard protocol,coated with gold-platinum coating, and were examined with SEM image analysis

5.3.3 Image analysis of anode sections

SEM images of four green anode sections after different cooling times were shown in Figure 5.28. It could be clearly seen that with increasing cooling time in air, pitch penetration increased up to 15 min (Figures 5.28 (a) to (c)). There did not seem to be any significant change after this time (Figures 5.28 (c) and (d)). This indicated that before

cooling in water, anode was still hot which allowed further penetration and redistribution of pitch after the forming process. Cooling by natural convection in air seemd to have improved the anode texture.

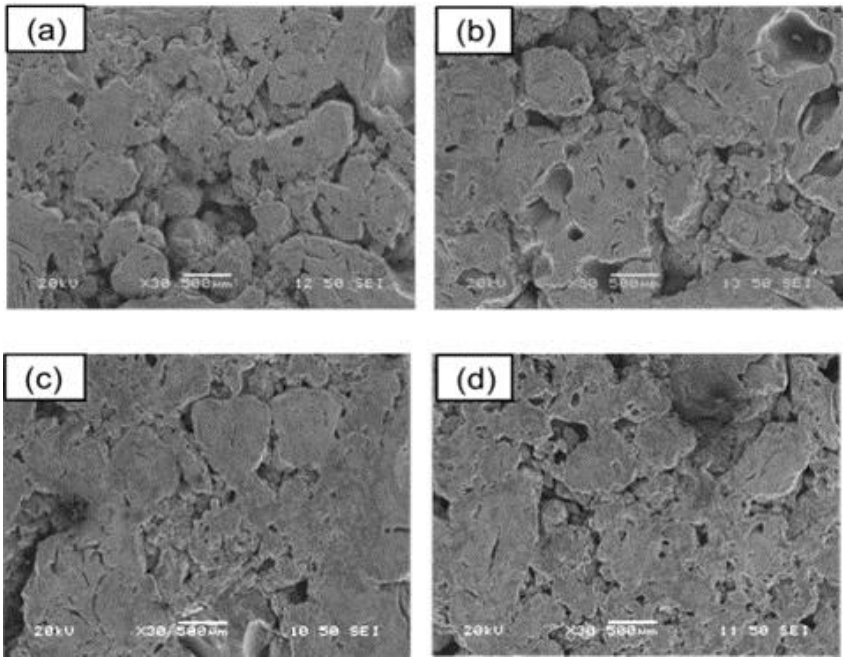

Figure 5.28 SEM images of green anode sections (500X) after different cooling times in air: (a) 5 min (b) 10 min (c) 15 min (d) 20 min

5.3.4 Concluding remarks

SEM micrograph of anode samples were examined after they were cooled in air for different periods. It showed that pitch penetration and redistribution continue even after the vibrocompaction of anodes for a certain period. It was found that this gradually improved the anode texture. This work was carried out with a laboratory anode. Depending on the anode size and cooling conditions, the period of redistribution is likely to change. Further work is needed to study the impact of such changes on anode quality.

CHAPTER 6

CHARACTERIZATIONS OF INDUSTRIAL ANODES

Production of high density and consistent quality anodes are one of the main interests of aluminum production process. Anode quality is associated with a large number of variables from raw material properties and different anode production parameters. Control over these parameters is a big challenge and which leads to inconsistence in the anode quality. A comprehensive study was carried out based on industrial measurement campaigns, mainly to understand the effect of four different industrial vibrocompactors, two different compaction times and temperature distribution during baking on the anode quality (green and baked densities, green and baked resistivities, air and CO_2 reactivities, pitch distribution, mechanical properties, kinetics, anode L_c, cracking, etc.) by the UQAC/AAI Chair [157, 172-176]. A detailed vibration measurement and analysis was also done for four industrial vibrocompactors and it is a subject of another project [177]. Eight green and twenty four baked anodes were produced to perform this complete study. Different cores from each anode were subjected to different analyses. In this chapter, the results analyzed for industrial anodes during this work as part of the major project described above are presented. The current study includes:

- Effect of vibrocompactor type and parameters on pitch distribution.
- Effect of anode position in the baking furnace on anode L_c.
- Effect of different anode production parameters and anode properties on CO_2 reactivity.

The first part of the chapter was concentrated to understand the effect of different industrial production steps specially vibrocompactor and baking cycle on pitch and pores distribution in industrial anodes. At the beginning of this study, optical microscope was used to take images and using a custom made software developed at UQAC to analyze the pitch and pores distribution of green anodes. Later another novel technique was developed by the personnel of UQAC/AAI Chair and incorporated to this project to analyse these industrial anodes using images taken by digital camera.

In the subsequent section, effect of different parameters on CO_2 reactivity of industrial anodes were studied using ANN. Crystalline length at different positions of the anode were measured to comprehend the orientation of anodes in baking furnace. These results were reported in the Appendix 2.

Anode recipe is one of the important factors and this recipe should be maintained to produce consistence quality of anode. In the following section, a study was carried out to closely monitor the kneader performances (whether it crushed the particles and reduced the size) during mixing of pitch and coke. A simple and environmentally feasible pitch extractive method was also developed further to carry out size distribution measurement after mixing.

6.1 Pitch distribution in industrial anodes

6.1.1 General

Anodes are made of calcined petroleum coke, recycled anode butts, and coal tar pitch. Since the coal tar pitch acts as a binder for the anode, its proper distribution in a green

anode has a great impact on the properties of the baked anode. There is presently no reliable method available to analyze and quantify the amount of coke, pitch, and pores/cracks in a green and baked anode sample. It is difficult to quantify the pitch in green anodes as it is well bonded with the coke and sometimes covers the coke particles. Also in baked anode, it is hard to distinguish between coke and cokified pitch by existing methods. An optical image analysis technique was developed by the Chair members, which can analyze as well as quantify the weight percentages of pitch [178]. The image analysis software quantifies the pitch on the surface of the sample and it was assumed that the surface represents the whole sample. The objective of this work is to study the effect of different vibrocompactors on pitch distribution in green and baked anodes using image analysis and to determine the impact of the compaction time, sample position and temperature in the baking furnace on pitch distribution in anodes.

6.1.2 Materials and methods

Initially a method to characterize four green (unbaked) carbon anodes was developed. The method was based on optical microscopy and digital image analysis [178, 179]. A method for distinguishing the pitch from the coke grains and the pores in the microscopic images was also established. The routine was used to examine the distribution of pitch, pores and coke grains in four industrial green anode samples produced under similar conditions and recipe but from different industrial vibrocompactors. Dividing the real value by an average value of all the samples, all the data were put to dimensionless form. The detailed sample preparation steps are described in the section 3.3.2. The sample positions

are schematically shown in the Figure 6.1. These four green anodes were divided in two major parts such as left and right side. Each side was divided in six sections. From each section, 1×1 cm samples were taken from top and bottom position for image analysis.

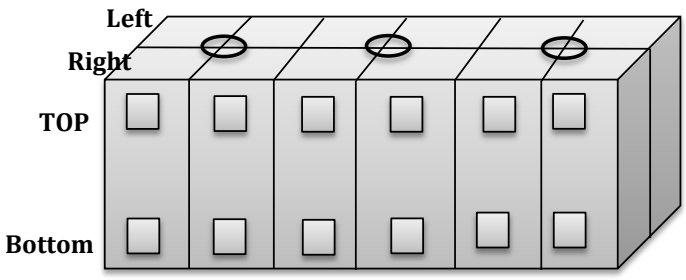

Figure 6.1 Sample positions in four green anodes

In the next part of this study, eight industrial green anodes and eight industrial baked anodes were studied to understand the influence of different production parameters on pitch distribution using digital camera available commercially. The anode paste recipes, and the production parameters were completely different compared to the four green industrial anodes previously received to measure their pitch content using optical microscopy. These sixteen industrial anodes were part of thirty two industrial anodes produced to perform a complete study of influence of different production parameters on anode properties in different projects as described earlier. In this study, anode quality assessment is widely focused on industrial tests undertaken on anode core samples. For analysis, four cores were taken from each anode. 13, 14, 22 and 23 were respective core numbers for pitch analysis. Each core was equally divided to four sections. The average pitch content of the uppermost two sections were considered as ‘Top’ and similarly the average pitch content of the lowermost two sections were considered as ‘Bottom’ (Figure 6.2 (a)). See Figure 6.2 for the

positions of the cores in the anode. It should be noted that cores 14 and 22 come from a partially chamfered region. This may have had some impact on the results.

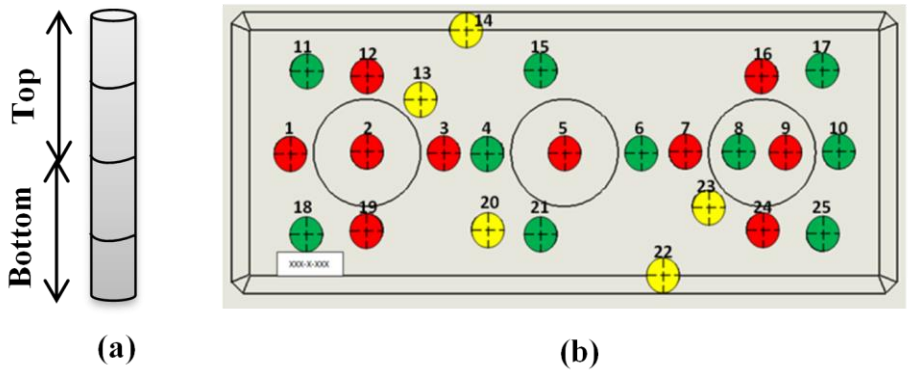

Figure 6.2 (a) Schematic of core sampling for image analysis **(b)** positions of the cores in an anode

The anode production parameters and recipe of eight green anodes studied by analyzing of images taken with digital camera are tabulated in the Table 6.1. In this study, four industrial vibrocompactor (‘A’, ‘B’, ‘C’, and ‘D’) were used to produce green anodes. Two anodes were produce from each compactor at two different compaction times (T1s and T1+7s). Two types of cokes (Coke A and Coke B) and pitches (Pitch A and Pitch B) were used to make anodes. The production parameters and recipes used to prepare each green anode are given in the Table 6.1. The conversion used to describe each parameter was that the lowest amount is considered as base and a value was just added to the base to quantify the difference. An example is T1 is lowest compaction time and difference between the two times is 7 s, i.e. T1+7 s. Similarly anode production parameters and recipes of baked anodes studied by analyzing the images taken with digital camera were presented in Table 6.2. Similar conversion was used to describe the parameters tabulated in Table 6.2

Table 6.1 Production parameters and recipes of green anodes studied by analyzing of images taken with digital camera

No. of Anode	1	2	3	4	5	6	7	8
Compaction Time (s)	T1	T1+7	T1	T1+7	T1	T1+7	T1	T1+7
Vibro-compactor	A	A	B	B	C	C	D	D
Type of Pitch	Pitch A	Pitch A	Pitch B	Pitch B	Pitch A	Pitch A	Pitch B	Pitch B
Type of Coke	Coke A+ Coke B	Coke A + Coke B	Coke B	Coke B	Coke A+ Coke B	Coke A+ Coke B	Coke B	Coke B
% Coke	Coke+0.5	Coke+0.5	Coke+12	Coke+12	Coke+0.5	Coke+0.5	Coke	Coke
% Green Reject	GR	GR	GR+0.5	GR+0.5	GR	GR	GR+0.5	GR+0.5
% Recycled Butt	Butt+12	Butt +12	Butt	Butt	Butt +12	Butt +12	Butt +12	Butt +12
% Pitch	Pitch	Pitch+0.12	Pitch+0.08	Pitch+0.02	Pitch+0.1	Pitch+0.04	Pitch+0.09	Pitch+0.07
% Coarse	Coarse	Coarse	Coarse+2	Coarse +2	Coarse+2	Coarse +2	Coarse +2	Coarse +2
% Medium	Medium+4	Medium+4	Medium+2	Medium+2	Medium	Medium	Medium	Medium
% Fine	Fine	Fine	Fine	Fine	Fine +4	Fine +4	Fine +4	Fine +4
% BMP	BMP	BMP	BMP+1	BMP+1	BMP+1	BMP+1	BMP+1	BMP+1
% FD	FD+1	FD+1	FD	FD	FD	FD	FD	FD
Top Bellow Pressure (Psi)	Pr	Pr	Pr+5	Pr+5	Pr+20	Pr+20	Pr+10	Pr+10

Table 6.2 Production parameters and recipes of baked anodes studied by analyzing the images taken with digital camera

No. of Anode	9	14	16	20	22	26	29	32
Compaction Time	T1	T1	T1	T1	T1+7	T1+7	T1+7	T1+7
Vibro-compactor	A	B	C	D	A	B	C	D
Type of Pitch	Pitch A	Pitch B	Pitch A	Pitch B	Pitch A	Pitch B	Pitch A	Pitch B
Type of Coke	Coke A+ Coke B	Coke B	Coke A+ Coke B	Coke B	Coke A+ Coke B	Coke B	Coke A+ Coke B	Coke B
% Coke	Coke+0.5	Coke+12	Coke+0.5	Coke	Coke+0.5	Coke+12	Coke+0.5	Coke
% Green Reject	GR	GR+0.5	GR	GR+0.5	GR	GR+0.5	GR	GR+0.5
% Recycled Butt	Butt+12	Butt	Butt+12	Butt+12	Butt+12	Butt	Butt+12	Butt+12

No. of Anode	9	14	16	20	22	26	29	32
% Pitch	Pitch+0.02	Pitch+0.05	Pitch+0.09	Pitch+0.09	Pitch+0.18	Pitch+0.04	Pitch+0.02	Pitch+0.03
% Coarse	Coarse	Coarse+2	Coarse	Coarse	Coarse	Coarse +2	Coarse	Coarse
% Medium	Medium +4	Medium+2	Medium	Medium	Medium +4	Medium+2	Medium	Medium
% Fine	Fine	Fine	Fine +4	Fine +4	Fine	Fine	Fine +4	Fine +4
% BMP	BMP	BMP+1	BMP+1	BMP+1	BMP	BMP+1	BMP+1	BMP+1
% FD	FD+1	FD	FD	FD	FD+1	FD	FD	FD

6.1.3 Image analysis by optical microscope

Figure 6.3 showed pitch distribution in four green anodes as a function of four industrial vibrocompactors used and sample positions (top, bottom, left and right sides of the anodes) using optical microscope (Figure 6.1). Some examples of mosaic optical images of anode sections were given in Appendix 2. Factorial anova analysis between the vibrocompactors, positions of the samples and side of the anode was done (marked in Figures 6.3 and 6.4). Pitch distribution was slightly different in right and left sides of the anodes. For all cases, considering the average values, the right side of the anode contained slightly higher pitch level at bottom compared to top of the anodes.

This trend was not followed on the left side of the anodes. It could be seen in Figure 6.3 that the opposite trend was observed for all anode samples except for the ones coming from the anode produced using vibrocompactor ‘A’. The pitch levels at the top and the bottom of the anode produced by vibrocompactor ‘C’ were significantly different.

Analysis of the available fabrication parameters indicated that the average pitch distributions in Figure 6.3 followed trends similar to those for the pitch temperature and the mixing intensity. Thus, these two parameters seemed to have influenced the pitch distribution observed.

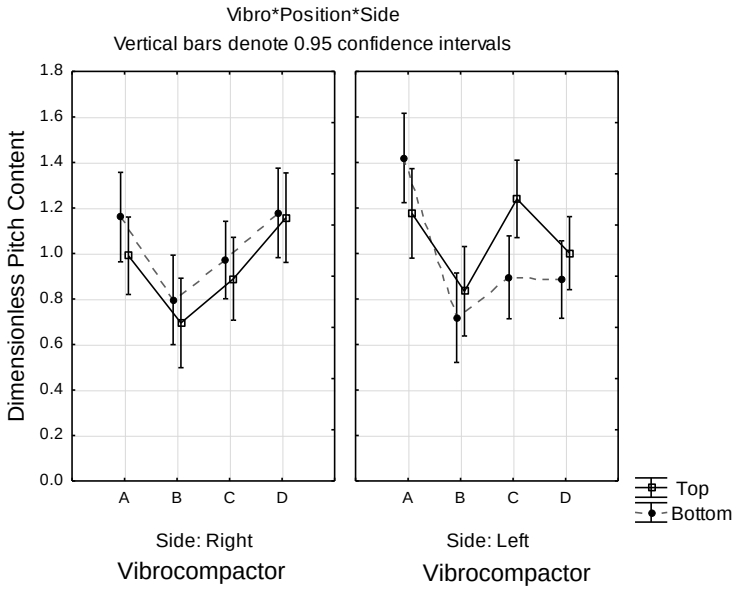

Figure 6.3 Effect of vibrocompactor and sample positions on pitch distribution of green anodes studied from the images taken with optical microscope

Figure 6.4 shows a comparison of the standardized effects for green anode open porosity. The results showed that anode produced from vibrocompactor 'C' comprised of highest porosity whereas the porosity was fairly low in the analyzed anode produced from vibrocompactor 'D'.

The analysis of different available green anode fabrication parameters showed that the vacuum applied in the vibrocompactors followed the same pattern as the pore distribution. Thus, this parameter seemed to have influenced the pore distribution in the anodes. The results also revealed that both sides of the anodes followed a similar trend. In most of the cases, the top part of the anodes contained marginally lower amount of pores compared to the bottom part of the anodes.

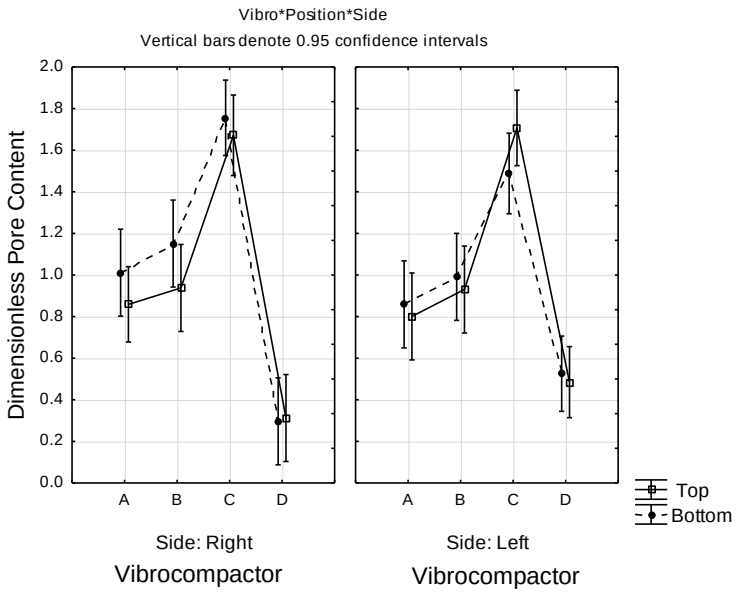

Figure 6.4 Effect of vibrocompactor and sample positions on pore distribution of green anodes studied from the images taken with optical microscope

The above analysis was carried out using the available data. However, not all the fabrication parameters were available. Thus, there might be other parameters that may have affected the pitch and pore distributions in the green anodes studied.

6.1.4 Image analysis by digital camera

6.1.4.1 Effect of different vibrocompactors and compaction times on pitch distribution of green anodes

Figures 6.5 (a) and (b) show the average pitch content for different positions of cores taken from four different anodes produced by different vibrocompactors (‘A’, ‘B’, ‘C’ and ‘D’) using a compaction time of T1 s. The error bars represent the standard deviations of the pitch content in the 4 sections (Figure 6.2 (a), 6.5 (e)) of each of the cores. Cores 13 and

23 were taken from positions close to the stub hole (interior) and cores 14 and 22 (exterior) were taken close to the anode side surfaces (Figure 6.2 (b), 6.5 (e)). Figure 6.5 (a) shows that cores 13 and 23 show similar pitch content for anodes produced by vibrocompactors ‘A’, ‘B’ and ‘C’; whereas, anode produced by vibrocompactor ‘D’ show higher values of pitch content. Cores 14 and 22 show different groups of anodes with similar pitch contents. Core 14 shows that vibrocompactors ‘A’ and ‘B’ form one group, and ‘C’ and ‘D’ form another group. It may be noted that vibrocompactors ‘A’ and ‘B’ are similar in terms of technology, and vibrocompactors ‘C’ and ‘D’ also use similar technology. Thus, pitch content in core 14 shows the effect of vibrocompactor type. Core 22, on the other hand, shows that vibrocompactors ‘B’ with ‘C’ and ‘A’ with ‘D’ form two groups. This might be due to the combined effects of different fabrication parameters, recipe used and vibrocompactor type. It can be seen that close to the stub holes (cores 13 and 23), each of the anodes showed similar levels of pitch. Thus, it can be concluded that pitch distribution inside the anodes are usually symmetrical irrespective of the raw materials used, fabrication conditions or compactor type. The pitch contents of the cores close to the outside surfaces show different levels in the anodes. The distribution of pitch close to the outside surfaces (exterior part of the anode) is not symmetrical compared to that observed for the cores taken from the interior part of the anode.

Figure 6.5 (b) shows that the anodes produced by vibrocompactors A and D show less variation of pitch content compared to that for vibrocompactors B and C. Thus, it can be concluded that uniform distribution of pitch cannot be attributed solely to vibrocompactor

type, raw material used or fabrication parameters. It is the result of the combined effect of different parameters.

Figures 6.5 (c) and (d) show the pitch content for different positions of cores taken from different anodes produced by different vibrocompactors (‘A’, ‘B’, ‘C’ and ‘D’) using a compaction time of T1 +7 s. The error bars represent the standard deviations of the pitch content in the 4 sections (Figure 6.2 (a), 6.5 (e)) of each of the cores. Figure 6.5 (c) shows that the cores 13 and 23 show similar pitch contents in each of the anodes except for those of vibrocompactor ‘A’. Also, cores 14 and 22 show somewhat different levels of pitch in each of the anodes except for vibrocompactor ‘C’ which had comparatively higher bellow pressure (Table 6.1). There is more scattering of data for the compaction time of T1 + 7 s.

Figure 6.5 (d) shows that the anodes produced by vibrocompactors ‘B’ and ‘D’ show less variation of pitch content compared to that for vibrocompactors ‘A’ and C. This is a different trend compared to that observed for the compaction time of T1 s. The raw materials used for the anodes produced by vibrocompactors ‘A’ and ‘C’ were different than those used for the anodes produced by vibrocompactors ‘B’ and ‘D’ (Table 6.1). Thus, the effect of raw materials on the pitch distribution seems to be more significant at longer compaction time.

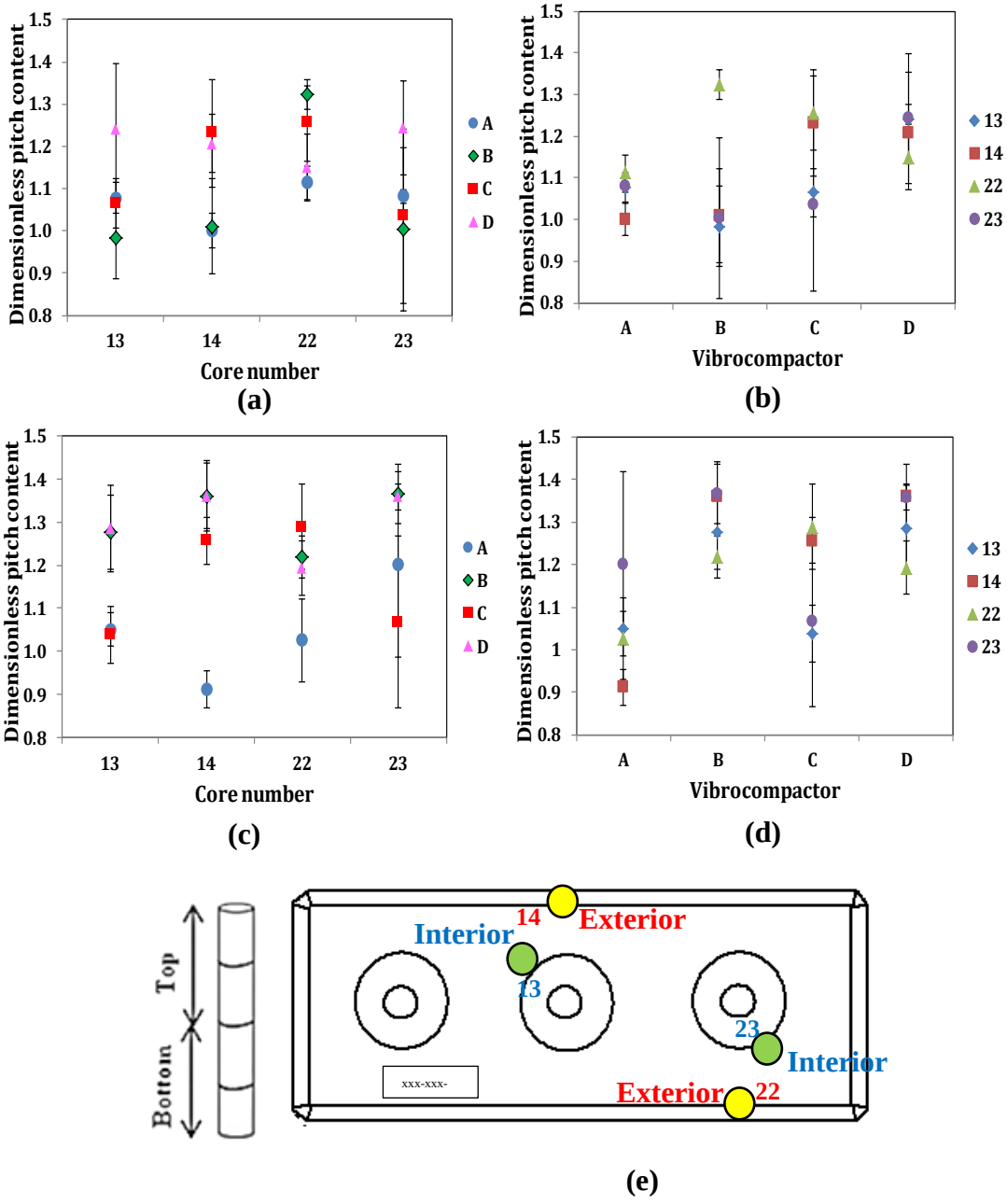

Figure 6.5 Effect of different (a) core positions at T1 s (b) vibrocompactors at T1 s (c) core positions at T1 +7 s (d) vibrocompactors at T1 +7 s on average green anode pitch content; (e) core positions and sections for each core

Figure 6.6 (a) represents the statistical analysis (Factorial ANOVA) of pitch distribution as a function of different vibrocompactors and times. The result shows that each vibrocompactor was statistically different; especially vibrocompactor A was completely different from the other three compactors. The results show that the pitch content of anodes produced from vibrocompactor 'A' comprises of lowest quantity of pitch; however, anode samples from vibrocompactor 'D' contained the highest amount of pitch. Anodes produced from vibrocompactor 'C' and 'D' contained higher amount of fine particles (<1μm) compared to anodes produced from vibrocompactor 'A' and 'B' (Table 6.1). In general, small particles have lower porosity and higher surface area, which creates pitch boundary surrounding the particles and increases the pitch content on the surface. It might be noted that here the pitch that surrounded the coke particles and covered the pores could only be measured with the image analysis, not the pitch that had already penetrated deep into the pores. This could be a possible reason for higher pitch content in the anodes produced from vibrocompactor 'C' and 'D' regardless of the type of coke used. In aaddition to this, Vibrocompactor 'C' and 'D' exhibited comparatively higher top bellow pressure and had higher acceleration of the lower vibration table [177] which could lead to higher percentage of pitch in the anode samples by reducing total pore area on the surface area of the anode sample. Also, each vibrocompactor is unique and type of vibrocompactor had an influence on the anode properties even after same technology was used.

It can be seen that the compaction time had a great influence on pitch content in green anodes as greater compaction time accumulated more pitch to cover the pores and well surrounded the coke particles (Figure 6.6). It was possible that higher compaction time

facilitated pitch to penetrate through the pores and filled the pore. In fact, increasing compaction time resulted in a diminution in total pore volume of the anode. It is also clear from Figure 6.6 that the pitch content in anodes were substantially different for vibrocompactor ‘B’ at two different compaction times but exact reason is unidentified.

Figure 6.6 (b) shows a similar trend between the groups for density and resistivity analysis. As it is known that density, electrical resistivity and porosity of the anodes are closely related to each other. The plot shows that anodes produced by vibrocompactor ‘C’ and ‘D’ were highly dense because they contained greater amount of fine fractions, additionally the top bellow pressure and acceleration of the lower vibration table was higher compared to those of vibrocompactor ‘A’ and ‘B’ which reduced the total pore volume in the anode. Furthermore, Coke B was used to produce anodes for vibrocompactor ‘C’ and ‘D’. In general, cokes from this supplier has less porosity and higher real density than Coke A. This could be probable reason of higher anode density and lower electrical resistivity for anodes produced from these two vibrocompactors. Also, anodes produced from vibrocompactor ‘B’ contained the lowest amount of recycled butt and the highest coarse to fine ratio; thus, had the lowest density. These results indicated that optimum amount of recycled butt is required to achieve higher density. Figure 6.6 (c) presents the electrical resistivity of anodes produced from different vibrocompactors. Due to the higher bellow pressure and acceleration of the table in vibrocompactor ‘C’, the resistivity values decreased as higher pressure increased the contact between the particles as well as reduced total porosity. The results were quite different for analysis done using optical microscope (Figure 6.4). Its showed anode produced from vibrocompactor ‘C’ containes highest pores,

which could increase the anode resistivity. This was due the difference in raw materials, paste recipe, and processing parameters. Due to that, it is impossible to compare image analysis results from optical microscope and digital camera. results Similarly for vibrocompactor 'D', bellow pressure was higher than vibrocompactor 'B' which resulted in lower electrical resistivity. Thus, higher bellow pressure lowers the electrical resistivity in green anodes irrespective of the coke type. It should be noted the final anode quality depends on the baked anode properties.

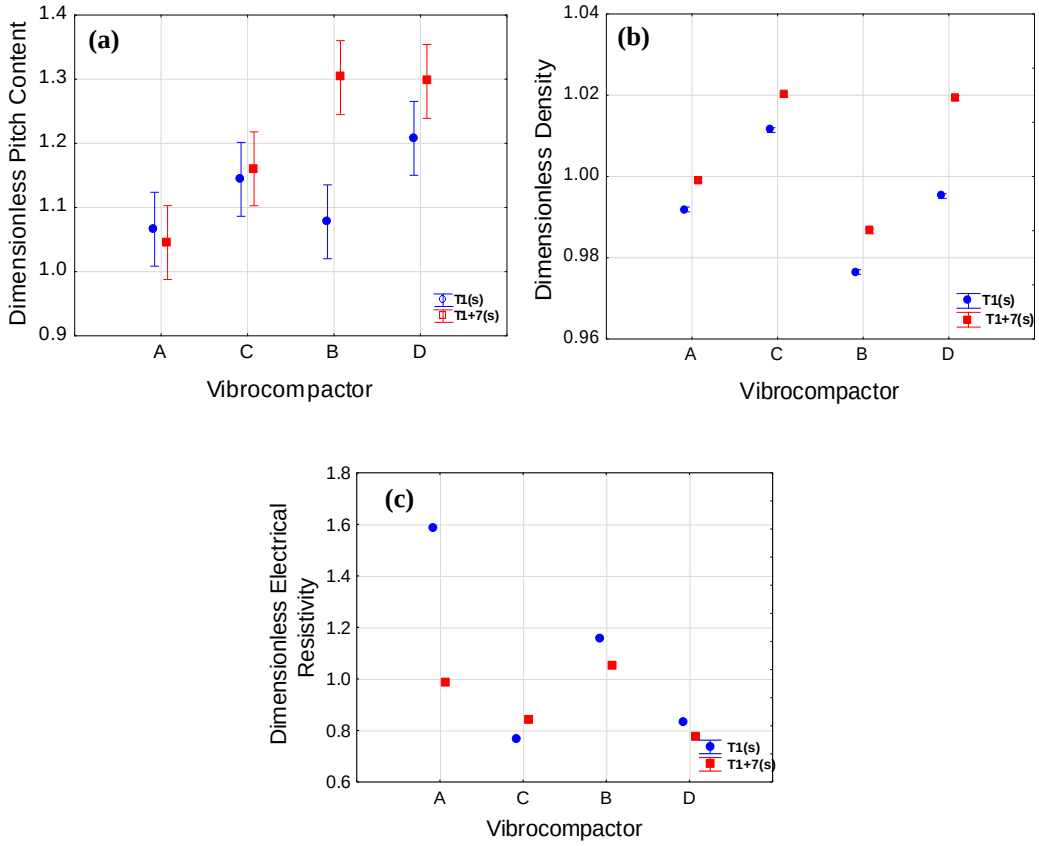

Figure 6.6 Factorial ANOVA for green anodes, combined effect of different vibrocompactors and compaction time on (a) pitch distribution (b) density (c) electrical resistivity (all the vertical bars represent 95% confidence interval)

The combined effect of vibrocompactor and sample positions (top and bottom) were analysed in Figure 6.7. It was observed that the overall pitch content in bottom part of the anodes was slightly higher compared to those at the top with the exception of the anode made with vibrocompactor 'B' but variations in pitch level were statistically insignificant. The reason could be the difference of bellow pressures at the top and bottom and variation in acceleration of the vibration tables at top and bottom.

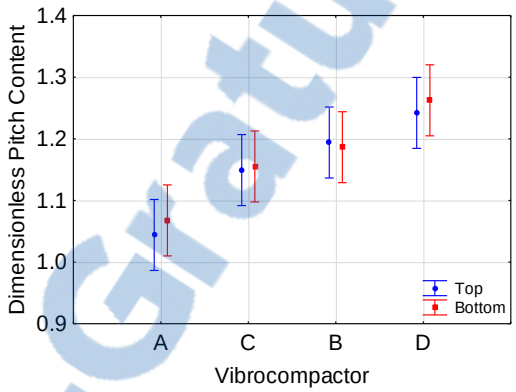

Figure 6.7 Factorial ANOVA for green anodes, effect of different core positions and vibrocompactors on pitch distribution (all the vertical bars represents 95% confidence interval)

It has been observed that there was difference in results and tendencies between the four green anodes studied previously, using the image analysis of optical microscopy and the eigth green anodes of 32 industrial anode measurement campaign using digital camera. In the first case, anode produced from vibrocompactor 'B' contained lowest pitch content (Figure 6.3). Also, anode produced from vibrocompactor 'C' contained highest amounts of pores which led to higher electrical resistivity and lower density (Figure 6.4). The situation wasn't the same with the second measurement with digital camera (Figures 6.6 and 6.7).

This was probably due to the difference in fabrication conditions, reparation of vibrocompactors and raw materials used. These two groups of measurements were taken during different periods which might mean the utilization of different raw materials and operating conditions. These are common and expected in industrial applications.

6.1.4.2 Effect of different vibrocompactors and compaction times on distribution of pitch on baked anode.

Anode baking, which is needed to obtain a mechanically stable and electrical current conductor anode for electrolysis, takes place in open top baking furnaces. A schematic of a baking furnace and the placement of the anodes in a pit are shown in Figure 6.8.

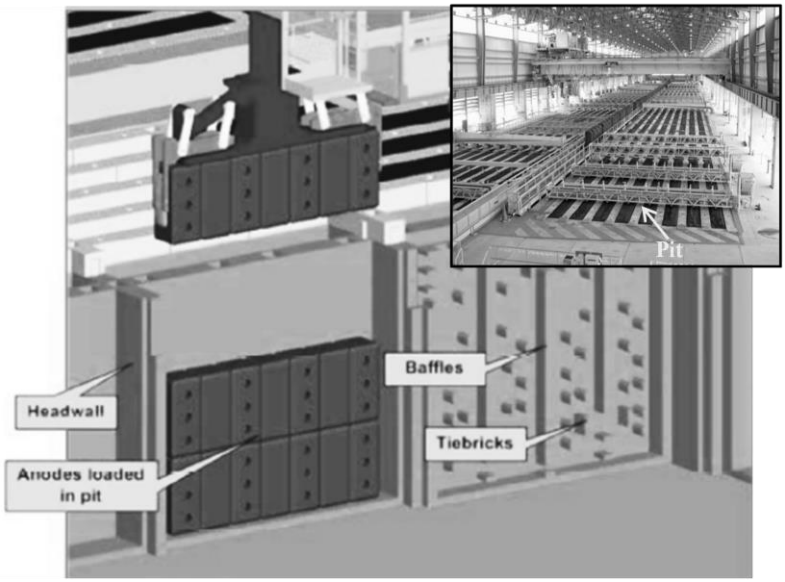

Figure 6.8 View of pits in the open top baking furnace and arrangements of anodes in pit [180, 181]

Figure 6.9 indicates the positions of the anode manufactured from different vibrocompactors in the baking furnace. In the Figure 6.9, 9, 14, 16 and 20 are the anode numbers (see Table 6.2) and 'A', 'B', 'C', and 'D' are the respective vibrocompactors in Chamber 1. Similarly 22, 26, 29 and 32 are anode numbers (see Table 6.2) and 'A', 'B', 'C', and 'D' are the respective vibrocompactors in Chamber 2. The color codes in the Figure 6.9 indicates the variation in the furnace temperatures. This study was done to comprehend the impact of different vibrocompactors, compaction times and baking temperatures on pitch distribution in baked anodes. The production parameters and anode recipe are given in Table 6.2. Temperature differences in baking furnaces are displayed Figure 6.9. The positions of the anodes were chosen in a way that difference of temperatures between the anodes would be minimum. The thermal gradient in the anodes were negligible. Thus, the effect of thermal stress was minimal.

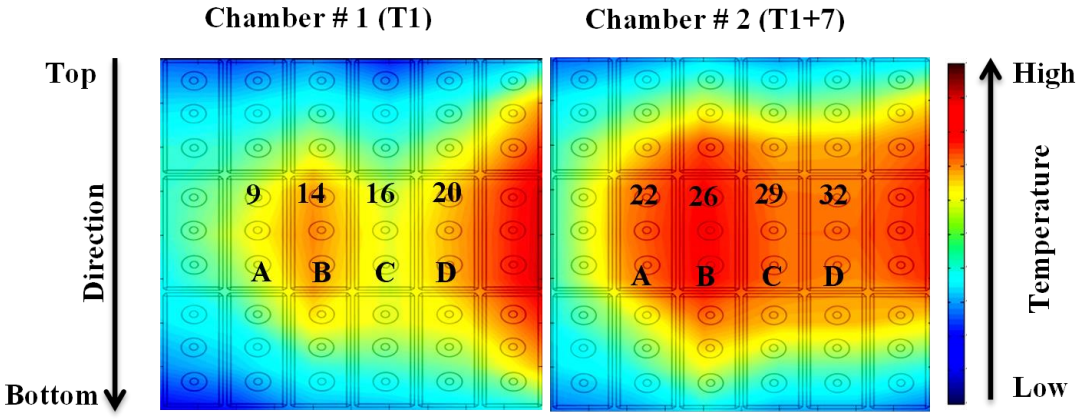

Figure 6.9 Baking level variations of anodes (produced from different vibrocompactor) baked in two different pits and position of the anodes in the pits

Figure 6.10 demonstrates that the pitch content of the baked anodes showed a similar trend to that of the green anodes, but the pitch content was reduced due to devolatization during baking. It can be also seen that the anodes in the chamber 2 was subjected to higher temperature compared to the anodes in chamber 1 (Figure 6.9). The effects of the baking temperature distribution within a pit had an influence on anode pitch distribution as well as anode density and resistivity. The results evidently displayed a decrease in pitch content and density of the anode samples for T1+7 s probably due to higher furnace temperature regardless of the vibrocompactor used for the anode production (Figure 6.10). Anodes produced from vibrocompactor 'B' which were exposed to highest temperature within pits (both in chamber 1 and chamber 2, see Figure 6.9) resulted in considerably low pitch content among all other anodes. The possible reasons for changes in pitch level also could be pitch redistribution into voids by pitch expansion and penetration of pitch between inter and intra particles void as pitch becomes liquid at 160°C [80]. Additionally during baking, release of volatile occurred in the furnace at around 450-600°C [80] which resulted in slightly lowered pitch level. Figure 6.10 seems to show that there is an optimum pitch level (around 1.0) which results in low resistivity and high density. Lower or higher pitch levels detoriate the anode properties.

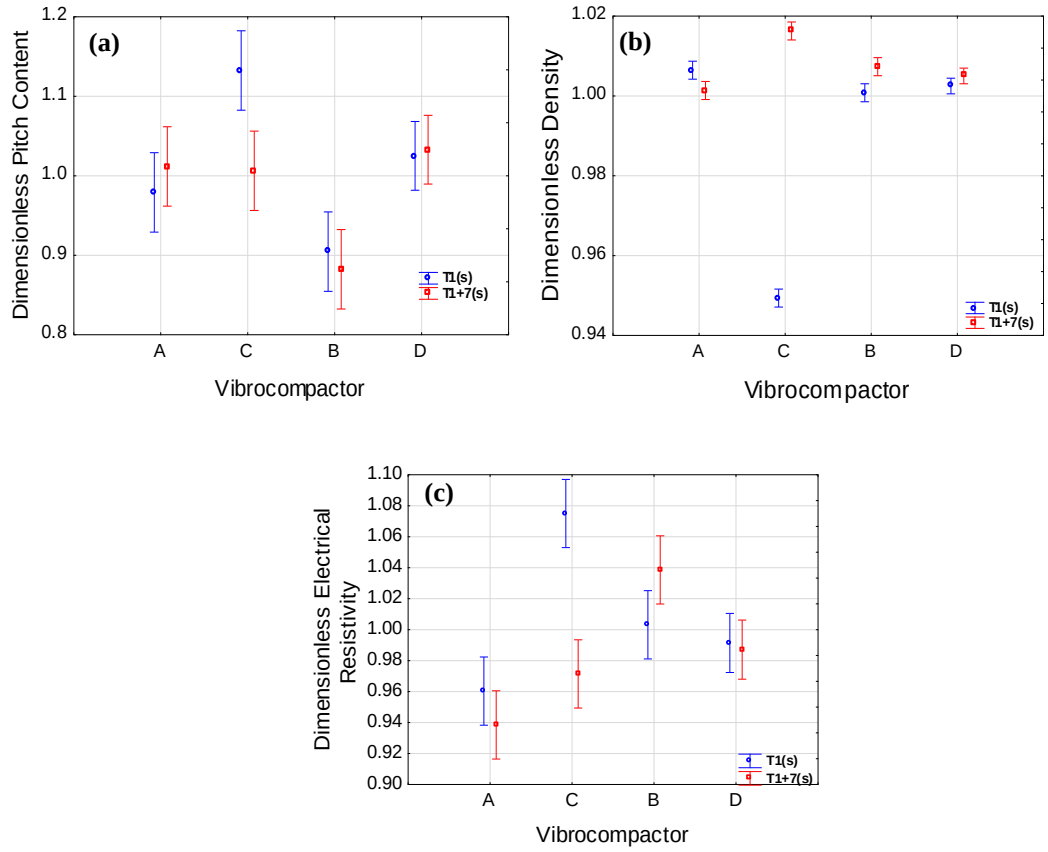

Figure 6.10 Factorial ANOVA for baked anodes, combined effect of different vibrocompactors and compaction times on (a) pitch distribution (b) density (c) electrical resistivity (all the vertical bars represent 95% confidence interval)

The distribution of pitch is essential for the electrical properties because carbonized pitch carries the electrical current from one coke particle to the next when the particles are not in direct contact. The uniform distribution of pitch is also important for anode density because that influences the various anode properties.

The overall pitch distribution results show that the pitch distribution is more homogeneous in baked anode compared to green anodes due to redistribution of pitch

during baking. Overall pitch content is slightly lower in baked anodes compared to green anodes because of volatile release during baking.

6.1.5 Concluding remarks

Two different image analysis techniques were developed by UQAC/AAI Chair personnel to analyze the weight percent of the pitch in green and baked anodes. In the first method, the image analysis using optical microscopy images gave a detailed structural analysis (pores) but was limited to a small surface area. Also sample preparation was a tedious and time consuming job. The second method, using images taken with a digital camera, was novel and simple; and this method was used to analyse the pitch distribution on larger surfaces.

The first method was applied to four industrial green anodes. It seemed that pitch temperature and mixing intensity affected the pitch distribution; whereas, the applied vacuum during compaction influenced the pore distribution. The lack of some of the fabrication parameters does not allow further analysis.

The second method was applied to eight green and twenty-four baked anodes. It seems that pitch distribution of green anodes was affected by a combination of factors such as raw materials, vibrocompactor type and fabrication parameters. The baked anodes showed somewhat more homogeneous pitch distribution compared to the green anodes.

Statistical ANOVA method was used to identify the significant controlling factors affecting the pitch distribution, density and electrical resistivity of green and baked anodes. Distribution of pitch in baked anodes was more homogeneous than that of green anodes.

The results can probably be explained with the redistribution of pitch during baking; as pitch transformed to liquid at 160ºC. The green anodes always contained high amount of pitch than baked anodes. The weight percentage of pitch in baked anodes reduced after baking due to the loss of volatiles from pitch during baking. Factorial ANOVA of green anodes revealed that vibrocompactor and compaction time used, and core positions predominantly influence the pitch distribution in green anodes. The vibrating time, acceleration of the tables and the bellow pressure, can be used to improve the green anode density and resistivity. The densification by the vibrocompaction is an important step in carbon anode production process, and an optimum vibrating time is mandatory to get a given density threshold. Analysis of baked anodes revealed that furnace temperature played a crucial role in pitch distribution within baked anodes as well as baked density and resistivity. It should also be noted that the anodes are not always produced under exactly the same conditions due to variations in operation; even during the same day. Slight differences in properties are expected in industrial applications. The image analysis technique by using digital camera was helpful in measuring the quantity of pitch in both green and baked anodes.

6.2 Effect of different factors on industrial anode CO_2 reactivity

6.2.1 General

Reducing the excess carbon consumption during electrolysis by the means of improving anode properties is important for decreasing the production cost as well as reducing the greenhouse emissions. CO_2 reactivity is one of the major reasons for excess carbon

consumption in pots. This work describes the development of a neural network model which was used to analyze the industrial data with the objective of studying the influence of number of parameters on CO_2 reactivity.

The CO_2 reactivity of the anodes depends on different parameters starting from raw materials and continuing to anode baking. Only the effects of few factors are taken into account based on available database. In this study, the influence of the fine content, butt content, in the recipe, impurities in the coke, bellow pressure of vibrocompactors and crystalline length and resistivity of anodes on CO_2 reactivity were considered. In general, fine grains are more prone to reactivity. Recycled butts also have significant effect on anode reactivity, since many aspects of their quality should be taken into consideration in order to gain a positive impact on the future anode performance. Impurties in raw materials have severe impact on the reactivity. Compaction parameters influence the anode density, porosity and cracks. These factors directly affect the anode reactivity. On the other hand, under baked anodes are prone to high dusting, due to poor resistance towards reactivity of binder matrix while over baked anodes might show higher reactivity due to the micro porosity and crack generation by the sulfur losses that occurred during baking.

6.2.2 Materials

In this study, 23 out of 24 baked anodes that were produced were used to study the influence of various factors on anode CO_2 reactivity using the standard ASTM D6558-00a. Core 20 from each baked anode was used for this purpose (see Figure 6.2).

6.2.3 Development of the ANN Model

ANN has two functions: learning and recalling. It can learn from past experiences (data used for training, learning and validation) and predict results for conditions different than those used for developing the model. To carry out the training process, the input data was divided randomly so that 20 data sets out of the 23 available experimental data sets were used for training of the network while remaining 3 data sets were used for verifying and testing the predictive accuracy of the proposed network model. ANN model with the highest R^2 value was used as the final model. In this study, the actual values of the collected data were normalized so that the values lie between 0 and 1. The plot of predicted outputs was presented in Figure 6.11. Regression analysis was the statistical tool for the establishment of relationships among variables and R^2 value for the present model was found to be 0.79.

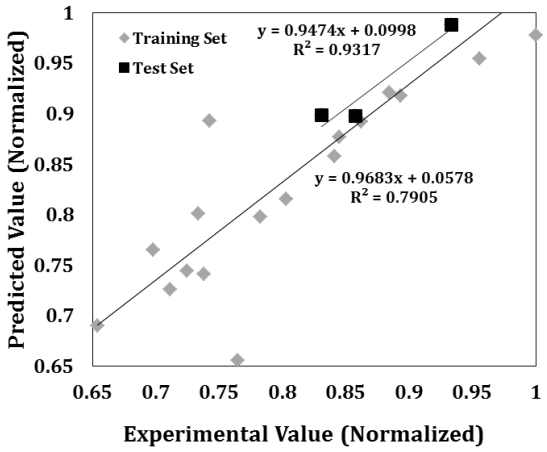

Figure 6.11 Normalized predicted and experimental values of CO_2 reactivity

Figure 6.12 presented the influence of different properties on anode CO_2 reactivity. The extent of the quantitative effect that the relevant properties had on anode reactivity could be

defined based on the results observed by ANN. In this ANN model, the effect of each parameter was studied while keeping all the others constant.

Crystalline length of the anodes was solely dependent on the anode baking temperatures. Higher baking temperatures resulted in higher crystalline length. Lower crystalline length of anodes indicates presence of more active sites of the carbon atoms such as higher amount of aromatic, aliphatic and sulfur components. CO_2 was not able to form bonds with these constituents during the gasification which seems to decrease the reactivity. Higher L_c of anodes denoted higher graphitized carbon. CO_2 could react with carbon to produce CO. This reaction was more pronounced at higher temperatures.

The addition of increasing amounts of butt material increased the CO_2 reactivity. This pronounced effect was due to an increase in impurity level when using higher quantity of butt which underlines the importance of manufacturing high purity anodes. Greater amounts of sodium were introduced into the recipe by butts and this increased the CO_2 reactivity. The magnitude of this effect depends on the sodium/sulfur sensitivity of the coke [96]. The influence of the butts' sodium content underlines the importance of having an efficient butt cleaning system to avoid issues related to reactivity.

A proper compaction was needed to obtain an appropriate level of anode density, which in turn would positively affect the reactivity behavior of anodes and would minimize the dust generation in the pots. Furthermore, an optimum bellow pressure was required in order to attain the adequate distribution of pitch for an efficient preparation of the anode paste, and thus a homogeneous anode texture, synonymous with a high density level. CO_2 reactivity is controlled by diffusion of CO_2 through the anode. Dense anodes have lower

porosity hence resistivity and CO_2 reactivity decreases with anode density. Correspondingly, the Figure 6.12 displays that an increase in electrical resistivity with increasing CO_2 reactivity. High electrical resistivity indicates the presence of pores and cracks which increases the diffusivity of CO_2 into the anode. Fine content on the recipe had direct influence on anode reactivity. High amount of fine grains increases the binder demand which in turn increased the reactivity. It is well-known that CO_2 attacks the cokified pitch more than the petroleum coke as explained in section 5.2.

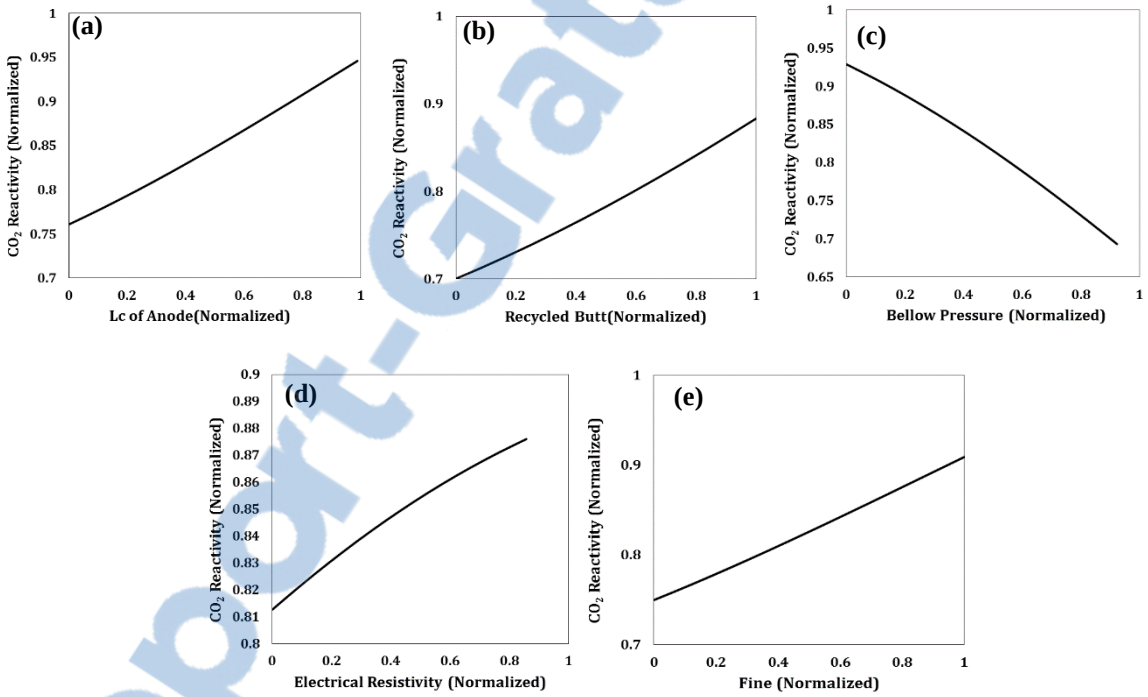

Figure 6.12 Effect of different parameters on CO_2 reactivity (a) L_c of anodes (b) butt (c) bellow pressure (d) electrical resistivity of baked anode (e) fine content in anode recipe

6.2.4 Concluding remarks

An ANN approach was employed in the simulation of CO_2 reactivity of anodes and was used to predict the effect of different parameters on CO_2 reactivity. The production parameters, which are necessary to have a lower CO_2 reactivity of anodes, could be predicted from the neural network. Thus, it is demonstrated that ANN could be used to estimate/predict the CO_2 reactivity of the baked anodes from its other properties such as L_c, density, electrical resistivity, etc. Results showed that CO_2 reactivity increased with increasing anode crystalline length, amount of fine particles, recycled butt content, and electrical resistivity. CO_2 reactivity decreased only with increasing bellow pressure. This probably has a limit. Too high pressure will result in overcompacted anodes with cracks hence increased reactivity. However, this limit was not reached during this study.

6.3 Analysis of industrial anode paste

6.3.1 General

Kneading is an important step for anode production where binder matrix and dry aggregates are mixed together to produce homogenous anode paste. Modern kneaders are large diameter machines with large rotating helical screw. The mixing could profoundly change the grain sizes and shapes during the kneading action. This changes the anode recipe resulting in anodes with properties not necessarily at their desired target values.

A systematic evaluation is required at regular time intervals to follow the effect of kneader. The paste samples have to be taken before and after the kneader and the coke

particle size distribution in paste has to be measured in order to see if the particles are reduced in size during kneading. There are industrial methods available to extract pitch from the paste and analyze the particle size of remaining residue but those methods are time consuming and use toxic solvent. Due to the ever increasing environmental legislations which are becoming more stringent with time, development of a nontoxic extraction method is necessary. An innovative technique was developed to extract pitch from the anode paste which could be used industrially. The method developed was applied for paste analysis in two different kneaders as explained below.

6.3.2 Materials

In this part of the work, 3 samples were collected before the preheater (before kneader) and 3 samples after the kneader at a time interval of 30 min. All the results were reported as the average of three samples (Each set of results are presented in Appendix 2). Detailed methodology is described in section 3.3.1.

6.3.3 Calculation of kneader residence time

A cross-sectional view of a kneader is shown in Figure 6.13. The calculation of the kneader residence time is presented in Table 6.3. The residence time is required so that the paste samples can be collected accordingly. This assures that same raw material is present in paste samples collected before and after the kneader. This is necessary since the raw material used can change any time in the plant.

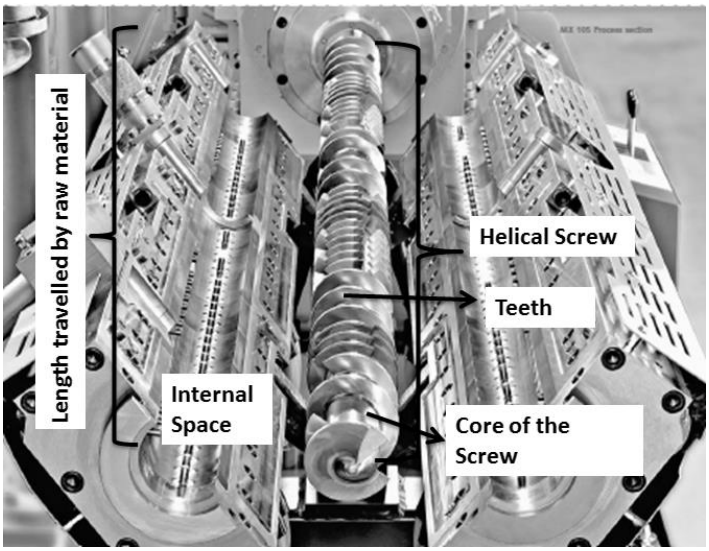

Figure 6.13 Cross-sectional view of a kneader [182]

Table 6.3 Calculation of kneader residence time

Internal diameter(mm)	D_1
Total volume (m^3) (V_1)	$[(\pi/4)\times (D_1/1000)^2]\times(L_1/1000)$
Core diameter(mm)	D_2
Length traveled by coke and pitch (mm)	L_1
Volume of the screw (m^3) (V_2)	$[(\pi/4)\times(D_1/1000)^2]\times(L_1/1000)$
Volume of the enclosed space(V_3) (m^3)	V_1-V_2
Percent of the void volume occupied by the teeth (%)	60
Percent of packing volume (%)	100
Used volume of enclosed space (V_4) (m^3)	$V_3\times(1\text{-}60/100)\times(100/100)$
Mass flow rate of the paste(kg/min)	$\dot{m}_1$
Density of the paste (kg/m^3)	d_1
Volumetric flow rate (m^3/min) (V_f)	$\dot{m}_1/d_1$
Residence time (min)	V_4/V_f

6.3.4 Performances of industrial kneaders

Emphasis was put on the effects of kneading on particle size distribution. Mainly, the effects of kneading actions on coarser fractions were taken into consideration as those were mostly affected by the kneading action. The effect of two industrial kneaders on aggregate distribution is illustrated in Figure 6.14. In this figure, particle size decreased from 1 to 6. It should be noted that very fine particles (ball mill product, filtered dust) were not included in this analysis because the emphasis was to investigate if the large particles were crushed during kneading. The results showed that there were some slight changes in particle size fractions of 1 and 2 only for Kneader 1 test; however, no significant changes in these fractions were detected in Kneader 2 test. The analysis suggested that Kneader 2 performance was slightly better than that of Kneader 1. Reduction in coarser size fractions resulted in increase in smaller size fractions (size 5 and size 6). Another reason for increase in size 5 and size 6 fractions was probably due to the agglomeration of very fine particles. It can be also seen from Figure 6.14 that the standard deviations of Kneader 2 results are greater compared to those of Kneader 1 results.

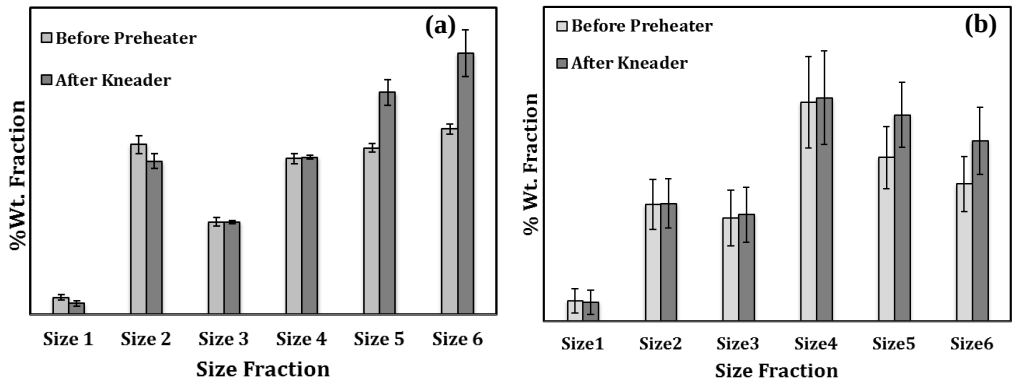

Figure 6.14 Distribution of coke fractions before and after kneader: (a) kneader 1 test (b) kneader 2 test

6.3.5 Concluding remarks

The technique developed was proven to be novel. This method involves nontoxic solvent which is easily available in the market and inexpensive. Also, this method consumed much less time compared to the time required for the method using sophisticated solvent extraction. Industry often requires simple and rapid methods for routine quality control. The simplicity of this technique made it beneficial for industrial use as it was also environmentally viable. The kneader tests demonstrated that the kneader performance was efficient and was not detrimental to the dry aggregate recipe in the paste.

CHAPTER 7

CONCLUSIONS AND RECOMMENDATIONS

7.1 Conclusions

The current project essentially focuses on the development of high density, low electrical resistivity, and low reactivity anodes. Three major goals were addressed:

- Characterization of raw materials and their interaction
- The development of new anode recipe, hence, improvement of anode quality
- Characterization of industrial anodes

Considerable effort was put forth to study the wetting characteristics of different anode raw materials. The main challenge was to determine the most important parameters that affect the pitch wetting and penetration behavior through calcined petroleum coke and recycled anode butts used in the production of anodes in aluminum industry. The coke-pitch interactions in anode paste have a significant influence on final anode properties. A number of experiments were conducted for a comprehensive study of chemical and physical interactions taking place during mixing. This may help facilitate the selection of raw materials and improve anode properties. The differences in pitch wetting and penetration behavior were assessed by contact angle measurements. The raw material properties which are relevant to pitch wetting were measured or estimated by different analytical tools.

It was found that dry aggregate's chemical, physical, and structural properties are important for their wettability by pitch. The results obtained from these studies indicated

that surface functional groups of both coke and pitch played a significant role in the wettability of coke by pitch. It was established that the presence of higher amounts of aromatic hydrocarbons, heteroatoms, and few impurities (silicon and sodium) improved the wetting behavior. It should be noted that some impurities (such as Na) increase the reactivities.

A clear increase in the wettability of coke by pitch with increasing mixing temperature was observed due to lower pitch viscosity at higher temperature. It was clearly established that the pitch wetting capability was considerably affected by coke particle porosity and shape. Highly porous cokes facilitated the pitch penetration and decreased the contact angle. Particle shape had a pronounced influence on the interaction between particles. Higher sphericity and lower irregularity of particles enhanced the packing properties and increased the wettability.

The crystalline length of coke (degree of coke calcination) affected wettability due to resulting differences in coke structure and surface chemistry. Under-calcined coke, which is wetted better by pitch, contained more aromatic hydrocarbons and heteroatoms as it was exposed to lower temperatures during the calcination process. This also suggested that the pre-graphitic order has a significant influence on pitch/coke wetting behavior.

Recycled butt is one of the major raw materials for anode production. The efficiency of pitch wetting and penetration into butt was compared with that of calcined petroleum coke. It was found that the wettability of recycled butt was significantly different than petroleum coke on both macroscopic and microscopic levels. The results suggested that recycled butt was better wetted by pitch due to presence of higher oxygen and sodium on the surface.

This probably accelerated the interfacial reaction. This result is in good agreement with the results obtained from the ANN model which suggested that an increase in oxygen and sodium improves the wetting. However, the presence of sodium is detrimental to anode reactivity. Also the particle shape and structure play a role.

The quality of petroleum coke used for the production of anodes for the aluminium industry is declining; and as a results of this, anode quality is deteriorating. Therefore, other anode-quality alternatives to petroleum coke should also be considered for anode production, and the quality of the anode should be ensured regardless of the raw material quality. Development of an alternative recipe could be one of the solutions to the problems concerning anode quality. In the second part of this thesis, an attempt was made to develop an ANN model and improve the anode paste recipe, which could be used in industry to reduce the excess carbon consumption in electrolysis. The challenge was to find an acceptable paste recipe within a practical range of each fraction. This attempt is justified since the quantity of each particle size fraction has an effect on anode properties. A primary objective was fulfilled by developing an ANN model where a tangible correlation was established between tapped bulk density of dry aggregates and ratio of dry aggregate density to green anode density. The scope of this study was also limited to the size fraction range used in industry so it was not possible to draw a definitive conclusion about the effect of each fraction on dry aggregate and green anode density. However, the study revealed the relative complexity to do so as the change in one fraction was followed by variations in other fractions simultaneously. The findings in this research highlighted the possibility of a significant improvement in green anode density that can be achieved by reducing the

medium fraction within a certain limit. Butt additions in bench scale anodes were proven to be beneficial from the density point of view. Optimum quantities of recycled butts were required to achieve desired density. Most of the other anode properties were in line with expectations. The improvement in anode density and reduction in electrical resistivity along with lower CO_2 reactivity indicated a promising case for industrial application of the novel recipe developed during this study. The objective of developing a new anode recipe part was also well accomplished, and the recipe developed during this study resulted in anodes with better properties than those of the standard anode recipe in the laboratory. The preparations are in progress for a trial for testing this recipe under industrial conditions.

A different approach was taken to reduce the anode reactivity and dusting by using under-calcined coke. Few separate studies are reported in the literature on the influence of coke crystalline length, baking temperature and sulfur content on anode properties. In this work, coke crystalline length was coupled with sulfur content and baking temperatures to study their combined effect on anode physical and chemical properties. The extent of the effect of L_c on these properties was also strongly affected by baking level and sulfur content. This study also revealed a number of results worth mentioning. Significant effect on anode air and CO_2 reactivity was noticed for under-calcined coke (UCC) at a lower baking temperature. Anode air and CO_2 dusting significantly reduced for anode produced from UCC at lower baking level. The reason behind reduced reactivity was due to the decrease in preferential consumption of the anode binder with oxygen or CO_2. However, there was a slight decrease in anode density for all anodes (anodes with and without doped sulfur) when the under-calcined coke was used due to the lower real density of this coke

compared to that of then calcined coke. The reduction in overall anode reactivity was observed for all the anodes (anodes with and without doped sulfur) baked at a high temperature but it was even more significant in anodes produced with UCC that were baked at a lower baking temperature. Also, wetting and interfacial analysis showed that UCC produced stronger interface compared to standard calcined coke. The results revealed that high sulfur based anode (both UCC and SCC) has higher air reactivity due to lower activation energy which easily destabilized the sulfur containing ring structure. Also, sulfur is highly prone to oxidation reaction and produces SO_2. Sulfur doped anodes had good resistance to CO_2 reactivity as sulfur acted as an inhibitor to metal catalyst. This study also revealed an interesting trend of an increase in anode density for standard calcined coke with addition of dibenzithiophene (DBT). The probable reason was explained by Sorlie *et al.* (1994) [91] that this sulfur dopant decreases the pitch viscosity, softening point. This study is the first one which investigates the combined effect of utilization of under-calcine coke, baking temperature and anode sulfur content.

Better understanding and control of the anode production parameters, and raw material properties can greatly contribute to the homogenous pitch distribution in anodes and consequently increase anode density. A method was developed to estimate the distribution of pitch and pores in the anodes using optical microscope. Further development and improvement of the method was required due to tedious sample preparation and limitation of surface area analysis. A novel technique was employed using digital camera and linear polarized light. Interpretation of results from the digital camera images showed that the characterizations of green and baked anodes are possible using this method. The analysis of

anode sections revealed useful information about pitch distribution during compaction. Anode pitch distribution and properties were significantly affected by type of industrial vibrocompactor, vibration time, paste recipe, bellow pressure and baking temperatures.

The different factors which have the most influence on industrial anode CO_2 reactivity were also studied using an ANN model. The elucidation of results showed that anode crystalline length had substantial effect on carboxy reactivity. A non-homogeneous temperature distribution in the baking furnace could create differences in anode crystalline length which could lead to non-homogenous reactivity in anodes. Additionally, bellow pressure during vibration improved the aggregate packing that produced dense anodes, which in turn reduced the CO_2 reactivity. Utilization of high amount of recycled butt and increasing sodium content of butt increased reactivity.

Paste characterization, specifically, the determination of particle size distribution in the paste before and after kneader may be used as an indicator to estimate anode quality. The kneader might crush the coke particles, hence, reduce the coke particle size. It is important to keep the dry aggregate sizing as intended as paste recipe has a significant influence on anode properties. A method, which is quick, nontoxic and inexpensive, is required for this purpose. However, most of the extraction methods available industrially use solvent which is toxic in nature. A new test was developed. The efficiency of the extraction method used in the new test was compared with industrial methods and found to be compatible. This test uses acetone as a solvent which is cheap and easily obtainable in marketplace and easy to dispose after use compared to other aromatic solvent such as xylene or toluene. It is also fast, which is one of the primary requirements of the industrial applications.

The overall results enlightened the unknown factors in this field of study. Therefore, it can be concluded that this work has significantly contributed to anode manufacturing.

7.2 Contribution to Québec and Canadian economies and environment

The main greenhouse gas emissions associated with primary aluminum production are CO_2 and perfluorocarbons (CF_4 and C_2F_6). The source of electric energy used for the electrolytic reduction is a very important factor influencing total CO_2 emissions from primary aluminum production. The specific emissions of CO_2 vary by a factor of five depending on whether coal or hydroelectricity is used as a source of power for the reduction cells. The aluminum in Québec is produced using hydroelectric power and it is considered "green". By contrast, emissions of PFCs are strictly the result of electrolytic reduction. They are formed only during the so-called anode effect when the electrolyte becomes depleted in alumina (Al_2O_3). CO_2 emission also occurs throughout the entire process of the electrolytic reduction of alumina. Produced CO_2 reacts with carbon anode (CO_2 reactivity) and produces CO. Improving the quality of anodes reduces the anode CO_2 reactivity, hence, contributes further to reduction of greenhouse emissions and the anode consumption. As explained above, the developed anode recipe reduced the anode CO_2 reactivity and increased the density which in turn decreases the greenhouse gas emissions, consequently, decreases anode consumption.

In this process, the high electrical resistance of anode is one of the main contributors to energy consumption, consequently, the cost of anode production. High density anodes have lower electrical resistivity; therefore, a small improvement in density as well as reduction

in electrical resistivity will improve the efficiency and economy of the operation. Characterization of raw materials and development of new recipe improved the quality of anode since the density is increased and the electrical resistivity is decreased. Consequently, the results of the project have a potential to contribute to reduction of the energy requirement and to increase anode life, hence, the productivity.

Aluminum is one of the major industries in Canada and Québec and this research will result in the improvement of product quality through technology transfer to the industry and economy of Québec and Canada.

7.3 Recommendations

Although an efficient model was developed which can determine the anode recipe to be used to improve the anode density and suggest an improved anode paste recipe, there is still a lot of room for improvement. As an extension of this work, studies on the prediction of alternate anode recipe can be conducted using ANN model. Also, this model can be improved further by training the network using more data. Another study can be conducted for understanding the effect of each particle size fraction on anode density on a wider scale.

The results of this study and available literatures showed that particle shape had greater influence on wettability, fluidity and furthermore overall packing behavior of the aggregate. The findings suggested that more spherical and regular shaped particles contribute to better wettability of coke by pitch. It was found that shot coke is wetted well by pitch. Additionally, it had higher real density. It might be possible that the spherical shape of shot coke particles and its high real density will result in anodes with improved properties. An

investigation can be carried out to study the effect of replacing some portion of anode grade coke by shot coke on anode properties.

Due to the constraints in time and budget and moreover availability of raw materials, it was not possible to make anodes from same cokes for which the wettability studies were conducted. Such a systematic study might help understand the impact of the wettability and surface properties of coke on green anode density.

It might be advantageous to continue the tests with under-calcined coke with larger range of crystalline lengths and various baking temperatures along with baking conditions (soaking, heating rate) in order to determine the optimum coke crystalline length and corresponding baking level. This could be one of the prerequisite for the industrialization of any attempt with under-calcined coke.

Optical test method with digital camera was found to be a promising method to study the distribution of pitch in green and baked anodes. However, this method might be extended for the determination of particle size distribution.

Appendix 1

WETTABILITY

A.1.1 Summary of contact angles of all coke/pitch pairs.

The contact angle data for all the wettability tests are tabulated in Table A.1.1. The table indicates the temperature of the experiments, contact angle (CA) at 1500s and contact angle at 80s. All the wettability tests were done under nitrogen atmosphere using sessile-drop setup.

Table A.1.1 Experimental results of contact angle with different coke-pitch pairs

Coke	Pitch	Temperature (°C)	Exp. CA at 1500 s (θ°)	Exp. CA at 80 s (θ°)
Coke 1	Pitch 2	170°C	18.37	83.1
Coke 1	Pitch 3	170°C	12.265	81.86
Coke 1	Pitch 4	170°C	24.33	73.9
Coke 1	Pitch 5	170°C	21.54	73.12
Coke 1	Pitch 1	170°C	25.13	62.05
Coke 3	Pitch 2	170°C	47.745	78.9
Coke 3	Pitch 3	170°C	43.16	83.05
Coke 3	Pitch 4	170°C	48.07	78.15
Coke 3	Pitch 5	170°C	41.305	82.32
Coke 6	Pitch 2	170°C	35.92	83.34
Coke 6	Pitch 3	170°C	20.49	78.15
Coke 6	Pitch 4	170°C	36.68	85.05
Coke 6	Pitch 5	170°C	37.94	75.12
Coke 6	Pitch 1	170°C	37.5	75.54
Coke 4	Pitch 2	170°C	22.05	75.12
Coke 4	Pitch 3	170°C	15.95	76.67
Coke 4	Pitch 4	170°C	29.145	77.6
Coke 4	Pitch 5	170°C	27.89	76.56
Coke 4	Pitch 1	170°C	28.44	70.285
Coke 2	Pitch 2	170°C	28.495	78.12
Coke 2	Pitch 3	170°C	36.53	79.18

Coke	Pitch	Temperature (°C)	Exp. CA at 1500 s (θ°)	Exp. CA at 80 s (θ°)
Coke 2	Pitch 4	170°C	39.02	80.132
Coke 2	Pitch 5	170°C	29.18	67.78
Coke 5	Pitch 2	170°C	29.325	78.23
Coke 5	Pitch 3	170°C	23.595	78.12
Coke 5	Pitch 4	170°C	32.41	83.88
Coke 5	Pitch 5	170°C	32.85	78.735
Coke 5	Pitch 1	170°C	30.47	64.93
Coke 1	Pitch 6	170°C	0	0
Coke 2	Pitch 6	170°C	0	47.5
Coke 3	Pitch 6	170°C	43.34	64.62
Coke 1	Pitch 7	170°C	0	35.42
Coke 2	Pitch 7	170°C	0	68.62
Coke 3	Pitch 7	170°C	46.68	75.53
Coke LS	Pitch 6	170°C	0	38.6
Coke HS	Pitch 6	170°C	0	0
Coke LS	Pitch 7	170°C	21.03	57.73
Coke HS	Pitch 7	170°C	0	58.1
Coke LS	Pitch 2	170°C	0	25.12
Coke HS	Pitch 2	170°C	0	0
Coke 2	Pitch 4	170°C	34.91	78.12
Coke 3	Pitch 1	170°C	50.47	76.81
Shot Coke	Pitch 7	170°C	0	80.62
Shot Coke	Pitch 1	170°C	0	67.63
Shot Coke	Pitch 2	170°C	0	66.14
Shot Coke	Pitch 3	170°C	0	71.14
Shot Coke	Pitch 4	170°C	0	74.12
Shot Coke	Pitch 5	170°C	0	61.83
Butt	Pitch 1	170°C	0	17.87
Butt	Pitch 7	170°C	13.44	65.58
Butt	Pitch 6	170°C	0	0
Coke 24 Lc	Pitch 8	170°C	0	8.63
Coke 30 Lc	Pitch 8	170°C	0	21.55
Coke 30 Lc	Pitch 8	170°C	0	22.93
Coke 34 Lc	Pitch 8	170°C	0	28.66
CPC 1	Pitch 8	170°C	53.71	67.19
Coke 1	Pitch 2	190°C	0	58.59
Coke 2	Pitch 2	190°C	0	61.39

Coke	Pitch	Temperature (°C)	Exp. CA at 1500 s (θ°)	Exp. CA at 80 s (θ°)
Coke 3	Pitch 2	190°C	32.96	66.02
Coke 4	Pitch 2	190°C	0	59.53
Coke 5	Pitch 2	190°C	0	72.09
Coke 6	Pitch 2	190°C	0	58.03
Coke 1	Pitch 2	190°C	0	50.64
Coke 2	Pitch 2	190°C	20.98	67.19
Coke 3	Pitch 2	190°C	32.17	75.49
Coke 4	Pitch 2	190°C	0	51.07
Coke 5	Pitch 2	190°C	25.83	52.04
Coke 6	Pitch 2	190°C	15.49	65.15

A.1.2 Wettability and characterization study of shot coke

A systematic study was undertaken to reveal shot coke wetting characteristic by different coal tar pitches and find a pathway to use of shot coke for anode production in aluminum industry. Shot coke-coal tar pitch wetting was characterized by monitoring the dynamic contact angle (Figure A.1.1) and coke morphology was macroscopically investigated by SEM microscopy (Figure A.1.4). Surface functional groups were mainly identified using spectroscopic techniques such as FT-IR and XPS along with SEM-EDX analyses (Figure A.1.2-A.1.3). The results obtained from wettability tests revealed that shot coke was wettable by all the coal tar pitches. Shot coke had a very unique and homogeneous structure. Shot coke particles were spherical in shape and constituted by very fine grains. FT-IR, XPS and SEM-EDX analyses revealed that shot coke contained similar surface functional groups as anode grade sponge coke (Table A.1.2). Furthermore, the previous findings of this thesis suggested that particle shape has great influence on coke/pitch wettability. It was found that spherical and regular particles exhibited greater wettability. Based on the previous findings in literatures and current results in this thesis, it seems that

shot coke has potential to be used in anode production and can be cautiously blended with regular anode grade coke.

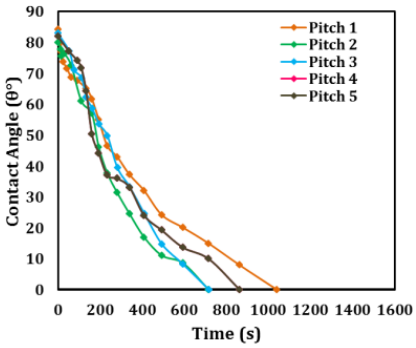

Figure.A.1.1 Dynamic contact angles of five different pitches on shot coke at 170°C

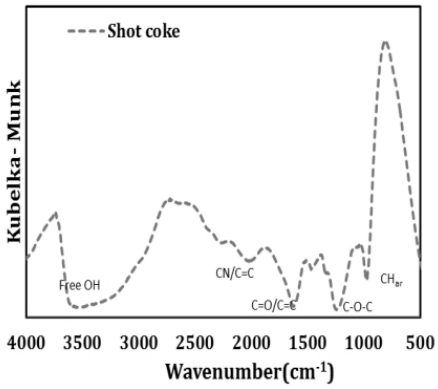

Figure.A.1.2 FT-IR spectra of shot coke

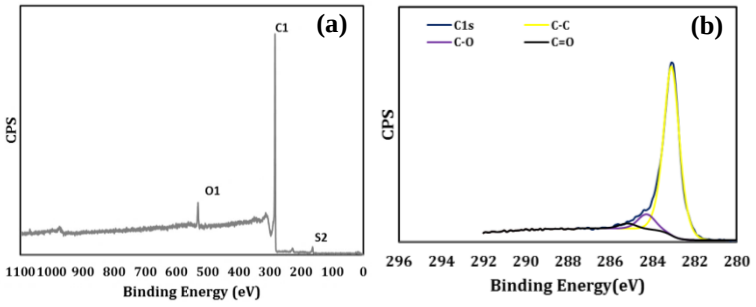

Figure.A.1.3 XPS spectra of shot coke (a) survey spectra (b) de-convoluted C1s spectra

Table A.1.2 Binding energy ranges used during deconvolution of C1s XPS spectra

Element	Peak	BE (eV)	Compound
C	1s	284.3-284.5	C=C
C	1s	285.1-285.5	C-C
C	1s	285.6-287.0	C-N/CO/CS
C	1s	287.5-287.9	C=O
C	1s	288.1-289.1	COOH/COOR

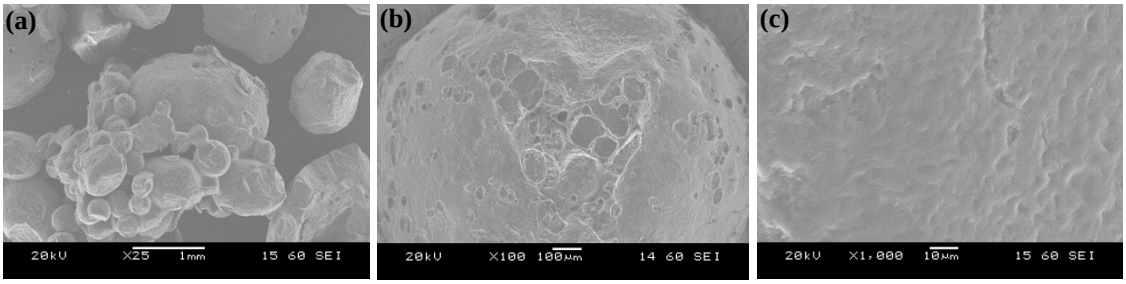

Figure.A.1.4. SEM images of shot coke at different magnification (a) 25X (b) 100X (c) 1000X

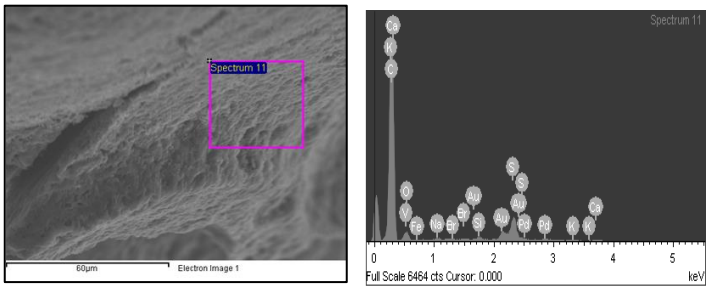

Figure.A.1.5 EDX analysis of shot coke

Table A.1.3 Atomic percentages of different elements in shot coke by EDX analysis

Element	*Atomic%*
C	94.85
O	2.38
Na	0.25
Si	0.17
S	1.60
K	0.08
Ca	0.11
V	0.04
Fe	0.07
Br	0.05
Pd	0.11
Au	0.31

A.1.3 Effect of sulfur on wettability

The pitch wetting capability was measured by determining the contact angle on a coke bed by using sessile-drop method. Several investigations were carried out in order to study effect of sulfur in coke on wettability using three different coal tar pitches. Study revealed that high sulfur coke had higher wettability (Figure.A.1.6).

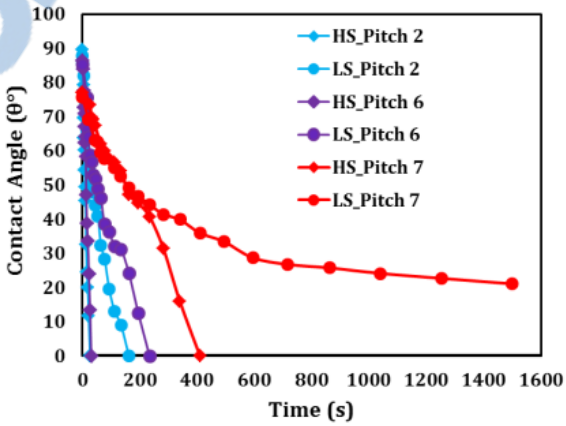

Figure.A.1.6 Dynamic contact angles of three different pitches on high and low sulfur coke at 170°C

Appendix 2

CHARACTERIZATIONS OF INDUSTRIAL ANODES

A.2.1 Pitch distribution in industrial anodes

Initially pitch distribution in anode was measured by optical microscope images. An example of mosaic picture is shown in the Figure A.2.1

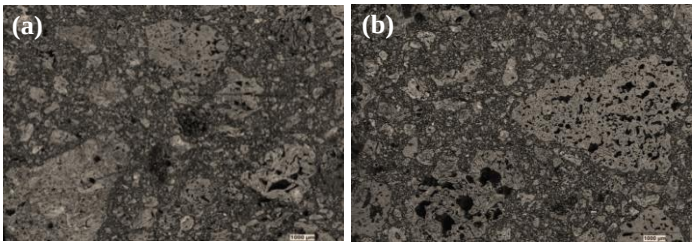

Figure.A.2.1 Optical microscopy mosaic images of samples of VA-G6 (a) top (b) bottom

A.2.2 Performances of industrial kneaders

Kneader performances are characterized by measuring the coke distribution before and after kneader. Results of each collected samples for Kneader 1 and 2 are presented in Figures A.2.2 and A.2.3.

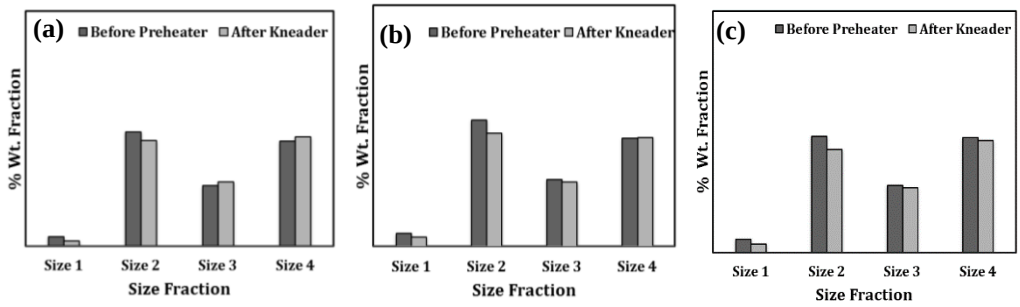

Figure.A.2.2 Distribution of coke fractions before and after kneader 1 (a) sample 1 (b) sample 2 (c) sample 3

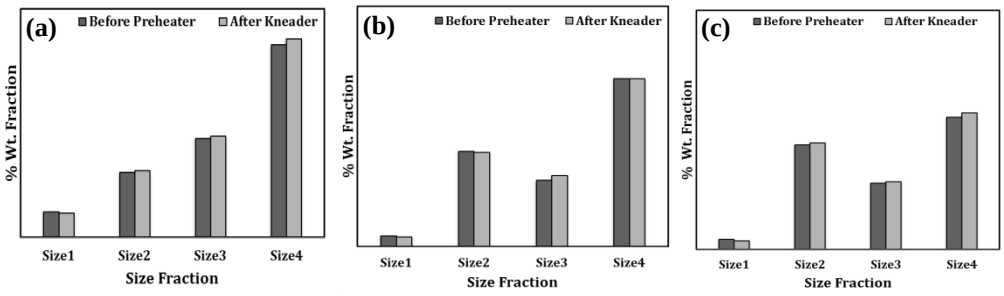

Figure.A.2.3 Distribution of coke fractions before and after kneader 2 (a) sample 1 (b) sample 2 (c) sample 3

A.2.3 Anode crystalline length

Figure 6.9 shows the positions of the anodes in the pits and Figure A.2.4 illustrate the core positions in the anodes. Crystalline length of the different anodes indicates that furnace temperature had significant influence on anode crystalline length. The nonhomogeneous temperature distribution in the pits greatly affected the crystalline length at different positions of the anodes. In the prior part of the works, it was found that anode crystalline length significantly affected the anode CO_2 reactivity. The nonhomogeneous temperature distribution in the pit, consequently, the nonhomogeneous distribution of Lc can affect the reactivity of the anodes in the pot room. Figure.A.2.5 presents the measured crystalline length of anode cores for different anodes.

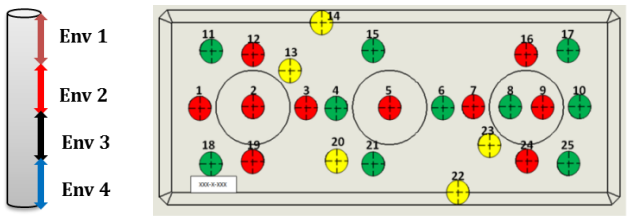

Figure.A.2. 4 Position of the core in an anode

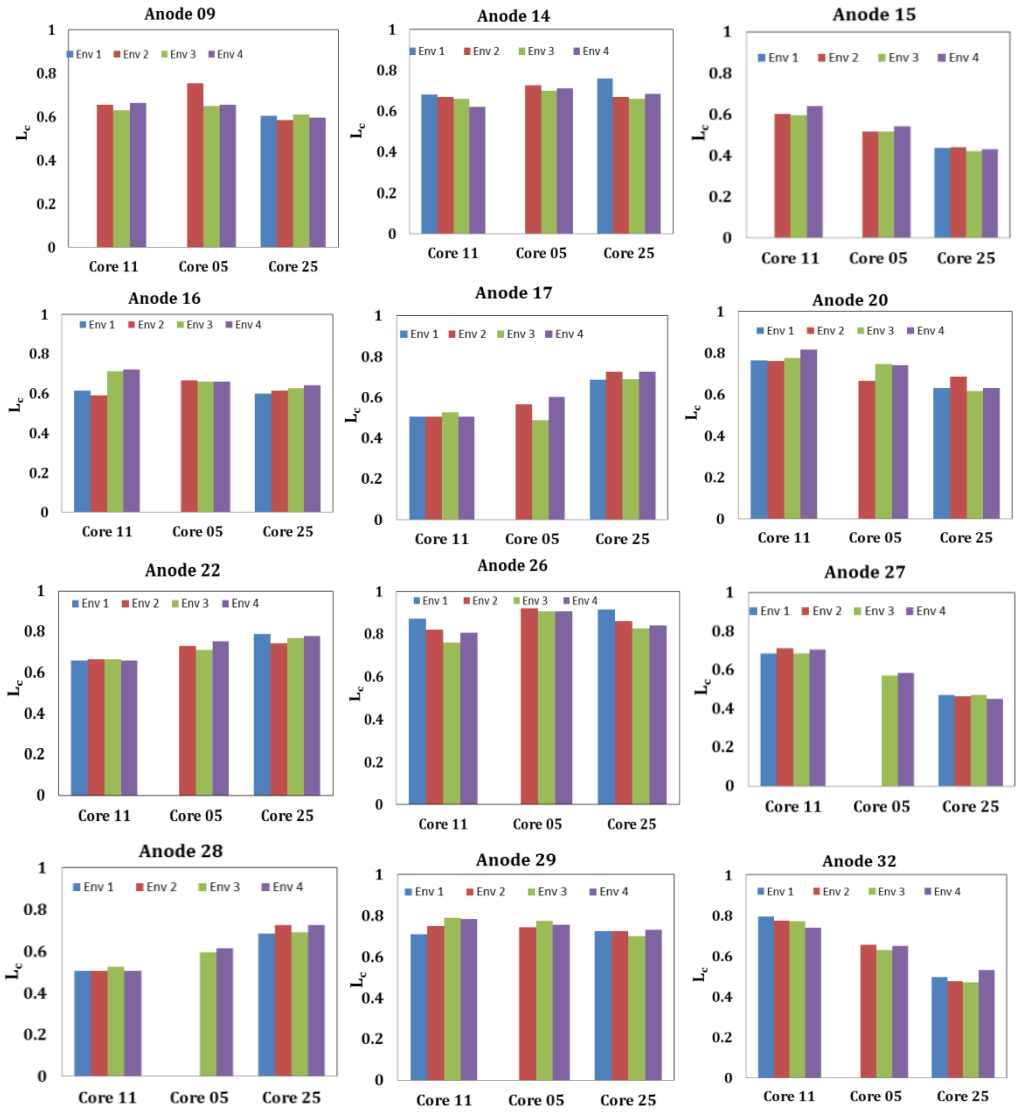

Figure.A.2.5 Crystalline length of anode cores for different anodes

REFERENCES

1. Carbon, R.D., *Anodes for the Aluminum Industry*. 4 ed. 2007, Sierre, Switzerland. 394.
2. Newsletter, T.A.A.O.C. 2011.
3. *World Aluminum - the website of the International Aluminium Institute*. 2014 [cited 2014; Available from: http://www.world-aluminium.org/.
4. *Aluminum Association of US.* 2014; Available from: http://www.aluminum.org/resources/industry-statistics.
5. Hulse, K.L., *Anode Manufacture:Raw Materials, Formulation and Processing Parameters*. 2000, Sierre, Switzerland: R&D Carbon Ltd. 416.
6. Couderc, P., Hyvernat, P.,Lemarchand, J. L., *Correlations between ability of pitch to penetrate coke and the physical characteristics of prebaked anodes for the aluminium industry.* Fuel., 1986. **65**(2): p. 281-287.
7. Adams, A.N., *Characterization of the pitch wetting and penetration behavior of petroleum coke and recycled butts in pre-baked carbon anode*, in *The Department of Energy and Geo-Environmental Engineering*. 2004, Pennsylvania State University: Pennsylvania. p. 1-220.
8. Rocha, V.G., Blanco, C., Santamaría, R., Diestre, E. I., Menéndez, R., Granda, M., *Pitch/coke wetting behaviour.* Fuel., 2005. **84**(12-13): p. 1550-1556.
9. Lhuissier, J., Bezamanifary, L., Gendre, M., Chollier, M. J., *Use of under-calcined coke for the production of low reactivity anodes.* Light Metals., 2009: p. 979-983.
10. Sulaiman, D., Garg, R., *Use of under calcined coke to produce baked anodes for aluminium reduction lines.* Light Metals., 2012: p. 1147-1151.
11. Brym, M.J.C., Gagnon, A., Boulanger, C., Lepage, D., Savard, G., Bouchard, G., Lagacé, C., Charette, A., *Anode reactivity: Effect of coke calcination level.* Light Metals., 2009: p. 905-908.
12. Fischer, W.K., Perruchoud, R., *Influence of coke calcining parameters on petroleum coke quality.* Light Metals., 1985: p. 811-826.
13. Kocaefe, Y.S., Dahmane, F., Bui, R. T., Proulx, A. L., *Study on coke dust generation in a rotary calcination kiln.* Light Metals., 1996: p. 485-489.
14. Al-Haj-Ibrahim, H., Morsi, B. I., *Desulfurization of petroleum coke: A review.* Industrial & Engineering Chemistry Research., 1992. **31**(8): p. 1835-1840.
15. Ibrahim, H.A.H., Ali, M. M., *Effect of the removal of sulphur and volatile matter on the true density of petroleum coke.* Periodica Polytechnica: Chemical Engineering., 2005. **49**(1): p. 19-24.
16. Siskin, M., Kelemen, S. R.,Eppig, C. P., Brown, L. D., Afeworki, M., *Asphaltene molecular structure and chemical influences on the morphology of coke produced in delayed coking.* Energy and Fuels., 2006. **20**(3): p. 1227-1234.
17. Hume, S.M., *Anode reactivity : influence of raw material properties*. 2 ed. 1999, Sierre Suisse 433.
18. Narvekar, R., Sardesai, A., *Performance of blended and unblended green cokes during calcination.* Light Metals., 2004: p. 483-488.

19. Tosta M, R.J., Inzunza, E. M., *Structural evaluation of coke of petroleum and coal tar pitch for the elaboration of anodes in the industry of the aluminum.* Light Metals, 2008: p. 887-892.
20. Narvekar, R.N., Sardesai, A., Prasad, A. B., *Importance of granulometry in calcined petroleum coke.* Light Metals., 2003: p. 525-530.
21. Tordai, T., *Anode dusting during the electrolytic production of aluminium*. 2007, École Polytechnique Fédérale de Lausanne: Lausanne. p. 1-351.
22. Belitskus, D., *Effects of petroleum coke calcination temperature and anode baking temperature on anode properties*, in *Light Metals* 1991. p. 557-563.
23. Edward, L.C., *Responding to changes in coke quality.* Rain Cii Technical paper., 2007.
24. Edwards, L., Backhouse, N.,Darmstadt, H.,Dion, M. J., *Evolution of anode grade coke quality.* Light Metals, 2012: p. 1207-1212.
25. Barry, S., *How important are coke and pitch quality changes and the fabrication process to anode performance in aluminium reduction.*, in *26 th International Aluminium Conference*. 2011.
26. Hays, D., J.W. Patrick, and A. Walker, *SEM characterization of cokes and carbons.* Fuel, 1983. **62**(9): p. 1079-1083.
27. Hays, D., J.W. Patrick, and A. Walker, *SEM study of binder coke in electrode carbon.* Fuel, 1983. **62**(8): p. 946-952.
28. Singh, A.K., Sharma, M.,Singh, M. P.,Choudhury, N. *SEM study of some Indian natural cokes (jhama)*. 2010.
29. Neyrey, K., Edwards, L.,Anthony Ross, J.,Vogt, F., *A tool for predicting anode performance of non-traditional calcined cokes*, in *Light Metals*. 2005. p. 607-612.
30. Coste, B., Schneider, J. P., *Influence of coke real density on anode reactivity consequence on anode baking.* Light Metals., 1994: p. 583-591.
31. jDreyer, C., Samanos, B.,Vogt, F., *Coke calcination levels and aluminum anode quality.* Light Metals, 1996: p. 535-542.
32. Hardin, E.E., Beilharz, C. L., Melvin, L. L., *Comprehensive review of the effect of coke structure and properties when calcined at various temperatures.* Light Metals., 1993: p. 501-508.
33. *Rain Cii certificate of calcined coke*. 2011.
34. Hume, S.M., Fischer, W. K., Perruchoud, R. C., Welch, B. J., *A model for petroleum coke reactivity.* Light Metals., 1993: p. 525-531.
35. Heintz, E.A., *Effect of calcination rate on petroleum coke properties.* Carbon., 1995. **33**(6): p. 817-820.
36. Tran, K.N., Bhatia, S. K., Tomsett, A., *Air reactivity of petroleum cokes: Role of inaccessible porosity.* Industrial and Engineering Chemistry Research., 2007. **46**(10): p. 3265-3274.
37. Boero, J.F.R., *The reaction of petroleum cokes with air.* Carbon., 1987. **25**(4): p. 477-483.
38. Tyler, R.J., *Intrinsic reactivity of petroleum coke to oxygen.* Fuel., 1986. **65**(2): p. 235-240.

39. Rørvik, S., Lossius, L. P., Petter Ratvik, A., *Determination of coke calcination level and anode baking level - Application and reproducibility of L-sub-c based methods.* Light Metals., 2011: p. 841-846.
40. Belitskus, D., Danka, D. J., *Comprehensive determination of effects of calcined petroleum coke properties on aluminum reduction cell anode properties.* Light Metals., 1989: p. 429-442.
41. Dreyer, C., *Anode reactivity influence of the baking process.* Light Metals., 1989: p. 595-602.
42. Bopp, A.F., Groff, G. B., Howard, B. H., *Influence of maximum temperature and heat-soak times on the properties of calcined coke.* Light Metals., 1984: p. 869-882.
43. Dion, M.J., Darmstadt, H., Backhouse, N., Canada, M., Cannova, F., *Prediction of calcined coke bulk density.* Light Metals., 2011: p. 931-936.
44. Marsh, H., Griffiths,J., *A high resolution electron microscopy study of graphitization of graphitizable carbons,* in *International Symposium on Carbon,* . 1982: Toyohashi, Japan. p. 113.
45. Tran, K.N., *Influence of raw material properties and heat treatment temperature on the reactivity of carbon anodes*, in *School of Chemical engineering*. 2011, University of Queensland: Australia. p. 1-194.
46. Neyrey, K., Edwards, L.,Marino, J., *Observations on the coke air reactivity test.* Light Metals., 2013: p. 1051-1056.
47. Cahill, R.A., Gehlbach, R. E., Tittle, G. S., *Factors influencing the carboxy reactivity of calcined coke.* Light Metals., 2000: p. 563-568.
48. Edwards, L.C., Neyrey, K. J., Lossius, L. P., *A review of coke and anode desulfurization.* Light Metals., 2007: p. 895-900.
49. Oberlin, A., *Carbonization and graphitization.* Carbon., 1984. **22**(6): p. 521-541.
50. Lavigne, L., Castonguay, L., *Prediction of anode performance from calcined coke properties.* Light Metals., 1993: p. 569-575.
51. Rolle, J.G., Czikall, R. A., *Use of coke air reactivity testing for predicting anode air reactivity.* Light Metals., 2001: p. 675-679.
52. Cutshall, E.R., Walsh, W. E., Blair, P. A., *Studies involving air reactivity of petroleum coke.* Light Metals., 1993: p. 555-562.
53. Samanos, B., Dreyer, C., *Impact of coke calcination level and anode baking temperature on anode properties.* Light Metals., 2001: p. 681-688.
54. Ameeri, J.G., Dreyer, C., Samanos, B., *Approach for a complete evaluation of resistance to thermal shock. [2]: Applying to the solution of an industrial problem at ALBA.* Light Metals., 1997: p. 591-596.
55. Narvekar, R., Sardesai, A., *Comparison of physical properties of finer grains of calcined cokes generated during calcination with those originally present in green cokes.* Light Metals., 2005: p. 601-605.
56. Belitskus, D., *Anode aggregate bulk density determinatiom using a Y-blender* Light Metals, 2015: p. 1061-1065.
57. Subero, J., *Quality of calcined petroleum coke and its influence on aluminium smelting.* Light Metals, 2013: p. 1085-1088.

58. Paz, M., Boero, J. R., Milani, F., *Coke density and anode quality*. Light Metals., 1993: p. 549-553.
59. Piffer, V., Woo, C.,Nicéas, F.,Bacelar, R.,Araujo, J.,Paulino, L., *Measures to prevent baked anode density drop when using high porosity cokes.* Light Metals, 2013: p. 1097-1100.
60. Ndjom, B., Malik, M. S.,Al Marzouqi, A.,Sahu, T. K.,Rabba, S. A., *Improving anode baked density and air permeability through process optimization and coke blending.* Light Metals, 2013: p. 1105-1110.
61. Belitskus, D., *Evaluating calcined coke for aluminum amelting by bulk density*, in *Essential Readings in Light Metals: Electrode Technology for Aluminum Production*. 2013. p. 148-155.
62. Khaji, K., Al Qassemi, M., *Factors influencing baked anode properties*, in *Light Metals*. 2015. p. 1135-1140.
63. Lossius, L.P., Lubin, M.,Edwards, L.,Wyss, J., *Relationships between coke properties and anode properties - Round robin 19.* Light Metals., 2013: p. 1183-1188.
64. Perruchoud, R., Fischer, W. K., *Granular carbon mechanical properties: their measurement and influence on paste production.* Light Metals., 1992: p. 695-700.
65. Leach, C.T., Brooks, D. G., Gehlbach, R. E., *Correlation of coke properties, anode properties, and carbon consumption.* Light Metals., 1997: p. 481-488.
66. Tran, K.N., Berkovich, A. J., Tomsett, A., Bhatia, S. K., *Crystalline structure transformation of carbon anodes during gasification.* Energy and Fuels., 2008. **22**(3): p. 1902-1910.
67. Perruchoud, R., Fischer, W., *Determination of the sodium sensitivity of petroleum coke.* Light Metals., 1991: p. 581-584.
68. Liu, F.Q., Liu, Y. X., Mannweiler, U., Perruchoud, R., *Effect of coke properties and its blending recipe on performances of carbon anode for aluminium electrolysis.* Journal of Central South University of Technology (English Edition). 2006. **13**(6): p. 647-652.
69. Rolle, J.G., Hoang, Y. K., *Studies of the impact of vanadium and sodium on the air reactivity of coke and anodes.* Light Metals., 1995: p. 741-745.
70. Farr-Wharton, R., Welch, B. J.,Hannah, R. C.,Dorin, R.,Gardner, H. J., *Chemical and electrochemical oxidation of heterogeneous carbon anodes.* Electrochimica Acta, 1980. **25**(2): p. 217-221.
71. Adams, A.N., Schobert, H. H., *Characterization of the surface properties of anode raw materials.* Light Metals., 2004: p. 495-498.
72. Smith, M., Perruchoud, R.,Fischer, W.,Welch, B. *Evaluation of the effect of dust granulometry on the properties of binder matrix bench scale electrodes*. 1991.
73. Figueiredo, F.E.O., Kato, C. R., Nascimento, A. S., Marques, A. O. F., Miotto, P., *Finer fines in anode formulation.* Light Metals., 2005: p. 665-668.
74. Bowers, R., Ningileri, S., Palmlund, D. C., Vitchus, B., Cannova, F., *New analytical methods to determine calcined coke porosity, shape, and size.* Light Metals., 2008: p. 875-880.

75. Xiao, J., Deng, S., Li, J., Lai, Y., Liu, Y., *Influence of ultrafine powder on the properties of carbon anode used in aluminum electrolysis.* Light Metals., 2011: p. 1143-1147.
76. Hulse, K.L., Perruchoud, R. C.,Fischer, W. K.,Welch, B. J., *Process adaptations for finer dust formulations: Mixing and forming.* Light Metals, 2000: p. 467-472.
77. Rørvik, S., A.P. Ratvik, and T. Foosnæs. *Characterization of green anode materials by image analysis*. in *TMS Light Metals*. 2006.
78. Vitchus, B., Cannova, F., *Practical air reactivity impacts on anode performance.* Light Metals., 2002: p. 553-559.
79. Sulaiman, D., Garg, R.,Toorani, M., Garg, R., *Baked anode quality improvement through optimization of green anode plant ultra fine content in ball mill product and process parameters.* Light Metals., 2012: p. 1165-1167.
80. Tkac, M., *Porosity Development in Composite Carbon Materials during Heat Treatment*, in *Department of Materials Science and Engineering*. April 2007, Norwegian University of Science and Technology.
81. Dreyer, C., Samanos, B., *Approach for a complete evaluation of resistance to thermal shock. [1]: Applying to the case of anodes and cathodes.* Light Metals., 1997: p. 585-590.
82. Meier, M.W., Fischer, W.K.,Perruchoud, R.C.,Gauckler, L.J., *Thermal shock of anodes-a solved problem?* Light Metals, 1994: p. 685-694.
83. Cao, J., Buckley, A. N., Tomsett, A., *Re-examining the pitch/coke wetting and penetration test.* JOM., 2002. **54**(2): p. 30-33.
84. Mannweiler, U., *Novel approach in anode technology*, in *International Conference "Aluminium industry of Russia, Strategy and development and new investments projects*. 1992.
85. Perruchoud, R.C., Meier, M. W., Fischer, W. K., *Survey on worldwide prebaked anode quality.* Light Metals., 2004: p. 573-578.
86. Fischer, W.K., Keller, F., Perruchoud, R.C., Oderbolz, S., *Baking parameters and the resulting anode quality.* Light Metals., 1993: p. 683-689.
87. Tran, K.N., Berkovich, A. J., Tomsett, A., Bhatia, S. K., *Influence of sulfur and metal microconstituents on the reactivity of carbon anodes.* Energy and Fuels., 2009. **23**(4): p. 1909-1924.
88. Rodríguez-Mirasol, J., Thrower, P. A.,Radovic, L. R., *On the oxidation resistance of carbon-carbon composites: Importance of fiber structure for composite reactivity.* Carbon, 1995. **33**(4): p. 545-554.
89. Lhuissier, J., *About the use of under-calcined coke for the production of low reactivity anodes.* International pitch and calcined petroleum coke conference-Industrial quimica del nalon and Jacobs consultancy, 2007.
90. Fang, N., Xue, J., Li, X.,Lang, G.,Gao,S.,Xia,B., Jiang, J., Bao.,C., *Effects of coke types and calcining levels on the properties of bench-scale anodes.* Light Metals, 2015: p. 1153-1156.
91. Cahill, R.A., Huang, X., Naidoo,V.,Cannova,F.,Canada,M., *Exploring the case for under calcined coke- prospectives from a calciner and smelter* p. 1-10.

92. Adams, A., Cahill, R., Belzile, Y., Cantin, K. , Gendron, M., *Minimizing impact of low sulfur coke on anode quality.* Light Metals., 2009: p. 957-962.
93. Sorlie, M., Kuang, Z.L, Thonstad, J., *Effect of sulphur on anode reactivity and electrolytic consumption.* Light Metals., 1994: p. 659-665.
94. Patra, B., Barik, R. K., *Studies on the impact of calcined petroleum coke from different sources on anode quality.* Light Metals, 2012: p. 1213-1217.
95. Jones, S.S., R.D. Hildebrandt, and M.C. Hedlund, *Influence of High Sulphur Cokes on Anode Performance*, in *Essential Readings in Light Metals: Electrode Technology for Aluminum Production*. 2013. p. 42-52.
96. Hume, S.M., Fischer, W. K.,Perruchoud, R. C.,Metson, J. B.,Terry, R.,Baker, K., *Influence of petroleum coke sulphur content on the sodium sensitivity of carbon anodes.* Essential Readings in Light Metals: Electrode Technology for Aluminum Production, 2013. **4**: p. 123-129.
97. Eidet, T., Sorlie, M. Thonstad, J., *Effects of iron and sulphur on the air and CO_2 reactivity of cokes.* Light Metals, 1997: p. 511-517.
98. Eidet, T., Sorlie, M., Thonstad, J., *Effects of the sulphur, nickel and vanadium on the air and CO_2 reactivity of cokes*. 1997. p. 436-437.
99. Pietrzyk, S., Thonstad, J., *Influence of the sulphur content in the carbon anodes in aluminium electrolysis - A laboratory study.* Light Metals., 2012: p. 659-664.
100. Belitskus, D., *Effect of carbon recycle materials on properties of bench scale prebaked anodes for aluminum smelting.* Metallurgical Transactions B, 1981. **12**(1): p. 135-139.
101. Suriyapraphadilok, U., Halleck, P.,Grader, A.,Andresen, J. M. *Physical, chemical and X-ray Computed Tomography characterization of anode butt cores*. 2005.
102. Fischer, W. and R. Perruchoud. *Interdependence between properties of anode butts and quality of prebaked anodes*. 1991.
103. Weng, T.L., Vera, V. M., *Effect of butt particle size and butt fraction on prebake anode properties.* Light Metals, 1984: p. 1005-1013.
104. Uthaiporn., S., *Characterization of coal and petroleum derived binder pitches and the interaction of pitch/coke mixtures in prebaked carbon anodes*, in *Department of Materials Science and Engineering*. 2008, The Pennsylvania State University: Pennsylvania. p. 1-335.
105. Grjotheim, K.W.B.J., *Aluminium Smelter Technology: A Pure and Applied Approach*. 2nd ed. 1988: Aluminium-Verlag. 328.
106. Arthur W. Adamson, A.P.G., *Physical chemistry of surfaces*. 1997: John Wiley & Sons Inc.
107. Mirchi, A.A., Savard, G.,Tremblay, J. P.,Simard, M., *Alcan characterisation of pitch performance for pitch binder evaluation and process changes in an aluminium smelter.* Light Metals, 2002: p. 525-533.
108. Rocha, V.G., Blanco, C., Santamaría, R., Diestre, E. I., Menéndez, R., Granda, M., *An insight into pitch/substrate wetting behaviour. The effect of the substrate processing temperature on pitch wetting capacity.* Fuel., 2007. **86**(7-8): p. 1046-1052.

109. Rocha, V.G., Blanco, C., Santamaría, R., Diestre, E. I., Menéndez, R., Granda, M., *The effect of the substrate on pitch wetting behaviour.* Fuel Processing Technology., 2010. **91**(11): p. 1373-1377.
110. Lahaye, J., Ehrburger, P., *Pitch-coke interactions.* Fuel., 1985. **64**(9): p. 1187-1191.
111. Dmitrieva, G.V., Ryss, M.A., Smirnova, A.S.,Shuvaev, E.A., *Wettability and impregnability of carbon materials by coal tar pitch.* International Chemical Engineering 7, 1967. **7**: p. 252-255.
112. Greenhalgh, E., and Moyse, M.E. I, *Contact angle of pitch on carbon surfaces.*, in *n 3rd Conference on Industrial Carbons and Graphite. .* 1970: Society of Chemical Industry: London, UK. p. 539-548.
113. Dell, M.B., Peterson, R. W., *Wettability of petroleum cokes by pitch.* Industrial and Engineering Chemistry Product Research and Development., 1970. **9**(2): p. 190-194.
114. Pinoir, J., Hyvernat, P., *Binding characteristic of coal tar pitches for prebaked anode mix-choice critera LRF Rport- 830.* Light Metals: Proceedings of Sessions, AIME Annual Meeting (Warrendale, Pennsylvania). 1980: p. 497-515.
115. Ehrburger, P., Lahaye, J., *Capillary-flow of liquid pitch.* Fuel 1984. **63**: p. 1677-1680.
116. Romain, J.L.S., Lahaye, J.,Ehrburger, P.,Couderc, P., *Anomalous capillary flow of coal tar pitches.* Fuel, 1986. **65**(6): p. 865-868.
117. Heintz, E.A., *Wetting of filler by binder-a simple apparatus for determining wetting temperatures.* Carbon, 1986. **24**(2): p. 131-134.
118. Saint-Romain, J.L., Cottinet, D.,Couderc, P., *Capillary flow of coal tar and petroleum pitches into a porous coke bed* Light Metals, 1987: p. 603-611.
119. Wolfrom, R.L., *Wetting characteristics of binder pitch on petroleum coke in the presence of surfactant additives.*, in *Department of Mineral Processing Engineering* 2002, The Pennsylvania State University, University Park.: Pennsylvania.
120. Rocha, V.G., Granda, M., Santamaría, R., Blanco, C., Diestre, E. I., Menéndez, R., *Pyrolysis behaviour of pitches modified with different additives.* Journal of Analytical and Applied Pyrolysis., 2005. **73**(2): p. 276-283.
121. Sakurovs, R., *Interactions between a bituminous coal and aromatic hydrocarbons at elevated temperatures.* Energy and Fuels, 1998. **12**(3): p. 631-636.
122. Vanvoren, C., *Recent improvement in paste plant design industrial application and results.* Light Metals., 1987: p. 525-531.
123. Cannova, F., Canada, M., Vitchus, B., *Calcined coke particle size and crushing steps affect its VBD result.* Light Metals., 2011: p. 937-939.
124. Azari, K., Ammar, H., Alamdari, H., Picard, D., Fafard, M., Ziegler, D., *Effects of physical properties of anode raw materials on the paste compaction behavior.* Light Metals., 2011: p. 1161-1164.
125. Cheshomi, A., A. Fakher, and C.J.F.P. Jones, *A correlation between friction angle and particle shape metrics in Quaternary coarse alluvia.* Quarterly Journal of Engineering Geology and Hydrogeology, 2009. **42**(2): p. 145-155.
126. Suriyapraphadilok, U., Jennis-McGroarty, C., Zel, A., Andresen, J. M., *The use of gasification pitch and coal tar pitch in carbon anodes.* Light Metals., 2004. **49**.

127. Daniel, C. and J.O. Besenhard, *Handbook of Battery Materials*. 2nd ed. Handbook of Battery Materials: Second Edition. 2011: John Wiley & Sons. .
128. Menéndez, J.A., Pis, J. J., Alvarez, R., Barriocanal, C., Fuente, E., Díez, M. A., *Characterization of petroleum coke as an additive in metallurgical cokemaking. Modification of thermoplastic properties of coal.* Energy and Fuels,, 1996. **10**(6): p. 1262-1268.
129. Michel, D., Pruski, M., Gerstein, B. C., *NMR of petroleum cokes I: Relaxation studies and quantitative analysis of hydrogen by magnetic resonance.* Carbon., 1994. **32**(1): p. 31-40.
130. Pruski, M., Gerstein, B. C., Michel, D., *NMR of petroleum cokes II: Studies by high resolution solid state NMR of 1H and 13C.* Carbon., 1994. **32**(1): p. 41-49.
131. Jiang, B., Zhang, Y., Zhou, J., Zhang, K., Chen, S., *Effects of chemical modification of petroleum cokes on the properties of the resulting activated carbon.* Fuel., 2008. **87**(10-11): p. 1844-1848.
132. Lee Jum.M, B.J.J., Rolle. Jeffrey G. , Llerena Robert ,, *Characterization of green and calcines coke properties used for aluminum anode grade carbon* p. 1-7.
133. Guillén, M.D., Iglesias, M. J., Domínguez, A., Blanco, C. G., *Semiquantitative FTIR analysis of a coal tar pitch and its extracts and residues in several organic solvents.* Energy & Fuels., 1992. **6**(4): p. 518-525.
134. Alcañiz-Monge, J., Cazorla-Amorós, D., Linares-Solano, A., *Characterization of coal tar pitches by thermal analysis, infrared spectroscopy and solvent fractionation.* Fuel., 2001. **80**(1): p. 41-48.
135. Malekshahian, M., Hill, J. *Chemical and thermal modification of petroleum coke*. in *8th World Congress of Chemical Engineering*. 2009.
136. Bo-Hye, K., Arshad, H. W., Kap S. Y., Yun H. B., Sung R. K., *Molecular structure effects of the pitches on preparation of activated carbon fibers from electrospinning* Carbon Letters., 2011. **12**(2): p. 70-80.
137. Zhang, X.l., Zhang, Y., Ding, F. S., Huang, Q. J., Li, Y., *Effect of the surface properties of an activated coke on its desulphurization performance.* Mining Science and Technology (China). 2009. **19**(6): p. 769-774.
138. Blyth, R.I.R., Buqa, H., Netzer, F. P., Ramsey, M. G., Besenhard, J. O., Golob, P., Winter, M., *XPS studies of graphite electrode materials for lithium ion batteries.* Applied Surface Science., 2000. **167**(1): p. 99-106.
139. Blyth, R.I.R., Buqa, H., Netzer, F. P., Ramsey, M. G., Besenhard, J. O., Winter, M., *X-ray photoemission studies of surface pre-treated graphite electrodes.* Journal of Power Sources., 2001. **97-98**: p. 171-173.
140. Mittal, K.L., Kohli, R., *Developments in Surface Contamination and Cleaning: Fundamental and Applied Aspects*. Vol. 1. 2008, Norwich, NY, USA: William Andrew.
141. Huang, X., Kocaefe, D.,Kocaefe, Y., Bhattacharyay, D., *Wettability of bio-coke by coal tar pitch for its use in carbon anodes.* Colloids and Surfaces A: Physicochemical and Engineering Aspects, 2016. **490**: p. 133-144.
142. Estrade-Szwarckopf, H., *XPS photoemission in carbonaceous materials: A "defect" peak beside the graphitic asymmetric peak.* Carbon, 2004. **42**(8-9): p. 1713-1721.

143. Lázaro, M.-J., Herod, A. A.,Cocksedge, M.,Domin, M.,Kandiyoti, R., *Molecular mass determinations in coal-derived liquids by MALDI mass spectrometry and size-exclusion chromatography.* Fuel, 1997. **76**(13): p. 1225-1233.
144. Díaz, C., Blanco, C. G., *NMR: A powerful tool in the characterization of coal tar pitch.* Energy and Fuels, 2003. **17**(4): p. 907-913.
145. Prouix, A.L., *Optimum binder content for prebaked anodes.* Light Metals., 1993: p. 657-661.
146. Adams, A.N., Mathews, J. P., Schobert, H. H., *The use of image analysis for the optimization of pre-baked anode formulation.* Light Metals., 2002: p. 547-552.
147. Lee, S.H., Choi, C. S., *Chemical activation of high sulfur petroleum cokes by alkali metal compounds.* Fuel processing technology., 2000. **64**(1): p. 141-153.
148. Pérez, S.P., Doval-Gandoy, J.,Ferro, A.,Silvestre, F. *Quality improvement for anode paste used in electrolytic production of aluminium*. in *Conference Record - IAS Annual Meeting (IEEE Industry Applications Society)*. 2005.
149. Azari, K., Alamdari, H.,Aryanpour, G.,Ziegler, D.,Picard, D.,Fafard, M., *Compaction properties of carbon materials used for prebaked anodes in aluminum production plants.* Powder Technology, 2013. **246**: p. 650-657.
150. Gao, S., Bao, C.,Zhang, S.,Wang, H.,Woo, J.,Cutshall, E., *Optimum vibration time for green anode production*, in *Light Metals*. 2013. p. 1123-1126.
151. *USGS Digital Spectral Library* Available from: http://speclab.cr.usgs.gov/spectral.lib06/ds231/.
152. Setnička, V. *FT-IR Reflection Techniques*. Available from: http://old.vscht.cz/anl/vibspec/FTIR%20Reflection%20Techniques.pdf.
153. *University of saarland, High Vacuum Lab*. Available from: http://www.uni-saarland.de/en/.
154. Parthiban, T., Ravi, R.,Kalaiselvi, N., *Exploration of artificial neural network [ANN] to predict the electrochemical characteristics of lithium-ion cells.* Electrochimica Acta, 2007. **53**(4): p. 1877-1882.
155. Milewski, J., Świrski, K., *Modelling the SOFC behaviours by artificial neural network.* International Journal of Hydrogen Energy, 2009. **34**(13): p. 5546-5553.
156. Madic M.J., M.V.J., *Assessing the sensitivity of the artificial neural network to experimental noise: a case study.* FME Transactions, 2010. **38**: p. 189-195
157. Bhattacharyay, D., Kocaefe, D.,Kocaefe, Y.,Morais,B. *Application of an artificial neural network to control the properties of baked anode* in *JER-REGAL*. 2013.
158. Sarkar, A., Kocaefe, D.,Kocaefe, Y.,Sarkar, D.,Bhattacharyay, D.,Morais, B.,Chabot, J., *Coke–pitch interactions during anode preparation.* Fuel, 2014. **117, Part A**(0): p. 598-607.
159. Kwan, A.K.H. and C.F. Mora, *Effects of various, shape parameters on packing of aggregate particles.* Magazine of Concrete Research, 2001. **53**(2): p. 91-100.
160. Azari, K., Hussein, A., Alamdari, H., Ziegler, D., Fafard, M.,, *Characterization of packing ability of coke particles.* Light Metals., 2014: p. 1117-1121.
161. Contreras, A., León, C. A.,Drew, R. A. L.,Bedolla, E., *Wettability and spreading kinetics of Al and Mg on TiC.* Scripta Materialia, 2003. **48**(12): p. 1625-1630.

162. Berlin, D.K., Clark, P. E.,Schroeder, J. T.,Hopper, D. G., *Synthesis of 1,2,3,4-Tetrahydrocarbazoles with Large Groups - Aromatization to Carbazoles.* Physical Sciences, 1966: p. 215-220.
163. Wikipedia. *Infrared spectroscopy correlation table*. Available from: http://en.wikipedia.org/wiki/Infrared_spectroscopy_correlation_table.
164. Eidet, T., Thonstad,J.,Sorlie,M., *Iron catalyzed reactivity of carbon anodes for aluminium electrolysis*, in *Conf. Carbon*. 1995: Bienn. p. 638-639.
165. Bhattacharyay, D., Kocaefe, D.,Kocaefe, Y.,Sarkar, A.,Morais, B.,Chabot, J. *Characterization of dry aggregates in carbon anodes by image analysis*. in *Light Metals*. 2014.
166. Aanvik Engvoll, M., *Reactivity of anode raw materials and anodes for production of aluminium*, in *Department of Inorganic Chemistry*. 2001, NTNU.
167. Zande, M., *Introduction to Carbon Technologies*. 1997, University of Alicante, Alicante.
168. Brooks, J.D., Taylor,G.H. , *Chemistry and Physics of Carbon*. Vol. 4. 1968, New York.
169. Schmidt-Hatting, W., A.A. Kooijman, and R. Perruchoud. *Investigation of the quality of recycled anode butts*. 1991.
170. Fischer, W.K., Perruchoud, R. C., *Interdependence Between Properties of Anode Butts and Quality of Prebaked Anodes*, in *Essential Readings in Light Metals: Electrode Technology for Aluminum Production*. 2013. p. 267-270.
171. Belitskus, D.L., *Evaluation of relative effects of coke, formulation, and baking factors on aluminum reduction cell anode performance.* Light Metals., 1993: p. 677-681.
172. Amrani, S., Kocaefe, D., Kocaefe, Y., Morais, B., Blaney, G., *Effect of heating rate on the crack formation during baking in carbon anodes used in aluminum industry.* Light Metals, 2014: p. 1175-1180.
173. Bhattacharyay, D., Kocaefe, D., Kocaefe, Y., Morais, B., Gagnon, M., *Application of the artificial neural network (ANN) in predicting anode properties.* Light Metals, 2013: p. 1189-1194.
174. Rebaïne, F., Bouazara, M.,Marceau, D.,Kocaefe, D., Morais, B., *Development of an analytical dynamic model of a vibro-compactor used in carbon anode production.* Light Metals, 2013: p. 1111-1115.
175. Bhattacharyay, D., Kocaefe, D., Kocaefe, Y. , Morais, B. , *Comparison of linear multivariable, partial least square regression, and artificial neural network analyses to study the effect of different parameters on anode properties.* Light Metals, 2014: p. 1129-1134.
176. Kocaefe, D., Sarkar, A., Lu, Y., Bhattacharyay, D., Kocaefe, Y, Morais, B., *Utilization of artificial neural network to analyze and predict the influence of different parameters on anode properties* in *Australasia*. 2014: Dubai.
177. Rebaine, F., *Étude de l'influence des paramètres de vibro-compaction sur les propriétés mécaniques des anodes crues en carbone.*, in *Department of Applied Science*. 2015, University of Quebec at chicoutimi: Chicoutimi, Canada. p. 1-235.

178. Bhattacharyay, D., Kocaefe, D.,Kocaefe, Y.,Sarkar, A.,Morais, B.,Chabot, J., *Characterization of dry aggregates in carbon anodes by image analysis.* Light Metals, 2014: p. 1111-1114.
179. Bhattacharyay, D., Kocaefe, D., Kocaefe,Y., Morais, B., *Determination of coke, pitch and pores/cracks in green anode by image analysis.* Journal of Surface Engineered Materials and Advanced Technology, 2013. **3**(3A): p. 1-6.
180. Keller, F., Schmidt-Hatting, W.,Kooijman, A.,Fischer, W.,Perruchoud, R., *Characterizing anode properties by quality figures.* Light Metals 1990: p. 479-483.
181. Akhtar, R.J., Meier, M. W.,Sulger, P. O.,Fischer, W. K.,Friedrich, R.,Janousch, T., *Anode quality and bake furnace performance of EMAL.* Light Metals, 2012: p. 1175-1179.
182. Buss. *Buss Kneader Tecnology*. Available from: http://www.busscorp.com/display.cfm?id=101990&disp_type=dmssimple&pageID=52640.

List of Publications

Journal Articles

- **Arunima Sarkar,** Duygu Kocaefe, Yasar Kocaefe, Dilip Sarkar, Dipankar Bhattacharyay , Brigitte Morais , Jérôme Chabot, Coke -pitch interaction during anode preparation. Fuel 117 (2014) 598–607
- **Arunima Sarkar,** Duygu Kocaefe, Yasar Kocaefe, Dipankar Bhattacharyay, Dilip Sarkar, Brigitte Morais, Effect of crystallinity on the wettability of petroleum coke by coal Tar Pitch. (submitted to the director and codirector for correction)
- **Arunima Sarkar,** Duygu Kocaefe, Yasar Kocaefe, Dipankar Bhattacharyay, Dilip Sarkar, Brigitte Morais, Influence of coke physical and chemical; properties on the wettability of different calcined petroleum cokes by coal tar pitch (submitted to the director and codirector for correction)
- **Arunima Sarkar,** Duygu Kocaefe, Yasar Kocaefe, Dipankar Bhattacharyay, Dilip Sarkar, Brigitte Morais, Influence of coke crystallinity and sulfur content on the reactivity of carbon anodes (in preparation)
- **Arunima Sarkar,** Duygu Kocaefe, Yasar Kocaefe, Dipankar Bhattacharyay, Dilip Sarkar, Brigitte Morais, Influence of coke granulometry on the properties of carbon anodes (in preparation)

Conference Articles

Refereed Conferences

- Duygu Kocaefe, **Arunima Sarkar**, Ying Lu, Dipankar Bhattacharyay, Yasar Kocaefe, Brigitte Morais; Utilization of artificial neural network to analyze and predict the influence of different parameters on anode properties. Australasia (2014) 29 -31 May.
- **Arunima Sarkar**, Duygu Kocaefe, Yasar Kocaefe, Dipankar Bhattacharyay, Brigitte Morais, Charles-Luc Lagacé; Determination of contact angle from raw material properties using linear multivariable analysis. TMS Light Metals (2014). 16-20 February.
- Dipankar Bhattacharyay, Duygu Kocaefe, Yasar Kocaefe, **Arunima Sarkar**, Brigitte Morais, Jerome Chabot; Charterization of dry aggregates in carbon anodes by image analysis. TMS Light Metals (2014). 16-20 February.
- Duygu Kocaefe, **Arunima Sarkar**, Shipan Das, Salah Amrani, Dipankar Bhattacharyay, Dilip Sarkar, Yasar Kocaefe, Brigitte Morais, Marc Gagnon; Review of different techniques to study the interaction between coke and pitch in anode manufacturing.; TMS Light Metals (2013). 3-7 March.
- **Arunima Sarkar**, Duygu Kocaefe, Yasar Kocaefe, Dipankar Bhattacharyay, Brigitte Morais, Martin Pouliot.; Characterization of petroleum coke and butts used in anode manufacturing in aluminum industry. COM (2013). 27-31 October.

Non-refereed Conferences

- **Arunima Sarkar,** Duygu Kocaefe, Yasar Kocaefe, Dipankar Bhattacharyay, Dilip Sarkar, Brigitte Morais, Prediction of anode recipe by artificial neural network (ANN) method, JER-REGAL (2014), 18th November. Québec, Canada

- **Arunima Sarkar,** Duygu Kocaefe, Yasar Kocaefe, Dipankar Bhattacharyay, Dilip Sarkar, Brigitte Morais, Marc Gagnon., Étude de l'impact des propriétés du coke de pétrole sur sa mouillabilité par le brai., Acfas (2013). Québec, Canada
- **Arunima Sarkar,** Duygu Kocaefe , Yasar Kocaefe, Brigitte Morais, A comparative surface characterization study between petroleum coke and recycled anode butt, JER-REGAL (2013), 22nd October, Québec, Canada
- **Arunima Sarkar,** Duygu Kocaefe, Yasar Kocaefe, Dipankar Bhattacharyay, Dilip Sarkar, Brigitte Morais, Marc. Gagnon., Effect of petroleum coke properties on coke/pitch wetting behavior., JER-REGAL (2012) , 15th November, Québec, Canada
- **Arunima Sarkar,** Duygu Kocaefe, Yasar Kocaefe, Pascal Coursol, Marc. Gagnon., Investigation of pitch-coke wetting behavior, JER-REGAL (2012) , 4th October, Québec, Canada